AN ABSTRACT OF THE THESIS OF

Pórdur Arason for the degree of Doctor of Philosophy in Geophysics presented on April 18, 1991.

Title: Paleomagnetic Inclination Shallowing in Deep-Sea Sediments.

Redacted for privacy

Abstract approved: _____

Dr. Shaul Levi

In this thesis anomalous downcore shallowing of paleomagnetic inclinations is interpreted to be caused by sediment compaction. Thus, compaction-induced inclination shallowing may influence tectonic reconstructions that are based on inclinations from deep-sea sediment cores.

Progressive downcore shallowing of the remanent inclination was observed in a 120-m section of Plio- Pleistocene sediments at Deep Sea Drilling Project (DSDP) site 578 in the northwest Pacific. Near the top of the section the average inclination corresponds to the expected geocentric axial dipole value of 53° but shallows downcore by about 6° to 8°. In sediments spanning the same time interval of neighboring site 576, no inclination shallowing was observed. This second site has considerably lower sedimentation rates, and the Plio- Pleistocene is represented by a 26-m sedimentary section. The inclination shallowing at site 578 was correlated to a downhole decrease in porosity, and these results are interpreted to suggest that both the downhole inclination

shallowing and decrease of porosity in site 578 were caused by sediment compaction.

Microscopic models demonstrate that sediment compaction may lead to inclination shallowing of the magnetic remanence. Furthermore, it is shown that inherent initial within-sample dispersion of the magnetic moments will transform any form of microscopic mechanism to an equation of a standardized form: $\tan(I - \Delta I) = (1 - a\,\Delta V)\tan I$, where I is the inclination of the ambient field, ΔI is the inclination shallowing, a is a constant and ΔV the compaction.

Paleomagnetic inclinations of Cretaceous DSDP sediments from the Pacific plate are known to be systematically shallower than predicted from paleolatitudes of hot spot reconstructions. Published paleomagnetic data were reexamined and the shallow Cretaceous inclinations explained as a result of sediment compaction. The Cretaceous data are used to estimate the parameter a. The resulting a values are comparable to those of previous studies of compaction-induced inclination shallowing, both from laboratory experiments and the considerably younger deep-sea sediments at site 578. Values of the parameter a suggest that it might be controlled by sediment lithology with greater shallowing for clayey than calcareous sediments.

Paleomagnetic Inclination Shallowing in Deep-Sea Sediments

by

Pórdur Arason

A THESIS

submitted to

Oregon State University

in partial fulfillment of

the requirements for the

degree of

Doctor of Philosophy

Completed April 18, 1991

Commencement June 1991

APPROVED:

Redacted for privacy

Professor of Geophysics in charge of major

Redacted for privacy

Dean of College of Oceanography

Redacted for privacy

Dean of Graduate School

Date thesis is presented April 18, 1991

Typed by Þórður Arason for Þórdur Arason

Dedication

Ég tileinka rit þetta stjúpömmu minni og minningu afa og ömmu minna.

Ragnhildur Steindórsdóttir
(fædd 11.5.1903)

Kristján Lárusson
(11.7.1905 – 5.12.1973)

Björg Steindórsdóttir
(18.5.1909 – 30.7.1935)

Þórður Valgeir Benjamínsson
(2.8.1896 – 10.11.1985)

Þorbjörg Sigurðardóttir
(26.10.1899 – 27.3.1987)

ACKNOWLEDGEMENTS

I would like to express my appreciation to my advisor, Shaul Levi, who has been a continuous source of support and encouragement during my seven years at Oregon State University. Simply put, he receives an A^+.

I would also like to thank the other faculty members who have served on my thesis committee: Gary D. Egbert, John L. Nábělek, Nicklas G. Pisias, J. Brookes Spencer, Erwin Suess, and William H. Menke. I am grateful for their constructive comments on my thesis and positive attitude through the years.

I appreciate all the assistance in the laboratory by Dennis Schultz and for keeping my spirits up.

It has been delightful to participate in this microcosm of the world, called Corvallis and I would especially like to thank all the geophysics students during my years at OSU: The Americans Bruce H. Dubendorff, Robert W. Foote, Steven C. Jaumé, Peter Middlebrooks, and John Rees. Also François Saucier from Quebec. Miguel Angel Alvarado-Omaña, Juan García-Abdeslem, and Osvaldo Sánchez-Zamora from Mexico. Ariel E. Solano-Borrego from Colombia. Ana L. G. Macario and Luiz Braga from Brazil. Rolin Chen and Shu-Fa Dwan from Taiwan. Xiao-Qing Li, Gui-Biao Lin and Gan-Yuan Xia from China. Muhammad A. Soofi and Akbar Khurshid from Pakistan. Pierre Doguin, Yannick Duroy, and Michel Poujol from France. Jochen Braunmiller, Rainer Ludwig, Peter Puster, and Daniel Sattel from Germany. Marijke van

Heeswijk from the Netherlands. And finally the Icelandic students Bryndís Brandsdóttir, Gudni Axelsson, and Haraldur Audunsson. I hope I didn't forget anyone and that I will not forget any of you. The geophysics faculty during this time included: Dallas H. Abbott, L. Dale Bibee, Y. John Chen, Richard W. Couch, J. Paul Dauphin, Gary D. Egbert, Randall S. Jacobson, Shaul Levi, Robert J. Lillie, William H. Menke, John L. Nábělek, Gordon E. Ness, and Anne M. Tréhu. I appreciate their attempts to guide me, and hope that I have learned something from all of them.

I am especially grateful to the late professor of geophysics and mathematics, Gunnar Bödvarsson. The many in-depth discussions with him on geophysics and all aspects of human activity on the porch overlooking his garden are unforgettable. His wife Tove and their children made us feel at home in Corvallis. Also special thanks to the Icelandic community of Corvallis who have enriched our stay here.

Marcia Turnbull, Donna Obert and Jefferson J. Gonor have been extremely helpful in minimizing bureaucracy for me. Thanks.

I thank Richard B. Kovar for supplying the geochemical data from DSDP leg 86 on digital form. Discussions with Robert A. Duncan on Pacific plate motions are greatly appreciated. Pierrick Roperch, Kenneth Kodama, and several anonymous reviewers made constructive comments on individual sections of this thesis.

This work would never have been accomplished without the encouragement of my wife, Elínborg G. Sigurjónsdóttir, and a little push every now and then from my energetic sons, Ari and Sigurjón.

This work was financially supported by grants from the U. S. National Science Foundation and loans from the Icelandic Government Student Loan Fund.

TABLE OF CONTENTS

LIST OF FIGURES

LIST OF TABLES

Paleomagnetic Inclination Shallowing in Deep-Sea Sediments

CHAPTER 1

Background

Use of the magnetic compass for navigation during the last millennium has been facilitated, largely by the fact that the geomagnetic field closely resembles a stationary dipole with an axis close to the Earth's rotation axis. The dipolar nature of magnets and of the magnetic field was determined in the 1500s, and it was found that the geomagnetic field varies over time in the 1600s. Paleomagnetism is the study of the geomagnetic field in the geologic past. In the 1960's it was demonstrated that when averaged over long enough time, the magnetic field does indeed resemble a geocentric axial dipole (GAD).

Paleomagnetic directions are often used to determine tectonic movements and for constraints on geomagnetic theories. An example is the study of changes in magnetic inclination observed in deep-sea sedimentary sections which maybe related to movement of large oceanic tectonic plates. This thesis deals with the study of paleomagnetic

inclinations within deep-sea sediments and the processes which may result in measured inclinations that are slightly shallower than expected. In this context it is important to keep in mind that a 1° inclination anomaly can be interpreted as a 200 km north-south translation of a terrane.

I will now briefly discuss four types of inclination anomalies that occur in paleomagnetism: (1) geomagnetic inclination anomaly, (2) depositional inclination error, (3) compaction-induced inclination shallowing, and (4) procedural inclination errors. Significant developments have been made towards understanding all of these inclination anomalies in the last decades. To some extent it is difficult to distinguish between the sources of these directional anomalies. The last two sub-fields are the topic of this thesis.

Although, the magnetic field averaged over thousands of years resembles a geocentric axial dipole [*Opdyke and Henry*, 1969], there is evidence for the existence of persistent non-dipole field components. The difference between the long term field inclination and the GAD-inclination is called inclination anomaly. The magnitude of the inclination anomaly seems to be latitude dependent and appears to be a few degrees [*Wilson*, 1970; 1971; *Coupland and Van der Voo*, 1980; *Merrill and McElhinny*, 1977; 1983; *Livermore et al.*, 1983; 1984; *Schneider*, 1988; *Schneider and Kent*; 1988*a*, *b*; 1990]. These studies indicate a negative inclination anomaly of 2° to 6° over the whole Earth; shallow inclinations in the northern hemisphere and steep inclinations in the south.

The earlier inclination anomaly studies did not take plate motions into account, which resulted in an overestimation of the anomaly, because most of the data are from northward moving plates. The estimated magnitude of the inclination anomaly has been decreasing in recent years, and the data from piston cores compiled by *Schneider and Kent* [1990] show on average no inclination anomaly (±1°) for the northern hemisphere.

In the 1950's and 1960's it was noticed that inclinations from recent glacial sediments were often shallower than the GAD value. Laboratory redeposition experiments showed that the laboratory magnetic field inclination could not be duplicated; the inclinations were systematically too shallow [e.g., *King*, 1955; *Griffiths et al.*, 1960]. This was termed the inclination error; the initial inclination was not parallel to the field. At that time, magnetization of sediments was thought to occur at the sediment/water interface. Theoretical models were developed that explained the inclination error to be caused by competing gravitational and magnetic forces; gravitational torques tend to rotate elongated grains into the horizontal, while the magnetic torques are trying to align the magnetic grains with the field [*King*, 1955; *Griffiths et al.*, 1960; *King and Rees*, 1966]. The theoretical models indicated that larger grains would be more affected by inclination error.

It was shown later that the laboratory magnetic field direction could be duplicated with carefully constructed experiments [e.g., *Irving and Major*, 1964; *Kent*, 1973; *Tucker*, 1979; 1980; *Barton et al.*, 1980; *Levi and Banerjee*, 1990]. It is now thought that the remanent magnetization of sediments is "locked-in" at some depth in the sediment [e.g., *Payne*

and Verosub, 1982], and that the processes leading to inclination error may not be important for fine-grained sediments. The results of *Levi and Banerjee* [1990] indicate that some of the previously documented inclination error in laboratory experiments may have been due to coarse magnetic particles, and insufficient stirring and breakup of the sediment matrix before redeposition.

Compaction-induced inclination shallowing is the main topic of this thesis. Suspicions of anomalously shallow inclinations have been reported from studies of deep-sea sediments, and it has been suggested that the shallow inclinations are due to sediment compaction [e.g., *Morgan*, 1979; *Kent and Spariosu*, 1982; *Tauxe et al.*, 1984]. Inclination shallowing has been associated with sediment porosity [*Arason and Levi*, 1986; 1990*b*; *Celaya and Clement*, 1988]. Furthermore, laboratory experiments have demonstrated that sediment compaction can lead to inclination shallowing [e.g., *Blow and Hamilton*, 1978; *Anson and Kodama*, 1987; *Deamer and Kodama*, 1990; *Lu et al.*, 1988; 1990].

Recently it was pointed out that if the processes controlling inclination shallowing and inclination error include physical rotation of the magnetic grains toward more horizontal positions then it might be detected by measurements of anisotropy of anhysteretic remanent magnetization (ARM) [*Collombat et al.*, 1990; *Jackson et al.*, 1991]. This approach is similar to the one suggested by *Cogné and Perroud* [1987]. In fact, some of the theories, interpretations and findings of this thesis can probably be tested by ARM anisotropy measurements of compacted samples from Deep Sea Drilling Project (DSDP) holes.

Sampling/measurement procedures as well as the data processing can also introduce an inclination bias. *Briden and Ward* [1966] demonstrated that arithmetic averages of inclination-only data would lead to systematic bias in the estimate of the mean inclination. *Kono* [1980*a*, *b*], *McFadden and Reid* [1982], and *Cox and Gordon* [1984] have found ways to correct for such bias. However, as we show in chapter 5 these methods are not always successful. *Calderone and Butler* [1988; 1991] showed that undetected random tilt may lead to slight systematic inclination shallowing. In fact it is possible that accepted sampling procedures may introduce systematic bias. It was shown by *Steele* [1989] that sample shape and a particular measurement procedure might result in too shallow inclinations. In chapter 6 we point out that the choice of averaging paleomagnetic data as either directions or poles may lead to systematic bias in the mean estimate.

One of the central assumptions in paleomagnetism is that the primary magnetization is acquired parallel to the local magnetic field. The validity of this assumption has not been sufficiently studied, even for igneous rocks. Although this thesis concerns the inclination shallowing in sediments, we note that there may also be inclination error problems in traditional paleomagnetic directions of igneous rocks. Recent comparisons of paleomagnetic directions from historical lava flows and the known field direction during emplacement have indicated minor, but systematic inclination shallowing of the remanence [e.g., *Castro and Brown*, 1987; *Tanguy*, 1990]. Furthermore, estimates of paleomagnetic poles from skewness of magnetic anomalies may also include slight

systematic biases [*Petronotis and Gordon*, 1989]. Therefore, it appears that slightly biased initial inclinations may not be confined to sediments.

This thesis is written in the manuscript format, and chapters 2 through 6 are considered as individual articles. In chapter 2 we show downcore inclination shallowing in paleomagnetic data from DSDP hole 578, which includes probably the most complete Neogene magnetostratigraphic data set from a single hole of the over 1100 holes cored in the DSDP-program. In appendix A we list the paleomagnetic data from DSDP hole 578. Chapter 2 was published in the *Journal of Geophysical Research* in April 1990 [*Arason and Levi*, 1990*b*]. In chapter 3 we review inclination shallowing models and describe several mechanical processes that might lead to inclination shallowing. In appendix B we derive some equations used in chapter 3. Chapter 3, and appendix B were published in the *Journal of Geophysical Research* in April 1990 [*Arason and Levi*, 1990*a*]. In chapter 4 we show that Cretaceous paleomagnetic data from the Pacific plate can be interpreted as being affected by inclination shallowing processes. We plan to submit chapter 4 for publication in the *Journal of Geophysical Research.* In chapter 5 we compare statistical methods that were designed for azimuthally unoriented cores of inclination-only data. In appendix C we list programs used in the simulations for chapter 5. We plan to submit chapter 5 for publication in the *Geophysical Journal International.* In chapter 6 we show that some inclination bias may be introduced by particular procedures of analyzing paleomagnetic data. We plan to submit chapter 6 for publication in the *Geophysical Research Letters.*

CHAPTER 2

Compaction and Inclination Shallowing in Deep-Sea Sediments From the Pacific Ocean

Progressive downcore shallowing of the remanent inclination has been observed in a 120-m section of marine sediments at Deep Sea Drilling Project site 578 in the northwest Pacific. This section represents the past 6.5 m.y. Near the top of the section the average inclination corresponds to the expected geocentric axial dipole value of 53° but shallows down section by about 6° to 8°. Northward translation of the Pacific plate accounts for only about a quarter of the inclination shallowing. Moreover, no inclination shallowing was observed at neighboring site 576, which has considerably lower sedimentation rates, and the last 5 m.y. are represented by a 26-m sedimentary section. The inclination shallowing at site 578 is correlated to an average decrease in porosity of 3-4%. The porosities in the top 26 m at site 576 are slightly higher than at site 578 and show no definite trend downhole. We interpret these results to suggest that both the downhole inclination shallowing and decrease of porosity in site 578 are caused by sediment

compaction. Compaction does not play a significant role for the section at site 576 due to its much shorter length.

2.1 INTRODUCTION

Paleomagnetism depends on accurate recording of the ancient geomagnetic field and the preservation of the magnetic remanence in the host rock. Many sediments have been shown to accurately preserve the paleomagnetic field direction; natural marine sediments often show no significant deviation from the expected geocentric axial dipole (GAD) inclination [e.g., *Harrison*, 1966; *Opdyke*, 1972; *Levi and Karlin*, 1989]. However, for some longer Deep Sea Drilling Project (DSDP) sedimentary sections, it was noticed that the inclinations at depth are shallower than expected, after correcting for tectonic movements, and these inclination anomalies have been qualitatively attributed to sediment compaction [e.g., *Morgan*, 1979; *Kent and Spariosu*, 1982; *Tauxe et al.*, 1984]. In these examples the postulated causal effects of compaction on the inclination shallowing have not been substantiated by independent quantitative methods. Inclination shallowing was associated quantitatively with sediment porosity in clays from the northwest Pacific Ocean [*Arason and Levi*, 1986], and *Celaya and Clement* [1988] reported correlations of inclination shallowing with dewatering in several cores from the Atlantic Ocean, where the carbonate contents are consistently greater than 80%. Laboratory studies have shown that compaction can contribute to inclination shallowing in sediments [e.g., *Blow and Hamilton*, 1978; *Anson and Kodama*, 1987]. In addition, *Arason and Levi* [1990*a*] have shown theoretically that a variety of mechanical models can produce inclination shallowing during compaction; the magnitude of the inclination shallowing may depend on factors such as

the sediment lithology and the dominant physical processes responsible for the shallowing.

As sediments are buried they experience the overburden pressure from the accumulating sediment, which expels pore water and decreases the porosity [*Hamilton*, 1959; 1976]. The decrease of porosity can be used as a first-order estimate of sediment compaction. *Nobes et al.* [1986] examined the physical properties, including porosity, of clay rich sediments from all oceans for DSDP legs 1 to 86. This data set shows that in clayey deep-sea sediments the porosity changes downhole, from a 50–90% range in the top of the holes, to 40–80% at about 200 m below the seafloor, and to 30–50% near 1000 m depths. From their data we estimate the porosity gradients to range on average from 0.02 to 0.08% m^{-1} in the top several hundred meters. Furthermore, these global porosity data suggest that sediment compaction in the top 100 m is a common property of marine sediments. Therefore, if sediment compaction can cause inclination shallowing, then slight inclination shallowing might be a common property of deep-sea sediments.

In this study we present paleomagnetic results from two DSDP sites. Interpretation of the magnetostratigraphy was straightforward due to the slowly changing sedimentation rates and excellent grouping of inclinations into antipodal polarities. The two sedimentary sections represent similar time intervals but different depths due to different sedimentation rates (site 578: 6.5 Ma in 120 m, and site 576: 5 Ma in 26 m). Although the inclinations near the top of both sections are close to the GAD value, the two sites do not show the same inclination changes back in time. We therefore conclude that the downhole inclination

trends at site 578 are probably not of geomagnetic origin. Although it is possible that lithological variability of the sediment, coring disturbance, and even nonvertical drilling contributed to the downhole inclination patterns, we correlate the inclination shallowing in site 578 to the parallel downhole decrease in sediment porosity and suggest that compaction of the sediment caused rearrangement of grains leading to the observed inclination shallowing.

2.2 DATA FROM PACIFIC OCEAN SEDIMENTS

In this study we consider results from DSDP sites 578 and 576 in the northwest Pacific Ocean (see Figure 2.1), cored in 1982 during leg 86 by the *D/V Glomar Challenger*. About 1000 km east of Japan (33.9°N, 151.6°E and 6010 m water depth) the hydraulic piston corer (HPC) was used to core a 177-m sedimentary section at site 578 with 99% recovery in the top 120 m. At site 576 (32.4°N, 164.3°E and 6217 m water depth) approximately 1200 km east of site 578, up to 75 m were cored in three holes using the HPC [*Heath et al.*, 1985*a*].

The top 120 m (~6.5 Ma) at site 578 consist of biosiliceous clay with locally abundant radiolarian-diatom ooze and numerous ash layers. This top section is composed of two units; the upper 77-m-thick unit is composed of gray anoxic clay which overlies a yellow-brown oxidized pelagic clay. The clay mineralogy of the sediment is approximately constant in the top 120 m, and the major clay minerals are 30% illite and 30% smectite. Below 120 m depth the mineralogy changes to 10% illite and 80% smectite and is more variable [*Lenôtre et al.*, 1985]. The sedimentation rate changes smoothly from about 10 m m.y.$^{-1}$ at 120 m depth, to 40 m m.y.$^{-1}$ near the top of the section. There are virtually no carbonates in the sediments at site 578 (less than 0.5% $CaCO_3$ [*Ku et al.*, 1985]). The top 27 m (~5 Ma) at site 576 consist of pelagic yellowish-brown, visibly burrowed, and slightly biosiliceous clay. The major clay minerals are approximately 30% illite and 30% smectite [*Lenôtre et al.*, 1985]. The sedimentation rate increases from about 2 m m.y.$^{-1}$ at 26 m depth, to 10 m m.y.$^{-1}$ near the top.

Samples for paleomagnetism were obtained during the cruise (approximately every 0.2 m at site 578, and 0.1 m at site 576) using a thin-walled, nonmagnetic stainless steel tube mounted in an oriented jig. The sediment was extruded from the 2 × 2 cm cross section sampling tube with a tightly fitting plastic piston into 8 cm^3 plastic sample boxes with lids. The samples were stored moist and at a temperature between 1° and 4°C. The intensities of the natural remanent magnetization (NRM) averaged about 50 mA m^{-1} at site 578 and 20 mA m^{-1} at site 576. The remanence directions are very stable, and minor secondary components were usually cleaned with 10 mT alternating field demagnetization (AFD), and the median demagnetizing fields of the NRM were about 30 mT. The remanence of all the paleomagnetic samples from site 576 (holes 576 and 576B) was measured, and they were demagnetized to at least 20 mT AFD [*Heath et al.*, 1985*b*]. Anomalous and pilot samples were taken to higher AFD levels. The subbottom depths for site 576 were adjusted according to correlations between the three holes by *Heath et al.* [1985*c*]. At site 578, initial measurements of the NRM and AFD to 10 mT were done for alternate samples [*Heath et al.*, 1985*b*]. Subsequently, we measured the remaining specimens in the top 120 m from site 578, which were demagnetized to at least 20 mT. No differences were observed between these two data sets for site 578.

Due to the excellent quality of the magnetic signal at site 578 and relatively rapid sedimentation rates, polarity magnetostratigraphy was possible down to 145 m subbottom, corresponding to about 15 Ma, but the quality of the magnetic signal deteriorates abruptly below 120 m

depth (~6.5 Ma) which coincides with significant change in sedimentation rate and mineralogy. For these reasons we limit the discussion in this study to the top 13 cores (119 m) of site 578. At site 576, magnetostratigraphy was only possible down to 26 m (~5 Ma). Below this depth there is a sudden change in lithology and a sharp decrease in sedimentation rate. The magnetostratigraphy at these two sites is shown in Figure 2.2. In Figure 2.3 we show vector projections of the remanence during AFD of selected pilot samples from sites 578 and 576. The demagnetization trajectories show a linear decay to the origin with no major secondary components. A minor normal overprint was observed in the reversed samples where the AFD of 10 mT removed usually only a minute net magnetization. Most samples showed no directional change after 10 mT AFD. Based on the relatively high intensities of the NRM and anhysteretic remanent magnetization (ARM) and their demagnetization characteristics, we presume that the remanence is carried predominantly by submicron magnetite particles.

Part of the observed inclination shallowing at site 578 can be explained by the northward translation component of the Pacific plate. If the observed inclination shallowing at site 578 were entirely due to northward displacement through time (using the magnetic polarity timescale [e.g, *Ness et al.*, 1980] to transform depths to time), a northward component of motion of 121 ± 28 km m.y.$^{-1}$ would be required. The uncertainty represents the 95% confidence limit of the slope of a least squares line (N = 563). *Duncan and Clague* [1985] estimated a Pacific plate Euler rotation pole at 68.0°N, 75.0°W and rotation rate of 0.95° m.y.$^{-1}$ since 42 Ma, using K-Ar dating of nine

linear island and seamount chains on the Pacific plate. This result indicates a 30 km m.y.$^{-1}$ northward velocity component at site 578, and 35 km m.y.$^{-1}$ at site 576. Several estimates have been made of Pacific plate motion, with slightly different rotations, indicating about 10 km m.y.$^{-1}$ uncertainty in the northward velocity components at these sites. Therefore it seems that only about 25% of the observed inclination shallowing at site 578 can be explained by Pacific plate motion.

Following the magnetic measurements, most of the samples were used in detailed geochemical studies. One of the estimated parameters was the water content (w), from $w = (m_w - m_d) / m_d$; m_w and m_d are the weights of the wet and dried sediment, respectively. We determined the porosity (ϕ) from the published water content data of *Heath et al.* [1985*c*], which we corrected for the salt content, using the relation

$$\phi = \frac{w}{w (1 - S r) + r (1 - S)} \qquad (2.1)$$

We assume sea water salinity, $S = 0.035$, and the ratio of the sea water density to the density of the sediment grains, $r = 1024/2700$.

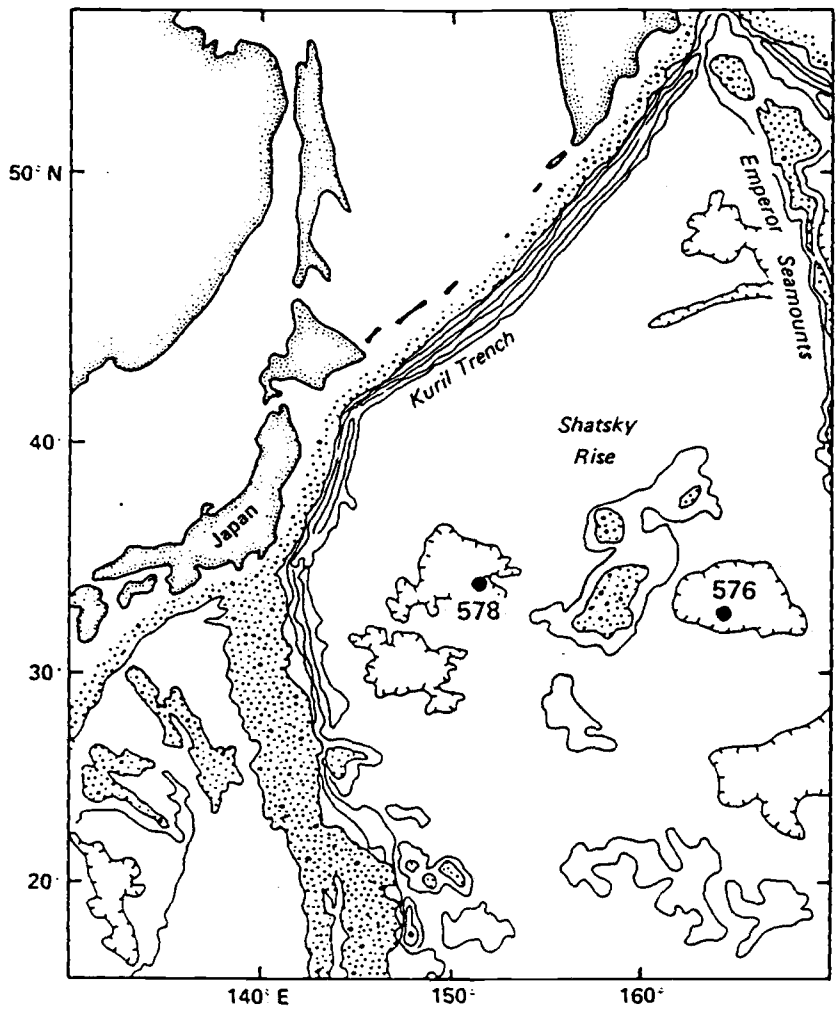

Figure 2.1. Location map of DSDP sites 578 and 576. This map was modified from *Heath et al.* [1985*a*].

Figure 2.2. Magnetostratigraphy at sites 578 and 576. The crosses represent excursional or transitional directions which were excluded from this study. (*a*) The inclination profile of the upper 120 m of hole 578, representing the most recent 6.5 m.y., showing all the recognized subchrons in this time-interval. (*b*) A composite section of inclinations in the top 26 m of holes 576 and 576B, representing the last 5 m.y. The downhole shallowing of the inclinations is visible in site 578, but there is no obvious trend at site 576.

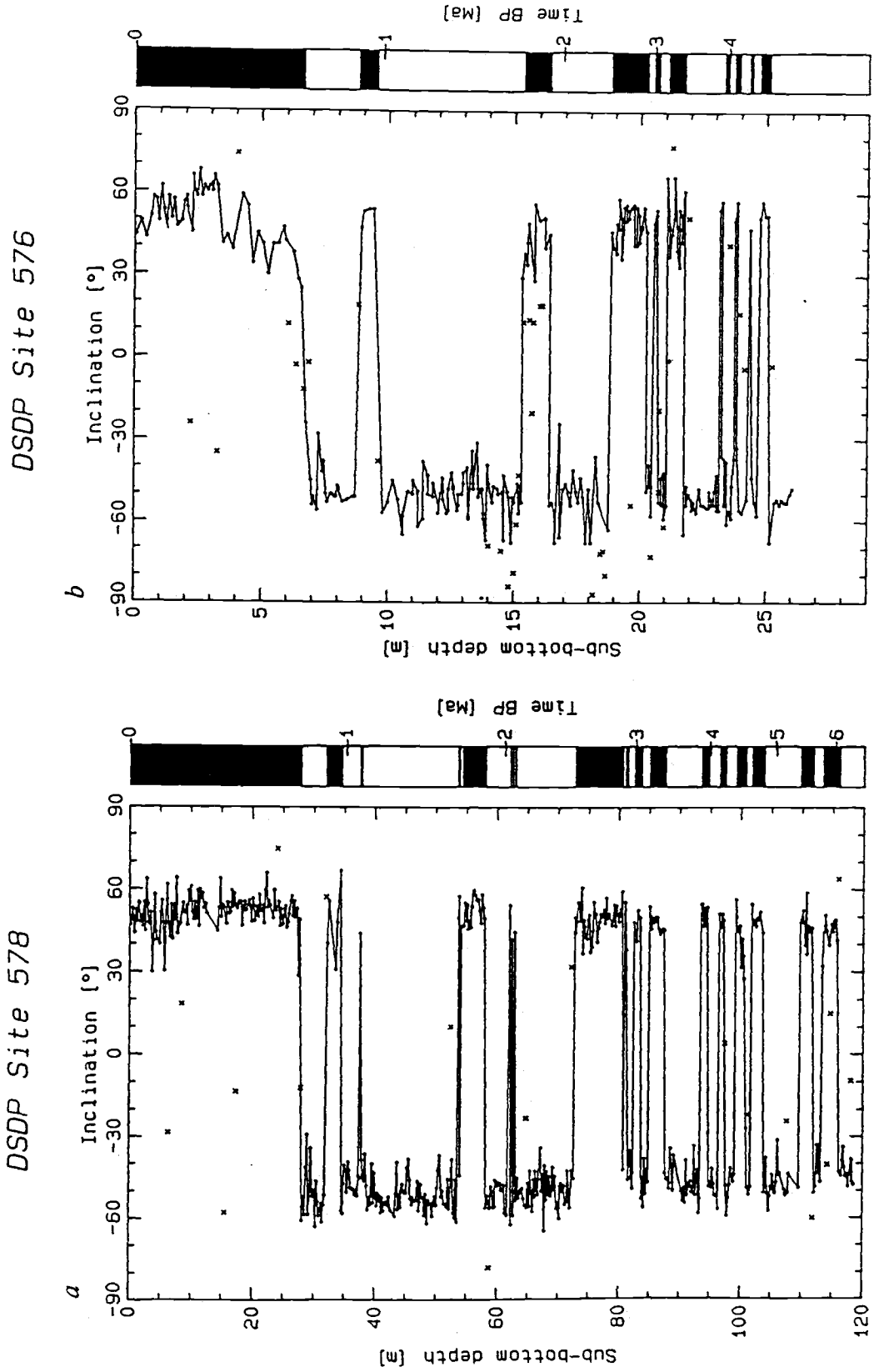
DSDP Site 578
a
Inclination [°]
Sub-bottom depth [m]
Time BP [Ma]
DSDP Site 576
b
Inclination [°]
Sub-bottom depth [m]
Time BP [Ma]

Figure 2.2.

Figure 2.3. Vector projections of selected pilot samples from sites 578 and 576. The ticks on the axes indicate 10 mA m^{-1}. Solid symbols show the inclination during demagnetization in an up (U) versus horizontal (H) projection, whereas open symbols show the relative declination during demagnetization in an north (N) versus east (E) projection. (*a*) – (*f*) Samples from site 578; NRM and demagnetization levels 10, 20, 30, 40, 60, 80, and 100 mT. (*a*) Sample 912 (578-1-2, 66) (hole-core-section, depth in section in centimeters) at 2.16 m depth below the seafloor. (*b*) Sample 946 (578-2-3, 128) at 9.06 m depth. (*c*) Sample 1074 (578-5-3, 26) at 36.56 m depth. (*d*) Sample 1198 (578-7-6, 106) at 60.76 m depth. (*e*) Sample 1290 (578-9-5, 83) 78.13 m depth. (*f*) Sample 1385 (578-11-5, 97) at 97.27 m depth. (*g*) – (*i*) Samples from site 576; NRM and demagnetization levels 10, 20, 30, and 40 mT. (*g*) Sample 36 (576-2-1, 96) at 7.91 m depth. (*h*) Sample 49 (576-2-2, 76) at 9.21 m depth. (*i*) Sample 192 (576-4-1, 106) at 19.96 m depth. The magnetization is very stable with only minor secondary components "cleaned" at the lowest demagnetization levels. The effect of minor overprinting are most noticeable in the reversed samples (Figures 2.3*c*, 2.3*d*, and 2.3*g*) where the demagnetization at 10 mT AFD removes only a minute net component.

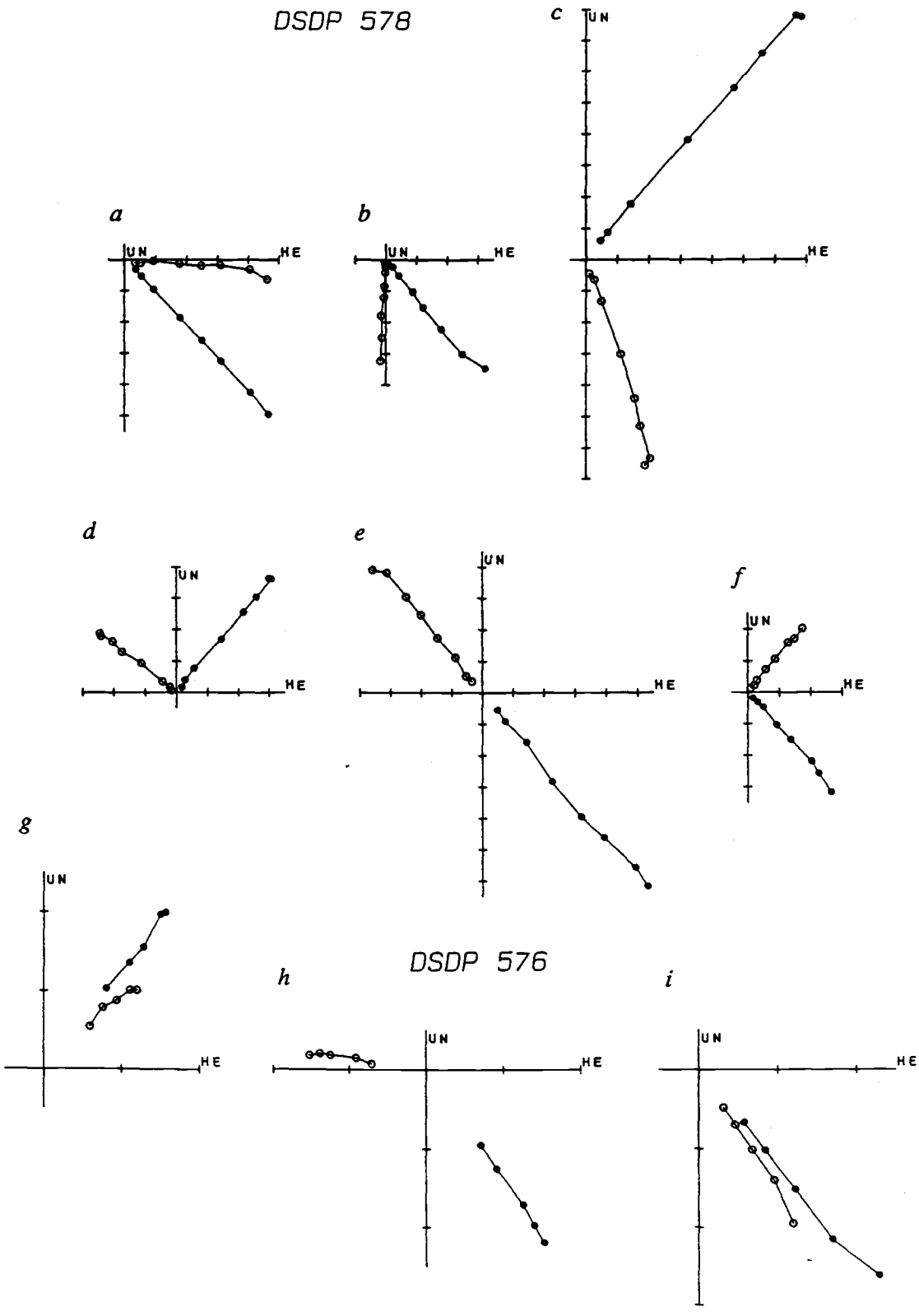

Figure 2.3.

2.3 DATA ANALYSIS

2.3.1 Paleomagnetic Data Selection

To focus on trends in the remanence, we analyzed the average behavior of the paleomagnetic directions. To be conservative, samples with excursion or transitional directions were omitted. Accordingly, using inclination and core-adjusted declination, we excluded specimens deviating from the GAD direction by more than 45°, as well as samples whose virtual geomagnetic pole latitudes deviated from the rotation axis by more than 20°, based only on the inclination data.

Of the 583 demagnetized specimens in the top 120 m of site 578, 20 were excluded from this study. Fourteen specimens were excluded because they deviated from the GAD direction by more than 45°, including eight excursions, five transitions, and one due to possible core top disturbance. An additional six samples were excluded because their virtual geomagnetic pole latitudes deviated from the rotation axis by more than 20°. These included two specimens with steep inclinations and four with shallow inclinations. Of the 328 demagnetized specimens in the top 26 m at site 576, 36 were excluded from this study. We omitted 16 specimens deviating from the GAD direction by more than 45°, including nine excursions, six transitions, and one possible core top disturbance. An additional 20 samples were excluded because their virtual geomagnetic pole latitudes deviated from the rotation axis by more than 20°. These included nine specimens with steep inclinations and 11 with shallow inclinations. To assess the influence of our data

selection on the results, we repeated the analysis with all the data included.

2.3.2 Analysis of the Average Inclinations

The selected "cleaned" inclination data (563 specimens from site 578 and 292 from site 576) are shown in Figure 2.4, transformed to positive inclinations. At site 578, there is a trend of downhole inclination shallowing of 6° to 8°, and a scatter of 10° to 15°. At site 576 we observe a slight but not significant inclination steepening trend of 1° to 2° and more scatter than at site 578. Since we are interested in the long-term trend, it is helpful to get rid of the high-frequency scatter, and this can be accomplished by averaging the inclinations over some depth or time interval. As these cores are azimuthally unoriented, the arithmetic means of the inclinations will have a bias, toward shallower inclinations. Therefore we used the method of *Briden and Ward* [1966] with formulas derived by *Kono* [1980*b*]. A square averaging window was used, because it is directly applicable to the Kono equations, whereas weighting functions, such as the Gaussian, cannot be so readily used in the equations. Of some concern is the sharpness of the boxcar window, which produces some high-frequency noise. The averaging window was varied for optimum results; a too narrow window increased the 95% confidence limits, so that the changes downhole were not significant, and too wide windows smoothed out all variability.

First, we compare the inclinations at these two sites in time domain to study possible time related geomagnetic expressions. Later in this paper we compare the inclinations in depth domain. The Kono average

inclinations, as well as several Fisher statistics parameters, including 95% confidence limits of the mean, were calculated in the time domain with a 1-m.y. running boxcar. The inclination shallowing, after correcting for the northward motion of the Pacific plate (30 km m.y.$^{-1}$ for site 578, and 35 km m.y.$^{-1}$ for site 576) is shown in Figure 2.5. The running averages were also calculated without excluding the anomalous directions with no significant changes in the average values, but there was a slight increase in the 95% confidence limits of the means.

Figure 2.5 shows the different downcore behavior of the average inclinations for sites 578 and 576 over a comparable time interval. In addition, *Bleil* [1985] studied the paleomagnetism of site 579 (38.6°N, 153.8°E), also situated on the Pacific plate, about 560 km north of site 578. The sediments at site 579 were deposited since 4.5 Ma, and the trend of the site 579 inclinations is very similar to that at site 576, showing slight but not significant steepening. Therefore the inclination shallowing at site 578 is unlikely to be of geomagnetic origin, and we are led to conclude that the inclination shallowing at site 578 is caused by a recording or preservation problem in the sediment. The running averages were therefore also calculated in depth domain. We chose a 10-m window width for site 578 and a 5-m window for site 576. To study possible effects of compaction on the remanent inclination, we examined changes in physical properties downhole particularly the sediment porosity.

2.3.3 Porosity Data

In analyzing the porosity data we omitted samples associated with ash layers, because they often show a very distinct porosity signature. Of 311 porosity determinations at site 578, five samples were excluded, and at site 576 we excluded three samples out of 480. The mean porosity at site 578 is 79% and 82% at site 576. The selected porosity data (306 specimens for site 578 and 477 specimens for site 576) are shown in Figure 2.6. The data from site 578 indicate a porosity decrease of about 3-4% in the top 120 m, which is similar to the general trend of 0.02-0.08% m^{-1} in clay-rich sediments of DSDP legs 1 to 86 (estimated from *Nobes et al.* [1986]). *Schultheiss* [1985] conducted consolidation experiments with a few samples from sites 578 and 576. From these data [*Schultheiss*, 1985, Figures 9 and 12] we can estimate that a sample with 80% initial porosity will experience a porosity decrease of 0.03-0.07% m^{-1} at 50–100 m depth, similar to the trend observed at site 578, suggesting that the observed porosity decrease is a good indicator of compaction. The porosity data from site 576 do not show simple downhole behavior that can be readily interpreted as compaction; after a sharp fluctuation in the top 5 m the porosity increases downhole to about 15 m depth followed by a gradual decrease. Indeed, if site 576 had the same porosity trend as site 578 (0.03% m^{-1}), it would result in less than 1% change in this considerably shorter section (26 m), which would be close to our detection limit.

A simple running boxcar arithmetic average was used to smooth the variability in the porosity data and to calculate the 95% confidence limits of the means. The boxcar window was chosen for compatibility with the

average inclination data, and its width was 10 m for site 578 and 5 m for site 576. The results are shown in Figure 2.7. The running averages were also analyzed when all the ash related porosities were included, and the results showed no noticeable changes.

Figure 2.4. The absolute values of the stable "cleaned" inclinations of the selected specimens used in this study. The curve on the graphs represents the geocentric axial dipole inclination of the sites with time transformed to depth. (*a*) The inclinations at site 578 show a definite trend with depth. The northward movement of the Pacific plate is not sufficient to account for the observed inclination shallowing with depth. (*b*) The inclinations at site 576 are more scattered, but there is no trend downcore.

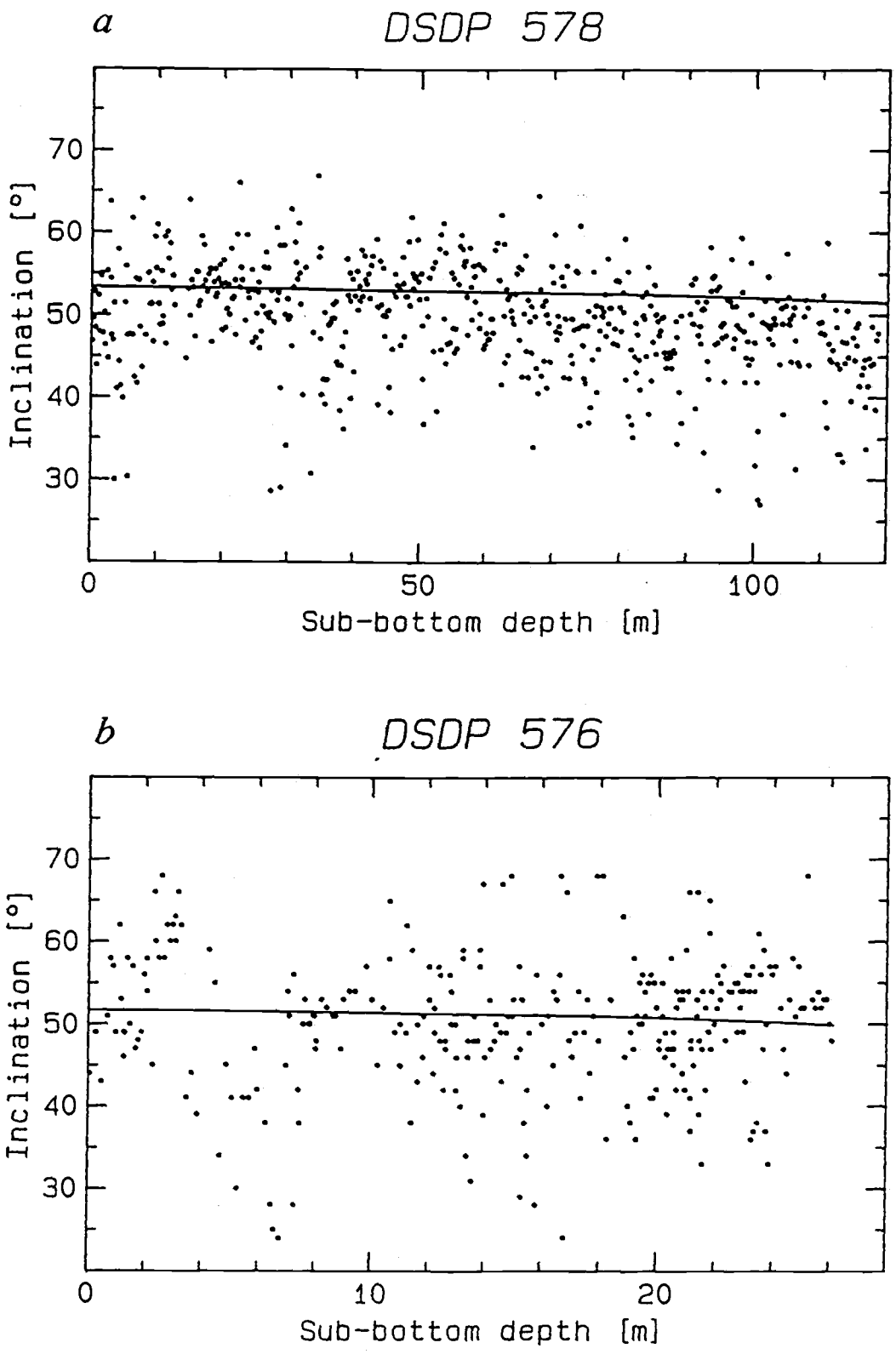
a
DSDP 578
Inclination [°]
70
60
50
40
30
0
50
100
Sub-bottom depth [m]
b
DSDP 576
Inclination [°]
70
60
50
40
30
0
10
20
Sub-bottom depth [m]

Figure 2.4.

Figure 2.5. A running 1-m.y. average of the inclination data back in time. The averages, shown by the bold curve, were calculated by the method of *Kono* [1980*b*]. The average inclinations are shown as inclination shallowing, compared to the GAD value, corrected for the northward movement of the Pacific plate. The envelopes around the averages represent 95% confidence limits of the means (α_{95}). (*a*) The inclinations at site 578 appear to have been much shallower than GAD prior to 2.5 Ma. (*b*) The running inclination averages for site 576 do not show shallowing back in time; rather they indicate a slight steepening.

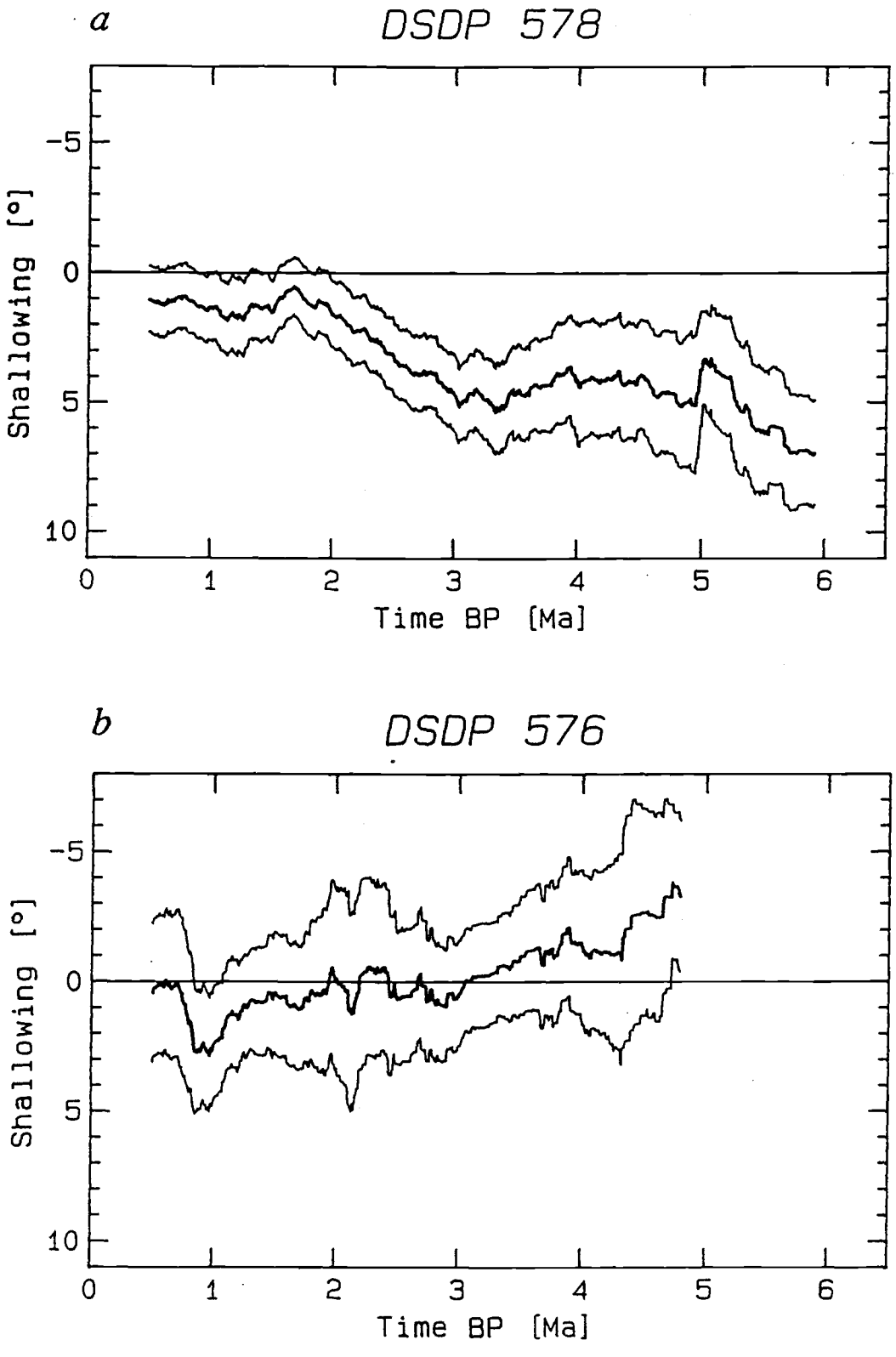
a
DSDP 578
Shallowing [°]
-5
0
5
10
0
1
2
3
4
5
6
Time BP [Ma]
b
DSDP 576
Shallowing [°]
-5
0
5
10
0
1
2
3
4
5
6
Time BP [Ma]

Figure 2.5.

Figure 2.6. The porosity of the sediments, calculated from drying individual samples. The horizontal line at 80% porosity was chosen arbitrarily for reference. (*a*) The porosities at site 578 show a definite downhole trend, which we interpret as dewatering due to gravitational compaction of the sediment. (*b*) The porosities at site 576 show no downhole trend mainly because of the difference of the depth scales. Note that site 576 has a higher mean porosity (i.e., is wetter) than site 578.

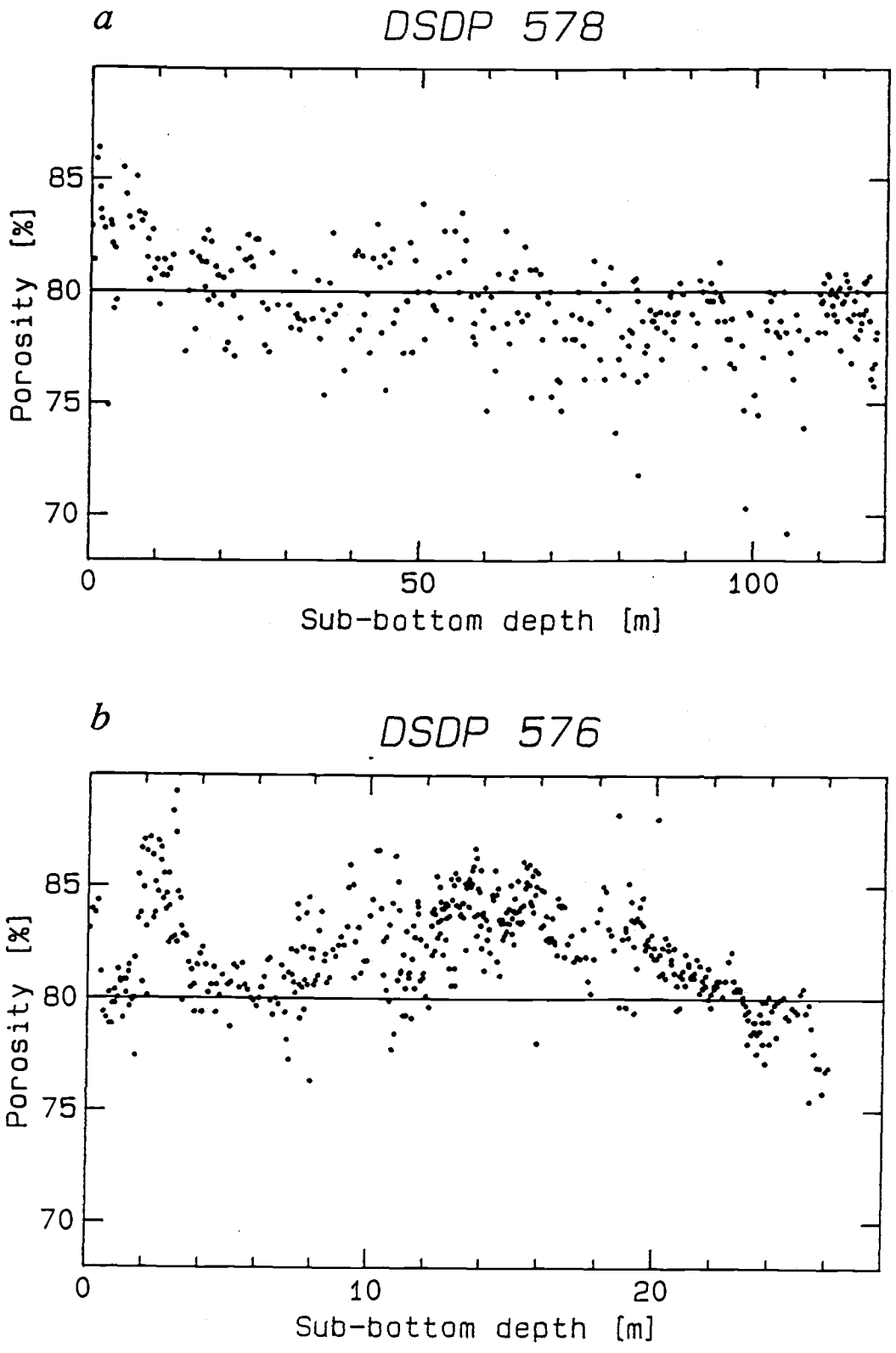
a
DSDP 578
Porosity [%]
85
80
75
70
0
50
100
Sub-bottom depth [m]
b
DSDP 576
Porosity [%]
85
80
75
70
0
10
20
Sub-bottom depth [m]

Figure 2.6.

Figure 2.7. A running average of the inclination and porosity data in depth domains. The shallowing was calculated with the same method as in Figure 2.5, with a fixed depth interval running window. The running averages are shown by a bold curve, enveloped by 95% confidence limits. (*a*) Average inclination shallowing at site 578. (*b*) Average porosities at site 578. The site 578 data were calculated every 0.2 m using a 10-m running window between 5.0 and 113.6 m (544 values). (*c*) Average inclination shallowing at site 576. (*d*) Average porosities at site 576. The site 576 averages were calculated every 0.1 m using a 5-m running window centered between 2.5 and 23.6 m (212 values). The downhole trends are now more visible than in Figures 2.4 and 2.6.

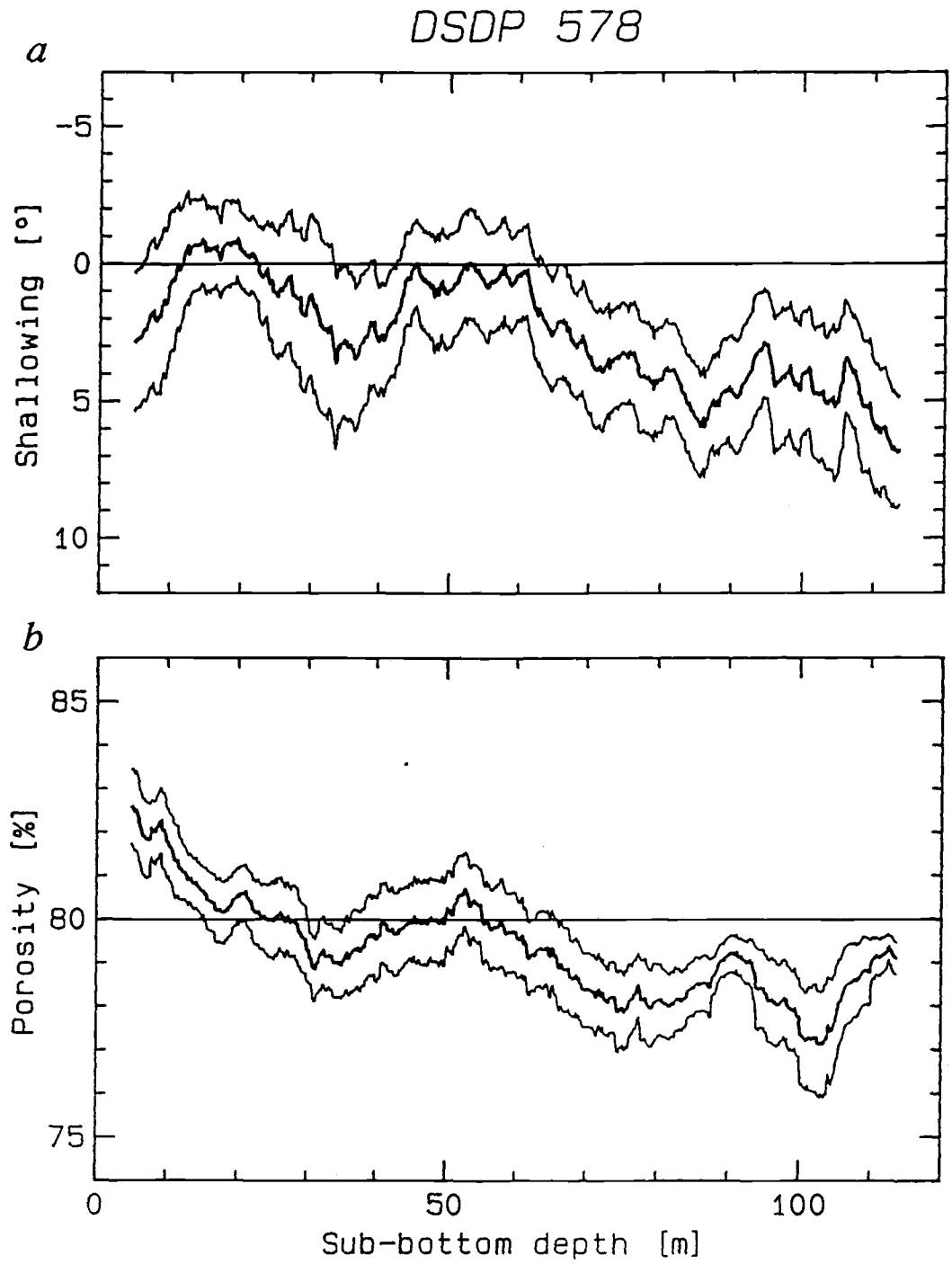
DSDP 578
a
-5
0
5
10
Shallowing [°]
b
85
80
75
Porosity [%]
0
50
100
Sub-bottom depth [m]

Figure 2.7.

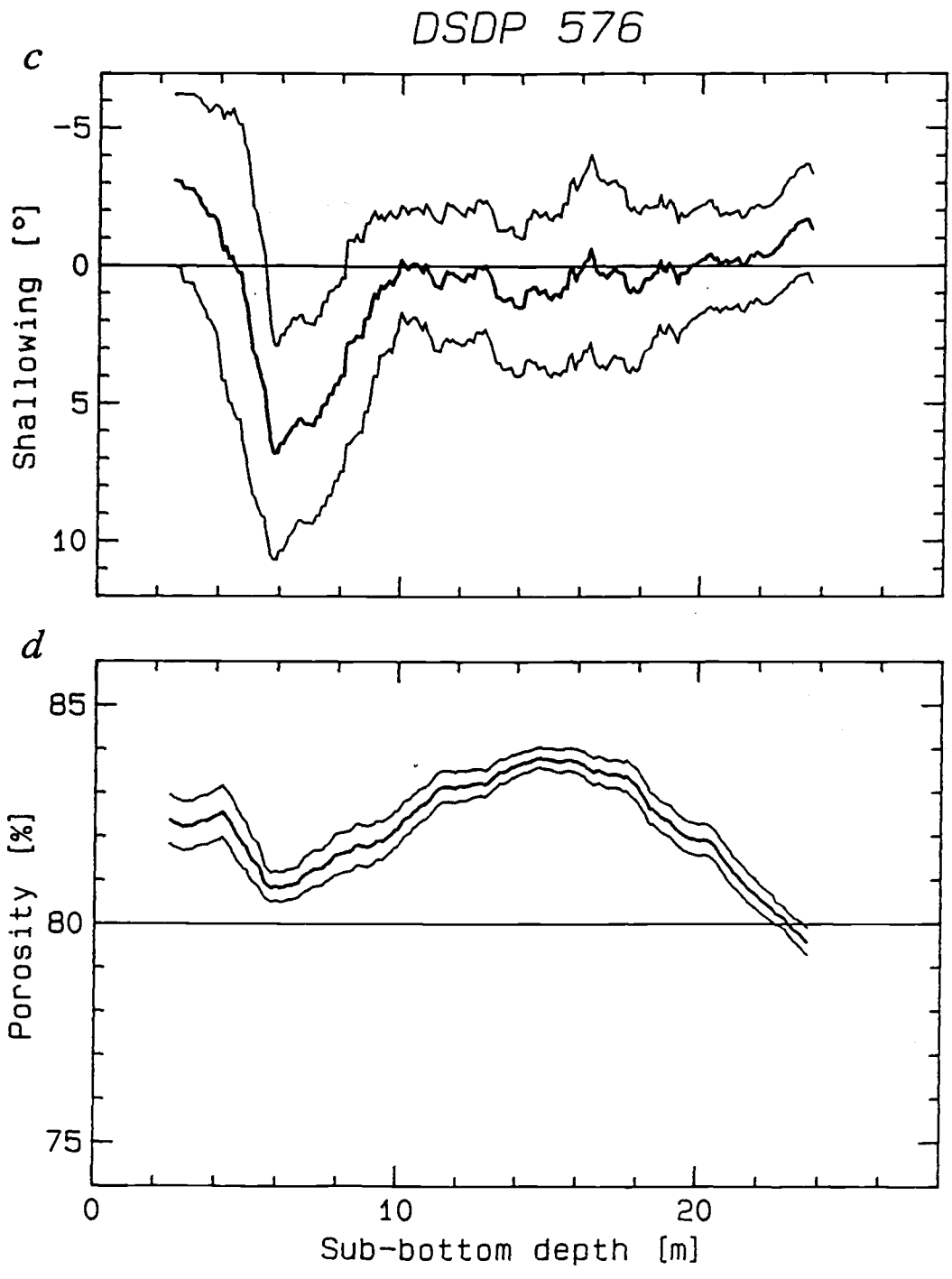

Figure 2.7 continued.

2.4 DISCUSSION

There is no apparent correlation between the magnetic and porosity data of individual specimens, which, we believe, is caused by high-frequency components in both signals, comparable or larger in amplitude than the trends (compare Figures 2.4 and 2.6 to Figure 2.7, noting that they show different scales). We have to average the direction over some time interval to decrease the effect of geomagnetic secular variation and other random noise in the magnetic signal. Similarly, the scatter in the individual porosity data also suggests that, strictly speaking, the initial porosity cannot be considered a constant through time. It may include high-frequency components in the initial porosity of the sediment, related to sedimentological variability due to climatic, lithologic, and provenance fluctuations. Therefore we have to integrate over these sediment fluctuations to be able to assume an on average constant initial porosity.

The running averages of the inclination shallowing and the porosity were calculated in depth domain and assigned the center depth of the running boxcar intervals (544 depths in site 578 centered from 5.0 to 113.6 m for 10-m windows at 0.2-m increments, and 212 depths in site 576 centered from 2.5 to 23.6 m using 5-m windows at 0.1-m increments). Note that these averages represent only a few independent estimates. The running averages of inclination shallowing and porosity for sites 578 and 576, together with 95% confidence limits, are shown in Figure 2.7. The depth domain running averages of the inclinations were plotted against the averages of the porosity in Figure 2.8, where it

is seen that for site 578, inclination shallowing increases progressively with decreasing porosity, when the porosity decreases below about 80%. At site 576 the porosity is predominantly greater than 80%, and there is no significant shallowing or steepening of the inclinations (apart from core 1). In addition, Figure 2.8 also shows that the inclinations of the top cores (5–10 m) at sites 578 and 576 are anomalous, showing high scatter and some shallowing of the inclinations, not associated with downcore compaction. Coring disturbance seems to be common in the top core of DSDP hydraulic piston cores and may be related to a particular coring practice, where the first core is shot from above the sediment-water interface. Our suspicions might be supported by the considerable porosity fluctuation in the top cores, whose depth variation is repeated for all three holes at site 576. Therefore we suspect that the upper 5–10 m at sites 578 and 576 suffered subtle coring disturbance. It is unlikely that the inclination shallowing downhole can be adequately explained by nonvertical drilling with vertical penetration near the top and gradual bending to southerly 6°-8° off-vertical drilling. Although, downhole measurements of DSDP holes indicate that the drillstring can deviate up to 5° from the vertical, the within hole variation of this angle is considerably lower [*Wolejszo et al.*, 1974]. The oxidation change at 77 m depth at site 578 is of concern, because it occurs in the zone of strongest change in inclination shallowing between 60 m and 85 m. However, this oxidation boundary is not accompanied by change in clay mineralogy. In addition, Figure 2.9 shows that there are essentially no downhole changes in the magnetic properties, as suggested by the

monotonous profiles of the NRM and ARM stability to alternating field demagnetization.

Tables 2.1 and 2.2 show the effect of polarity on the inclination shallowing. At first glance, the results of site 578 (Table 2.1) indicate that when the data are divided by chron, the reversed periods show more inclination shallowing than normal times. However, these differences are not significant at the 95% confidence levels. When all the data are considered together there is no significant difference in the inclination shallowing between normal and reversed polarity. For site 576 (Table 2.2) there is no significant inclination shallowing or steepening when the normal and reversed polarity data are divided by chron, or when all the normal and reversed data are pooled together. The present field inclination (IGRF 1985 [*Barker et al.*, 1986]) at sites 578 and 576 is about 8° shallower than the GAD value. Significant unidentified overprinting by the present field would cause normal zones to show inclination shallowing and reversed zones inclination steepening. Similarly, any biasing overprint during sampling and storage should affect normal and reversed samples in opposite directions. Since there is no systematic difference in the inclinations of normal and reversed samples, we can rule out problems due to possible unidentified overprinting.

Because of the proximity of sites 578 and 576 and their location on the same lithospheric plate, their different downcore inclination patterns cannot be caused by recent anomalous plate motions, true polar wander or long-term variations in the nondipole components of the Earth's magnetic field. Thus we interpret the results to indicate that the

progressive inclination shallowing at site 578 is caused by increasing compaction. Interestingly, there is no evidence for significant inclination shallowing in the top 50 m of site 578 or at site 576, where the porosities are generally greater than 80%. Hence there might be a threshold porosity for each sediment, which delineates the onset of inclination shallowing, which would be expected to be highly dependent on the sediment lithology.

The decrease in porosity, from an initial porosity ϕ_0 to the porosity ϕ, can be transformed to the normalized compaction values ΔV by the relation

$$\Delta V = \frac{\phi_0 - \phi}{1 - \phi} \tag{2.2}$$

The average porosity data from site 578 were transformed to compaction, using equation (2.2). The initial porosity was estimated to be 80.3% from Figure 2.8*a*. The results are shown in Figure 2.10, which excludes the data from disturbed core 1. In estimating the compaction we have assumed constant average initial porosity of the sediments. However, in the time interval represented by these sediments the sites had undergone long term sedimentation rate changes by a factor of four from the preglacial Pliocene to Pleistocene glaciations. In addition, slight variations in lithology may produce different initial sediment porosities. To investigate whether the onset of Pleistocene glaciations has significantly affected the porosity, we have compared the porosities of DSDP sites 576, 578, 579, and 580 (41.6°N, 154.0°E) in time domain but observed no consistent similarities that might be

attributed to global climatic changes. Therefore we conclude that porosity changes can give a good first order estimate of sediment compaction, but further refinements may still be possible.

In Figure 2.10 we also show curves representing two values of the parameter a defined by the equation

$$\tan (I - \Delta I) = (1 - a \, \Delta V) \tan I \qquad (2.3)$$

[*Arason and Levi*, 1990*a*; *Anson and Kodama*, 1987] describing compaction-induced inclination shallowing ΔI, where I is the inclination of the ambient field and ΔV is the compaction. For the results from site 578 the parameter a is between 1 and 2. In comparison, we estimated the parameter a to be about 4 for the inclination shallowing versus compaction for the carbonate-rich sediments studied by *Celaya and Clement* [1988]. Further studies are needed to determine if the parameter a has characteristic values for particular lithologies.

Paleomagnetists cannot generally use porosity as a check for compaction, because sufficient porosity data are usually unavailable for most cores and also because of the lack of successful theories and models to predict and subsequently correct the inclinations for compaction effects. However, the results of this study indicate that more careful attention must be paid to possible occurrences of inclination shallowing due to sediment compaction, and for the need to identify sediment lithologies and physical conditions which are likely to cause inclination anomalies. This, of course, has obvious implications for the use of inclination data from sediments for tectonic reconstructions and for

studies of the long-term behavior of the geomagnetic field. In addition, there is a need for predictive models, that may eventually be used to correct for compaction produced inclination shallowing.

Figure 2.8. Correlation between the running averages of the inclination shallowing and sediment porosity data. These data sets were shown versus depth in Figure 2.7. The encircled tails are presumably disturbed data from the top core in each hole. The error bars represent the average 95% confidence limits from Figure 2.7. (*a*) Site 578: 10-m running averages (544 data) of inclination shallowing and porosity at identical depths. (*b*) Site 576: 5 m running averages (212 data) of inclination shallowing and porosity at identical depths. Apart from anomalous behavior in cores 1, site 576 shows no significant inclination shallowing or steepening.

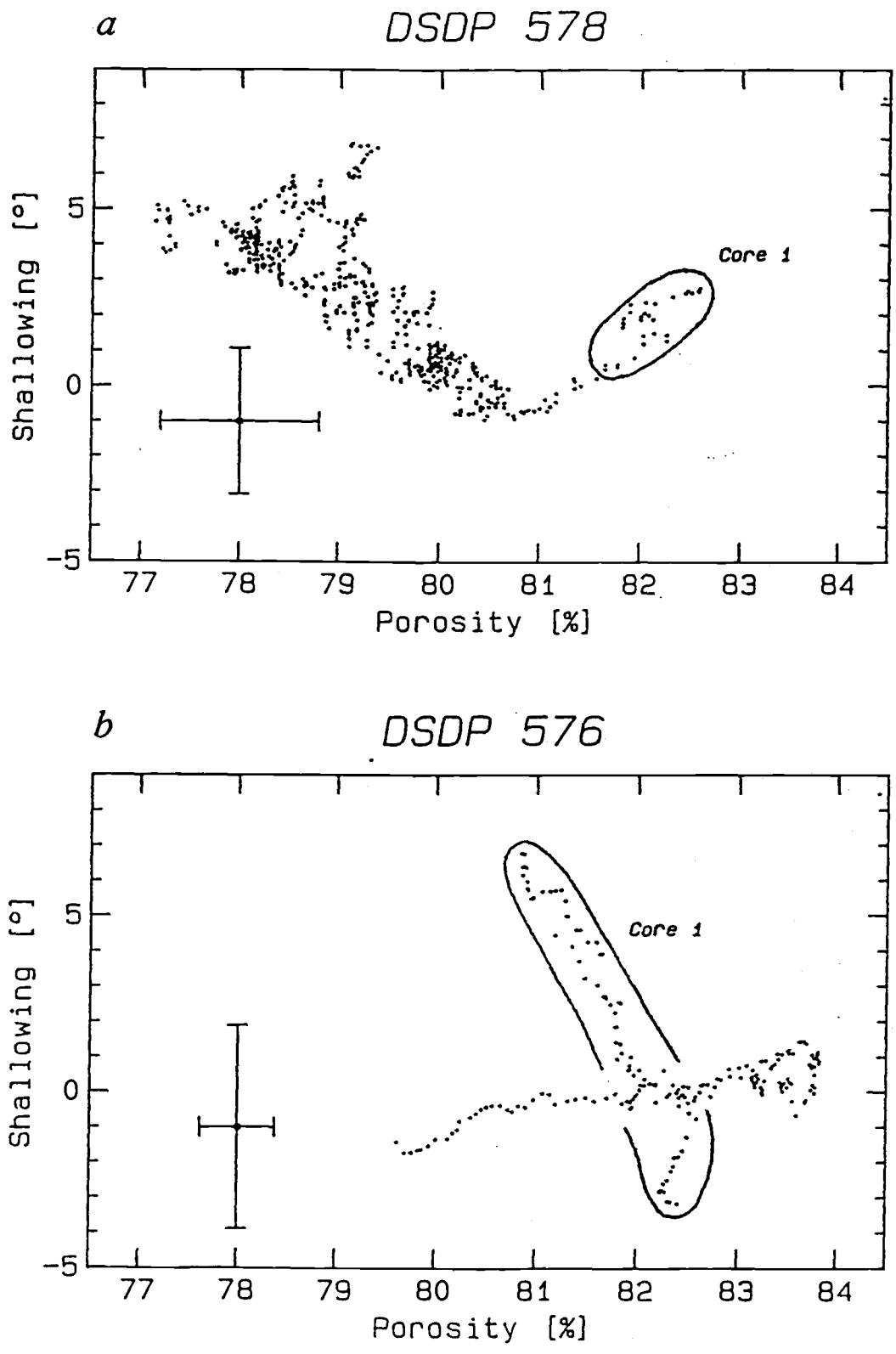
a
DSDP 578
Shallowing [°]
5
0
-5
77
78
79
80
81
82
83
84
Porosity [%]
Core 1
b
DSDP 576
Shallowing [°]
5
0
-5
77
78
79
80
81
82
83
84
Porosity [%]
Core 1

Figure 2.8.

Figure 2.9. Downhole stability of remanence of samples from site 578. The stability of natural remanent magnetization (NRM) and anhysteretic remanent magnetization (ARM), as measured by the ratio J_{20}/J_{10} of the intensity after 10 and 20 mT alternating field demagnetization (AFD). Of the 563 selected paleomagnetic samples used in this study we have measured ARM of 165. (*a*) Downhole NRM stability for the 165 samples for which ARM data is available. Most samples were cleaned at 10 mT. Note the small residual overprint at 10 mT, apparent in differences between polarities (higher and more dispersed for Matuyama 27.8–72.7 m). (*b*) Downhole stability of ARM. Note the similarity of the stability downhole, indicating the relative homogeneity of the magnetic properties.

DSDP 578

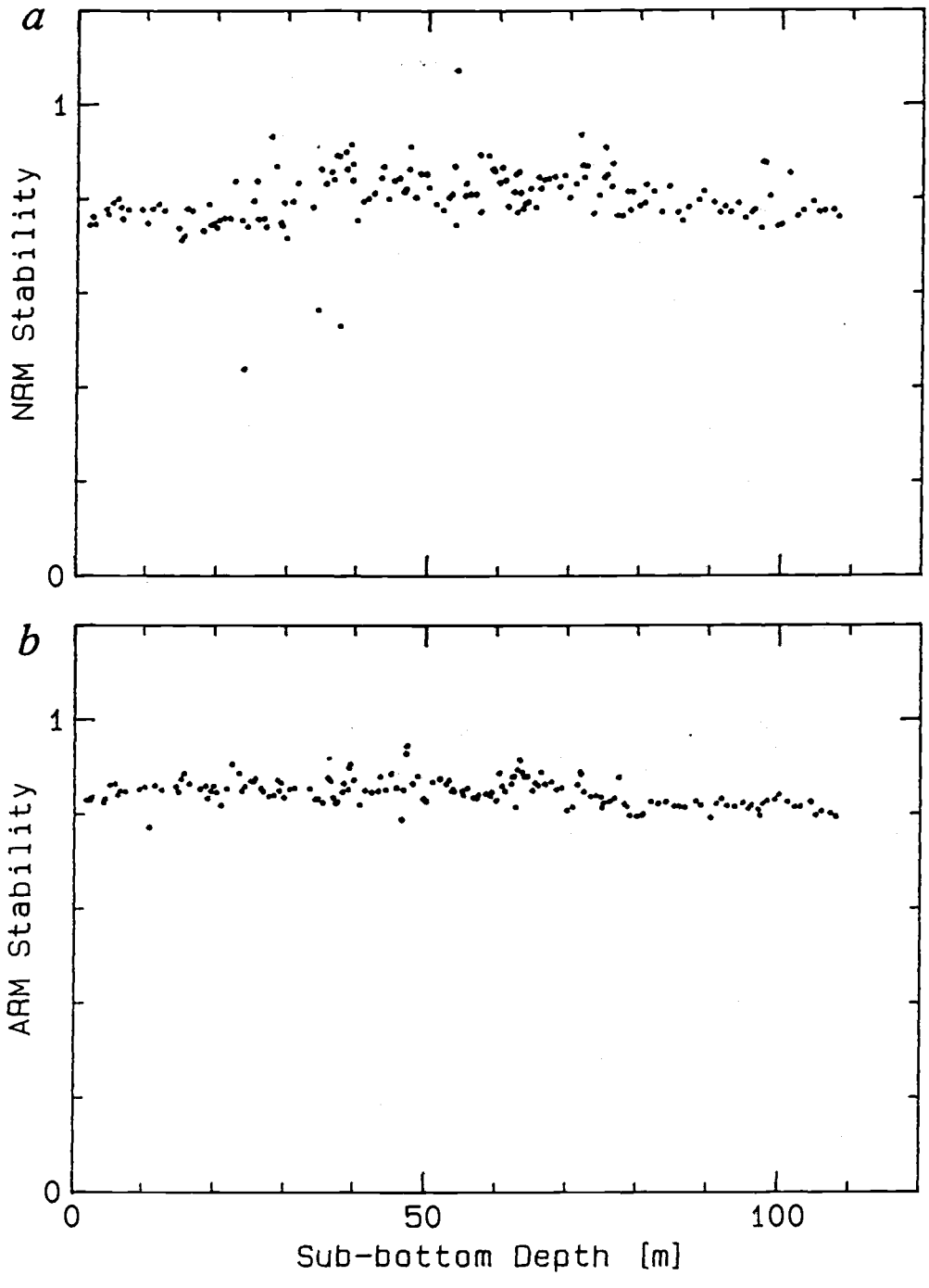

Figure 2.9.

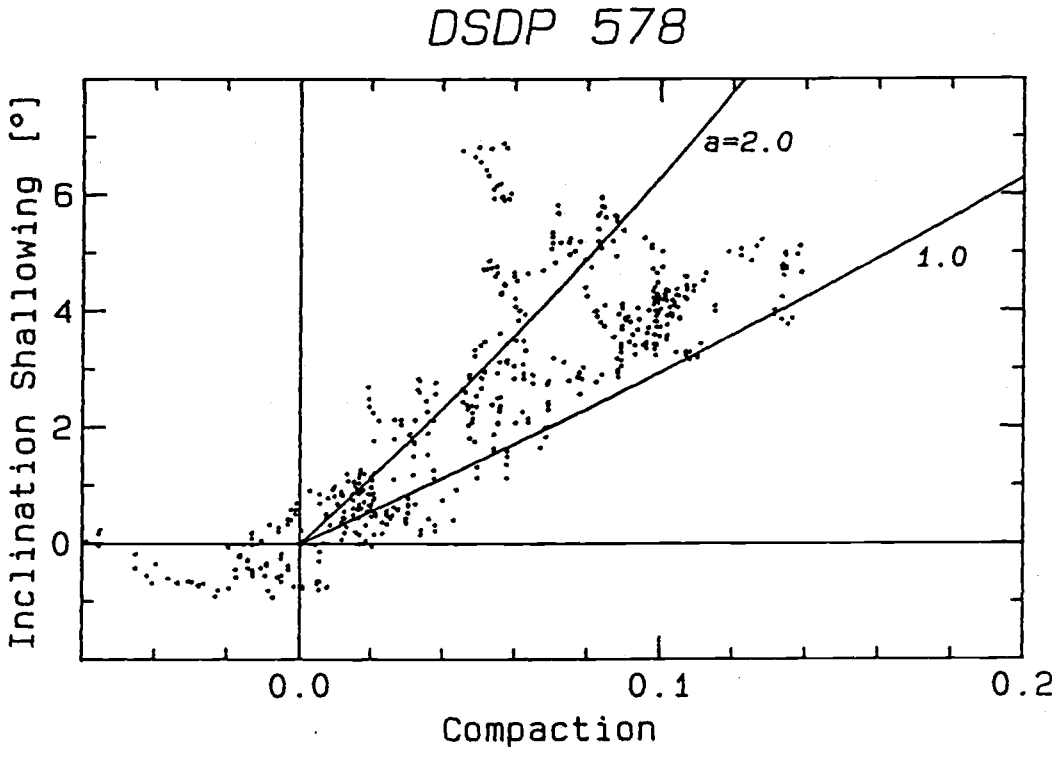

Figure 2.10. Inclination shallowing versus sediment compaction at site 578. The data are the same as in Figure 2.8*a*, with porosities converted to compaction, assuming a constant initial porosity of 80.3%. The results of the disturbed core at the top of the hole are not shown. The data are compared to two values of the parameter a in equation (3); $a = 1$ and 2. The best fit in a least squares sense is $a = 1.3$.

TABLE 2.1. Average Directions in DSDP Site 578

Chron	Polarity	Depth Range, m	Number of Samples	Average Depth, m	Average Inclination, deg	Average GAD Inclination, deg	Inclination Shallowing, deg	α_{95}, deg
Brunhes	N	0.0–27.8	128	14.0	52.2	53.3	1.1	1.4
Matuyama	N	31.9–63.0	32	52.4	51.6	52.9	1.3	3.2
	R	27.8–72.7	186	50.6	–51.2	–52.9	1.7	1.2
Gauss	N	72.7–87.6	64	79.5	48.7	52.6	3.9	1.6
	R	80.7–85.0	14	83.1	–45.2	–52.5	7.3	4.1
Gilbert	N	93.5–103.7	28	99.0	48.1	52.1	4.0	3.4
	R	87.6–109.7	68	97.4	–47.8	–52.2	4.4	2.1
Pre-Gilbert	N	109.7–116.1	23	112.7	45.9	51.7	5.8	2.9
	R	111.8–118.6	20	115.7	–43.2	–51.6	8.4	3.0
Selected	N	0.0–116.1	275	50.6	50.4	52.8	2.4	1.0
	R	27.8–118.6	288	67.7	–49.6	–52.6	3.0	1.0
	A	0.0–118.6	563	59.4	±50.0	±52.7	2.7	0.7
All	N	0.0–116.1	283	51.0	50.5	52.8	2.3	1.3
	R	27.8–118.6	300	67.6	–49.5	–52.6	3.1	1.3
	A	0.0–118.6	583	59.6	±50.0	±52.7	2.7	0.9

The selected data are grouped by chrons and subchrons of normal (N) and reversed (R) polarity. Pre-Gilbert includes data between 5.41 and 6.42 Ma. The Selected normal and reversed data are grouped together, and also all absolute values (A). We also calculate the results for all samples (including transitions and excursions). Subbottom depth range of the samples is shown and the average of the sample depths in each group. Average inclinations were calculated using the method of *Kono* [1980*b*], assuming the directions to be Fisherian [*Fisher*, 1953]. By assuming the poles to be Fisherian we get steeper average inclinations by 0.0°–0.2°. Average of the estimated geocentric axial dipole (GAD) inclinations were estimated assuming constant sedimentation rate between reversal boundaries, and 30 km m.y.$^{-1}$ northbound movement of site 578. The present location of site 578 is 33.926°N, 151.629°E with GAD inclination of 53.4°. Inclination shallowing is the difference between average GAD inclination and the average of the observed inclinations. When the observed inclination is more horizontal than the GAD inclination, inclination shallowing is taken positive. Finally, the 95% confidence limits of the average inclination were estimated, and it is the same for the inclination shallowing since the GAD inclinations have very low uncertainty.

TABLE 2.2. Average Directions in DSDP Site 576

Chron	Polarity	Depth Range, m	Number of Samples	Average Depth, m	Average Inclination, deg	Average GAD Inclination, deg	Inclination Shallowing, deg	α_{95}, deg
Brunhes	N	0.0–6.7	49	2.9	52.1	51.6	–0.5	3.9
Matuyama	N	8.8–16.4	15	14.0	45.5	51.2	5.7	6.3
	R	6.7–18.8	107	12.8	–51.1	–51.2	0.1	2.1
Gauss	N	18.8–21.8	51	20.4	49.2	50.7	1.5	2.4
	R	20.3–21.1	13	20.7	–50.6	–50.7	0.1	4.4
Gilbert	N	23.2–25.1	9	24.2	53.1	50.2	–2.9	3.0
	R	21.8–26.1	48	23.5	–52.3	–50.3	–2.0	2.7
Selected	N	0.0–25.1	124	13.0	50.2	51.1	0.9	2.0
	R	6.7–26.1	168	16.5	–51.4	–50.9	–0.5	1.6
	A	0.0–26.1	292	15.0	±50.9	±51.0	0.1	1.2
All	N	0.0–25.1	136	13.2	50.0	51.1	1.1	2.9
	R	6.7–26.1	192	16.3	–53.3	–50.9	–2.4	2.7
	A	0.0–26.1	328	15.0	±51.9	±51.0	–0.9	2.0

See Table 2.1 footnotes for description of individual columns. Negative inclination shallowing indicate steeper average inclinations than the GAD value. The present location of Site 576 is 32.356°N, 164.276°E with present GAD inclination of 51.7°. The northbound velocity of site 576 is assumed 35 km m.y.$^{-1}$.

2.5 REFERENCES

Anson, G. L., and K. P. Kodama, Compaction-induced shallowing of the post-depositional remanent magnetization in a synthetic sediment, *Geophys. J. R. Astron. Soc.*, *88*, 673-692, 1987.

Arason, P., and S. Levi, Inclination shallowing recorded in some deep sea sediments (abstract), *Eos Trans. AGU*, *67*, 916, 1986.

Arason, P., and S. Levi, Models of inclination shallowing during sediment compaction, *J. Geophys. Res.*, *95*, 4481-4499, 1990*a*.

Barker, F. S., et al., International geomagnetic reference field revision 1985, *Eos Trans. AGU*, *67*, 523-524, 1986.

Bleil, U., The magnetostratigraphy of northwest Pacific sediments, Deep Sea Drilling Project leg 86, *Initial Rep. Deep Sea Drill. Proj.*, *86*, 441-458, 1985.

Blow, R. A., and N. Hamilton, Effect of compaction on the acquisition of a detrital remanent magnetization in fine-grained sediments, *Geophys. J. R. Astron. Soc.*, *52*, 13-23, 1978.

Briden, J. C., and M. A. Ward, Analysis of magnetic inclination in borecores, *Pure Appl. Geophys.*, *63*, 133-152, 1966.

Celaya, M. A., and B. M. Clement, Inclination shallowing in deep sea sediments from the north Atlantic, *Geophys. Res. Lett.*, *15*, 52-55, 1988.

Duncan, R. A., and D. A. Clague, Pacific plate motion recorded by linear volcanic chains, in *The Ocean Basins and Margins*, vol. 7A, edited by A. E. M. Nairn, F. G. Stehli, and S. Uyeda, pp. 89-121, Plenum, New York, 1985.

Fisher, R., Dispersion on a sphere, *Proc. R. Soc. London, Ser. A, 217*, 295-305, 1953.

Hamilton, E. L., Thickness and consolidation of deep-sea sediments, *Geol. Soc. Am. Bull., 70*, 1399-1424, 1959.

Hamilton, E. L., Variations of density and porosity with depth in deep-sea sediments, *J. Sediment Petrol., 46*, 280-300, 1976.

Harrison, C. G. A., Paleomagnetism of deep sea sediments, *J. Geophys. Res., 71*, 3035-3043, 1966.

Heath, G. R., et al., *Initial Reports of the Deep Sea Drilling Project, 86*, 804 pp., U.S. Government Printing Office, Washington, D.C., 1985*a*.

Heath, G. R., D. H. Rea, and S. Levi, Paleomagnetism and accumulation rates of sediments at sites 576 and 578, Deep Sea Drilling Project leg 86, western north Pacific, *Initial Rep. Deep Sea Drill. Proj., 86*, 459-502, 1985*b*.

Heath, G. R., R. B. Kovar, C. Lopez, and G. L. Campi, Elemental composition of Cenozoic pelagic clays from deep sea drilling project sites 576 and 578, western north Pacific, *Initial Rep. Deep Sea Drill. Proj., 86*, 605-646, 1985*c*.

Kent, D. V., and D. J. Spariosu, Magnetostratigraphy of Caribbean site 502 hydraulic piston cores, *Initial Rep. Deep Sea Drill. Proj., 68*, 419-433, 1982.

Kono, M., Statistics of paleomagnetic inclination data, *J. Geophys. Res., 85*, 3878-3882, 1980*b*.

Ku, T. L., J. R. Southon, J. S. Vogel, Z. C. Liang, M. Kusakabe, and D. E. Nelson, ^{10}Be distributions in deep sea drilling project site 576 and

site 578 sediments studied by accelerator mass spectrometry, *Initial Rep. Deep Sea Drill. Proj., 86*, 539-546, 1985.

Lenôtre, N., H. Chamley, and M. Hoffert, Clay stratigraphy at Deep Sea Drilling Project sites 576 and 578, leg 86 (western north Pacific), *Initial Rep. Deep Sea Drill. Proj., 86*, 571-579, 1985.

Levi, S., and R. Karlin, A sixty thousand year paleomagnetic record from Gulf of California sediments: Secular variation, late Quaternary excursions and geomagnetic implications, *Earth Planet. Sci. Lett., 92*, 219-233, 1989.

Morgan, G. E., Paleomagnetic results from DSDP site 398, *Initial Rep. Deep Sea Drill. Proj., 47*, 599-611, 1979.

Ness, G., S. Levi, and R. Couch, Marine magnetic anomaly timescales for the Cenozoic and Late Cretaceous: A précis, critique, and synthesis, *Rev. Geophys., 18*, 753-770, 1980.

Nobes, D. C., H. Villinger, E. E. Davis, and L. K. Law, Estimation of marine sediment bulk physical properties at depth from seafloor geophysical measurements, *J. Geophys. Res., 91*, 14,033-14,043, 1986.

Opdyke, N. D., Paleomagnetism of deep-sea cores, *Rev. Geophys., 10*, 213-249, 1972.

Schultheiss, P. J., Physical and geotechnical properties of sediments from the northwest Pacific: Deep Sea Drilling Project leg 86, *Initial Rep. Deep Sea Drill. Proj., 86*, 701-722, 1985.

Tauxe, L., P. Tucker, N. P. Petersen, and J. L. LaBrecque, Magnetostratigraphy of leg 73 sediments, *Initial Rep. Deep Sea Drill. Proj., 73*, 609-621, 1984.

Wolejszo, J., R. Schlich, and J. Segoufin, Paleomagnetic studies of basalt samples, Deep Sea Drilling Project, leg 25, *Initial Rep. Deep Sea Drill. Proj.*, *25*, 555-572, 1974.

CHAPTER 3

Models of Inclination Shallowing During Sediment Compaction

We construct microscopic models of compacting sediment which lead to inclination shallowing of the magnetic remanence. The models can be classified as (1) rotation of elongated magnetic grains to more horizontal orientations; (2) rotation toward the horizontal of flat nonmagnetic fabric grains to which smaller magnetic grains are attached; (3) randomization of the sediment by grain rotations which lead to decreased intensity of magnetization and possibly also to inclination shallowing; and (4) finally, we show that the initial within-sample dispersion of the magnetic moments dampens the amount of inclination shallowing of all the models and transforms any form of microscopic mechanism to an equation of a standardized form. The physically realistic models give rise to different magnitudes of inclination shallowing, which to the first order obey an equation of the form $\tan (I - \Delta I) = (1 - a \, \Delta V) \tan I$, where I is the inclination of the ambient field, ΔI is the inclination shallowing and ΔV the compaction. For these models we also calculate the effect of compaction on the intensity of magnetization, and the results show that considerable randomization is needed to offset the increased

intensity due to higher concentrations of magnetic particles caused by compaction. If random rotations of the grains are biased toward rolling about horizontal axes and the randomization is sufficient to cancel the effect of greater concentrations, then the random grain rolling due to the compaction would give rise to considerable inclination shallowing.

3.1 INTRODUCTION

Anomalous shallowing of the magnetic inclination with depth in deep-sea sediments has been noted in several studies, and it has been suggested that the observed shallowing is due to compaction of the sediment [e.g., *Morgan*, 1979; *Kent and Spariosu*, 1982; *Tauxe et al.*, 1984]. The inclination shallowing has been associated quantitatively with the sediment porosity in clays from the Northwest Pacific ocean [*Arason and Levi*, 1986; 1990*b*] and in carbonates from the North Atlantic ocean [*Celaya and Clement*, 1988]. Furthermore, laboratory experiments have demonstrated that compaction of sediment can lead to inclination shallowing in redeposition of natural deep-sea silty clays [*Blow and Hamilton*, 1978] and in synthetic sediment composed of kaolinite and magnetite [*Anson and Kodama*, 1987]. *Verosub* [1977] reviewed the important processes in the magnetization of sediments.

The probable occurrence of inclination shallowing in some sediments is of great significance and concern for paleomagnetism with respect to the tectonic and geomagnetic interpretations of remanent magnetism. North-south translations of plates, microplates, and terranes as well as tilting of blocks are deduced from remanent inclinations of sediments. Alternatively, information about the paleomagnetic field, such as the correctness of the geocentric axial dipole hypothesis, and secular variation including polarity transitions have been derived from sediments. In all these applications it is assumed that sedimentary processes such as compaction do not alter the primary remanence direction. The development (circa 1978) of the Hydraulic Piston Coring

system for the Deep Sea Drilling Project (DSDP) and subsequently Ocean Drilling Program (ODP) provides means of obtaining undisturbed marine sedimentary sections of up to 200 m in length, at present, with good global coverage. To be able to utilize fully this growing body of data, it is crucial to understand and account for compaction-related effects on the remanent magnetism in sediments.

Available models that predict shallowing of the magnetic inclination due to sediment compaction were derived intuitively and by analogy with mechanisms for inclination shallowing in noncompacting environments, and they were designed to fit specific observations, but they lack physical rigor. The detailed behavior of remanent magnetism in compacting environments is complex and probably never fully known. It would therefore be valuable to be able to simulate the compaction effects on remanent magnetism with a simple model(s). We present here simple but physically plausible mechanical models that cause inclination shallowing during compaction. For the proposed microscopic mechanisms we derive exact mathematical expressions which relate the inclination shallowing to sediment compaction.

3.2 DEFINITIONS

The terms inclination shallowing and compaction are used extensively in this chapter, so a brief description of them is appropriate.

3.2.1 Inclination Shallowing

Inclination shallowing, ΔI, is taken as the difference between the initial magnetic inclination and the inclination after compaction. Inclination changes toward lower absolute values (more horizontal) are taken as positive inclination shallowing. In this chapter we only consider positive inclinations, but due to symmetry the conclusions are fully valid for negative inclinations. However, the equations may have some ambiguity concerning negative inclinations, due to the way inclination shallowing is defined with use of absolute values. The inclination shallowing is sometimes called inclination error, and, its negative value, inclination anomaly.

3.2.2 Compaction

As a measure of the degree of compaction, we choose the change in the normalized volume, ΔV. The initial volume of a sample is $V = 1$ with $\Delta V = 0$; later, the volume decreases to $V = (1 - \Delta V)$ for an arbitrary compaction ΔV. In squeezing a sample it is assumed that only the pore fluid is taken out of the sample, decreasing its porosity. The compaction ΔV is closely related to the settlement, Δh, a term commonly used in soil mechanics, where a sediment of initial thickness h decreases (settles) by Δh upon compaction, $\Delta V = \Delta h / h$ [e.g., *Hamilton*, 1959, p.

1424; *Tschebotarioff*, 1951, p. 105; *Tomlinson*, 1980, p. 135]. The compaction is related to the sediment porosity, ϕ, by

$$\phi = \frac{\phi_0 - \Delta V}{1 - \Delta V} \tag{3.1}$$

where ϕ_0 is the initial porosity (porosity of 80% enters the equation as 0.80). From the data of *Nobes et al.* [1986] we estimate the compaction in natural clay-rich sediments to be $\Delta V \approx 0.1$ at 50–100 m subbottom depth, $\Delta V \approx 0.3$ at 200–400 m depth and $\Delta V \approx 0.5$ for 500–1500 m depth. Therefore we are mainly interested in compaction values between 0 and 0.5. Changes in porosity with compaction from equation (3.1) are shown in Figure 3.1 for various initial porosities. We note that the relationship is quite smooth and close to linear for the lower compaction values.

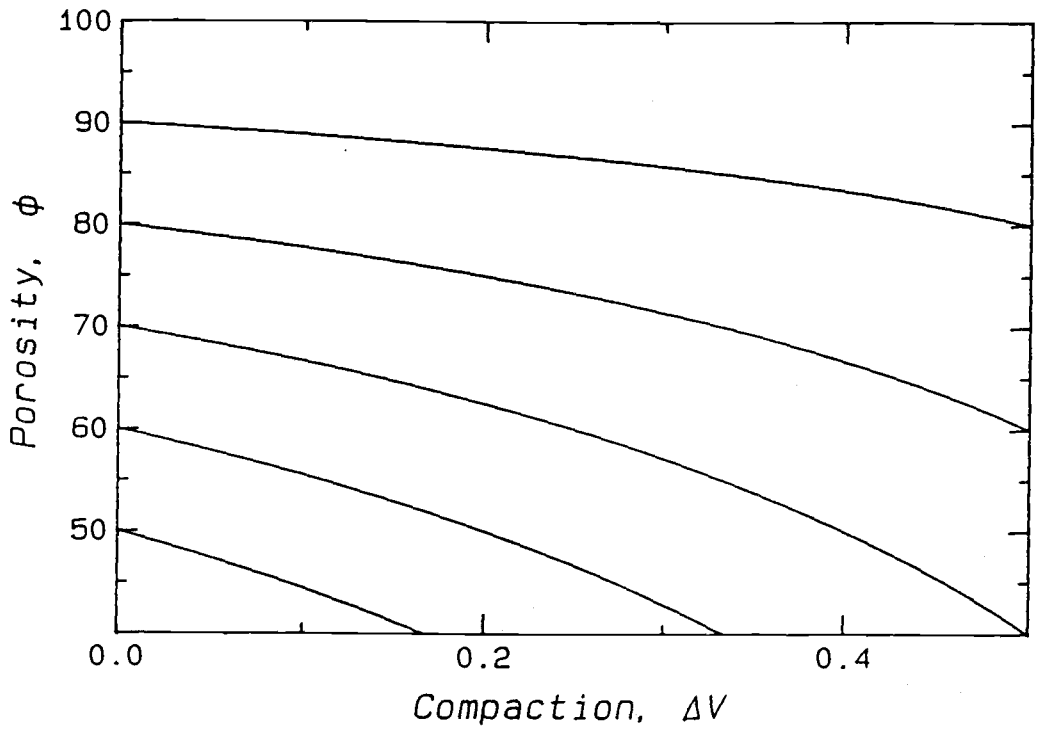

Figure 3.1. Sediment porosity ϕ (%) as a function of compaction ΔV determined from equation (3.1) for initial porosities of ϕ_0 = 50, 60, 70, 80, and 90%. For typical deep-sea sediment with porosities from 50 to 90% and compactions between 0 and 0.5 the relationship is very smooth and close to linear.

3.3 PREVIOUSLY PUBLISHED MODELS

Several models have been proposed to explain observed inclination shallowing, and we shall describe those relevant for this study. We refer to the models by the initials of their author(s). For the purpose of easy comparisons we have changed the symbols of some variables in the quoted references. The correct field inclination is denoted by I, and the observed inclination by $(I - \Delta I)$, where ΔI is the inclination shallowing.

3.3.1 Noncompacting Environment

For historical reasons we begin by describing two early models that predict inclination shallowing in noncompacting environments: first, the model by *King* [1955], which has influenced later models for compacting environments, and second, a model by *Griffiths et al.* [1960], which has been adapted for compaction in this study.

Model K. From redeposition studies of glacial sediments, *King* [1955] proposed a model to explain the observed inclination shallowing. He assumed two types of magnetic carriers: (1) a fraction f_K of platelike grains, magnetized parallel to their flat side, which would be lain down horizontally on contact at the sediment interface with zero inclination, and (2) a fraction $(1 - f_K)$ of spherical grains that accurately record the field inclination on average. By taking into account that initial dispersions affect the horizontal grains more, since there is a weaker aligning force ($\cos I$), he obtained the expression

$$\tan (I - \Delta I) = (1 - f_K) \tan I \qquad (3.2)$$

[*King*, 1955, equation 5, p. 123]. His observations suggested that $f_K \approx 0.6$. This model has influenced several later models for inclination shallowing. *Nagata* [1962] criticized King for assuming the alignment to be proportional to the field strength, and he adjusted the equation to include strong alignment of individual grains, when the net moment is not proportional to the external field strength. However, we believe that King's argument is fully justified for geomagnetic field strengths, as will be discussed later.

Model GKRW. *Griffiths et al.* [1960] noted that sediment can usually not be clearly divided into well-contrasted groups of spherical and platelike particles, as required by model K. They were primarily interested in mechanisms at the sediment-water interface, which produce inclination shallowing. One of their models deals with rolling magnetized spheres into adjacent holes. The azimuth of the direction to the holes is random, but all the particles rotate about horizontal axes.

Consider first an example of four spheres, that prior to rotation, faithfully recorded the field direction, say, inclination I and declination zero. Now let these four particles rotate through an angle $\Delta\theta$, one toward north, one south, one east, and one west. For the northward and southward rotations, the declinations are unaffected and the changes of inclination will cancel. For the eastward and westward rotations the declination changes will cancel, but both the eastward and westward rotations will result in a shallowed inclination. The resultant direction

of these four grains, after rotation, will preserve the declination but give shallow inclination.

Griffiths et al. [1960] solved this problem explicitly, starting with an ensemble where all the grains have initially an identical magnetic unit vector $\mathbf{m} = (\cos I, 0, \sin I)$. They obtained an exact expression for this vector after rotation through an angle $\Delta\theta$, about a horizontal axis with the azimuth λ. By integrating through all possible horizontal azimuthal directions λ, they found that the average magnetic vector after rotation is

$$\mathbf{m}_G = [(1/2) (1 + \cos \Delta\theta) \cos I, 0, \cos \Delta\theta \sin I] \qquad (3.3)$$

The inclination shallowing can then be obtained by the exact expression

$$\tan (I - \Delta I) = \frac{2 \cos \Delta\theta}{1 + \cos \Delta\theta} \tan I \qquad (3.4)$$

[*Griffiths et al.*, 1960, equation 3, p. 377]. If we now define f_G as

$$f_G \equiv \frac{1 - \cos \Delta\theta}{1 + \cos \Delta\theta} \qquad (3.5)$$

equation (3.4) becomes

$$\tan (I - \Delta I) = (1 - f_G) \tan I \qquad (3.6)$$

which has the same form as equation (3.2) derived by *King* [1955] for a totally different model. The dependence of ΔI on $\Delta\theta$ for a fixed I, in equation (3.6) is shown in Figure 3.2*a*, and Figure 3.2*b* gives the

intensity deduced from equation (3.3) for various I. The rolling of magnetic spheres at the sediment water interface is analogous to the random rolling of grains due to rearrangement of sediment fabric in a compaction environment, which we explore further in this chapter.

3.3.2 Compacting Environment

Blow and Hamilton [1978] proposed a compaction model which *Anson and Kodama* [1987] modified slightly to provide a better fit to their experimental data. The equations of these two models turn out to be very similar to the results of two of our rotating needle models, even though we start from totally different points of view.

Model BH. *Blow and Hamilton* [1978] proposed a compaction model, where the magnetization shallows in the same way as a passive line marker, which can be thought of as a sloping imagined soft line in the sediment, which shallows due to the shrinking vertical dimension. One way to view this model is to assume that the vertical axis of the remanence is reduced in the same proportion as the compaction of the vertical dimension of the sediment, with no alteration of the horizontal magnetization. Keeping in mind the form of the equation obtained by *King* [1955] for inclination shallowing (see model K), and using simple trigonometry, they deduced the mathematical expression

$$\tan (I - \Delta I) = (1 - \Delta V) \tan I \qquad (3.7)$$

[*Blow and Hamilton*, 1978, Figure 6, p. 20]. However, the equation was not accompanied by a microscopic physical model, and their laboratory redepositional data were only marginally supportive of their model. *Ozima* [1980] conducted compaction experiments with ferromagnetic Co particles in a Cu matrix and found the inclination to follow the passive line marker upon deformation. Equation (3.7) of model BH is identical to equation (3.18) obtained for model 1b of this study.

Model AK. *Anson and Kodama* [1987] applied model BH to data from their laboratory compaction experiments with synthetic sediments. Their results suggested that model BH overestimates the inclination shallowing, and they modified equation (3.7) by a coefficient, a, such that

$$\tan (I - \Delta I) = (1 - a \, \Delta V) \tan I \qquad (3.8)$$

[*Anson and Kodama*, 1987, equation 2, p. 685]. Best fits to the data were achieved for $a = 0.63 \pm 0.18$ for the acicular magnetite particles and $a = 0.54 \pm 0.18$ for the equidimensional magnetite. They proposed that the magnetite particles were electrostatically attached and rotated to the clay flake planes. Upon compaction the clay flakes would rearrange to more horizontal positions, resulting in inclination shallowing. Equation (3.8) turns out to be very similar to the equations of models 1c and 4a of this study (equations (3.22) and (3.72)).

Figure 3.2. Predictions of a model from *Griffiths et al.* [1960], here called model GKRW. (*a*) The inclination shallowing ΔI (deg) is shown as a function of the rolling angle $\Delta\theta$ (deg), for a fixed initial inclination of $I = 45°$, equation (3.6). Note that for small rolling angles, there is very little inclination shallowing; a rolling angle of 60° is needed to produce $\Delta I \approx 10°$. The nonlinearity of this function shows that for variable rolling angles the grains with very high rolling angles can outweigh those with lower values. (*b*) The intensity decrease, M/M_0, with rolling angle $\Delta\theta$ (deg) of model GKRW, from equation (3.52), for initial inclinations of $I = 0°$, 45°, and 90°.

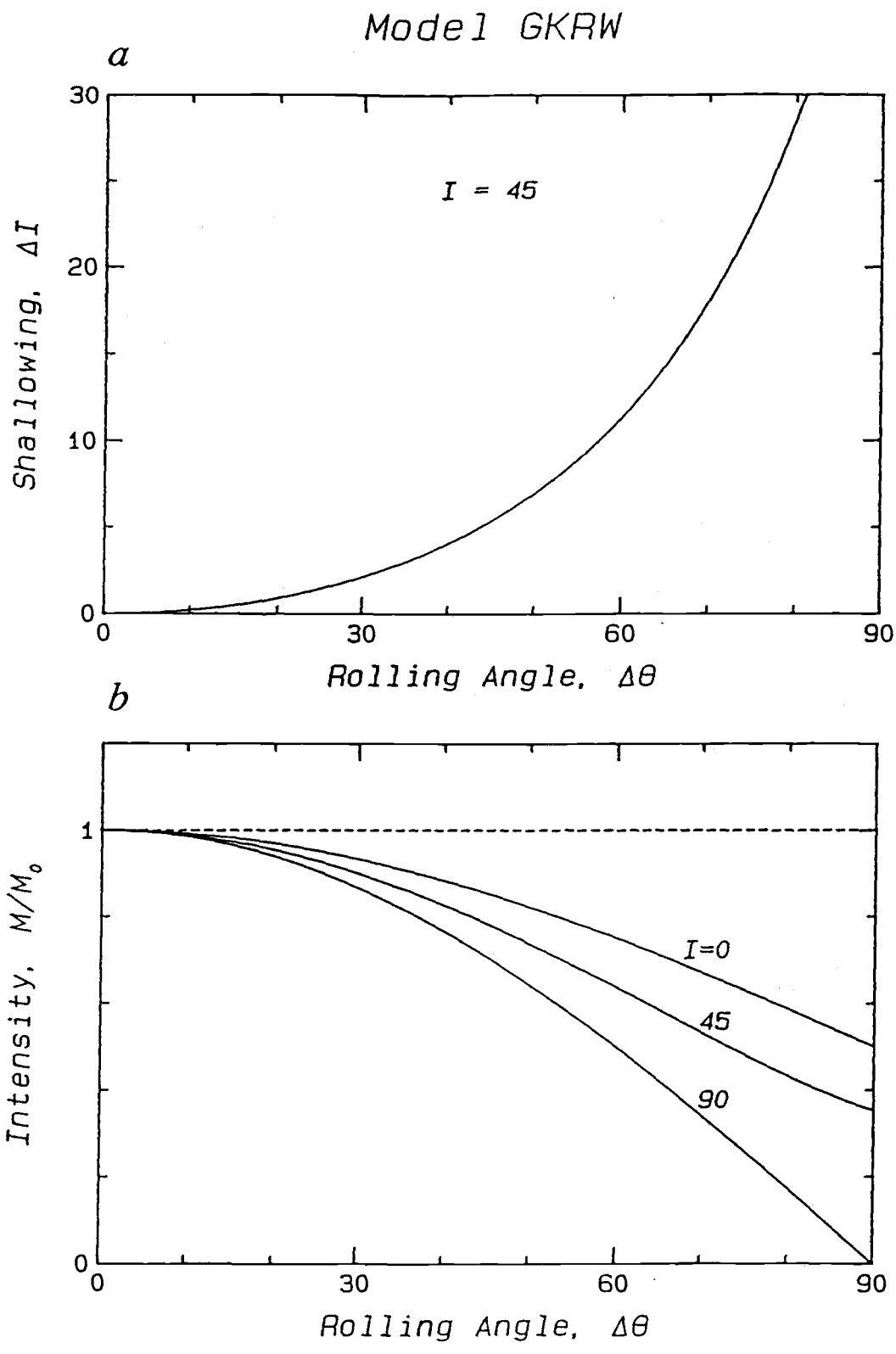
Model GKRW
a
30
20
10
0
Shallowing, ΔI
I = 45
0
30
60
90
Rolling Angle, Δθ
b
1
0
Intensity, M/M₀
I=0
45
90
0
30
60
90
Rolling Angle, Δθ

Figure 3.2.

3.4 MODELS OF THIS STUDY

In this chapter we propose several microscopic mechanisms to explain the compaction-induced inclination shallowing in sediments. The proposed models are used to derive mathematical expressions, relating inclination shallowing to sediment compaction. The proposed models can be categorized as (1) rotation of elongated or platy magnetic particles to more horizontal orientations, (2) rotation toward the horizontal of flat nonmagnetic fabric grains to which smaller magnetic grains are attached, (3) particle randomization leading to intensity decrease and possibly to inclination shallowing, and (4) the effects of expected initial within-sample dispersion.

3.4.1 Rotating Magnetic Needles

The simplest inclination shallowing models consider the rotation of elongated magnetic grains during sediment compaction. For simplicity we consider only very elongated needlelike grains magnetized along their long axis. We first assume perfect initial alignment of the needles with the external field, but later in this chapter we examine the consequences of relaxing this constraint.

In the first less sophisticated model the needles are enclosed between two converging, rigid horizontal layers, the rigid matrix. In a second more realistic case we consider the surrounding sediment matrix as a soft compressible medium. The two fundamental assumptions in these first two models are that the magnetic grains are acicular and that the surrounding nonmagnetic sediment grains behave as a soft compressible

medium around the rigid needles. Because the shapes of the magnetic particles in natural sediments probably range between being needles and equidimensional particles, these models predict an upper limit of inclination shallowing. Therefore we consider an additional model where a fraction of the remanence carriers rotates during compaction and the rest of the carriers are unaffected. The needle models are also applicable to magnetized flakes, if they are magnetized along the flake dip. For the surrounding sediment to approximate a soft medium with respect to the magnetic particles, one would expect that the nonmagnetic matrix grains are much smaller than the magnetic needles. Although observations show that fabric grains are often considerably larger than the magnetic grains, the matrix framework supported by organic binder might on average respond as a soft compressible medium, because of random and nondiscriminatory behavior, rotating some needles (flakes) more and some less than predicted. This random grain rotation will lead to an intensity decrease, which we consider later.

Model 1a: Rotating magnetic needles in rigid matrix. For this very simple model it is assumed that the remanence is carried by needle-shaped particles of length L, magnetized along their long axes. We assume that only compaction affects the remanence in the sediment. As compaction proceeds, the needles are not allowed to intrude into the sediment above or below; only particle rotation is permitted. This mechanical model is shown in Figure 3.3*a*. From the left part of Figure 3.3*a* we find the trigonometric relation: $1 = L \sin I$, and from the right

part we obtain $(1 - \Delta V) = L \sin (I - \Delta I)$. These can be connected through L to give

$$\sin (I - \Delta I) = (1 - \Delta V) \sin I \qquad (3.9)$$

which relates the inclination shallowing to the compaction. The dependence of ΔI on I in equation (3.9) is shown in Figure 3.3*b*, for various ΔV and the dependence of ΔI on ΔV for a fixed initial inclination I in Figure 3.3*c*. For this model we note that the maximum effect of inclination shallowing is at very steep initial inclinations, but for lower initial inclinations the relationship between inclination shallowing and compaction is close to linear. For low initial inclinations this model predicts similar inclination shallowing as model BH.

The constraint of the model that the needles cannot penetrate the overlying and underlying sediment appears to be unrealistic, especially for very steep inclinations, but it may be more compatible for shallow initial inclinations. For very steep initial inclinations, we would expect the needles to intrude into the oncoming sediment from above and below as the surrounding sediment is compacted, accompanied by relatively smaller grain rotation. This situation is considered in the next model.

Model 1b: Rotating magnetic needles in soft matrix. We now consider a single needle of length L, sloping at an angle I from the horizontal; see Figure 3.4*a*. We set the coordinate system such that the center of the needle is the origin which remains fixed through the compaction. From this perspective there is no translation of the needle

but only rotation about a horizontal axis. The horizontal plane through the origin is called plane O. As seen from plane O, the sediment surrounding the needle will compact both from above and below. We restrict the surrounding sediment from moving horizontally, so in fact we can view this as a solid walled container depressed by a porous piston. We define r as the length along the needle from the origin; r is positive above the plane O and negative below; s is the vertical component of r: $s = r \sin I$. As the sediment compacts, by a small increment δV, the sediment at height s above the plane O will experience a movement toward the plane O: $s \rightarrow s - \delta s = s\ (\ 1 - \delta V\ )$, leading to $\delta s = s\ \delta V$. The vertical force of the compacting sediment per unit length of the needle can be related to the displacement of the surrounding sediment by

$$F_v(r) = \alpha\ \delta s = \alpha\ r\ \delta V \sin I \tag{3.10}$$

where α is some constant, and the normal force on an element dr of the needle is

$$dF_n = F_v \cos I\ dr \tag{3.11}$$

which exerts a torque trying to rotate the needle toward shallower inclinations:

$$\tau = \int_{-L/2}^{L/2} r\ F_v(r) \cos I\ dr \tag{3.12}$$

with the solution

$$\tau = (\alpha L^3 / 24) \delta V \sin I \cos I \qquad (3.13)$$

Now it is reasonable to expect that this torque will affect the rotation of the elongated particles, against the internal friction in the sediment. For a small compaction step, δV, the inclination shallowing, δI, is assumed to be proportional to the torque; $\delta I \sim \tau$, so

$$\delta I = \eta \, \delta V \sin I \cos I \qquad (3.14)$$

where η is an efficiency parameter, indicating how effective the sediment is in rotating the needle. From equation (3.14) we can get the following differential equation:

$$\frac{dI}{dV} = \eta \sin I \cos I \qquad (3.15)$$

and by definition we know that the inclination goes from I to $(I - \Delta I)$ as the volume goes from 1 to $(1 - \Delta V)$. Here we note that dV is not a linear measure of translation, so we transform dV to settlements dh, where $dV = dh/h$, and the thickness decreases from $h = 1$ to $h = (1-\Delta V)$. We obtain

$$\int_I^{I-\Delta I} \frac{dI}{\eta \sin I \cos I} = \int_1^{1-\Delta V} \frac{dh}{h} \qquad (3.16)$$

with the exact solution

$$\tan (I - \Delta I) = (1 - \Delta V)^{\eta} \tan I \qquad (3.17)$$

One way to estimate the constant η is to assume that for very shallow initial inclinations ($I \approx 0°$), the inclination shallowing is predicted by model 1a (equation (3.9)), but then $\tan I \approx \sin I$, and $\tan (I - \Delta I) \approx \sin (I - \Delta I)$, and we therefore must have $(1 - \Delta V)\eta \approx (1 - \Delta V)$, leading to $\eta = 1$, and the equation for model 1b

$$\tan (I - \Delta I) = (1 - \Delta V) \tan I \qquad (3.18)$$

This equation is identical to equation (3.7) of model BH. The dependence of ΔI on I in equation (3.18) is shown in Figure 3.4*b*, for various ΔV, and the dependence of ΔI on ΔV for a fixed initial inclination I, in Figure 3.4*c*.

For small compaction the maximum shallowing is predicted to be around initial inclinations of 45°, and the maximum moves toward slightly higher initial inclinations with increasing compaction. From equation (3.14) we see that for small compactions $\Delta I \approx \{180/\pi\}$ (1/2) $\Delta V \sin 2I$ (the term $\{180/\pi\}$ gives ΔI in degrees), so for a fixed initial inclination I, the inclination shallowing ΔI is approximately linear with compaction ΔV, and that behavior extends over the compaction values of interest, as shown in Figure 3.4*c*.

Increased concentration of magnetic material. The previous two magnetic needle models (1a and 1b) do not account for random

rotations of the magnetic grains, and during compaction the intensity increases with increasing concentration of magnetic particles per unit volume

$$M/M_0 = \frac{1}{1 - \Delta V} \tag{3.19}$$

In the absence of randomization, the needle models predict significant increases in intensity with compaction.

Model 1c: Two types of magnetic grain shapes in soft matrix. Magnetic particles in natural sediments have a range of shapes, and we therefore consider a mixture of magnetized grains; a fraction, f_n, are needles that obey the relation of model 1b (equation (3.18)) and the rest ($1 - f_n$) are equidimensional particles that do not rotate and preserve the initial inclination I during compaction. Upon compaction ΔV the inclination of the fraction f_n shallows by Δi

$$\tan (I - \Delta i) = (1 - \Delta V) \tan I \tag{3.20}$$

The resultant vector is the sum of two vectors; one of length f_n dipping at ($I - \Delta i$); the other of length ($1 - f_n$) dipping at I: ($f_n \cos (I - \Delta i)$, $f_n \sin (I - \Delta i)$) + (($1 - f_n$) $\cos I$, ($1 - f_n$) $\sin I$), and we can find the total inclination shallowing from the total vector

$$\tan (I - \Delta I) = \frac{f_n \sin (I - \Delta i) + (1 - f_n) \sin I}{f_n \cos (I - \Delta i) + (1 - f_n) \cos I} \tag{3.21}$$

Using equation (3.20) and manipulating the trigonometric functions in equation (3.21), we obtain

$$\tan (I - \Delta I) = (1 - c f_n \Delta V) \tan I \qquad (3.22)$$

where the correction factor c is

$$c = \frac{1}{f_n+(1-f_n)\sqrt{\cos^2 I+(1-\Delta V)^2\sin^2 I}} \qquad (3.23)$$

Although c is weakly a function of f_n, ΔV, and I, it is practically equal to unity over values of interest. For $\Delta V = 0$, or $I = 0°$, $c = 1$, and for the range of compaction values ΔV from 0 to 0.5, initial inclinations I of 0° to 90°, and fractions f_n from 0 to 1, the correction factor c is always between 1 and 2. Indeed, if we further restrict our values to be $f_n > 0.5$, $I < 60°$, and $\Delta V < 0.3$, then c will be between 1.00 and 1.12.

We note that equation (3.22) is nearly identical to the formula used by *Anson and Kodama* [1987] (equation (3.8) of model AK in this chapter), where we replace their arbitrary constant a by $c f_n$. The predictions of model 1c are compared to that of model AK in Figure 3.5. The dependence of ΔI on I in equations (3.8) and (3.22) is shown in Figure 3.5*a*, for various ΔV, and the dependence of ΔI on ΔV for a fixed initial inclination I is shown in Figure 3.5*b*. We note that the predictions are quite similar.

Figure 3.3. Model 1a, rotating magnetic needles in rigid matrix, equation (3.9). (*a*) The magnetic needle of length L is enclosed between two rigid horizontal layers. Initially, on left the magnetic needle has the inclination I, and the sediment has the porosity ϕ_0. On right the layers have converged by ΔV and the water has been squeezed out so the porosity drops to ϕ and the inclination is shallower by ΔI. (*b*) The predicted inclination shallowing ΔI (deg) as a function of initial inclination I (deg), for different compactions ΔV = 0.1, 0.3, 0.5. (*c*) The predicted inclination shallowing ΔI (deg) as a function of compaction ΔV, for initial inclination of $I = 45°$. The model predicts maximum ΔI at the magnetic poles ($I \approx \pm 90°$) but is thought to be unrealistic for steep inclinations.

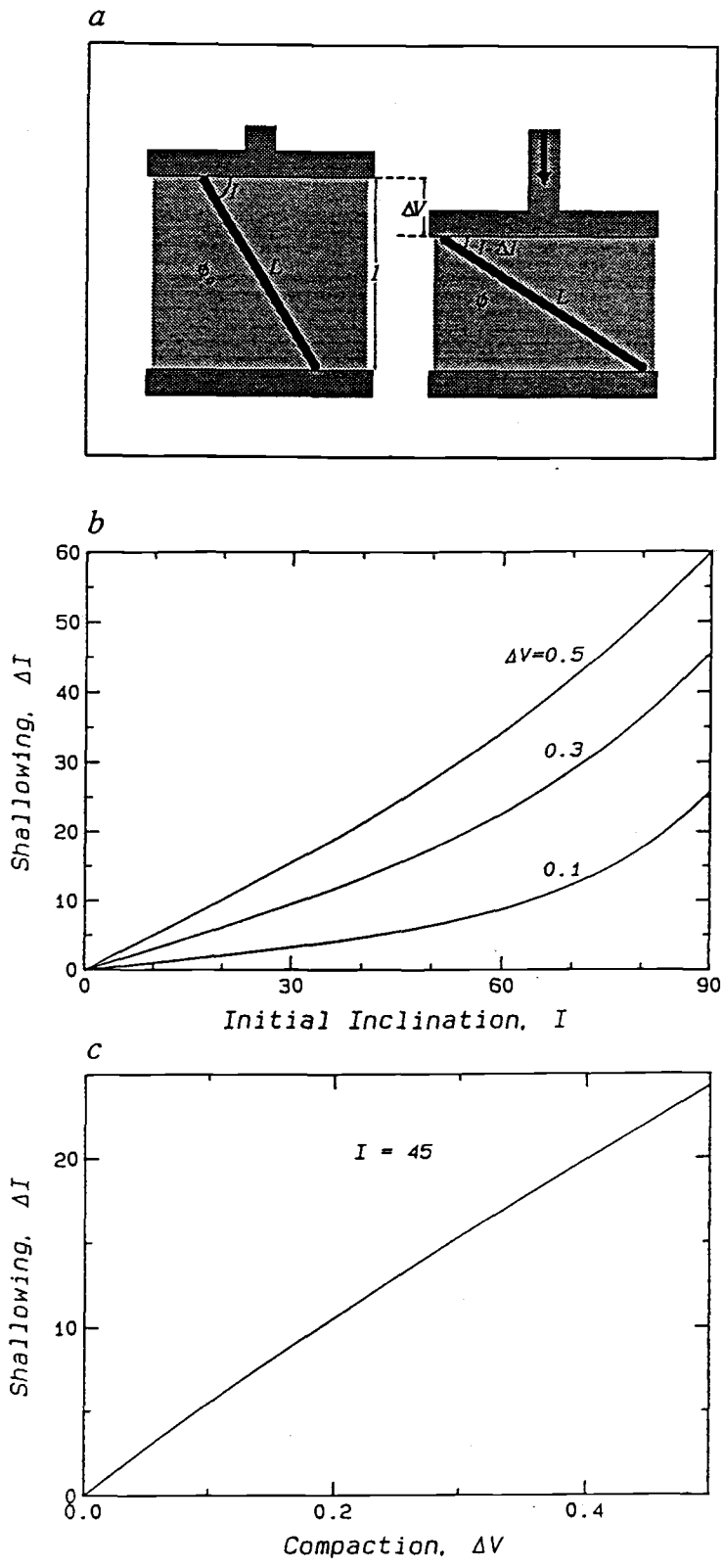
Model 1a
a
ΔV
I
I - ΔI
b
Shallowing, ΔI
ΔV=0.5
0.3
0.1
Initial Inclination, I
c
Shallowing, ΔI
I = 45
Compaction, ΔV

Figure 3.3.

Figure 3.4. Model 1b, rotating magnetic needles in soft matrix, equation (3.18). (*a*) The magnetic needle of length L is surrounded by soft material. As the material compacts, toward the plane O, it exerts torques on the needle, tending to rotate it to shallower inclinations. (*b*) The predicted inclination shallowing ΔI (deg) as a function of initial inclination I (deg), for different compactions $\Delta V = 0.1, 0.3, 0.5$. (*c*) The predicted inclination shallowing ΔI (deg) as a function of compaction ΔV, for initial inclination of $I = 45°$. For $I \approx \pm 90°$ the needle will not rotate but rather will intrude into the oncoming sediment above and below.

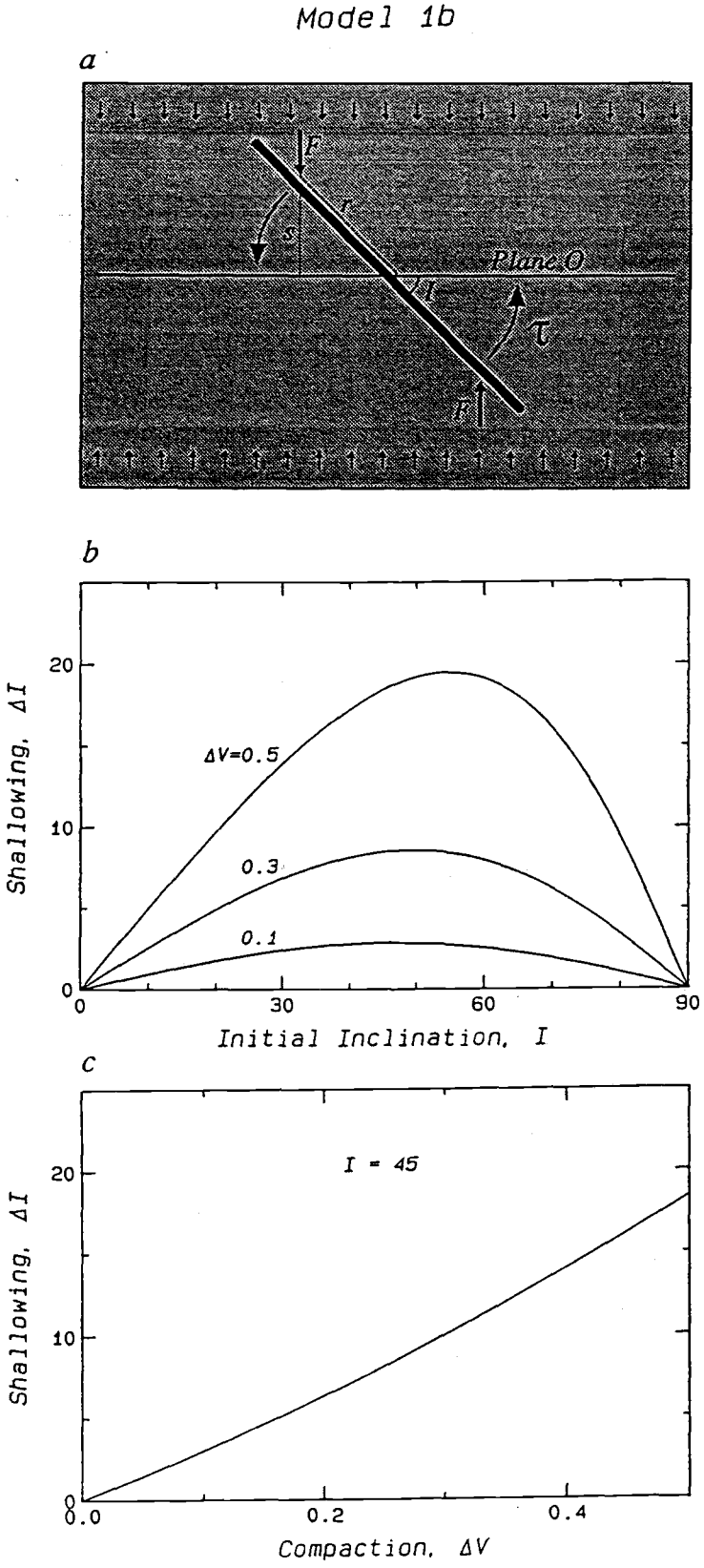
Model 1b
a
F
s
r
Plane O
I
τ
F
b
Shallowing, ΔI
20
10
0
ΔV=0.5
0.3
0.1
0
30
60
90
Initial Inclination, I
c
Shallowing, ΔI
20
10
0
I = 45
0.0
0.2
0.4
Compaction, ΔV

Figure 3.4.

Figure 3.5. Model 1c, two types of magnetic grain shapes in soft matrix, equation (3.22), where a fraction f_n of the magnetic carriers obey model 1b, and the rest ($1 - f_n$) are invariant upon compaction. Model 1c (solid lines) with $f_n = 0.62$, is compared to model AK (dashed lines), equation (3.8) with $a = 0.65$. (*a*) The inclination shallowing ΔI (deg) with initial inclination I (deg) for compactions $\Delta V = 0.1, 0.3, 0.5$. (*b*) The inclination shallowing ΔI (deg) with compaction ΔV for initial inclination of $I = 45°$. The two models show very similar results.

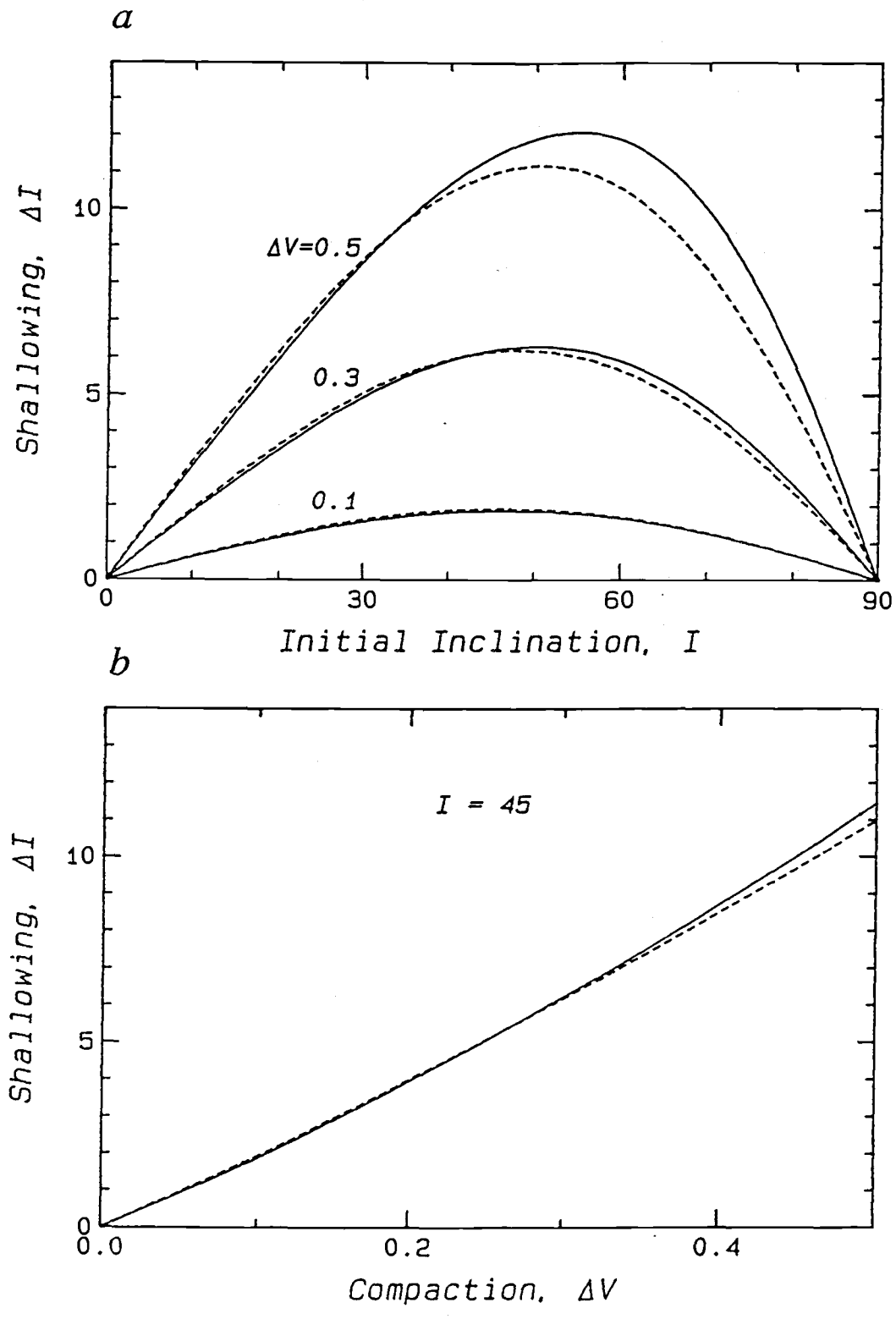
a
Shallowing, ΔI
10
5
0
ΔV=0.5
0.3
0.1
0
30
60
90
Initial Inclination, I
b
Shallowing, ΔI
I = 45
10
5
0
0.0
0.2
0.4
Compaction, ΔV

Figure 3.5.

3.4.2 Collapsing Sediment Fabric

The most stable magnetic grains are expected to be small compared to the sediment fabric grains. If the magnetic grains are attached to fabric grains, they may rotate together during rearrangement of the matrix upon compaction. Clay flakes have strong shape anisotropy; however, any fabric with elongated or flat grains will give rise to a similar effect. In fact, any sediment, even composed of spherical grains, is subject to random grain rotations which may be predominantly about horizontal axes and will therefore give rise to the same effect. As the sediment compacts, the grains will rearrange themselves. Slight rearrangement of an individual grain can be described by a translation and rotation through an angle about some axis. The primary forces responsible for this rearrangement are the vertical forces of the gravitational compaction, and viscous drag due to the pore fluid flowing around grains mainly upwards to escape the decreasing pores. These forces will rotate the grains, predominantly about horizontal axes, analogous to model GKRW but now in compactional environments. This process will cause some randomization in the directions of the magnetic grains and also inclination shallowing.

In the following two collapsing fabric models we assume no relation between the orientations of flakes and magnetic grains. Similar to the needle models we assume perfect initial alignment of the magnetic moments with the external field, even though the fabric flakes may be oriented in a random fashion. Later in this chapter we examine the consequences of allowing for initially dispersed magnetic moments. We

assume now that the small magnetic carriers are somehow attached to the relatively large fabric flakes in the sediment surface layers subsequent to the initial blocking of the remanence, and subsequently they rotate with the flakes during compaction. We define a normal vector perpendicular to the upper flat side of a flake. That normal deviates by the angle θ from the vertical, and θ is therefore also the dip of the flake plane from horizontal. The normal vector has the azimuthal direction λ from north. The normalized probability distribution of flakes with particular angle θ is $P_f(\theta)$, $0 \leq \theta \leq \pi/2$, $P_f(\theta)$ will change with compaction, as more of the flakes acquire shallower dips.

As the sediment compacts by ΔV, each flake with the initial dip θ will rotate through the angle $\Delta\theta$ to a shallower dip $(\theta - \Delta\theta)$. By analogy to model GKRW we see that these flakes will transform the initial magnetic unit vector (cos I, 0, sin I) to an equivalent of equation (3.3)

$$\mathbf{m}_G(\theta) = [(1/2)\,(\,1 + \cos\Delta\theta\,)\cos I,\ 0,\ \cos\Delta\theta \sin I\,] \qquad (3.24)$$

We note that this is no longer a unit vector.

By connecting $\Delta\theta$ to a given ΔV and θ, we can find the resultant remanent magnetization after compaction by integrating equation (3.24) over all the fabric flakes

$$\mathbf{m}_f = \int_0^{\pi/2} \mathbf{m}_G(\theta)\, P_f(\theta)\, d\theta \qquad (3.25)$$

By considering equation (3.24), we can split $\mathbf{m}_f$ in equation (3.25) into the three components (m_x , m_y , m_z):

$$m_x = \int_0^{\pi/2} (1/2)\,(1 + \cos\Delta\theta\,)\cos I\, P_f(\theta)\, d\theta \qquad (3.26)$$

$$m_y = 0 \qquad (3.27)$$

$$m_z = \int_0^{\pi/2} \cos\Delta\theta \sin I\, P_f(\theta)\, d\theta \qquad (3.28)$$

Now we can calculate the magnetic inclination after the compaction through the relation $\tan(I - \Delta I) = m_z / m_x$:

$$\tan(I - \Delta I) =$$

$$= \frac{\sin I \int_0^{\pi/2} \cos\Delta\theta\, P_f(\theta)\, d\theta}{(1/2)\cos I \left[\int_0^{\pi/2} P_f(\theta)\, d\theta + \int_0^{\pi/2} \cos\Delta\theta\, P_f(\theta)\, d\theta\right]} \qquad (3.29)$$

The probability distribution is assumed to be normalized, and by defining

$$F(\Delta V) = \int_0^{\pi/2} \cos\Delta\theta\ P_f(\theta)\ d\theta \qquad (3.30)$$

we get

$$\tan(I - \Delta I) = \frac{2\,F(\Delta V)}{1 + F(\Delta V)} \tan I \qquad (3.31)$$

Equation (3.31) can now be written on the same form as equation (3.2),

$$\tan (I - \Delta I) = (1 - f_f) \tan I \tag{3.32}$$

where

$$f_f \equiv \frac{1 - F(\Delta V)}{1 + F(\Delta V)} \tag{3.33}$$

So far we have avoided relating $\Delta\theta$ to θ and ΔV in equation (3.30), which in general is rather complex. However, two simple models can be set up. In the absence of other randomization one probably represents an overestimate and the other an underestimate of the flake rotation $\Delta\theta$. These models are intuitively similar to the rotating magnetic needle models, and are here called model 2a, collapsing rigid matrix, and model 2b, collapsing soft matrix.

Model 2a: Collapsing rigid matrix. A simplified flake-fabric model will give an overestimate of the rotation toward horizontal alignment in the absence of other randomization if we assume that each individual fabric flake is enclosed between two rigid horizontal surfaces through compaction. By analogy to model 1a (equation (3.9)), the rearrangement of the flakes is described by

$$\sin (\theta - \Delta\theta) = (1 - \Delta V) \sin \theta \tag{3.34}$$

See also Figure 3.3*a*. Through this equation we have connected $\Delta\theta$ to θ and ΔV. Furthermore, we assume that the flakes are initially spherically randomly distributed; hence

$$P_f(\theta)\, d\theta = \sin\theta\, d\theta \tag{3.35}$$

Now we can solve equation (3.30) by use of equations (3.34) and (3.35). The derivation is shown in Appendix B, and the solution is found to be exactly

$$F(\Delta V) = 1 - \frac{(2\,\Delta V - \Delta V^2)^{3/2} - 3\,\Delta V^2 + 2\,\Delta V^3}{3 - 6\,\Delta V + 3\,\Delta V^2} \tag{3.36}$$

We use equation (3.33) to define a function f_a which can be approximated for ΔV between 0 and 0.5 as $f_a \approx 0.101\,\Delta V + 0.245\,\Delta V^2$. The equation for model 2a has the same form as equation (3.2)

$$\tan(I - \Delta I) = (1 - f_a)\tan I \tag{3.37}$$

The dependence of f_a on ΔV (from equations (3.33) and (3.36)) is shown in Figure 3.6*a*. The dependence of ΔI on I in equation (3.37) is shown in Figure 3.6*b*, for various ΔV, and the dependence of ΔI on ΔV for a fixed initial inclination I is shown in Figure 3.6*c*. The function f_a takes on much lower values than ΔV, leading to a very small inclination shallowing effect. Note that the function f_a is no longer linear with compaction, ΔV.

Model 2b: Collapsing soft matrix. As an underestimate of the flake rotation we use an analogy to model 1b (equation (3.18)), for the rotation of the fabric flakes. As before we assume that the initial dip θ diminishes to ($\theta - \Delta\theta$) after a compaction ΔV. Therefore

$$\tan (\theta - \Delta\theta) = (1 - \Delta V) \tan \theta \qquad (3.38)$$

Equation (3.30) is solved in Appendix B, using equations (3.38) and (3.35). It is found to be exactly

$$F(\Delta V) = \frac{1}{2(2-\Delta V)} +$$

$$+ \frac{(2-\Delta V)^2 - 1}{4\,(2-\Delta V)\sqrt{\Delta V(2-\Delta V)}} \ln \left[\frac{1 + \sqrt{\Delta V(2-\Delta V)}}{1 - \sqrt{\Delta V(2-\Delta V)}} \right] \qquad (3.39)$$

As before, we define the function f_b using equation (3.33); f_b is shown in Figure 3.7*a* and can be approximated for low ΔV as $f_b \approx 0.0384\ \Delta V^2 + 0.1149\ \Delta V^4$. Therefore the equation for model 2b has the same form as equation (3.2):

$$\tan (I - \Delta I) = (1 - f_b) \tan I \qquad (3.40)$$

The dependence of ΔI on I in equation (3.40) is shown in Figure 3.7*b*, for various ΔV, and the dependence of ΔI on ΔV for a fixed initial inclination I is shown in Figure 3.7*c*. This underestimate of the inclination shallowing in collapsing fabric is about a factor of 10 lower than by model 2a. For compaction values lower than 0.5 this model

predicts a maximum inclination shallowing less than 0.5° which would be very difficult to detect in nature.

Magnetization intensities due to fabric rearrangement. With the rearrangement of fabric flakes in models 2a and 2b there is some dispersion of the magnetic moments and an associated intensity decrease. The concentration of magnetic material will increase as we sample more compacted sediment, as in model 3a. By connecting equation (3.33) to (3.30) and (3.26) – (3.28) we get the intensity

$$M/M_0 = \frac{\sqrt{1 - (2 f_f - f_f^2) \sin^2 I}}{(1 - \Delta V) (1 + f_f)} \qquad (3.41)$$

By inserting f_a for f_f in equation (3.41), we get the predicted intensity with compaction for model 2a, and by inserting f_b we get the prediction for model 2b. The intensity with compaction in model 2a is shown in Figure 3.8, for various initial inclinations I. We do not show the effect of model 2b, since the change is so small that it becomes indistinguishable from the bold reference curve, representing the increased concentration of magnetic material during compaction, equation (3.19). We note that even our overestimate (model 2a) does not decrease the intensity enough to account for the increased concentration effect. Therefore, in the absence of other randomization, the intensity will increase with compaction.

Figure 3.6. Model 2a, collapsing rigid matrix, equation (3.37). This is thought to be an overestimate, when other randomization processes are omitted, of the inclination shallowing associated with rotation of the fabric grains to which smaller magnetic grains are attached. (*a*) The dependence of the function f_a on compaction ΔV, according to equations (3.33) and (3.36). (*b*) The predicted inclination shallowing ΔI (deg) as a function of initial inclination I (deg) for different compactions $\Delta V = 0.1$, 0.3, 0.5. (*c*) The predicted inclination shallowing ΔI (deg) as a function of compaction ΔV for initial inclination of $I = 45°$. There are strong similarities to models BH, AK, 1b, and 1c, but a factor of 3–10 in magnitude of the inclination shallowing.

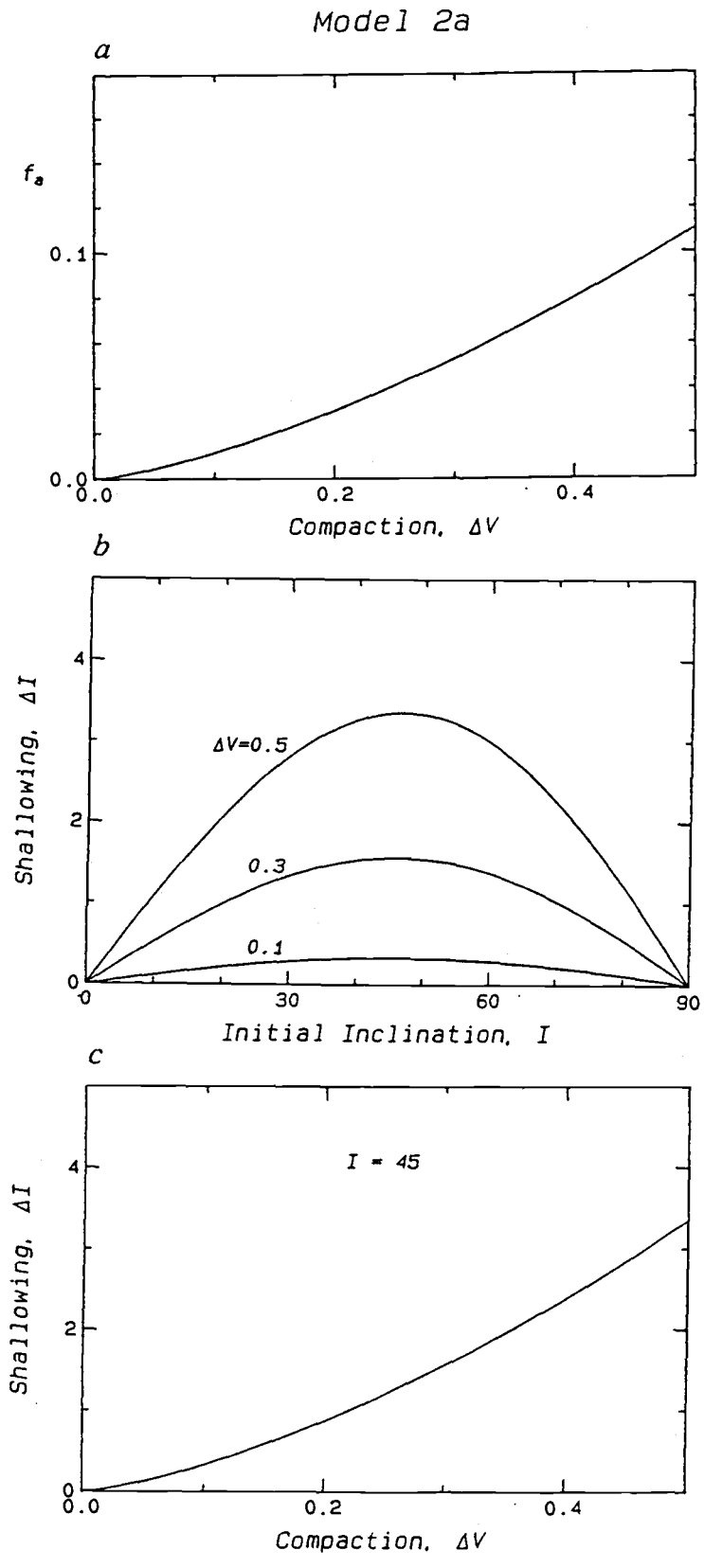
Model 2a
a
f_a
0.1
0.0
0.0
0.2
0.4
Compaction, ΔV
b
Shallowing, ΔI
4
2
0
ΔV=0.5
0.3
0.1
0
30
60
90
Initial Inclination, I
c
Shallowing, ΔI
4
2
0
I = 45
0.0
0.2
0.4
Compaction, ΔV

Figure 3.6.

Figure 3.7. Model 2b, collapsing soft matrix, equation (3.40). Note that all vertical scales differ by a factor of 10 from Figure 3.6. This is considered an underestimate of the inclination shallowing associated with the collapsing fabric. (*a*) The dependence of the function f_b on compaction ΔV, according to equations (3.33) and (3.39). (*b*) The predicted inclination shallowing ΔI (deg) as a function of initial inclination I (deg), for different compactions ΔV = 0.1, 0.3, 0.5. (*c*) The predicted inclination shallowing ΔI (deg) as a function of compaction ΔV, for initial inclination of $I = 45°$. Note that this model predicts less than 0.5° inclination shallowing, which is hard to detect.

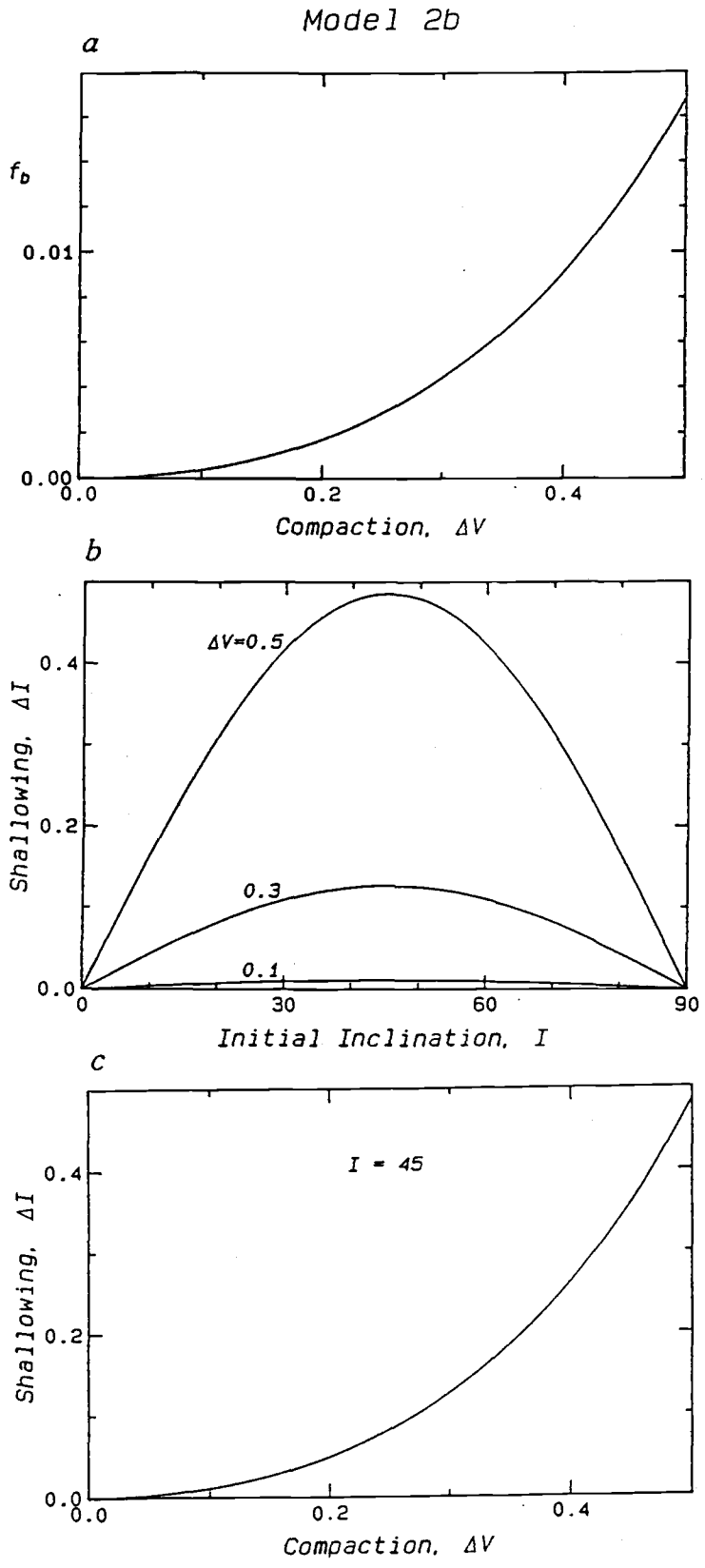
Model 2b
a
f_b
0.01
0.00
0.0
0.2
0.4
Compaction, ΔV
b
ΔV=0.5
0.3
0.1
Shallowing, ΔI
0.4
0.2
0.0
0
30
60
90
Initial Inclination, I
c
I = 45
Shallowing, ΔI
0.4
0.2
0.0
0.0
0.2
0.4
Compaction, ΔV

Figure 3.7.

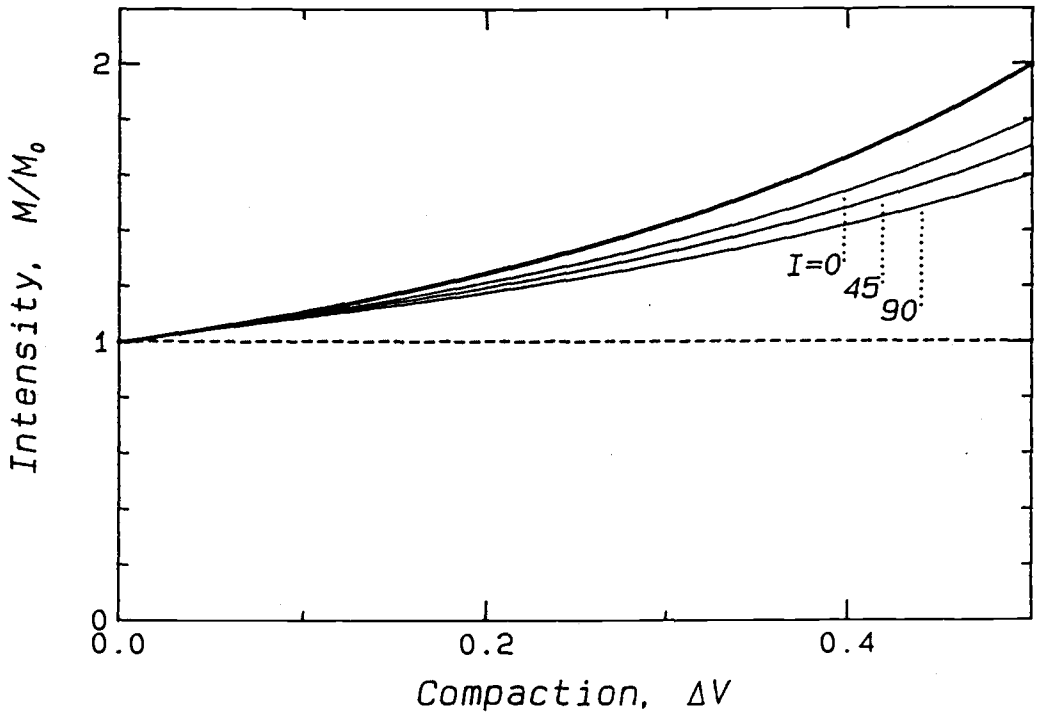

Figure 3.8. Normalized intensity as a function of compaction for models 1 and 2. The bold curve represents the increased concentration of magnetic material, assuming no randomization, equation (3.19). The higher intensities are caused by more magnetic material per unit volume. Also shown is the intensity predicted by model 2a, collapsing rigid matrix (the three plain curves), equation (3.41), for initial inclinations $I = 0°$, 45°, and 90°. The effect of model 2b (not shown in the figure) is so minute that the intensities become indistinguishable from the bold reference curve. The two collapsing fabric models (2a and 2b) do not predict enough dispersion of the magnetic moments to account for the increased concentration of magnetic material due to the compaction.

3.4.3 Microscopic Kneading of the Sediment

The previous models are deterministic descriptions of inclination and intensity changes with compaction. Decrease of the intensity of magnetizations have been observed during compaction, both with depth (or time) in sediment cores and compaction in laboratory experiments. This effect has been attributed to randomization or misalignment of the magnetic grains [*Stober and Thompson*, 1979; *Karlin and Levi*, 1982]. As seen in Figure 3.8 it is impossible to decrease the intensity with the models 1a, 1b, 2a, and 2b, so we consider two models of random grain rotations. Model 3a, unbiased randomization of grains, will not affect the inclination but will decrease the intensity, and model 3b, random rolling of grains about horizontal axes, will decrease the intensity and also will introduce inclination shallowing through the rolling spheres effect described by *Griffiths et al.* [1960] (model GKRW). The magnetic torques of the grains are negligible compared to the mechanical forces responsible for their rearrangements, so for these two models we assume that growth of secondary remanence during grain randomization [e.g., *Tucker*, 1980] can be neglected.

Model 3a: Unbiased randomization of grains. A simple way of looking at an unbiased randomization process is to assume a group of initially parallel magnetic moments, which will be rotated through some angles, θ. Some grains will experience small rotations, and others greater. It is reasonable to assume that these angular deviations can be

described by the Fisher distribution P_F, which is analogous to the normal distribution on a sphere [*Fisher*, 1953]

$$P_F(\theta)\, d\theta = \frac{\kappa}{2 \sinh \kappa}\, e^{\kappa \cos \theta} \sin \theta\, d\theta \qquad (3.42)$$

where κ is the precision parameter of the distribution. Due to the symmetry of the random rotations we expect that the average magnetic direction of the sample will not change. The magnetic intensity of a unit vector, that has rotated through θ, will therefore only add cos θ to the total intensity, which can then be calculated by

$$M/M_0 = \int_0^{\pi} P_F(\theta) \cos \theta\, d\theta \qquad (3.43)$$

To solve equation (3.43), it is convenient to make the substitution $s \equiv \cos \theta$, which transforms it to

$$M/M_0 = \frac{\kappa}{2 \sinh \kappa} \int_{-1}^{1} s\, e^{\kappa s}\, ds \qquad (3.44)$$

with the solution

$$M/M_0 = \coth \kappa - 1/\kappa \qquad (3.45)$$

which is the Langevin function $L(\kappa)$. Convenient approximations to the Langevin function ($L(\kappa) \approx \kappa/3$ for low κ, and $L(\kappa) \approx 1 - 1/\kappa$ for high κ) are not fully applicable since we are also interested in intermediate values. We can also take into account the increased concentration effect

due to an arbitrary compaction ΔV, even though we are not relating κ to ΔV

$$M/M_0 = \frac{\coth \kappa - 1/\kappa}{1 - \Delta V} \tag{3.46}$$

where κ can, for instance, be related to θ_{63}, the angular standard deviation, that is, 63% of the moments are rotated through an angle less than θ_{63}

$$\cos \theta_{63} = 1 + (1/\kappa) \ln [\, 1 - 0.63 \, (1 - e^{-2\kappa}) \,] \tag{3.47}$$

The normalized intensity in equation (3.46) is shown as a function of θ_{63} in Figure 3.9*a* for various ΔV.

So far in this model we have assumed no initial within-sample dispersion. To address the problem of initial dispersion, we consider a partially randomized sample where different subsets of grains have parallel magnetic moments. The total magnetization of the *i*th subset is m_i, and the magnetization direction of the *i*th subset is at angle θ_i to the average direction of the whole sample, and it contributes $m_i \cos \theta_i$ to the sample's total intensity. Upon randomization the subset under consideration retains its average direction, due to symmetry, but there is a decrease in intensity $m_i L(\kappa)$ (as described by equation (3.45)), because all the moments of the subset were initially parallel. Since neither the subset's direction nor the direction of the whole sample have changed during randomization, our subset will contribute $m_i L(\kappa) \cos \theta_i$ to the total intensity. The intensity contributions of all subsets will decrease as

$L(\kappa)$, and the total moment will therefore also decrease as $L(\kappa)$. Therefore randomization in samples with initial dispersion also obeys equation (3.45).

From this result we see that a sample undergoing randomization by κ_1 will have intensity $M_1/M_0 = L(\kappa_1)$. If we take this randomized sample and randomize it again by arbitrary chosen κ_2, its intensity will be $M_2/M_0 = L(\kappa_1)\, L(\kappa_2)$ and so on. We now define the term randomization, ξ,

$$\xi \equiv -\ln [\, L(\kappa) \,] / \ln 2 \tag{3.48}$$

The factor (1/ln 2) gives ξ the property that by increasing the randomization by 1 will decrease the intensity by a factor of 2. With the aid of equation (3.45) we see

$$M = M_0\, e^{-\xi \ln 2} \tag{3.49}$$

and for a randomization ξ_1 followed by ξ_2, followed by ξ_3 and so on, we see that the total randomization is partially additive

$$\xi_{total} = \xi_1 + \xi_2 + \xi_3 + \cdots \tag{3.50}$$

This additivity of randomization is valid for all κ values, $0 \leq \kappa \leq \infty$. In Figure 3.9*b* we show how the intensity decreases with randomization. For high κ, $L(\kappa) \approx 1 - 1/\kappa$, and ln $(1 - \varepsilon) \approx -\varepsilon$; therefore, from equation (3.48) we get $\xi \sim 2/\kappa$ for high κ values. This is the variance of

the Fisher distribution. However, for low κ, neither $2/\kappa$ nor the variance are partially additive as is the randomization.

From equation (3.49) we note that for a sedimentary section with constant reworking per unit depth (or even unit of time) we can define $\zeta \equiv \ln 2\ \xi/h$ (where h is the thickness of the section) and we would expect an intensity profile with depth z

$$M(z) = M_0\, e^{-\zeta z} \tag{3.51}$$

where M_0 would now represent intensity at the top ($z = 0$). We therefore predict exponential decrease of intensities in sediments where the randomization is constant per unit depth.

This model predicts no directional changes but leads to the next model where we consider what happens if the randomization is limited to rotations about horizontal axes.

Model 3b: Random rolling of grains about horizontal axes. Instead of trying to relate $\Delta\theta$ to θ and ΔV in the collapsing fabric models (2a and 2b), we can consider what effect a grain rotation about horizontal axes would have on the intensity of the remanent magnetization, independent of how much compaction it would require. For a rotation of the magnetic grains about randomly distributed horizontal axes, by some fixed characteristic angle $\Delta\theta$, we get the inclination shallowing shown in equation (3.6). From equation (3.3) (in model GKRW) one easily obtains the intensity decrease as

$$M/M_0 = \sqrt{(1/4)(1+\cos\Delta\theta)^2\cos^2 I + \cos^2\Delta\theta \sin^2 I} \quad (3.52)$$

Note that we do not relate $\Delta\theta$ to ΔV in this model. The effect of equation (3.52) is shown in Figure 3.2*b* for various initial inclinations.

Model GKRW shows the inclination shallowing when all grains roll by the same rolling angle $\Delta\theta$. Furthermore, we have connected rolling of grains to compaction in models 2a and 2b in a particular deterministic way. In reality, one would expect some grains to roll more and others less, depending on many unpredictable factors. Therefore an obvious extension of model GKRW is to allow for a distribution in $\Delta\theta$, where rolling occurs about horizontal axes. Distribution of rotation angles about a fixed axis can be described as a distribution on a circle. The "normal" distribution on a circle is the Von Mises distribution, closely related to the Fisher distribution on a sphere [*Von Mises*, 1918; *Fisher*, 1953; *Mardia*, 1972, p. 57]

$$P_M(\Delta\theta)\, d(\Delta\theta) = \frac{1}{2\pi I_0(\kappa)} e^{\kappa\cos\Delta\theta}\, d(\Delta\theta) \quad (3.53)$$

where $I_0(\kappa)$, the hyperbolic Bessel function of order zero (sometimes also called the modified Bessel function), is used to normalize the distribution. $I_0(\kappa)$ can not be written in terms of elementary functions. In choosing the Von Mises distribution to describe the rolling angles, we do not take into account that some grains are elongated and will resist rolling through the horizontal. However, in the absence of detailed knowledge of individual grain behavior, we take the Von Mises distribution with zero mean (symmetric rolling) as a good first-order

estimate. The Von Mises distribution is shown in Figure 3.10*a*, for selected values of κ.

Now we use the result of *Griffiths et al.* [1960], ($\mathbf{m}_G$ in equation (3.3) in this chapter) to determine how the unit vector $\mathbf{m} = (\cos I, 0, \sin I)$ rotates to $\mathbf{m}_H$

$$\mathbf{m}_H = \int_{-\pi}^{\pi} P_M(\Delta\theta)\, \mathbf{m}_G(\Delta\theta)\, d(\Delta\theta) \tag{3.54}$$

or split into the components (m_{Hx} , m_{Hy} , m_{Hz})

$$m_{Hx} = \int_{-\pi}^{\pi} \frac{1}{2\pi I_0(\kappa)} e^{\kappa \cos\Delta\theta}\, (1/2)(1+\cos\Delta\theta)\, \cos I\, d(\Delta\theta) \tag{3.55}$$

$$m_{Hy} = 0 \tag{3.56}$$

$$m_{Hz} = \int_{-\pi}^{\pi} \frac{1}{2\pi I_0(\kappa)} e^{\kappa \cos\Delta\theta}\, \cos\Delta\theta\, \sin I\, d(\Delta\theta) \tag{3.57}$$

with the solutions

$$m_{Hx} = (1/2)\, [\, 1 + I_1(\kappa) / I_0(\kappa)\,]\, \cos I \tag{3.58}$$

$$m_{Hz} = [\, I_1(\kappa) / I_0(\kappa)\,]\, \sin I \tag{3.59}$$

where $I_1(\kappa)$ is the hyperbolic Bessel function of first order.

Now we can calculate the inclination shallowing

$$\tan (I - \Delta I) = \frac{2\, I_1(\kappa) / I_0(\kappa)}{1 + I_1(\kappa) / I_0(\kappa)} \tan I \tag{3.60}$$

and by defining

$$f_h \equiv \frac{1 - I_1(\kappa) / I_0(\kappa)}{1 + I_1(\kappa) / I_0(\kappa)} \tag{3.61}$$

we get the common form

$$\tan (I - \Delta I) = (1 - f_h) \tan I \tag{3.62}$$

The intensity is

$$M/M_0 = \sqrt{(1/4)[1+I_1(\kappa)/I_0(\kappa)]^2\cos^2 I + [I_1(\kappa)/I_0(\kappa)]^2\sin^2 I} \tag{3.63}$$

We note that the hyperbolic Bessel functions always occur as the ratio $I_1(\kappa)/I_0(\kappa)$, and even though both $I_0(\kappa)$ and $I_1(\kappa)$ blow up very fast with increasing κ, their ratio is very similar to the Langevin function. For high κ, $I_1(\kappa)/I_0(\kappa) \approx 1 - 1/(2\kappa) \approx L(2\kappa)$, and for low κ, $I_1(\kappa)/I_0(\kappa) \approx \kappa/2 \approx L(1.5\kappa)$. The Langevin function and the ratio of the hyperbolic Bessel functions is shown in Figure 3.10*b*. The characteristics of model 3b are shown in Figure 3.11, where we show the exact solutions of equations (3.62) and (3.63), using the inverse of the precision parameter, which we call the "spread" parameter ($1/\kappa$), as a measure of random rolling. We note that random rolling about horizontal axes, leading to intensity decreases of 20–50%, results in significant inclination shallowing.

We believe that microscopic randomization of sediment is an important mechanical factor in sediments. The random rolling about horizontal axes may be much less important than the isotropic randomization but still sufficiently significant for producing inclination shallowing. Different lithologies and physical properties may control the amount of isotropic randomization relative to random rolling about horizontal axes, making it difficult to predict the magnitude of this effect. However, the ratio between these two processes may be unique for a given lithology and once established, prediction is possible.

Figure 3.9. Model 3a, unbiased randomization of grains, equation (3.46). (*a*) Normalized intensity predicted as a function of the characteristic rotation angle θ_{63} (angular standard deviation), equation (3.47), for different compaction values $\Delta V = 0$ (bold curve), and 0.1, 0.3, 0.5. Here we are only considering how much randomized grain rotation is needed to depress the intensity. Note that a considerable grain rotations are needed to offset the intensity of magnetization. (*b*) Normalized intensity versus the randomization parameter ξ, equation (3.49). The term randomization is introduced as a fundamental property of the net magnetic moment of a sedimentary sample. Randomizations are independent of distribution of magnetic moments and other initial properties of a given sediment. Randomizations are additive.

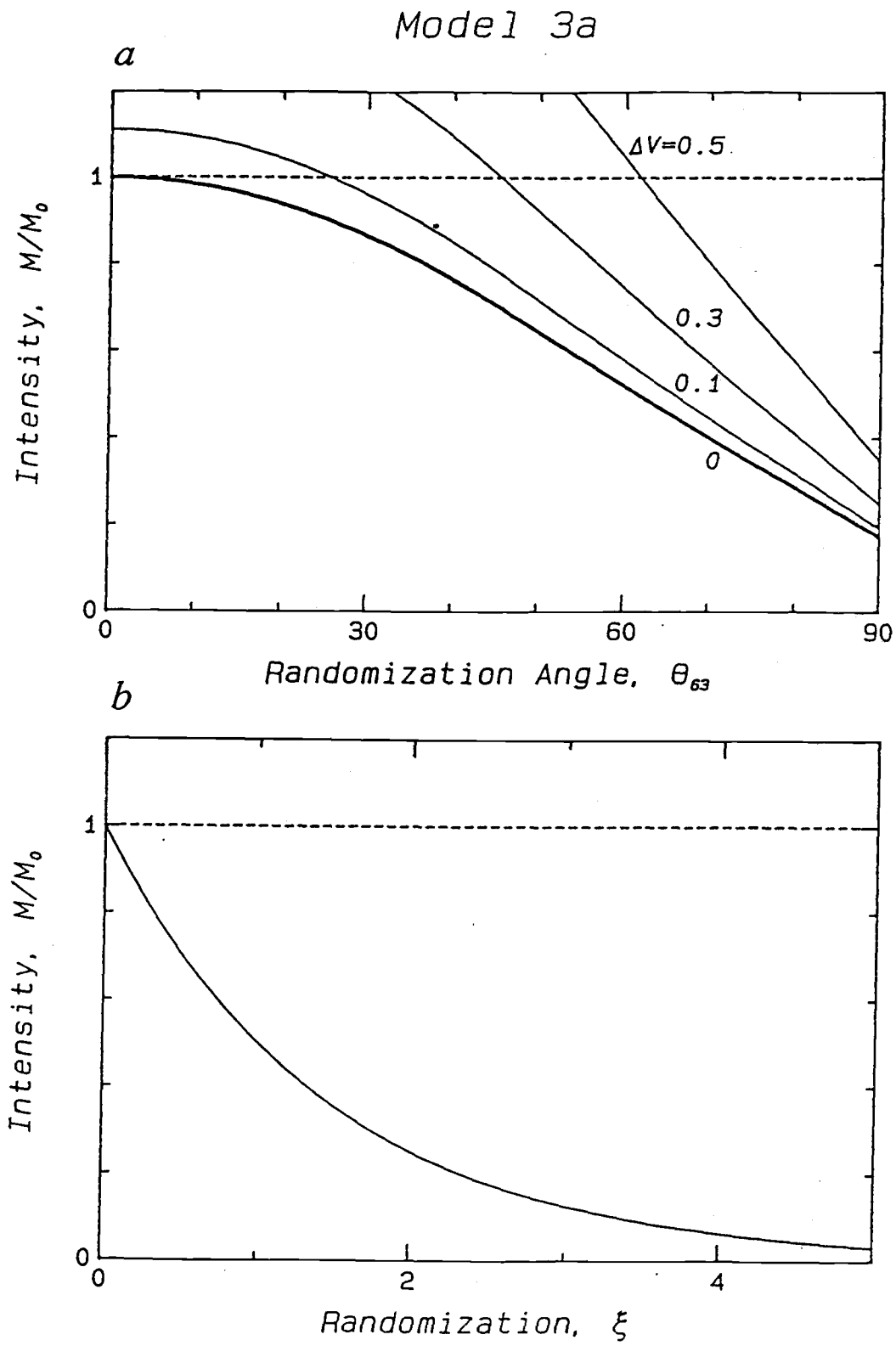
Model 3a
a
ΔV=0.5
0.3
0.1
0
1
0
30
60
90
Intensity, M/M₀
Randomization Angle, θ₆₃
b
1
0
0
2
4
Intensity, M/M₀
Randomization, ξ

Figure 3.9.

Figure 3.10. Fundamental functions used in models 3a and 3b. (*a*) The Von Mises distribution, equation (3.53), is shown versus the rolling angle $\Delta\theta$ (deg), for spread parameters of $1/\kappa = 0.2, 0.6, 1.0$. We note that these spread values call for considerable grain rolling. (*b*) The Langevin function $L(\kappa)$ (bold), equations (3.45) and (3.65), compared to the ratio of the hyperbolic Bessel functions $I_1(\kappa)/I_0(\kappa)$ (thin), that appears in equations (3.58) through (3.63). These functions are very similar. For low κ ($\kappa < 0.5$) they can be approximated as $L(\kappa) \approx \kappa/3$, and $I_1(\kappa)/I_0(\kappa) \approx \kappa/2$, and for high κ ($\kappa > 3$) they can be approximated as $L(\kappa) \approx 1 - 1/\kappa$, and $I_1(\kappa)/I_0(\kappa) \approx 1 - 1/(2\kappa)$.

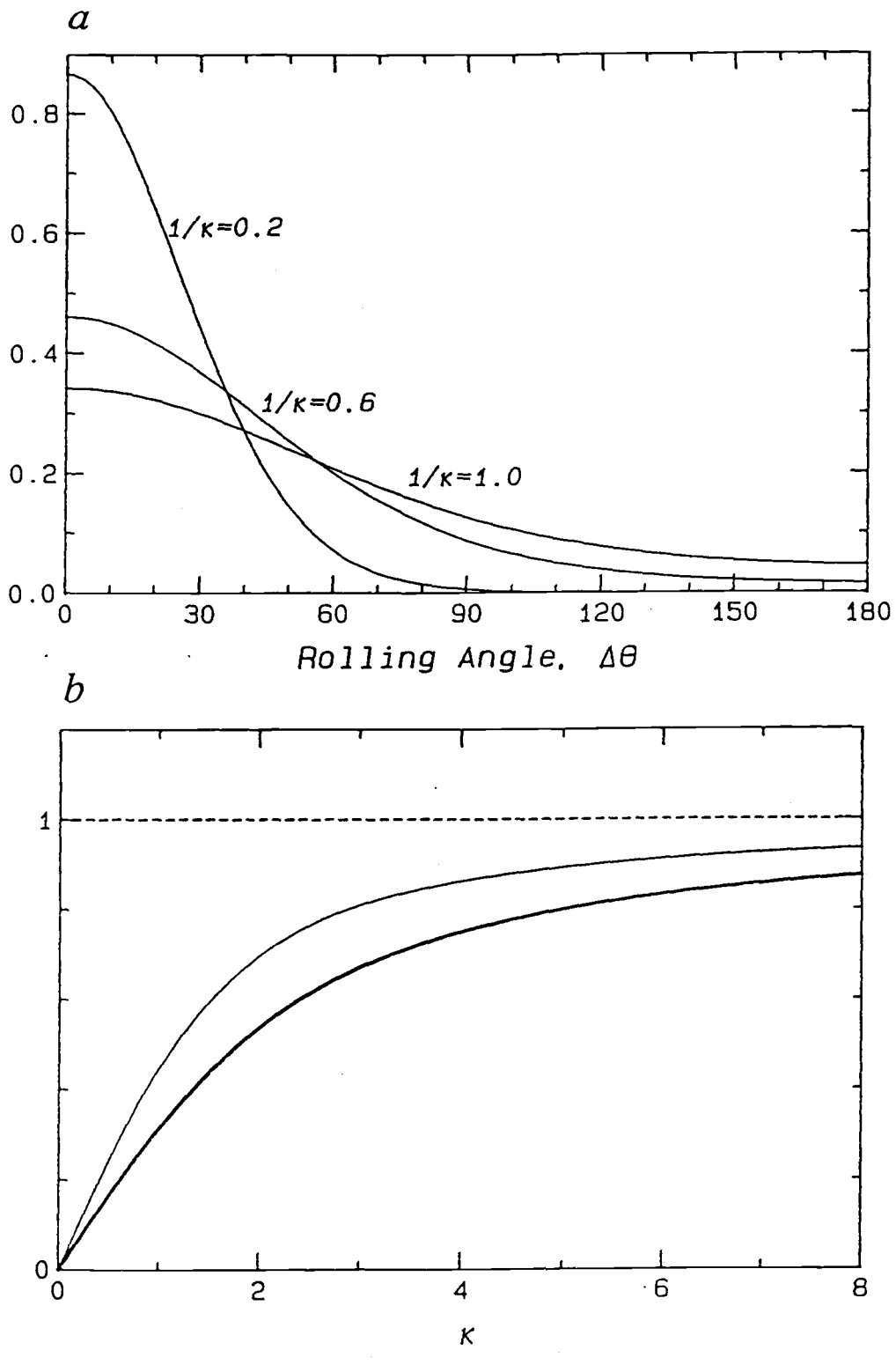
a
0.8
0.6
0.4
0.2
0.0
1/κ=0.2
1/κ=0.6
1/κ=1.0
0
30
60
90
120
150
180
Rolling Angle, Δθ
b
1
0
0
2
4
6
8
κ

Figure 3.10.

Figure 3.11. Model 3b, random rolling of grains about horizontal axes, equation (3.62). (*a*) The inclination shallowing ΔI (deg) versus initial inclination I (deg), for fixed amounts of random rolling of sediment grains about horizontal axes, measured by the "spread" parameter $1/\kappa =$ 0.2, 0.6, 1.0. (*b*) The inclination shallowing ΔI (deg) versus spread parameter $1/\kappa$, for a fixed initial inclination $I = 45°$. (*c*) The normalized intensity changes with the spread parameter $1/\kappa$, for initial inclinations $I = 0°$, 45°, and 90°. In essence we have transformed a model by *Griffiths et al.* [1960], model GKRW in this chapter, to allow for a distribution in rolling angle, resulting in significant inclination shallowing.

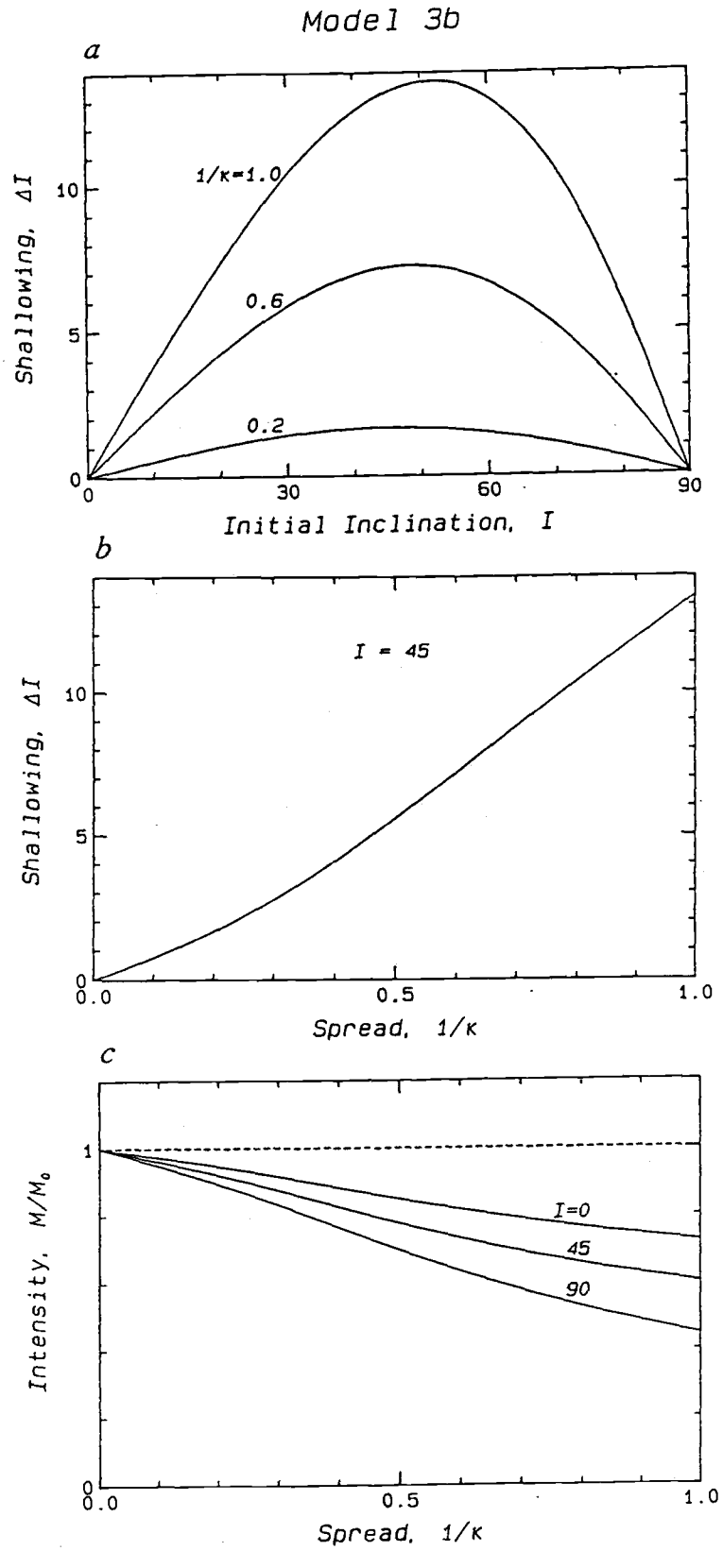
Model 3b
a
Shallowing, ΔI
1/κ=1.0
0.6
0.2
0
5
10
0
30
60
90
Initial Inclination, I
b
Shallowing, ΔI
I = 45
0
5
10
0.0
0.5
1.0
Spread, 1/κ
c
Intensity, M/M₀
I=0
45
90
0
1
0.0
0.5
1.0
Spread, 1/κ

Figure 3.11.

3.4.4 Initial Dispersion of the Magnetic Moments

Initial distribution. We are interested in the initial within-sample distribution of magnetic moments. *King* [1955] assumed relatively low degree of alignment of magnetic moments within the sediment, so that the intensity of magnetization would be proportional to the external field strength. *Nagata* [1962] was first to study distributions of within-sample dispersions. To study the probable initial distribution of magnetic moments, we consider the acquisition of remanence in the sediment close to the sediment water interface. A magnetic particle of net moment m oriented at an angle θ to the external magnetic field H will have a torque, $m\,H \sin\theta$, which will tend to rotate the grain toward the field direction, while thermal agitations due to Brownian motions compete with this aligning force [*Collinson*, 1965]. This problem is identical to Langevin's classical theory of paramagnetism of the alignment of molecules with magnetic moments in an external magnetic field [*Langevin*, 1905; *Chikazumi*, 1964, pp. 60-62]. In fact, any randomization agent, such as bioturbation, will fight the alignment. The distribution of the magnetic moments in Langevin's theory is

$$P(\theta)\,d\theta = \frac{N\,(mH/kT)}{2\sinh\,(mH/kT)}\,e^{(mH/kT)\cos\theta}\,\sin\theta\,d\theta \qquad (3.64)$$

where k is Boltzmann's constant, T the absolute temperature, and N is the number of individual moments (Nm is the total moment, when all moments are parallel). We note that if we normalize this distribution to

unity ($N = 1$), this is the Fisher distribution with $\kappa = m\,H\,/\,k\,T$. *Langevin* [1905] found the net moment to be

$$M/M_0 = \coth \kappa - 1/\kappa \tag{3.65}$$

since then called the Langevin function $L(\kappa)$. Even though it has been shown that the distribution and the net moment may vary with grain size [*Stacey*, 1972], we consider equations (3.64) and (3.65) as an adequate first-order estimate of the initial within-sample distribution of the magnetic moments and its net moment.

It should be possible to estimate the amount of initial dispersion in sediments. *Kent* [1973] obtained a linear dependence of the remanence on the external field for redeposited deep-sea sediments in fields up to 120 μT. This implies that the external fields were still in the linear range of the Langevin function, indicating that M/M_0 is less than 10% and $\kappa < 0.3$. Similarly, *Khramov* [1968] observed linear behavior to fields 10 times the present value, leading to the estimate $M/M_0 < 3\%$ and $\kappa < 0.1$. These estimates provide an upper limit to the alignment, but they indicate relatively poor alignment.

In laboratory depositional experiments with synthetic sediment one has better control of the concentration and domain state of the magnetic material, which might lead to better estimates of M/M_0. Our best estimate of probable values of M/M_0 comes from the data of *Anson and Kodama* [1987]. From their description we estimate that each of their samples contain approximately 10^{-5} kg of magnetite. Their acicular magnetite (0.45 μm × 0.07 μm) is clearly single domain [e.g., *Levi and*

Merrill, 1978], for which we can assign the saturation magnetization of magnetite 92 A m^2 kg^{-1}. Therefore, if all the magnetite needles in a sample (10^{-5} kg) were aligned parallel, the sample would have the magnetic moment 10^{-3} A m^2. The magnetic moments of their samples average to 15.5×10^{-7} A m^2 ranging from 4.1 to 36.3 at the lowest compaction values of the 14 samples [*Anson and Kodama*, 1987, Table 1]. Therefore we can estimate the alignment for these samples: $M/M_0 \approx 0.2\%$, and $\kappa \approx 0.005$. By taking into account possible impurities, crystal imperfections, and probable grain size distribution of their magnetite we note that this will be a slight underestimate of alignment, but accounting for such factors can probably not bring the estimate of the alignment above 1%. We conclude that the orientation of submicron magnetic grains is probably nearly random in natural sediments, redeposited natural sediments, and synthetic sediments. Of course, there is a small but sufficient orientation bias toward the ambient field direction to account for the net observed remanent magnetism.

Model 4a: Initial within-sample dispersion. So far we have ignored any effects of initial within-sample dispersion of magnetic moments on the inclination shallowing. Within-sample dispersion would tend to smear out the dependence of ΔI on I. By assuming that individual grains obey an equation of the form

$$\tan (i - \Delta i) = (1 - \varepsilon) \tan i \qquad (3.66)$$

we see that Δi at middle inclinations (about 45°) will be less than predicted by equation (3.66) due to smearing. From symmetry of the expected dispersion we note that the inclination shallowing, Δi, will still be zero at $I = 0°$ and $\pm 90°$.

We solve the problem of initial dispersion by starting with a unit vector composed of inclination, i, and declination, d:

$$\mathbf{m} = (\cos i \cos d , \cos i \sin d , \sin i) \qquad (3.67)$$

This vector makes the angle θ with the sample's mean direction (inclination I and declination of zero) which can be calculated from the scalar product of $\mathbf{m}$ and ($\cos I$, 0, $\sin I$)

$$\cos \theta = \sin I \sin i + \cos I \cos i \cos d \qquad (3.68)$$

The unit vector, $\mathbf{m}$, is subsequently rotated to a new shallower inclination $(i - \Delta i)$, defined by equation (3.66), but the declination is kept unaltered at d. The unit vector $\mathbf{m}$ is therefore transformed to

$$\mathbf{m}' = [\cos(i - \Delta i) \cos d , \cos(i - \Delta i) \sin d , \sin(i - \Delta i)] \qquad (3.69)$$

The vectors $\mathbf{m}$ are assumed to obey the Fisher distribution about the mean direction; hence the frequency density of the vector $\mathbf{m}$ is proportional to

$$e^{\kappa \cos \theta} \qquad (3.70)$$

To get the total inclination shallowing, we therefore integrate over all directions (d,i), weighted by equation (3.70) and a geometrical factor of cos i:

$$\tan (I - \Delta I) = \frac{m_{z\text{-average}}}{m_{x\text{-average}}} =$$

$$= \frac{\int_{-\pi/2}^{\pi/2} \int_{0}^{2\pi} \cos i \; e^{\kappa \cos\theta} \sin(i-\Delta i) \; dd \; di}{\int_{-\pi/2}^{\pi/2} \int_{0}^{2\pi} \cos i \; e^{\kappa \cos\theta} \cos(i-\Delta i) \cos d \; dd \; di} \qquad (3.71)$$

where $(i - \Delta i)$ and θ are functions of I, i, d, and ε through equations (3.66) and (3.68). To solve this analytically turns out to be complicated; instead we make the approximation

$$e^{\kappa \cos \theta} \approx 1 + \kappa \cos \theta \qquad (3.72)$$

which is reasonable for small κ. With this approximation, equation (3.71) is solved in Appendix B and has the solution

$$\tan (I - \Delta I) = (1 - b \, \varepsilon) \tan I \qquad (3.73)$$

where

$$(1 - b \, \varepsilon) =$$

$$= \frac{2(1-\varepsilon)\arccos(1-4\varepsilon+2\varepsilon^2) - 4(1-\varepsilon)^2\sqrt{2\varepsilon-\varepsilon^2}}{-(1-4\varepsilon+2\varepsilon^2)\arccos(1-4\varepsilon+2\varepsilon^2) + 2(1-\varepsilon)\sqrt{2\varepsilon-\varepsilon^2}} \quad (3.74)$$

Exact solutions to equation (3.71) may be written on the form of equation (3.73), where b would be a function of ε and also slightly dependent on κ and I. However, with the approximation in equation (3.72), b becomes independent of κ and I. We have studied numerical solutions to the exact form of equation (3.71) and found the solution to start deviating from the approximation in equations (3.73) and (3.74) when $\kappa > 0.5$ (1% error in b). Furthermore, if the initial distribution were not exactly Fisherian, this would affect the function b. Therefore we believe the approximation in equation (3.72) to be adequate. For ε between 0 and 0.5 we can estimate b in equation (3.74) as

$$b \approx 0.593 + 0.232\varepsilon \quad (3.75)$$

The choice between equations (3.74) and (3.75) depends on the need for accuracy. The results of this model are shown in Figure 3.12. We note that a sediment obeying the equation of model BH on a microscopic level but composed of rather dispersed moments will appear to be obeying model AK macroscopically with the numerical value $a \approx 0.65$, within error bounds of the estimate of a that *Anson and Kodama* [1987] obtained experimentally. We therefore compare the predicted inclination shallowing of model AK with $a = 0.65$, model 1c with $f_n = 0.62$, and model 4a with $\varepsilon = \Delta V$, in Figure 3.13*a*. They are very similar.

For the above estimate of b, we have assumed that the sediment obeys equation (3.66) on microscopic level. All our models are of this form, except model 1a. In Appendix B we show that assuming equation (3.9) (model 1a) on a microscopic level results macroscopically in the same form as equation (3.73) but with a different constant b, which we call b'. In this appendix we show that b' is

$$(1 - b' \varepsilon) = \frac{2 (1-\varepsilon)^3}{((1-\varepsilon)^2-1) \boldsymbol{K}(1-\varepsilon) + ((1-\varepsilon)^2+1) \boldsymbol{E}(1-\varepsilon)} \quad (3.76)$$

where the special functions $\boldsymbol{K}$ and $\boldsymbol{E}$ are the complete elliptic integrals of the first and second kind, respectively. For compaction values between 0 and 0.5 ($\varepsilon = \Delta V$ for model 1a) we can approximate b' in equation (3.76) by

$$b' \approx 1.43 - 0.66 \, \Delta V \quad (3.77)$$

One remarkable result of the derivation in the appendix is that for the assumed form of the initial within-sample dispersion, we will obtain macroscopically an equation of the form

$$\tan (I - \Delta I) = (1 - F) \tan I \quad (3.78)$$

independent of the form of the equation of the microscopic mechanism responsible for the inclination shallowing. The microscopic mechanism serves only to define the function F. The effects of the expected initial within-sample dispersion on the models discussed in this chapter will be

to dampen the resultant inclination shallowing in equations (3.18), (3.22), (3.32), (3.37), (3.40), and (3.62) according to equation (3.73). This effect transforms the different form of equation (3.9) of model 1a to this standard form, with the modifying constant b' instead of b. We compare the transformed versions of models 1a and 1b in Figure 3.13*b*. The effect of initial dispersion should also affect equations (3.2), (3.6), (3.7), and (3.8), even though one may say that it is built in equation (3.8). Because of the low initial alignment in natural sediments, the intensity variation in equations (3.41), (3.52), and (3.63) should be nearly independent of the initial inclination I. In these equations, I should be replaced by the effective average inclination I_{eff} which is constant about 30° (the average I over positive inclinations, weighted by the area of the directional sphere (cos I)). In equation (3.23) the correction factor c, should also be nearly independent of I, which makes it still closer to unity and it can probably be omitted in practical situations.

Figure 3.12. Model 4a, initial within-sample dispersion, equation (3.73). (*a*) The function b as a function of ε, (b turns out to be close to a constant $b \approx 0.65$). (*b*) The inclination shallowing ΔI (deg), versus initial inclination I (deg) for various $\varepsilon = 0.1, 0.3, 0.5$. (*c*) The inclination shallowing ΔI (deg) versus ε, for initial inclination $I = 45°$. The effect of initial dispersion on a sediment that on a microscopic level satisfies $\tan (I - \Delta I) = (1 - \varepsilon) \tan I$ is to make it appear macroscopically to satisfy $\tan (I - \Delta I) = (1 - b\, \varepsilon) \tan I$.

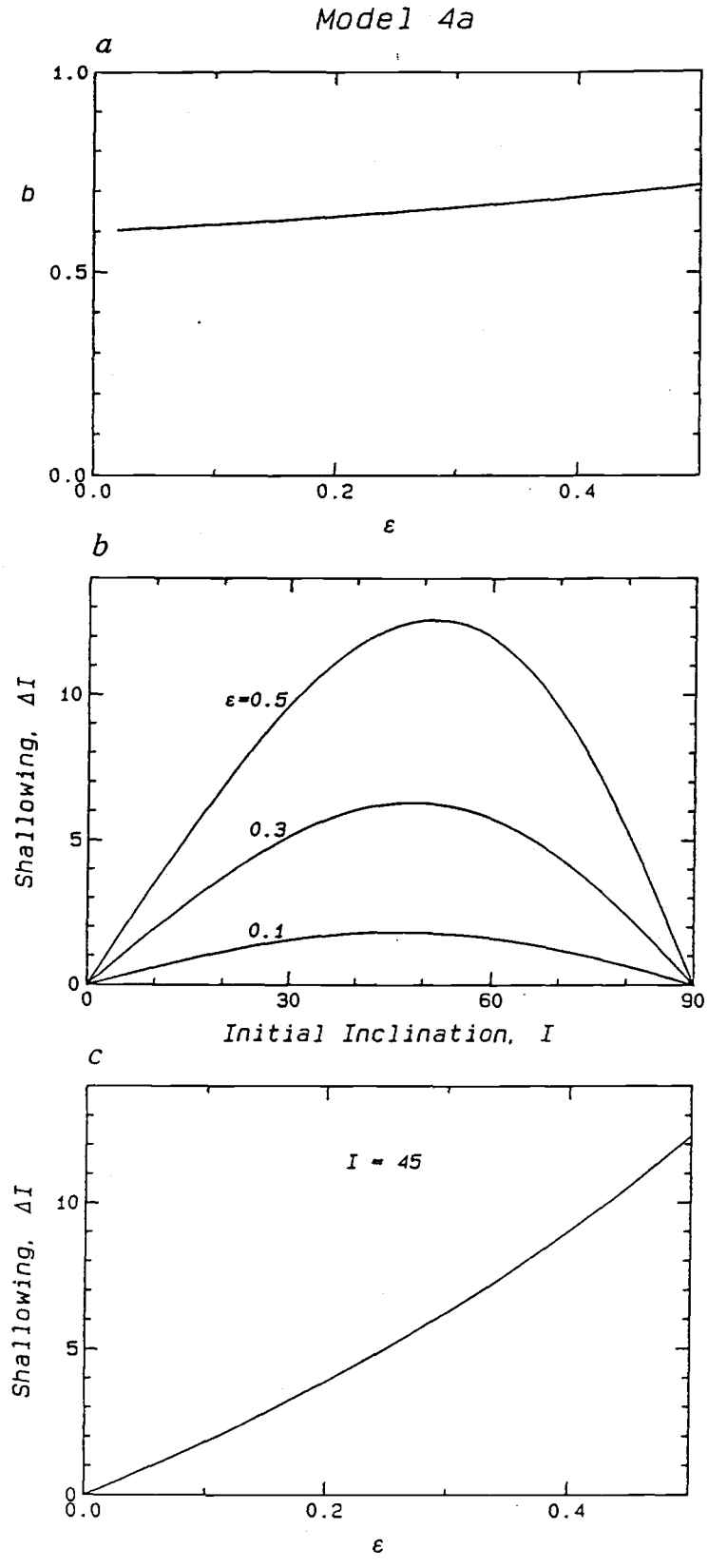
Model 4a
a
1.0
b
0.5
0.0
0.0
0.2
0.4
ε
b
Shallowing, ΔI
10
5
0
ε=0.5
0.3
0.1
0
30
60
90
Initial Inclination, I
c
Shallowing, ΔI
10
5
0
I = 45
0.0
0.2
0.4
ε

Figure 3.12.

Figure 3.13. Comparison of the predicted inclination shallowing of some of the models. (*a*) Comparison of model 1b (bold), equation (3.18) when model 4a, equation (3.72) with $\varepsilon = \Delta V$, has been taken into account, model AK (dashed), equation (3.8) with $a = 0.65$, and model 1c (thin), equation (3.24) with $f_n = 0.62$, all for initial inclination of $I = 45°$. We note that the predictions of these models are very similar. (*b*) Comparison of macroscopic predictions of models 1a (dashed) and model 1b (thin), when the effect of initial within-sample dispersion (model 4a) has been taken into account. For reference we also show the microscopic form of model 1b (bold), equation (3.18), when the effect of model 4a has not been taken into account. All curves are for compaction values $\Delta V = 0.5$, where $b = 0.716$ and $b' = 1.123$ (from the exact equations (3.74) and (3.76), respectively).

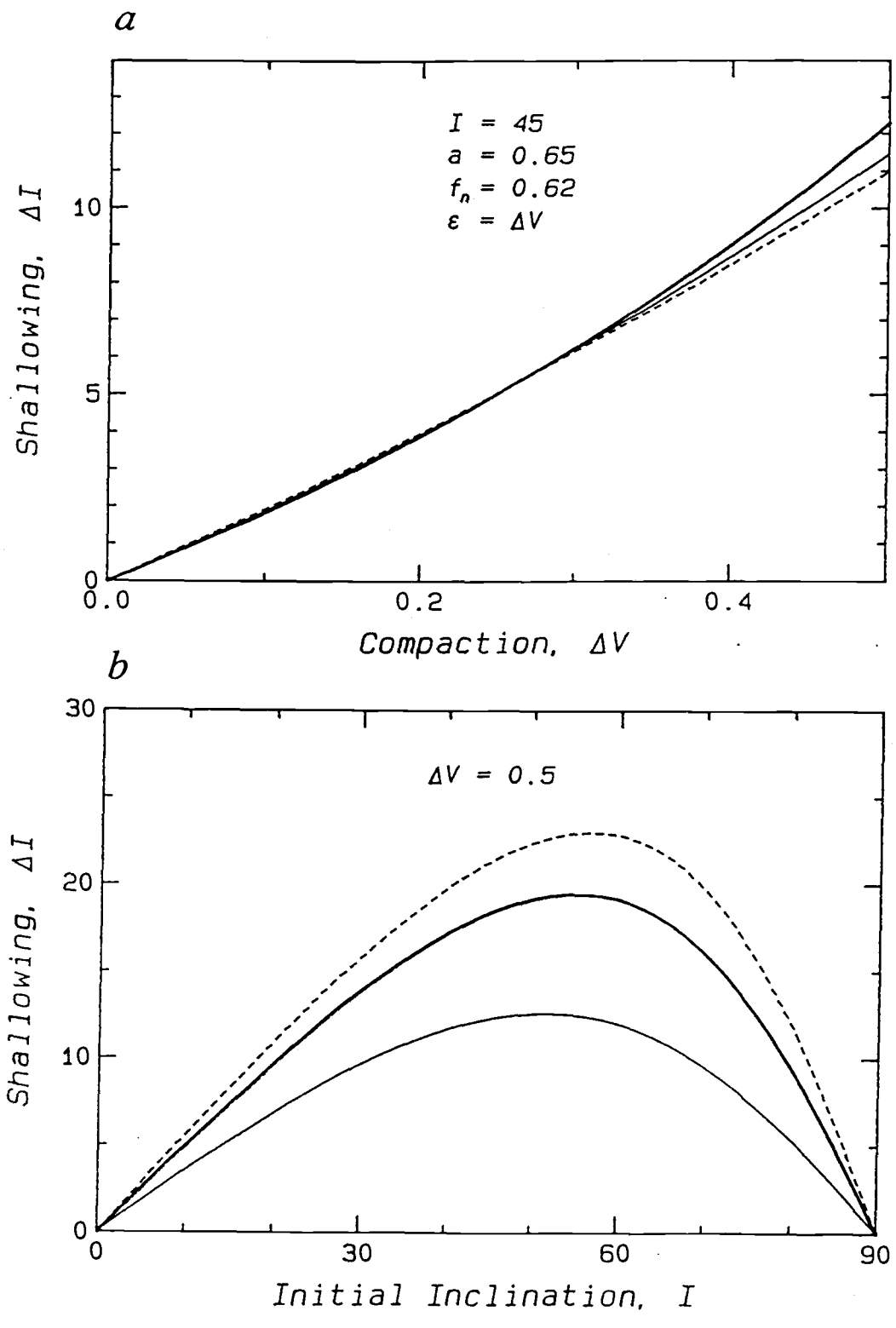
a
I = 45
a = 0.65
f_n = 0.62
ε = ΔV
Shallowing, ΔI
Compaction, ΔV
0
5
10
0.0
0.2
0.4
b
ΔV = 0.5
Shallowing, ΔI
Initial Inclination, I
0
10
20
30
0
30
60
90

Figure 3.13.

3.5 CONCLUSIONS

We have shown three possible mechanisms for inclination shallowing and a fourth process dampening the effect of all the other models slightly. The described models are realistic to different degrees. It is not usually known to what extent the magnetic minerals rotate directly, or whether they are attached to fabric flakes and are rotated through fabric rearrangements of the sedimentary matrix. Our calculations show that fabric rearrangement can not be a major source of inclination shallowing or intensity decrease. Sometimes deep-sea sediments show intensity decrease downhole, in otherwise homogeneous sections. Neglecting chemical alterations, this can be explained by directional randomization of the magnetic grains. The dispersion of magnetic moments predicted by the collapsing fabric, reduces the intensity less than the increased concentration due to compaction, and therefore leads to an intensity increase (Figure 3.8). In contrast, the randomization models readily predict the intensity decrease and in addition some inclination shallowing. We are therefore inclined to favor random rolling of sediment grains about horizontal axes as a significant process in sediments, leading to intensity decrease and inclination shallowing. The dampening of the inclination shallowing predicted by considering the effect of initial within-sample dispersion of moments is inevitable, and we believe that it has to be taken into account in all inclination shallowing models.

Studies of the fabric of clay rich sediments indicate that near the surface, the clay flakes are more or less randomly oriented, but

compaction tends to collapse the matrix and reorient the particles to lie down with their flat surface horizontal [*Bennett et al.*, 1981]. Clay flakes have been reported to rearrange to nearly-horizontal orientations at depths of about 100 m in clay-rich deep-sea sediments [*Faas and Crocket*, 1983].

We have not been concerned with geochemical processes and possible dissolution of the magnetic grains in this chapter, even though dissolution may be responsible for significant intensity decreases in some sediments [*Karlin and Levi*, 1985]. Neither have we addressed the effect of grain size. It is possible that in the randomization models larger grains may be less affected than the smaller ones. However, the grain size dependence is diminished whenever the magnetic grains are immobilized by being attached to larger fabric grains, because the matrix grains are usually considerably larger than the particles responsible for the stable remanence in sediments.

Inclination shallowing due to sediment compaction is clearly of great concern for paleomagnetism and the interpretation of paleomagnetic data. In this study we introduce simple mechanical models to derive mathematical expressions for the inclination shallowing during sediment compaction. We believe that all the models represent realistic physical processes active in sediments (except for model 1a at high values of I). The relative importance of the different mechanisms depends on the nature of the sediment and cannot yet be predicted a priori. However, several or all the processes may be active in any compacting sedimentary environment. In Table 3.1 we summarize the equations for the inclination shallowing models, taking into account the effect of initial

within-sample dispersion (model 4a). We note the parallel structure of the equations, which arises because model 4a transforms any microscopic mechanism into this macroscopic form.

If a mechanism obeying the equation $\tan(I-\Delta I)= (1-p\Delta V)\ \tan I$ is followed by another mechanism obeying $\tan (I - \Delta I) = (1 - q\ \Delta V)\ \tan I$, they will together result in $\tan (I - \Delta I) = (1 - p\ \Delta V)\ (1-q\Delta V)\ \tan I \approx (1 - (p+q)\ \Delta V)\ \tan I$. Therefore, until there is more specific knowledge of inclination shallowing mechanisms in sediments, we recommend the use of an equation of the form

$$\tan (I - \Delta I) = (1 - a\ \Delta V)\ \tan I \qquad (3.79)$$

where I is the ambient field inclination, ΔI the inclination shallowing, ΔV the compaction, and a is a constant, chosen to fit inclination shallowing data from laboratory experiments and natural sediments.

TABLE 3.1. Summary of the Equations of the Inclination Shallowing Models

Model	Author(s)	Equation of Model	Equation Number in Text
		Previously published models:	
K	[*King*, 1955]	$\tan(I-\Delta I) = (1-f_K)\tan I$	(3.2)
GKRW	[*Griffiths et al.*, 1960]	$\tan(I-\Delta I) = (1-f_G)\tan I$	(3.6)
BH	[*Blow and Hamilton*, 1978]	$\tan(I-\Delta I) = (1-\Delta V)\tan I$	(3.7)
AK	[*Anson and Kodama*, 1987]	$\tan(I-\Delta I) = (1-a\,\Delta V)\tan I$	(3.8)
		Models of this study: *	
1a: Rotating magnetic needles in rigid matrix		$\tan(I-\Delta I) = (1-b'\,\Delta V)\tan I$	(3.9)
1b: Rotating magnetic needles in soft matrix		$\tan(I-\Delta I) = (1-b\,\Delta V)\tan I$	(3.18)
1c: Two types of magnetic grain shapes in soft matrix		$\tan(I-\Delta I) = (1-b\,c\,f_n\,\Delta V)\tan I$	(3.22)
2a: Collapsing rigid matrix		$\tan(I-\Delta I) = (1-b f_a)\tan I$	(3.37)
2b: Collapsing soft matrix		$\tan(I-\Delta I) = (1-b f_b)\tan I$	(3.40)
3b: Random rolling of grains about horizontal axes		$\tan(I-\Delta I) = (1-b f_h)\tan I$	(3.62)

* The effects of model 4a, equation (3.73), are included in all the models of this study. The functions (nearly constants) b and b' are given in equations (3.75) and (3.77).

3.6 REFERENCES

Anson, G. L., and K. P. Kodama, Compaction-induced shallowing of the post-depositional remanent magnetization in a synthetic sediment, *Geophys. J. R. Astron. Soc.*, *88*, 673-692, 1987.

Arason, P., and S. Levi, Inclination shallowing recorded in some deep sea sediments (abstract), *Eos Trans. AGU*, *67*, 916, 1986.

Arason, P., and S. Levi, Compaction and inclination shallowing in deep-sea sediments from the Pacific ocean, *J. Geophys. Res.*, *95*, 4501-4510, 1990*b*.

Bennett, R. H., W. R. Bryant, and G. H. Keller, Clay fabric of selected submarine sediments: Fundamental properties and models, *J. Sediment. Petrol.*, *51*, 217-232, 1981.

Blow, R. A., and N. Hamilton, Effect of compaction on the acquisition of a detrital remanent magnetization in fine-grained sediments, *Geophys. J. R. Astron. Soc.*, *52*, 13-23, 1978.

Celaya, M. A., and B. M. Clement, Inclination shallowing in deep sea sediments from the North Atlantic, *Geophys. Res. Lett.*, *15*, 52-55, 1988.

Chikazumi, S., *Physics of Magnetism*, 554 pp., John Wiley, New York, 1964.

Collinson, D. W., Depositional remanent magnetization in sediments, *J. Geophys. Res.*, *70*, 4663-4668, 1965.

Faas, R. W., and D. S. Crocket, Clay fabric development in a deep-sea core: Site 515, Deep Sea Drilling Project leg 72, *Initial Rep. Deep Sea Drill. Proj.*, *72*, 519-535, 1983.

Fisher, R., Dispersion on a sphere, *Proc. R. Soc. London, Ser. A, 217*, 295-305, 1953.

Griffiths, D. H., R. F. King, A. I. Rees, A. E. Wright, Remanent magnetism of some recent varved sediments, *Proc. R. Soc. London, Ser. A, 256*, 359-383, 1960.

Hamilton, E. L., Thickness and consolidation of deep-sea sediments, *Geol. Soc. Am. Bull., 70*, 1399-1424, 1959.

Karlin, R., and S. Levi, Preliminary paleomagnetic results of laminated sediments from deep sea drilling project hydraulic piston core site 480, Guaymas basin, Gulf of California, *Initial Rep. Deep Sea Drill. Proj., 64*, 1255-1258, 1982.

Karlin, R., and S. Levi, Geochemical and sedimentological control of the magnetic properties of hemipelagic sediments, *J. Geophys. Res., 90*, 10,373-10,392, 1985.

Kent, D. V., Post-depositional remanent magnetization in deep-sea sediment, *Nature, 246*, 32-34, 1973.

Kent, D. V., and D. J. Spariosu, Magnetostratigraphy of Caribbean site 502 Hydraulic Piston Cores, *Initial Rep. Deep Sea Drill. Proj., 68*, 419-433, 1982.

Khramov, A. N., Orientational magnetization of finely dispersed sediments, *Izv. Acad. Sci. USSR Phys. Solid Earth, 1*, 63-66, 1968.

King, R. F., Remanent magnetism of artificially deposited sediments, *Mon. Not. R. Astron. Soc., Geophys. Suppl., 7*, 115-134, 1955.

Langevin, P., Magnétisme et théorie des électrons (in French), *Ann. Chim. Phys., 5*, 70-127, 1905.

Levi, S., and R. T. Merrill, Properties of single-domain, pseudo-single-domain, and multidomain magnetite, *J. Geophys. Res.*, *83*, 309-323, 1978.

Mardia, K. V., *Statistics of Directional Data*, 357 pp., Academic, San Diego, Calif., 1972.

Morgan, G. E., Paleomagnetic results from DSDP site 398, *Initial Rep. Deep Sea Drill. Proj.*, *47*, 599-611, 1979.

Nagata, T., Notes on detrital remanent magnetization of sediments, *J. Geomagn. Geoelectr.*, *14*, 99-106, 1962.

Nobes, D. C., H. Villinger, E. E. Davis, and L. K. Law, Estimation of marine sediment bulk physical properties at depth from seafloor geophysical measurements, *J. Geophys. Res.*, *91*, 14,033-14,043, 1986.

Ozima, M., Effects of plastic deformation on the remanent magnetization of a Cu-Co alloy, *Earth Planet. Sci. Lett.*, *47*, 121-123, 1980.

Stacey, F. D., On the role of Brownian motion in the control of detrital remanent magnetization of sediments, *Pure Appl. Geophys.*, *98*, 139-145, 1972.

Stober, J. C., and R. Thompson, Magnetic remanence acquisition in Finnish lake sediments, *Geophys. J. R. Astron. Soc.*, *57*, 727-739, 1979.

Tauxe, L., P. Tucker, N. P. Petersen, and J. L. LaBrecque, Magnetostratigraphy of leg 73 sediments, *Initial Rep. Deep Sea Drill. Proj.*,*73*, 609-621, 1984.

Tomlinson, M. J., *Foundation Design and Construction*, 793 pp., 4th ed., Pitman Advanced Publishing Program, Boston, Mass., 1980.

Tschebotarioff, G. P., *Soil Mechanics, Foundations and Earth Structures*, 655 pp., McGraw-Hill, New York, 1951.

Tucker, P., Stirred remanent magnetization: A laboratory analogue of post-depositional realignment, *J. Geophys.*, *48*, 153-157, 1980.

Verosub, K. L., Depositional and postdepositional processes in the magnetization of sediments, *Rev. Geophys.*, *15*, 129-143, 1977.

Von Mises, R., Über die "ganzzahligkeit" der atomgewichte und verwandte fragen (in German), *Phys. Z.*, *19*, 490-500, 1918.

CHAPTER 4

Compaction-Induced Inclination Shallowing in Cretaceous DSDP Sediments From the Pacific Plate

Paleomagnetic inclinations of Cretaceous Deep Sea Drilling Project (DSDP) sediments from the Pacific plate are known to be systematically shallower than predicted from paleolatitudes of hot spot reconstructions. In this study we reexamine published data and try to explain the shallow Cretaceous inclinations as a result of sediment compaction. We obtain mean paleomagnetic inclinations I_P of published paleomagnetic data from DSDP sediments; the expected inclinations I_H are from hot spot paleolatitude reconstructions, which are in agreement with sedimentless apparent polar wander paths. Sediment compaction ΔV is estimated from DSDP density and porosity data, assuming lithology dependent initial values. These data and the equation for compaction-induced inclination shallowing, $\tan I_P = (1 - a\ \Delta V)\ \tan I_H$, are used to calculate the free parameter a. The resulting a values are comparable to those of previous studies of compaction-induced inclination shallowing, both from laboratory experiments and Plio- Pleistocene DSDP sediments. Values of the parameter a suggest that it might be controlled by sediment

lithology with greater shallowing for clayey sediments ($a \approx 1.1$) than in calcareous sediments ($a \approx 0.7$). The apparent predictability of the parameter a offers the hope for restoring shallow inclinations when sediment compaction is known.

4.1 INTRODUCTION

In this study we examine mean inclinations in compacted deep-sea sediments. In finding a mean inclination for a paleomagnetic data set it is very important to be able to distinguish between normal and reversed polarities. A reversed direction that is accidentally averaged with normal period data causes the mean to become too shallow. This problem of polarity mixing becomes serious for low latitudes where the polarity is not necessarily reflected in the sign of the inclination. This problem is amplified when the magnetostratigraphy is not clear. On the other hand, this problem is diminished by considering data from known long polarity chrons. The Cretaceous long normal polarity chron from about 83-118 Ma provides one such opportunity of old sequences where the polarity should be fairly certain. These sediments are often deeply buried and compacted. We limit this study to the Pacific plate because its motion in the hot spot reference frame is relatively well documented, and several Cretaceous sedimentary sections have been sampled from a large area of a single plate. Furthermore, we undertake this study because the reliability of the Cretaceous sediment paleomagnetic data from the Pacific plate has been questioned [e.g., *Gordon*, 1990].

When Cretaceous deep-sea sedimentary sections became available through the Deep Sea Drilling Project (DSDP), it became possible to calculate paleolatitudes and tectonic movements from paleomagnetic inclinations [e.g., *Jarrard*, 1973; *Hammond et al.*, 1975; *Cockerham and Jarrard*, 1976; *Steiner*, 1981; *Sayre*, 1981; *Bleil*, 1985; *Ogg*, 1986]. However, significant paleolatitude discrepancies were observed between

sites. This led to speculations on local block tilting and/or the existence of independent microplates in the past [e.g., *Cockerham and Hall*, 1976]. *Cockerham and Hall* [1976, p. 4221] discussed the possibility that some paleomagnetic data may be affected by an inclination error.

Gordon [1990] compared Cretaceous age paleomagnetic poles for the Pacific plate obtained by four different methods; (1) skewness of magnetic anomalies, (2) inversion of seamount magnetic anomalies, (3) paleomagnetism of basement rocks from DSDP holes, and (4) paleomagnetism of sediments from DSDP holes. While the paleomagnetic poles were comparable for the first three data sets, the sedimentary DSDP data resulted in significantly different poles than the other methods. The inclinations from the DSDP sediments were too shallow. *Gordon* [1990] speculated on three possible causes for this bias; bias imparted by the rotary drilling process, compaction-induced inclination shallowing, or Brunhes viscous overprint. He recommended discarding all reference poles based on these apparently unreliable data, and suggested that paleolatitude discrepancies between sites is due to inclination bias rather than tectonic movements.

Tarduno [1990] compared inclinations from Cretaceous DSDP sediments from the Pacific plate to the expected inclination as determined by apparent polar wander (APW) paths. He noticed that sites which reconstruct to positions farthest south in the southern hemisphere show the largest inclination anomaly while data from sediments deposited closer to the equator agree with the APW poles from sedimentless data. Therefore, he concluded that the data could not be explained by possible inaccurate pole determinations, but rather as an

inclination shallowing effect. *Tarduno* [1990] did not introduce quantitative estimates of compaction or mention depth differences between the DSDP cores. He suggested that subtle differences in composition and sediment diagenesis might explain differences between sites.

Suspicions of too shallow inclinations have been reported from studies of deep-sea sediments, and it has been suggested that the shallow inclinations are due to sediment compaction [e.g., *Morgan*, 1979; *Kent and Spariosu*, 1982; *Tauxe et al.*, 1984]. Inclination shallowing was associated with the sediment porosity in clays from the Northwest Pacific ocean [*Arason and Levi*, 1986; 1990*b*], and in carbonates from the North Atlantic ocean [*Celaya and Clement*, 1988]. Laboratory experiments have demonstrated that sediment compaction can lead to inclination shallowing in redeposition of natural deep-sea silty clays [*Blow and Hamilton*, 1978] and in synthetic clays [*Anson and Kodama*, 1987; *Deamer and Kodama*, 1990]. Furthermore, in laboratory experiments with synthetic sediments *Lu et al.* [1988; 1990] observed increased inclination shallowing versus increased clay concentration, indicating that lithology may be a controlling factor on inclination shallowing processes.

In this article we examine whether compaction-induced inclination shallowing can explain the apparent inclination bias in Cretaceous DSDP sediments. The DSDP sites from the Pacific plate where Cretaceous sediments have been recovered and studied for paleomagnetism are shown in Table 4.1 and Figure 4.1. Compaction-induced inclination shallowing obeys the relation

$$\tan (I - \Delta I) = (1 - a \, \Delta V) \tan I \qquad (4.1)$$

[*Arason and Levi*, 1990*a*] where I is the initial inclination; ΔI the compaction-induced inclination shallowing, ΔV the sediment compaction, and a is a constant. It is important to realize that the parameter a is not well known and especially the extent to which lithology and other factors can modify it. In this study we try to use the Cretaceous DSDP sediments to understand factors that control the parameter a.

The parameter a is estimated by manipulating equation (4.1) using the mean paleomagnetic inclinations I_P as ($I - \Delta I$), the dipole inclination of the hot spot paleolatitude I_H as the initial inclination I, and the compaction estimate based on the density-porosity data for calculating ΔV:

$$a = \frac{1 - \dfrac{\tan I_P}{\tan I_H}}{\Delta V} \qquad (4.2)$$

This is of course done in the hope that if the parameter a is predictable one might restore the shallow inclinations by calculating the initial or compaction-corrected inclination I_{corr} in the sediment

$$I_{corr} = \arctan \left(\frac{\tan I_{obs}}{(1 - a \, \Delta V)} \right) \qquad (4.3)$$

The corrected inclinations could then be used to calculate more accurate site paleolatitudes.

TABLE 4.1. Location of DSDP Sites Considered in this Study.

DSDP Leg	DSDP Site	Present Location Latitude, deg N	Present Location Longitude, deg E	Water Depth, m
7	66	2.39	−166.12	5293
17	164	13.20	−161.52	5499
17	165	8.18	−164.86	5053
17	166	3.76	−175.08	4962
17	167	7.07	−176.83	3176
17	169	10.67	173.55	5407
17	170	11.80	177.62	5792
17	171	19.13	−169.46	2290
20	199	13.51	156.17	6100
30	288	−5.97	161.83	3000
30	289	−0.50	158.51	2206
33	315	4.17	−158.53	4152
33	316	0.09	−157.13	4451
33	317	−11.00	−162.26	2598
61	462	7.24	165.03	5181
62	463	21.35	174.67	2525
62	465	33.82	178.92	2161
86	577	32.44	157.72	2675
86	578	33.93	151.63	6010
89	585	13.48	156.82	6109

Figure 4.1. Map of DSDP and ODP sites where Cretaceous sediments have been recovered and studied for paleomagnetism. (*a*) Outline of the Pacific plate is shown (based on *Le Pichon* [1968]); crustal ages were derived from magnetic anomalies with darker shades for older crust (Tertiary/Cretaceous/Jurassic) (based on *Pitman et al.* [1974]). The ODP sites are shown as squares and the DSDP sites as circles. (*b*) Closer look at the sites with site numbers. The most useful DSDP sites of this study are shown as filled circles. Location of the DSDP sites is listed in Table 4.1.

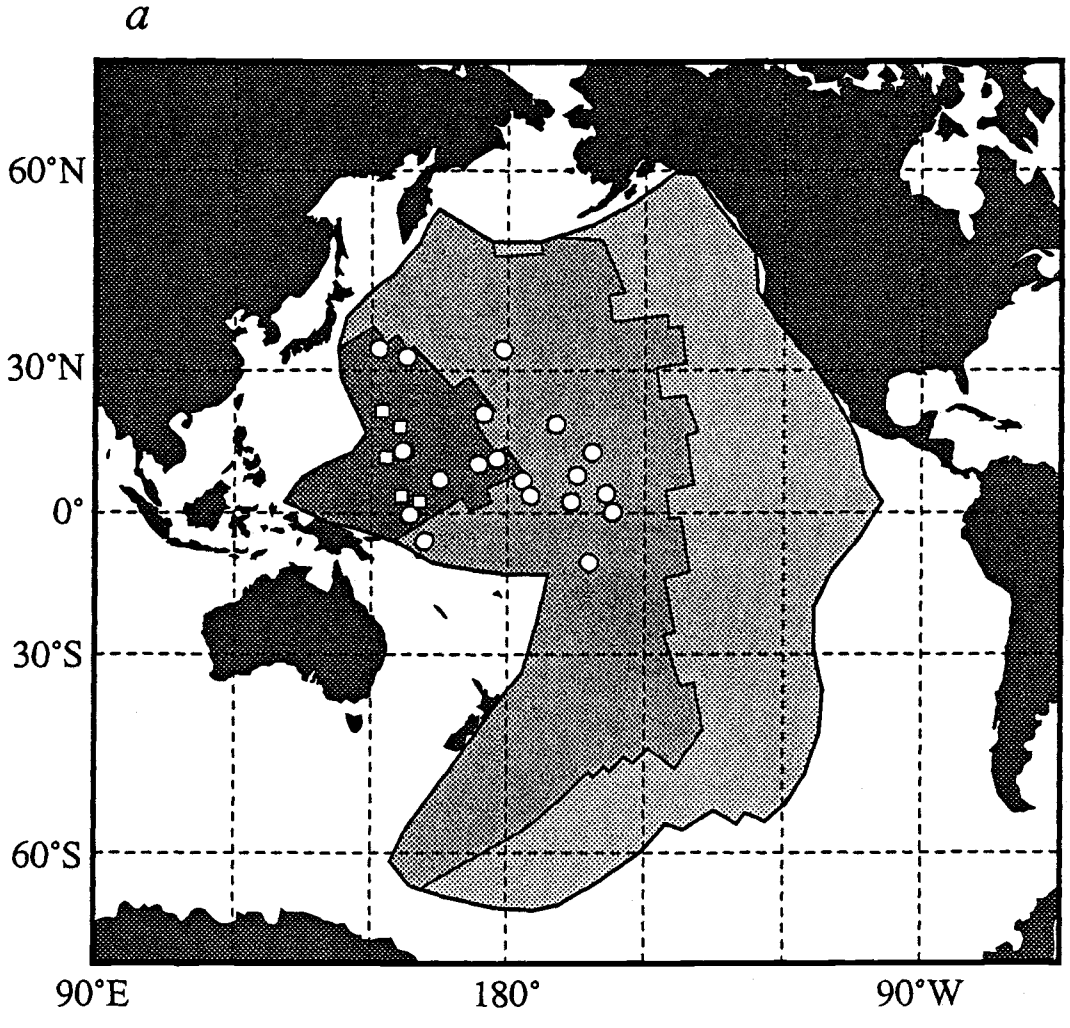

Figure 4.1.

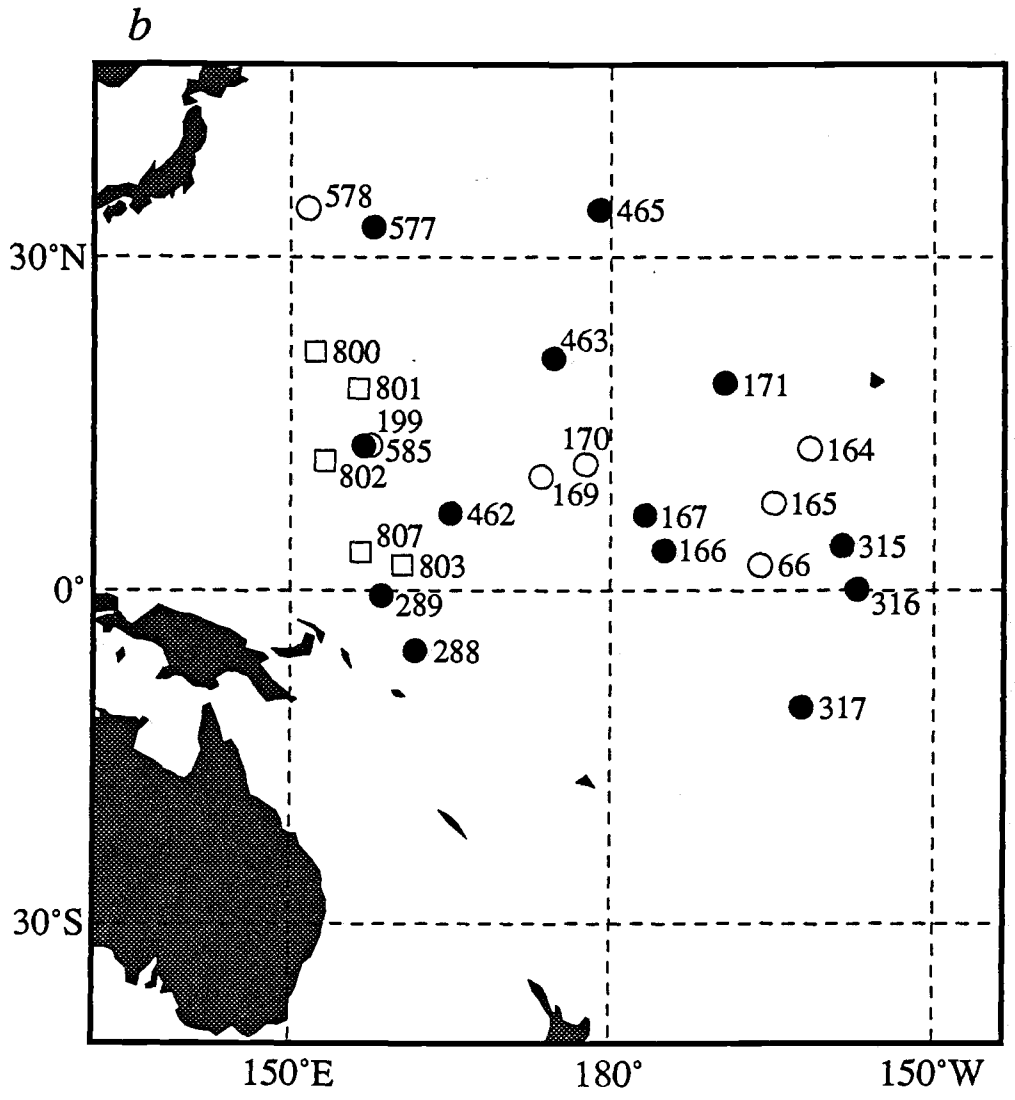

Figure 4.1 continued.

4.2 DSDP PALEOMAGNETIC DATA

We analyze the available paleomagnetic data from Cretaceous DSDP sediments from the Pacific plate. *Gordon* [1990] used published mean inclinations and paleolatitudes in his analysis. The published mean values were calculated using different methods, including arithmetic means of inclinations, a method known to cause a bias toward shallow inclinations. Furthermore, the original averages were usually split into several arbitrary age periods. Because most of the original data were published, we decided to recalculate the mean inclinations, along with the 95% confidence limits of the mean, in a standardized fashion, using Kono statistics [*Kono*, 1980*a*, *b*]. Our estimates are listed in Table 4.2.

To examine the effects of different lithologies on the inclination shallowing, we grouped the data from each hole by lithology. The lithological description of the depth intervals was taken from the DSDP data base [*DSDP CD-ROM*, 1989]. In most of the holes the samples are predominantly from one main lithology; data from anomalous horizons were deleted.

TABLE 4.2. Mean Inclinations in DSDP Sediments.

Hole	Data Depth Range, m	Average Depth, m	*N*	Mean Inclination and 95% CI, deg	Angular Standard Deviation, deg
		Clayey sediments:			
DSDP 315A	807.72-849.26	830.24	25	−17.0 ± 2.8	7.7
DSDP 315A*	807.72-849.26	828.68	43	−16.9 ± 2.1	7.8
Normal*	818.57-849.26	833.09	35	−15.9 ± 2.3	7.7
Reversed*	807.72-811.85	809.37	8	+20.9 ± 4.0	5.8
DSDP 462	513.58-551.42	525.99	19	−12.8 ± 3.9	9.3
Normal	513.58-551.42	529.24	12	−13.9 ± 4.7	8.7
Reversed	516.85-524.17	520.42	7	+10.8 ± 7.2	9.6
DSDP 462A	517.08-555.55	532.45	24	−16.0 ± 3.9	10.5
Normal	517.08-555.55	538.07	16	−18.4 ± 4.5	9.8
Reversed	518.36-525.08	521.20	8	+11.1 ± 5.8	8.4
DSDP 585	485.67-679.95	549.86	49	−17.2 ± 3.9	15.3
DSDP 585A	503.07-829.75	666.29	39	−21.5 ± 3.8	13.1
		Calcareous sediments:			
DSDP 167	787.22-863.77	831.82	46	−23.2 ± 5.1	19.3
Normal	787.22-863.77	833.74	26	−17.1 ± 4.9	13.7
Reversed	828.20-831.31	829.33	20	+31.3 ± 9.0	21.6
DSDP 167**	(861-975)	(880)	95	−29.1 ± 2.0	13.3
DSDP 288A**	(742-896)	(880)	41	−41.6 ± 2.6	11.6
DSDP 289**	(1231-1262)	(1235)	11	−37.6 ± 5.8	12.1
DSDP 315A	809.21-843.55	826.50	18	−16.6 ± 3.4	8.0
DSDP 316**	(571-730)	(640)	132	−17.1 ± 1.7	13.9
DSDP 317A	584.30-662.78	620.54	23	−46.8 ± 5.6	14.8
DSDP 463	481.01-671.14	561.98	47	−28.3 ± 3.2	12.2
DSDP 465A	277.03-402.36	342.74	8	+1.6 ± 3.6	5.2
DSDP 577	109.10-117.20	112.42	45	+23.3 ± 1.8	7.0
Normal	112.70-117.20	114.93	20	+21.6 ± 1.5	3.7
Reversed	109.10-112.50	110.41	25	−24.6 ± 3.0	8.4
DSDP 577A	109.67-122.93	116.27	53	+28.3 ± 2.6	10.8
Normal	113.16-122.93	118.42	34	+31.4 ± 2.4	7.8
Reversed	109.67-121.55	112.41	19	−22.5 ± 4.3	10.2
		Volcanic sediments:			
DSDP 171	287.00-329.19	297.10	16	−15.4 ± 4.4	9.5
Normal	287.00-329.19	309.42	7	−18.8 ± 7.4	9.8
Reversed	287.02-288.17	287.51	9	+12.7 ± 4.8	7.5

* Includes both the clayey and calcareous samples.
** Estimates from *Tarduno* [1990], for which we have added rough depth estimates.

4.3 SEDIMENT COMPACTION

To quantify the sediment compaction we calculate the compaction parameter ΔV [e.g., *Arason and Levi*, 1990*a*]. The compaction ΔV describes the change in the normalized sediment volume. The initial volume of a sample is $V = 1$ with $\Delta V = 0$; later the volume decreases to $V = (1 - \Delta V)$ for an arbitrary compaction ΔV. The compaction can be calculated from the decrease in pore space in the sediment [*Skempton*, 1970; *Baldwin*, 1971]. This approach assumes that gravitational forces squeezing out the pore water are dominant during compaction over chemical processes. Some sediments of this study experienced considerable diagenesis. However, distinction between gravitational compaction and chemical dissolution and recrystalization of the matrix may not be important for this study because both processes are expected to be responsible for reorganization of the matrix. Such reorganization may lead to rotations and randomizations of the magnetic grains, which ultimately causes the inclination shallowing [*Arason and Levi*, 1990*a*]. The relation between compaction and porosity due to dewatering is

$$\Delta V = \frac{\phi_0 - \phi}{1 - \phi} \tag{4.4}$$

where ϕ_0 is the initial sediment porosity, and ϕ is the porosity after the compaction (porosity of 81% enters the equation as 0.81). Similarly the increase in wet bulk density can be related to compaction

$$\Delta V = \frac{\rho - \rho_0}{\rho - \rho_w} \tag{4.5}$$

where ρ_0 is the initial wet bulk density of the sediment, ρ_w is density of the pore water, and ρ is the wet bulk density of the compacted sediment. Water content data can also be used to estimate the compaction

$$\Delta V = \frac{\frac{w_0}{(1-w_0)} - \frac{w}{(1-w)}}{\frac{w_0}{(1-w_0)} + \frac{\rho_w}{\rho_g}} \tag{4.6}$$

where w_0 is the initial water content (here: weight of water over weight of wet sediment), w is the water content after the compaction (water content of 61% enters the equation as 0.61), and ρ_w and ρ_g are the densities of the pore water and the sediment grains, respectively.

In order to estimate the compaction we calculated averages of the available water content, porosity and density data from the DSDP data base [*DSDP CD-ROM*, 1989] for the depth ranges of the paleomagnetic data along with the 95% confidence intervals of the means. For some holes we found additional data in the literature. We use these averages in equations (4.4)-(4.6), and adopt the lithology dependent initial values used by *Hamilton* [1976]; calcareous sediments ρ_0 = 1510 kg m^{-3}, ϕ_0 = 72.0%, w_0 = 49.4%; clayey sediments ρ_0 = 1360 kg m^{-3}, ϕ_0 = 81.2%, w_0 = 62.1%; volcanic sediment ρ_0 = 1530 kg m^{-3}, ϕ_0 = 72.0%. The densities are assumed ρ_w =1024 kg m^{-3} and ρ_g = 2700 kg m^{-3}. We list the water content, porosity and density averages for the DSDP holes in Table 4.3 along with our compaction estimates. The water content, porosity, and density data are usually measured/calculated for the same samples, and are not independent

estimates. However, for a consistency check we calculated the compaction for all three data sets, and in all cases there is excellent agreement.

The initial porosity of sediments seems to be relatively constant for a given lithology. For instance, in a study of a depth transect at 160°E on the equator *Johnson et al.* [1977] studied physical properties in calcareous sediments in numerous box cores from 1.6 to 4.4 km water depth. Although dissolution of the calcareous sediment was found to affect some of the physical properties, it did not affect the density or porosity of the sediment. At 20 cm depth in the cores the average wet bulk density was 1500 kg m^{-3} and porosity 71.9% and varied very little between cores on the depth transect.

We have compared the compaction estimates of this study to published compaction curves based on the subbottom depth of the sediment using lithology dependent average porosity curves versus depth [*Hamilton*, 1976; *Baldwin and Butler*, 1985]. This comparison is shown in Figure 4.2. The estimates of this study are comparable to the curves of *Hamilton* [1976] down to about 300 m, but are similar to the curve of *Baldwin and Butler* [1985] below 300 m. This should not be surprising since the *Baldwin and Butler* [1985] curve is based on deeper data.

TABLE 4.3. Compaction Estimates for DSDP Sediments.

Hole / Data	*N*	Average Depth, m	Mean Value and 95% CI*	Initial Value*	Compaction
DSDP 167 Calcareous:					
Water content data	6	822	18.7 ± 5.2	49.4	0.55 ± 0.06
Compaction estimate					0.55 ± 0.06
DSDP 171 Volcanic:					
Porosity data	6	311	61.5 ± 8.0	72.0	0.27 ± 0.16
Density data	6	311	1.688 ± 0.139	1.53	0.24 ± 0.17
Compaction estimate					0.26 ± 0.16
DSDP 288A Calcareous:					
Water content data	19	835	14.8 ± 2.3	49.4	0.59 ± 0.02
Porosity data	17	838	31.6 ± 3.8	72.0	0.59 ± 0.02
Density data	17	838	2.142 ± 0.074	1.51	0.57 ± 0.03
Compaction estimate					0.58 ± 0.03
DSDP 289 Calcareous:					
Water content data	3	1233	9.7 ± 14.6	49.4	0.64 ± 0.12
Porosity data	3	1233	22.5 ± 29.2	72.0	0.64 ± 0.15
Density data	3	1233	2.327 ± 0.541	1.51	0.63 ± 0.19
Compaction estimate					0.64 ± 0.19
DSDP 315A Clayey:					
Water content data	7	835	11.3 ± 4.7	62.1	0.75 ± 0.03
Porosity data	7	835	26.4 ± 9.5	81.2	0.74 ± 0.03
Density data	7	835	2.281 ± 0.098	1.36	0.73 ± 0.02
Compaction estimate					0.74 ± 0.02
DSDP 315A Calcareous:					
Water content data	16	821	7.9 ± 1.3	49.4	0.66 ± 0.01
Porosity data	16	821	19.3 ± 3.0	72.0	0.65 ± 0.01
Density data	16	821	2.389 ± 0.056	1.51	0.64 ± 0.01
Compaction estimate					0.65 ± 0.01
DSDP 316 Calcareous:					
Water content data	42	667	8.3 ± 1.2	49.4	0.65 ± 0.01
Compaction estimate					0.65 ± 0.01
DSDP 317A Calcareous:					
Water content data	21	627	11.4 ± 2.0	49.4	0.63 ± 0.02
Porosity data	19	627	26.9 ± 4.2	72.0	0.62 ± 0.02
Density data	19	627	2.314 ± 0.089	1.51	0.62 ± 0.03
Compaction estimate					0.62 ± 0.02

TABLE 4.3 continued.

Hole / Data	*N*	Average Depth, m	Mean Value and 95% CI*	Initial Value*	Compaction
DSDP 462 Clayey:					
Water content data	11	533	27.7 ± 4.6	62.1	0.62 ± 0.04
Porosity data	10	531	49.4 ± 6.2	81.2	0.63 ± 0.05
Density data	10	531	1.869 ± 0.108	1.36	0.60 ± 0.05
Compaction estimate					0.62 ± 0.04
DSDP 462A Clayey:					
Water content data	13	535	28.0 ± 3.6	62.1	0.62 ± 0.03
Porosity data	13	535	51.2 ± 4.9	81.2	0.61 ± 0.04
Density data	13	535	1.851 ± 0.075	1.36	0.59 ± 0.04
Compaction estimate					0.61 ± 0.03
DSDP 463 Calcareous:					
Water content data	41	561	11.3 ± 1.1	49.4	0.63 ± 0.01
Porosity data	41	561	24.9 ± 2.1	72.0	0.63 ± 0.01
Density data	41	561	2.241 ± 0.052	1.51	0.60 ± 0.02
Compaction estimate					0.62 ± 0.01
DSDP 465A Calcareous:					
Water content data	12	343	11.6 ± 4.6	49.4	0.62 ± 0.04
Porosity data	12	343	24.6 ± 7.8	72.0	0.63 ± 0.04
Density data	12	343	2.257 ± 0.160	1.51	0.61 ± 0.05
Compaction estimate					0.62 ± 0.04
DSDP 577 Calcareous:					
Grape porosity	(5)	113	55.8 ± 2.1	72.0	0.37 ± 0.03
Grape density	(5)	113	1.772 ± 0.038	1.51	0.35 ± 0.03
Compaction estimate					0.36 ± 0.03
DSDP 577A Calcareous:					
Porosity data	3	118	58.7 ± 11.2	72.0	0.32 ± 0.20
Density data	3	118	1.690 ± 0.194	1.51	0.27 ± 0.23
Grape porosity	(9)	116	61.7 ± 3.3	72.0	0.27 ± 0.06
Grape density	(9)	116	1.668 ± 0.051	1.51	0.25 ± 0.06
Compaction estimate					0.26 ± 0.06
DSDP 585 Clayey:					
Water content data	9	547	24.5 ± 3.3	62.1	0.65 ± 0.03
Porosity data	9	547	45.9 ± 5.2	81.2	0.65 ± 0.03
Density data	9	547	1.890 ± 0.081	1.36	0.61 ± 0.04
Compaction estimate					0.64 ± 0.03

TABLE 4.3 continued.

Hole / Data	*N*	Average Depth, m	Mean Value and 95% CI*	Initial Value*	Compaction
DSDP 585A Clayey:					
Water content data	23	678	25.1 ± 2.4	62.1	0.65 ± 0.02
Porosity data	23	678	47.3 ± 3.2	81.2	0.64 ± 0.02
Density data	23	678	1.917 ± 0.053	1.36	0.62 ± 0.02
Compaction estimate					0.64 ± 0.02

* The water content and porosity estimates are expressed in %, and density in 10^{-3} kg m^{-3}.

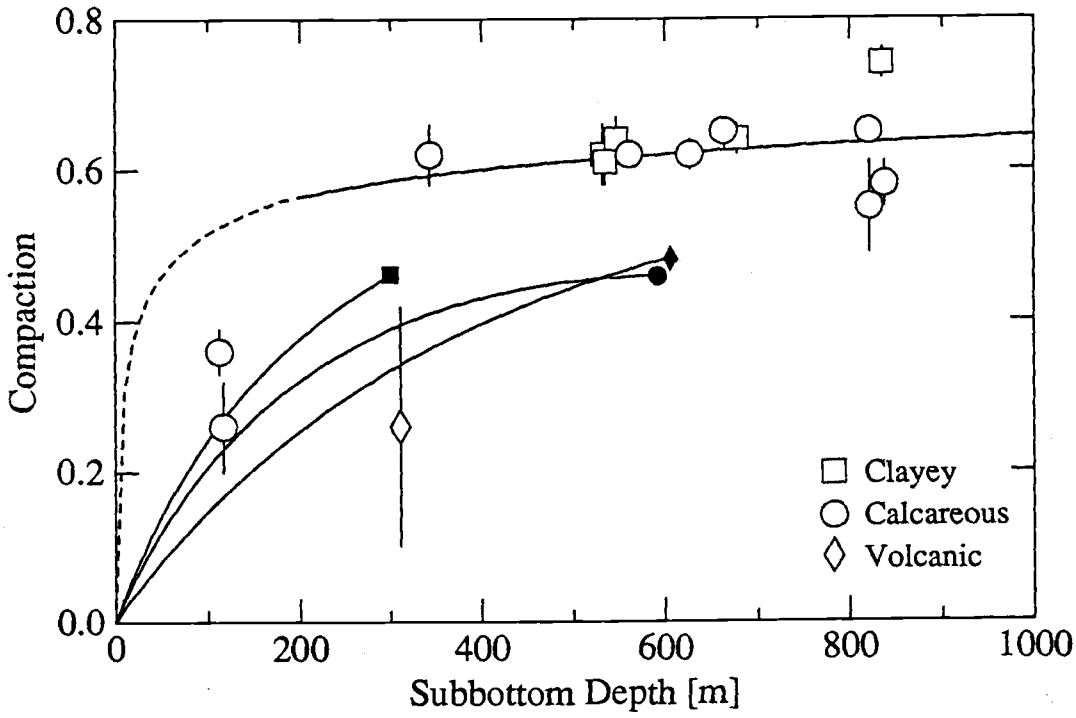

Figure 4.2. Estimates of sediment compaction versus depth. Comparison of compaction estimates for DSDP holes of this study and compaction models. The compaction estimates for the DSDP holes in Table 4.3 are shown with open symbols. Error bars represent 95% confidence intervals. The highest curve represents the compaction model of *Baldwin and Butler* [1985] for shales and limestone, assuming initial porosity values at 1 m. The top part (~200 m) of this curve is thought to be unrealistic. The three shorter curves are based on the regression equations of *Hamilton* [1976] (laboratory values) for pelagic clay (curve with a filled square on the end), calcareous sediment (filled circle), and terrigenous sediment (filled diamond).

4.4 PALEOLATITUDES

Several independent methods can be used to estimate paleolatitudes of sites for comparison to sedimentary paleomagnetic inclinations. First, it is possible to use the apparent polar wander (APW) path of the Pacific plate. This would be desirable since any variations in the long term non-dipole components of the magnetic field would be canceled out. The main problem with this approach is that the APW path for the Pacific plate is based on relatively few pole determinations, due to lack of land masses on the plate. The 66, 81, and 90 Ma poles of *Gordon* [1983] are all based on inversion of seamount magnetic anomalies. However, many APW poles have been derived by compilation of paleomagnetic results from both sediments and igneous rocks. For example, *Sager and Pringle* [1988, Table 2, p. 11,764] list eleven Cretaceous mean paleomagnetic poles, all of which include sedimentary paleomagnetic data, except their 95 Ma pole, which includes a pole for Makarov seamount used by *Gordon* [1983] in his 90 Ma mean pole.

Second, paleolatitude constraints can be obtained from sedimentary facies in cores, recording time of equatorial transit of sites. The upwelling which causes the high equatorial productivity is due to a change in the sign of the Coriolis force. Therefore, the latitude of this zone of increased biogenic sedimentation is forced to be at the equator by the rotation of the Earth.

Third, the Pacific plate has abundant hot spot tracks, and their movements in the hot spot reference frame are probably better constrained than for other plates. The hot spot reference frame is

desirable due to its continuity and smoothness back in time, although the hot spot tracks become more uncertain with age. One of the problems with the hot spot reference frame is that there may be movements between the hot spots and the rotation axis. Several studies have attempted to compare the hot spot reference frame to APW paths, the difference interpreted as true polar wander (TPW). The hot spot reference frame is better documented for the Pacific than other areas, where as the APW paths are better constrained for continental plates. Unfortunately, the relative movement between the Pacific and the rest of the world is ambiguous [e.g., *Duncan and Richards*, 1991], and data from the Pacific plate are commonly omitted in TPW studies. Eliminating data from whole regions of the Earth and systematic biases in paleomagnetic data, such as recording bias and non-dipole components of the field, may affect TPW estimates.

Andrews [1985] compared paleomagnetic data for the last 180 m.y. to plate motions in the hot spot reference frame. Her model suggests a TPW movement of about 10° at 30 to 50 Ma, then a rebound occurs and her TPW analysis for the late-Cretaceous results in insignificant effect on paleolatitudes for the sites of this study (<5° for 65 to 100 Ma). Using the same data, *Schneider and Kent* [1986] showed that much of the polar offset interpreted by *Andrews* [1985] as TPW, could be explained by long term non-dipole field. *Courtillot and Besse* [1987], and *Besse and Courtillot* [1991] defined a TPW path of about 10° towards the Atlantic at 10 to 50 Ma. Similar to *Andrews* [1985], their TPW path turns around and results in an insignificant paleolatitude anomaly for the Pacific sites of this study during the late-Cretaceous. Therefore, it

appears that TPW paleolatitude corrections may be omitted for this study. However, the strong TPW during the Tertiary in these models is not supported by equatorial transits of DSDP sites from the Pacific as we discuss later. The TPW path of *Livermore et al.* [1984] is similar, but is weaker in amplitude. Their path indicates that the amplitude of TPW has been about 5° for the last 90 m.y. This polar offset may not be significantly different from zero. Before 90 Ma there are discrepancies. *Gordon and Livermore* [1987] show that there has been approximately no true polar wander in the last 70 m.y., but before that time there are differences, and they mention that lower quality and quantity of data may be to blame. Magnitudes of possible TPW have been estimated from the Pacific plate. Igneous rock paleomagnetic inclinations from the Hawaiian-Emperor chain indicate that the Hawaiian hot spot has remained at a similar latitude (±5°) during the Tertiary [*Kono*, 1980*a*; *Sager*, 1984]. However, *Sager and Bleil* [1987] show paleolatitude discrepancies of data from the Pacific plate and interprete it as increased TPW between 40 and 70 Ma. On closer inspection it appears that this trend may partly be due to their choice of a hot spot model. Furthermore, their sediment paleomagnetic data for 30-50 Ma is from piston cores (~20 m depth); data for 50-70 Ma is based on hydraulic piston cored (HPC) DSDP Site 577 (~100 m depth); and data for 64-75 Ma is from deeply buried DSDP cores. Therefore, compaction-induced inclination shallowing may affect their TPW estimates.

For this study we compared hot spot paleolatitudes to paleolatitude estimates based on APW path, and saw no evidence of an appreciable difference. Furthermore, the hot spot model is in agreement with the

equatorial transit data summarized by *Sager* [1984]. Therefore, it seems that the true polar wander for the time and locations of this study may not be important, and we omit TPW corrections for this study.

We have chosen to estimate the paleolatitude of the sites in a hot spot reference frame defined by *Duncan and Clague* [1985], which includes probably the most up to date estimate for the Cretaceous period. The Pacific plate Euler rotation poles are listed in Table 4.4. In order to estimate a paleolatitude for a site we need the sediment age. We have transformed the depth to geological boundaries and intervals in the DSDP sediments to ages based on the geological time scale of *Harland et al.* [1982]. The Pacific plate motion in the hot spot reference frame is well constrained in the Tertiary. The constraints on the motions during the late-Cretaceous come from age progression of the Line Island chain, and Musician Seamounts [*Schlanger et al.*, 1984; *Duncan and Clague*, 1985]. Before 100 Ma the motion is constrained by the east-west trend of the Mid-Pacific Mountains, but age progression is poorly documented.

In order to estimate the uncertainty of the hot spot paleolatitude estimates, we compared the *Duncan and Clague* [1985] model to other independent estimates. First, we compare the paleolatitudes from *Duncan and Clague* [1985] to a more recent hot spot model of *Watts et al.* [1988]. The model of *Watts et al.* [1988] is based on a careful study of the Louisville Ridge, but extends only to 68 Ma. We compare the paleolatitude of the sites in Table 4.1 as predicted from these two hot spot models at the Tertiary/Cretaceous boundary at 65 Ma. The comparison is shown in Figure 4.3. The difference in predicted

paleolatitude of these two hot spot models is about ±2° at 65 Ma, and neither model gives consistently higher latitudes.

In a second test we compare the paleolatitude estimates of the hot spot model to the APW poles at 66 Ma, 81 Ma, and 90 Ma defined by *Gordon* [1983]. The comparison is shown in Figure 4.4. The difference appears to be about ±4°, comparable to the uncertainty in the APW paleolatitudes. Note that the paleolatitudes at 66 Ma plot slightly above the diagonal and the 81 Ma paleolatitudes slightly below.

In a third assessment, we compare the time of equatorial passage of several DSDP sites to the prediction of the hot spot model. In Table 4.5 we show the age estimates of equatorial transits of DSDP sites, taken from *Sager* [1984, Table 3, p. 6281]. In the same table we show the predicted paleolatitudes of the hot spot model (latitude range corresponds to age range). This data is shown in Figure 4.5. Of the 15 sites, seven are predicted to cross the equator during the estimated age range, and 14 of them come within 2.5° of the equator. Only DSDP site 199 shows disagreement with the hot spot paleolatitudes. We note that these data indicate less than 5° TPW to or from the Pacific in the last 70 m.y. contrary to the TPW paths of *Andrews* [1985], and *Besse and Courtillot* [1991].

Errors in sediment dating and in dates used to construct the hot spot model will affect the paleolatitude estimates. To account for paleolatitude errors inherent in the hot spot model, due to age uncertainties, possible true polar wander, and long term non-dipole geomagnetic field we take the paleolatitude errors to be probably less than ±5°.

The expected inclination I_H of the hot spot paleolatitudes λ is then calculated from the dipole equation

$$I_H = \arctan [2 \tan \lambda] \qquad (4.7)$$

and the inclination uncertainty is calculated corresponding to a $\pm 5^\circ$ uncertainty in the paleolatitude. Table 4.6 summarizes the age estimates and the calculated paleolatitudes in the hot spot reference frame.

TABLE 4.4. Rotation Poles for the Pacific Plate over a Hot Spot Reference Frame

Age, Ma	Euler Rotation Pole		
	Latitude, deg N	Longitude, deg E	Rotation Angle, deg ccw
	Duncan and Clague [1985]:		
0-42	68.0	–75.0	34.0
42-65	17.0	–107.0	14.0
65-74	22.0	–95.0	7.5
74-100	36.0	–76.0	15.0
100-150	85.0	165.0	24.0
	Watts et al. [1988]:		
0-43	65.0	–60.0	33.0
43-68	15.0	–100.0	14.0

From [*Duncan and Clague*, 1985, Table IV, p. 113; *Watts et al.*, 1988, Figure 26, p. 3076].

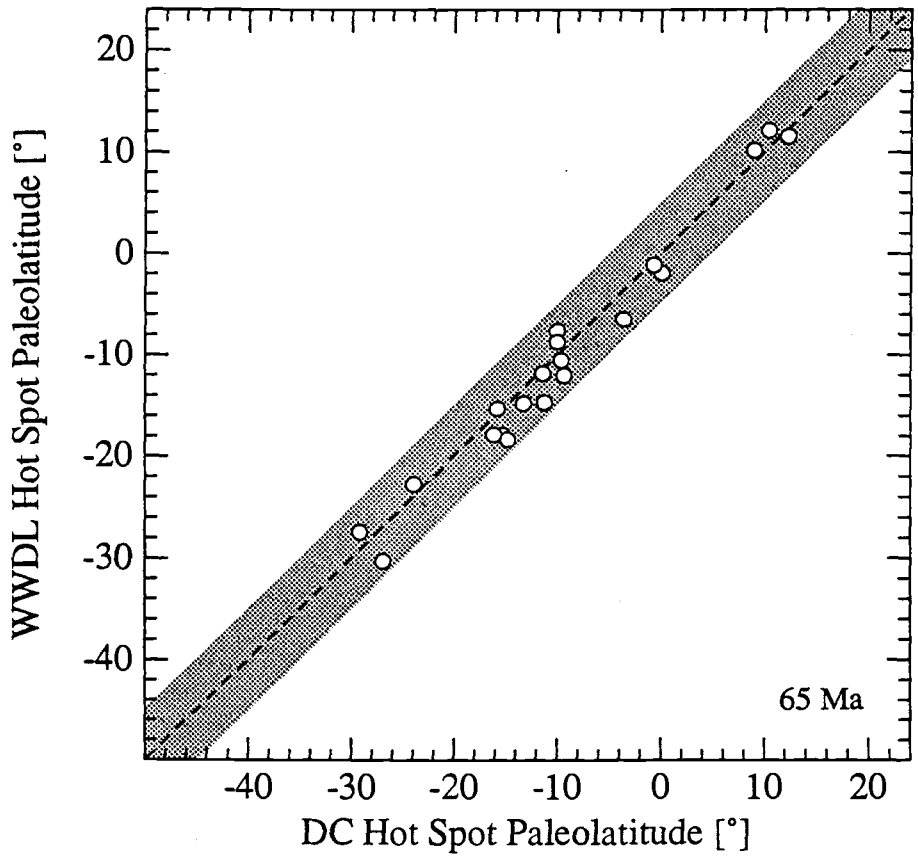

Figure 4.3. Paleolatitudes of two hot spot models compared. The predicted paleolatitudes of the 20 DSDP sites in Table 4.1 are compared for the model of *Duncan and Clague* [1985] (DC) and *Watts et al.* [1988] (WWDL) at 65 Ma. The rotation poles are listed in Table 4.4. This graph indicates good agreement, but paleolatitude discrepancies of about ±2° are common.

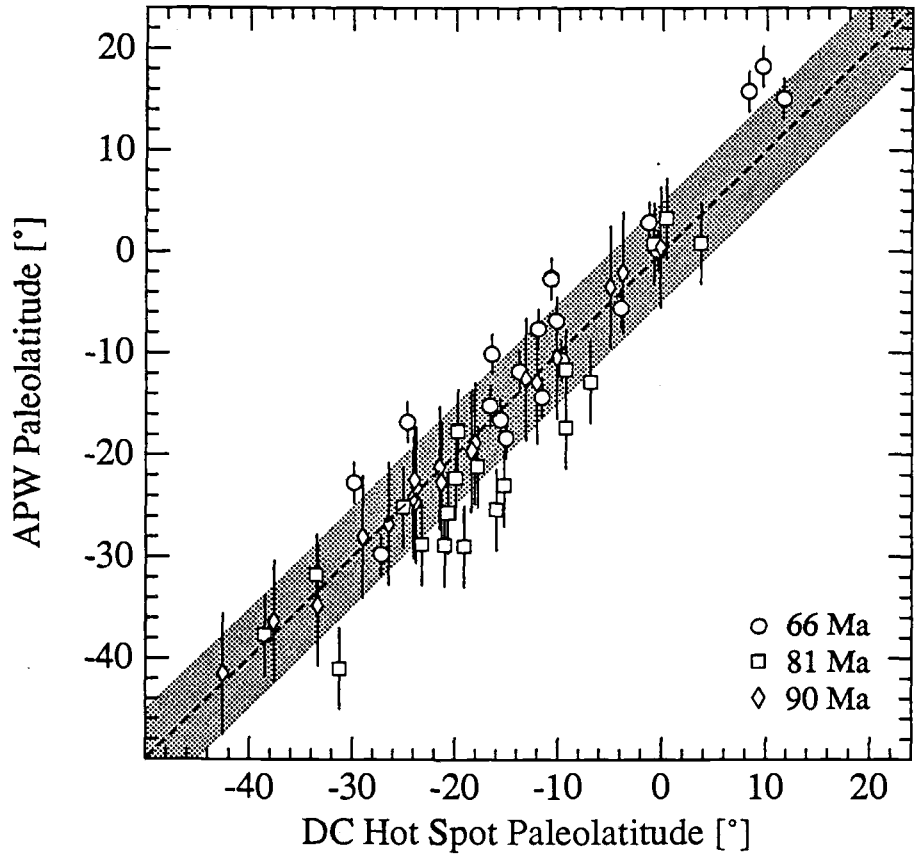

Figure 4.4. Apparent polar wander path compared to hot spot model. Paleolatitude of the hot spot model of *Duncan and Clague* [1985] (DC) is compared to the paleolatitudes predicted by the 66, 81 and 90 Ma APW poles of *Gordon* [1983]. The approximate 95% confidence intervals of the APW paleolatitudes are shown. Generally there is good agreement, but discrepancies of about ±4° are common.

TABLE 4.5. Equatorial Transits of DSDP Sites.

DSDP Leg	DSDP Site	Present Location Latitude, deg N	Present Location Longitude, deg E	Equatorial Transit Age Range *, Ma	Hot Spot Paleo-latitude Range, deg N	
8	69	6.00	–152.87	22–32	–0.2	–2.8
8	70	6.33	–140.36	20–32	1.2	–1.4
8	71	4.47	–140.32	12–24	1.3	–1.6
16	161	10.67	–139.95	24–34	4.6	2.5
16	163	11.24	–150.29	37–49	1.5	–0.5
17	165	8.18	–164.86	30–38	–0.7	–2.9
17	166	3.76	–175.08	12–16	0.1	–1.1
17	167	7.07	–176.83	22–32	0.4	–2.6
17	171	19.13	–169.46	67–76	–0.8	–5.0
20	199	13.51	156.17	56–76	–5.4	–17.4
32	313	20.18	–170.95	69–76	–1.2	–4.4
33	315	4.17	–158.53	14–24	0.0	–2.8
62	463	21.35	174.67	68–72	–2.5	–5.0
85	572	1.43	–113.84	3–6	0.9	0.3
85	574	4.21	–133.33	12–22	1.3	–0.9

* Equatorial transit ages are from *Sager* [1984].

Figure 4.5. Comparison of equatorial transit of sites and hot spot paleolatitudes. The data for this figure is shown in Table 4.5. Circles centered above the line segments show the present latitude of the DSDP sites. Each line segment represents the hot spot paleolatitude of a site versus age over a short are range. The age range indicates the age of equatorial transit of sites based on sedimentary facies in the cores. We note that there is excellent agreement between the hot spot model and the sedimentary facies data.

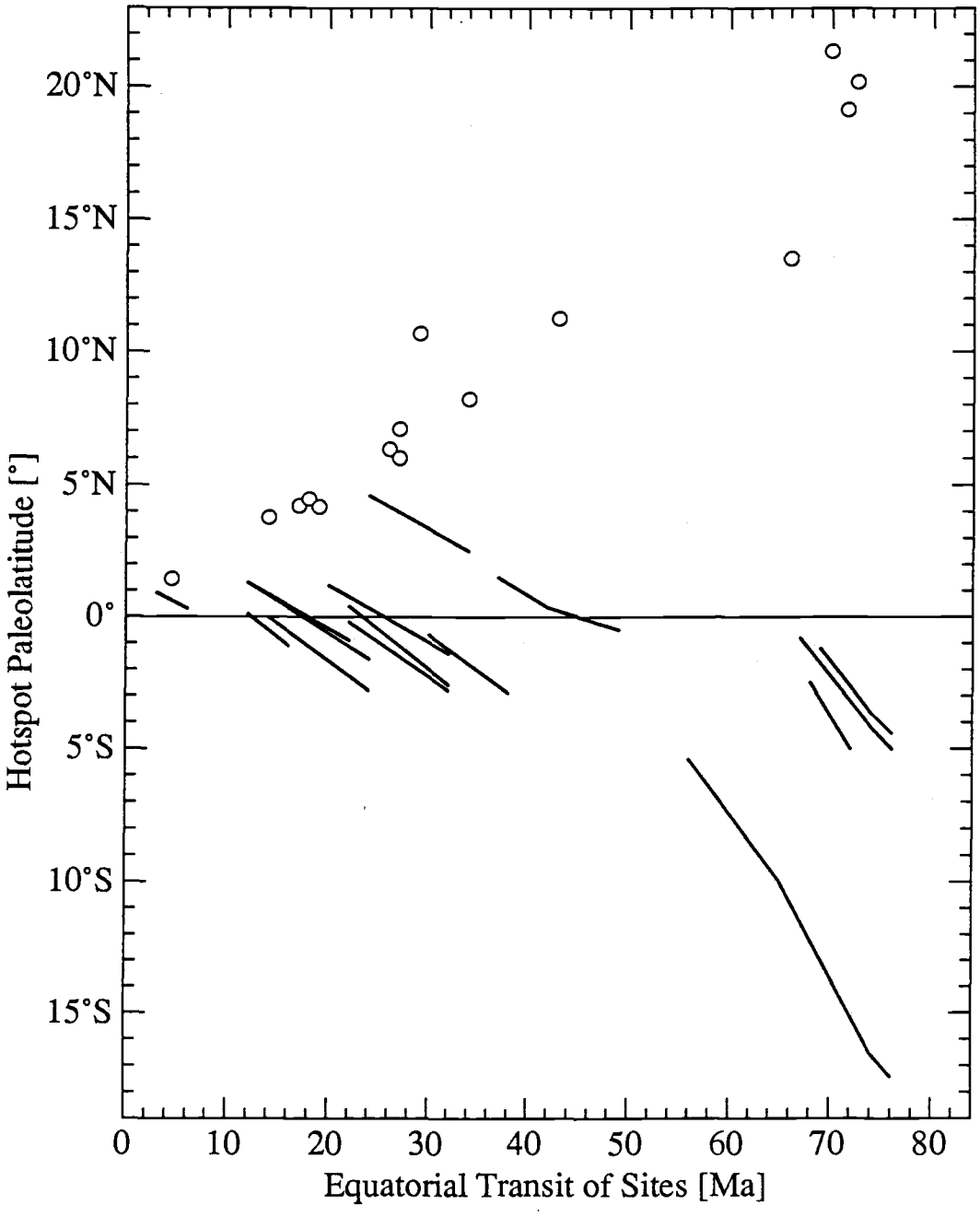
20°N
15°N
10°N
5°N
0°
5°S
10°S
15°S
Hotspot Paleolatitude [°]
0
10
20
30
40
50
60
70
80
Equatorial Transit of Sites [Ma]

Figure 4.5.

TABLE 4.6. Estimates of Hot Spot Paleolatitude and Initial Inclination for DSDP Sediments.

Hole	Data Depth, m	Age, Ma	Paleolatitude, deg N	Northward Velocity, deg m.y.$^{-1}$	Estimate of Initial Inclination*, deg
DSDP 167	832	83	–21.4	0.38	–38.1 ± 7.2
DSDP 167	(880)	115	–28.2	0.04	–47.0 ± 6.0
DSDP 171	297	88	–9.4	0.36	–18.3 ± 9.2
DSDP 315A (C)**	830	71	–13.1	0.30	–25.0 ± 8.6
DSDP 315A (L)**	827	70	–12.8	0.30	–24.4 ± 8.7
DSDP 316	(640)	70	–16.2	0.27	–30.2 ± 8.1
DSDP 317A	621	110	–35.8	0.04	–55.3 ± 5.0
DSDP 288A	(880)	92	–43.5	0.44	–62.2 ± 4.1
DSDP 289	(1235)	115	–42.6	0.03	–61.5 ± 4.2
DSDP 462	526	84	–26.3	0.45	–44.7 ± 6.3
DSDP 462A	532	87	–27.7	0.45	–46.4 ± 6.1
DSDP 463	562	114	–17.8	0.03	–32.7 ± 7.8
DSDP 465A	343	98	–3.5	0.41	–7.0 ± 9.8
DSDP 577	112	65	+9.0	0.73	+17.6 ± 9.3
DSDP 577A	116	66	+8.3	0.73	+16.3 ± 9.4
DSDP 585	550	93	–25.3	0.46	–43.4 ± 6.5
DSDP 585A	666	102	–28.6	0.03	–47.5 ± 5.9

* The inclination is the GAD-inclination of the hot spot paleolatitude, and the effect on the inclination of a ±5° latitude uncertainty is calculated.
** Separate estimates are for the claystone (C) and limestone (L) intervals in hole 315A.

4.5 CRETACEOUS DSDP SEDIMENTARY SECTIONS

The DSDP data base [*DSDP CD-ROM*, 1989] was searched for Cretaceous sections from the Pacific plate. Of the 1112 holes in the data base, paleomagnetic studies are listed for 276 holes. Of these 276, 117 holes are from the Pacific ocean. The data base includes only 17 holes from the Pacific plate containing Cretaceous sediments that have been studied for paleomagnetism. These are DSDP holes 66, 164, 165A, 166, 167, 169, 170, 171, 315A, 317A, 462, 462A, 463, 465A, 578, 585, and 585A. In addition, we consider estimates from holes 199, 288A, 289, 316, 577, and 577A which are not listed in the DSDP data base but have been published elsewhere [*Hammond et al.*, 1975; *Cockerham*, 1979; *Bleil*, 1985; *Sager and Bleil*, 1987; *Tarduno*, 1990].

Of the available data from these 23 DSDP holes we omit the data from the following seven holes: DSDP hole 66 contains only four inclinations of Turonian to Cenomanian age (core 9: 187-192 m) [*Winterer et al.*, 1971; *Sclater and Jarrard*, 1971]. Due to the few data points and short interval we omit these data. We note that *Peirce* [1976] used additional data from hole 66 by assuming that cores 6, 7, 8 and 9 are all of Cretaceous age. DSDP hole 164 contains 20 inclinations of Cretaceous age (80-203 m). We exclude these data because polarity stratigraphy is highly uncertain and the age is so ambiguous that even position of the long Cretaceous normal is not known [*Jarrard*, 1973]. DSDP hole 165A contains four inclinations of upper-Campanian age (291-293 m) which should represent normal polarity in a 1.11 m long interval [*Jarrard*, 1973]. Due to the short interval and few data points

we exclude this data from further study. *Sager and Bleil* [1987] show paleolatitude estimates for DSDP 165 for 70-78 Ma. Their estimate indicates shallower inclination than expected. We do not have access to the number of samples that they used or the depths, and therefore, we do not consider these estimates further for this study. DSDP hole 169 contains seven inclinations of Campanian to Cenomanian age from a 0.38 m thick section (200-202 m) [*Jarrard*, 1973]. Due to the short section we omit these data. DSDP hole 170 contains 25 very scattered inclinations of middle to early-Campanian (106-122 m) [*Jarrard*, 1973], probably representing either anomaly 33n or 33r or both. Due to the scattered directions it is impossible to identify polarities in the data and DSDP 170 is not considered further in this study. *Sager and Bleil* [1987] show paleolatitude estimates from DSDP hole 199 for 62-67 Ma. Their low latitude estimate indicates shallower inclination than expected, but we do not consider these estimates because no information is given on number of samples or measure of spread. DSDP hole 578 may have penetrated 0.81 m of Cretaceous sediments (core 20) [*Heath et al.*, 1985*a*], but dating was poor, and the section contains too few paleomagnetic data to be useful, in addition to the possibility of polarity mixing. Therefore, we do not analyze the Cretaceous data from DSDP hole 578 in this study.

Following is a description of the 16 DSDP holes studied further in the current analysis along with description of the data processing and some discussion of our estimates. As it turns out, we reject data from DSDP hole 166, because of noise problems. In addition, data from four of the

holes cannot constrain the parameter a due to their low paleolatitude (less than ±10°). These are DSDP holes 171, 465A, 577, and 577A.

4.5.1 DSDP Hole 166

Hole 166 was cored during leg 17 in 1971 [*Winterer et al.*, 1973]. Paleomagnetic samples from 7 to 292 m, and demagnetized Cretaceous inclinations from 221-292 m were studied by Richard Jarrard. Apart from one section near the bottom (291.6-291.8 m), most of the data are from pelagic clay between 221-232 m. The published data [*Jarrard*, 1973, Table 2, p. 369-370] include 31 inclinations from this zone. Biostratigraphy of hole 166 shows late-Albian to Cenomanian age (91-105 Ma) at 202-272 m. Picking the average age (98 Ma) we estimate the hot spot paleolatitude to be $\lambda = -29.2°$ (the associated dipole inclination would be $I_H = -48.2° \pm 5.9°$) and northward movement of 0.33° m.y.$^{-1}$. This indicates that the paleomagnetic data are from the central part of the Cretaceous long normal. The "cleaned" inclinations are very scattered in a nearly uniform distribution between –77° and +78°, 20 samples with positive inclinations and 11 negative. At first glance these data appear to be very noisy, however since this data set has previously been used to calculate paleolatitudes [e.g., *Cockerham*, 1979; *Gordon*, 1990] some further discussion is needed.

First, we calculate the mean assuming that these samples represent the Cretaceous long normal, resulting in $I = +39.5° \pm 23.1°$, and angular standard deviation $\theta_{63} = 55.6°$ indicating a northern hemisphere location, but extreme uncertainty. Another possibility would be to assume that the age of the remanence is wrong and that the data represents both

polarities. Average of the absolute values results in $I = 44.1° \pm 9.9°$, still with high scatter $\theta_{63} = 29.3°$, and a third of the inclinations is over 20° away from the mean. This estimate is similar to the value obtained by *Cockerham* [1979] $I = -44.2°$ ($\lambda = -25.9°$) and used by *Gordon* [1990]. In the following discussion we use the value of *Cockerham* [1979] and estimate the 95% confidence interval of his mean as double the standard error ($I = -44.2° \pm 4.8°$).

It is difficult to estimate the compaction in this interval since the calculated grain density is about 5000 kg m^{-3} [*Winterer et al.*, 1973, Appendix B, p. 113] and our assumptions in calculating compaction may break down. However, we estimate that the compaction is probably within $\Delta V = 0.3 \pm 0.2$ ($N = 3$). These rough estimates ($I_P = -44.2° \pm 4.8°$, $I_H = 48.2° \pm 5.9°$, and $\Delta V = 0.3 \pm 0.2$) indicate that the parameter $a = 0.4 \pm 0.9$, and the uncertainty in the parameter a comes equally from the observed inclination, initial inclination and the compaction estimate. However, the extremely high scatter in the paleomagnetic data indicates strongly that the data set is contaminated with noise, and we reject the data from DSDP hole 166 from further discussion in this study.

4.5.2 DSDP Hole 167

Hole 167 was cored during leg 17 in 1971 [*Winterer et al.*, 1973]. Paleomagnetic samples were obtained between 104 and 1160 m subbottom depth, including demagnetized Cretaceous specimens from 787-864 m [*Jarrard*, 1973]. The Cretaceous section is composed of nannofossil chalk, nannofossil limestone and marly limestone. Of the

published paleomagnetic data [*Jarrard*, 1973, Table 2, p. 370-371], we deleted two possibly transitional samples (823.92 and 824.39 m). This leaves 46 stable inclinations from limestone, with mean inclination of $-23.2° \pm 5.1°$, using Kono statistics [*Kono*, 1980*b*]. This is comparable to previous estimates of $I = -21.4°$ ($N = 48$) [*Peirce*, 1976], and $I = -22.1°$ ($\lambda = -11.5°$) [*Cockerham*, 1979]. The normal polarity inclinations are shallower ($-17.1° \pm 4.9°$) than the reversed ($+31.3° \pm 9.0°$) which could be attributed to a slight persistent present field overprint. Our mean inclination is slightly steeper than the estimates of *Tarduno* [1990] (Campanian $I = -15.7° \pm 3.6°$, and Turonian-Cenomanian $I = -20.0° \pm 6.3°$). Recently, *Tarduno et al.* [1989] obtained additional samples from Albian-Hauterivian (98-131 Ma) interval of limestone from DSDP hole 167 (861-975 m subbottom depth). The mean inclination of this deeper interval was $I = -29.1° \pm 2.0°$ ($\theta_{63} = 13.3°$, $N = 95$) [*Tarduno et al.*, 1989].

From the depth range of the paleomagnetic data and limestone intervals a total of 6 water content data points were found in the DSDP data base [*DSDP CD-ROM*, 1989]. The average is shown in Table 4.3. This was used to estimate sediment compaction of 0.55 ± 0.06. No density-porosity data were found for the deeper section, studied by *Tarduno et al.* [1989].

Biostratigraphy of Hole 167 shows late-Campanian (73-78 Ma) at 750-769 m, early-Campanian (78-83 Ma) at 777-824 m, Santonian to Coniacian (83-88.5 Ma) at 827-836 m, late-Turonian (88.5-90 Ma) at 841-843 m, Cenomanian (91-97.5 Ma) at 851-853 m, and early-Cenomanian to late-Albian (95-105 Ma) at 860-901 m [*Winterer et al.*,

1973; *Harland et al.*, 1982]. The paleomagnetic data includes a reversed interval between 823.8-831.4 m, which fits well in age to anomaly 33r (78.53-82.93 Ma). This indicates that the paleomagnetic data used for this study is within 78-105 Ma and the age of the average depth 831.82 m is about 83 Ma. The expected paleolatitude at 83 Ma is $\lambda = -21.4°$ and northward motion 0.38° m.y.$^{-1}$. *Tarduno et al.* [1989] revised the original biostratigraphy below 850 m, and *Tarduno* [1990] estimated mean age of the data from 861-975 m to be 115 Ma. The expected hot spot paleolatitude at 115 Ma is $\lambda = -28.2°$ and northward motion 0.04° m.y.$^{-1}$.

The estimates of this study result in the parameter $a = 0.82 \pm 0.37$, and the uncertainty in a comes equally from the observed inclination and initial inclination. We cannot estimate the parameter a for the deeper part of the hole, studied by *Tarduno* [1990] since we lack information on compaction. However, taking the compaction value to be $\Delta V = 0.6 \pm 0.1$, results in $a = 0.80 \pm 0.24$. This value is very similar to the previous one, but is not used for this study.

4.5.3 DSDP Hole 171

Hole 171 was cored during leg 17 in 1971 [*Winterer et al.*, 1973]. Paleomagnetic samples were obtained from 90 to 330 m subbottom depth, including demagnetized Cretaceous specimens from 287-330 m [*Jarrard*, 1973]. The Cretaceous section is composed of volcanic sandstones and siltstones. From the published paleomagnetic data [*Jarrard*, 1973, Table 2, p. 372-373] we obtained 16 stable inclinations, with mean inclination of $-15.4° \pm 4.4°$, using Kono statistics [*Kono*,

1980*b*]. This is comparable to a previous estimate of $I = -13.1°$ [*Peirce*, 1976]. John Tarduno analyzed 5 samples from 316-330 m depth and obtained the inclination $I = -5.7° \pm 11.3°$ ($\theta_{63} = 12.8°$), and he suspects that previously determined reversals may be artifacts of drilling disturbance [*Tarduno*, 1990, p. 101].

From the depth range of the paleomagnetic data no density-porosity information was found in the DSDP data base [*DSDP CD-ROM*, 1989]. *Winterer et al.* [1973, Appendix B, p. 300-301] give ranges of density and porosity of sections, and the averages are shown in Table 4.3. These were used to estimate sediment compaction of 0.26 ± 0.16.

Biostratigraphy of Hole 171 shows late-Campanian (73-78 Ma) at 269-287 m, early-Santonian to Campanian (73-87.5 Ma) at 287-292 m, Coniacian (87.5-88.5 Ma) at 297-300 m, and Turonian (88.5-91 Ma) at 306-329 m [*Winterer et al.*, 1973; *Harland et al.*, 1982]. The paleomagnetic data includes a reversed interval between 287.0-288.2 m, which fits well in age to anomaly 33r (78.53-82.93 Ma). This indicates that the paleomagnetic data is within 73-91 Ma and average age of about 88 Ma. The expected paleolatitude in the hot spot reference frame at 88 Ma is $\lambda = -9.4°$ moving northward at $0.36°$ m.y.$^{-1}$.

These estimates can not constrain the parameter a and significant uncertainty comes from all estimates.

4.5.4 DSDP Hole 288A

Hole 288A was cored during leg 30 in 1973 [*Andrews et al.*, 1975]. Paleomagnetic samples from cores 15-30 (approximately 742-990 m) were studied by John Tarduno. This interval is composed of nannofossil

chalk and limestone. *Tarduno* [1990, Table 1, p. 101] estimates the inclination $I = -41.6° \pm 2.6°$ ($\theta_{63} = 11.6°$, $N = 41$) for the younger and larger subset. He estimates the average age to be 92 Ma corresponding to approximately 880 m depth. We do not have access to the original data but accept these estimates.

From the depth range of the paleomagnetic data and chalk/limestone intervals we located 19 water content and 17 porosity and density determinations in the DSDP data base [*DSDP CD-ROM*, 1989]. These were used to estimate sediment compaction $\Delta V = 0.58 \pm 0.03$.

The expected paleolatitude for site 288 at 92 Ma is $\lambda = -43.5°$ moving northward at 0.44° m.y.$^{-1}$. These estimates result in the parameter $a = 0.92 \pm 0.17$. *Tarduno* [1990] gives a second estimate of inclination for this hole corresponding to age 113 Ma. The a value for this deeper data does not change $a = 0.91 \pm 0.17$, but is not used in this study.

4.5.5 DSDP Hole 289

Hole 289 was cored during leg 30 in 1973 [*Andrews et al.*, 1975]. Sedimentary paleomagnetic samples from 923 to 1235 m subbottom depth were studied by Stephen Hammond, Loren Kroenke and Fritz Theyer. The paleomagnetic data contains 9 samples of Cretaceous age [*Hammond et al.*, 1975, Table 1, p. 416]. This part of the hole consists of limestone. However, the Cretaceous data are separated by about 40 m.y. hiatus, and rapid movement of the plate in that period forces splitting of the data into 5 limestone samples of Maastrichtian age and 4 Aptian samples. The younger data have a mean inclination of $I = -18.9° \pm 2.1°$. *Tarduno* [1990] obtained additional samples from the Aptian

sequence, with average inclination $I = -37.6° \pm 5.8°$ ($\theta_{63} = 12.1°$, $N = 11$), and age estimate of 115 Ma.

The five density-porosity data points in the Maastrichtian interval [*DSDP CD-ROM*, 1989] indicate a compaction of $\Delta V = 0.58 \pm 0.09$. The compaction estimate for the older part of the data is based on only 3 density-porosity determinations, $\Delta V = 0.64 \pm 0.19$. The average depth of 1170 m corresponds to middle-Maastrichtian, we choose 68 Ma. The hot spot paleolatitude at 68 Ma is $\lambda = -26.0°$, and $\lambda = -42.6°$ at 115 Ma.

For the 68 Ma age estimate $a = 1.12 \pm 0.24$. Similarly, $a = 0.91 \pm 0.35$ at 115 Ma. However, due to the abnormally low angular standard deviation of the inclinations at 68 Ma ($\theta_{63} = 2.3°$) we suspect that these samples are too few ($N = 5$) for adequate portrayal of average geomagnetic behavior. Therefore, we only use the older data from DSDP hole 289 in further discussions of this study.

4.5.6 DSDP Hole 315A

Hole 315A was cored during leg 33 in 1973 [*Schlanger et al.*, 1976]. Paleomagnetic samples from 778 to 914 m subbottom depth were studied by Robert Cockerham and Richard Jarrard. The lithology in this interval fluctuates between clayey nannofossil limestone and nannofossil claystone. We have split the data in two groups (limestone and claystone) according to these classifications [*Schlanger et al.*, 1976]. Of the published paleomagnetic data [*Cockerham and Jarrard*, 1976, Table 2, p. 637-638], we extracted the most reliable (their A < 5°) inclinations from 807 to 850 m where dense sampling shows clear correspondence to the magnetic polarity time scale. From the data we deleted two very

steep transitional samples (817.04 and 817.06 m), and brief polarity chrons or excursions (819.17, 823.55-824.81, 837.20-837.22 m). Also sandstone samples (842-843 m, and 847-848 m) were deleted. A total of 17 samples were omitted. This leaves 25 stable inclinations from claystone, and 18 from limestone intervals, with mean inclination (inverting the reversed directions) of $-17.0° \pm 2.8°$ (claystone), and $-16.6° \pm 3.4°$ (limestone), using Kono statistics [*Kono*, 1980*b*]. This is comparable to the original median estimate of $I = -17.8°$ ($N = 82$) [*Cockerham and Jarrard*, 1976, Table 5, p. 647], and $I = -18.1°$ ($\lambda = -9.3°$) [*Cockerham*, 1979]. We note that there appears to be no inclination difference between these two lithological groups. The calcium carbonate content is about 50% in these intervals and there appears to be insignificant differences between intervals of "clayey limestone" and "limey claystone". We have also calculated the mean inclination of the claystone and limestone together $I = -16.9° \pm 2.1°$ ($N = 43$). The difference between normal polarity ($-15.9° \pm 2.3°$) and reversed polarity ($+20.9° \pm 4.0°$) is not significant. *Tarduno* [1990] gives slightly steeper inclination $I = -20.5° \pm 2.6°$ ($\theta_{63} = 9.9°$, $N = 30$) for an older part of the hole (78 Ma). We do not incorporate these additional data, but note that they are consistent with the current analysis.

From the depth range of the paleomagnetic data and intervals characterized as claystone 7 water content data were found in the DSDP data base [*DSDP CD-ROM*, 1989]. Additional porosity and density data are from *Schlanger et al.* [1976, Table 3, p. 50-52]. The averages are shown in Table 4.3, and are used to estimate sediment compaction,

$\Delta V = 0.74 \pm 0.02$. From intervals characterized as limestone 16 water content data were found in the DSDP data base [*DSDP CD-ROM*, 1989]. Additional porosity and density data are from *Schlanger et al.* [1976, Table 3, p. 50-52]. The averages are shown in Table 4.3, and are used to estimate sediment compaction of 0.65 ± 0.01.

Biostratigraphy of Hole 315A shows the Tertiary/Cretaceous boundary (65 Ma) between 780-788 m, middle-Maastrichtian (67-71 Ma) at 787-820 m, lower-Maastrichtian to upper-Campanian (71-76 Ma) at 820-843 m, middle Campanian to lower-Campanian (76-83 Ma) at 844-912 m [*Schlanger et al.*, 1976; *Harland et al.*, 1982]. The paleomagnetic data include a clear reversal boundary at 817.05 m that fit very well in age to boundary 31r/32 (69.48 Ma), the data also include the short reversed intervals 32.1r (69.72-69.96 Ma) at 824 m and 32r (71.40-72.06 Ma) between 836.9-837.7 m. The magnetostratigraphy fits very well to the biostratigraphy and indicates that the paleomagnetic data is within 67-80 Ma with average age of 71 Ma (claystone) and 70 Ma (limestone). The expected paleolatitude for the claystone data set is $\lambda = -13.1°$ in the hot spot reference frame and $\lambda = -12.8°$ for the limestone data. The northward movement of the site at this time was $0.30°$ m.y.$^{-1}$.

These estimates result in insignificant differences between the two groups the parameter $a = 0.47 \pm 0.42$ (claystone) and $a = 0.53 \pm 0.51$ (limestone), and the uncertainty in a comes mainly from the initial inclination due to relatively low paleolatitude.

4.5.7 DSDP Hole 316

Hole 316 was cored during leg 33 in 1973 [*Schlanger et al.*, 1976]. The original paleomagnetic data was not available for this study. However, *Cockerham* [1979] published a mean paleocolatitude indicating that the inclination is $I = -18.3° \pm 4.4°$. We use the estimate of *Tarduno* [1990] for cores 17-26 (approximately 571-730 m) with mean age of 70 Ma: $I = -17.1° \pm 1.7°$ ($\theta_{63} = 13.9°$, $N = 132$). The lithology is predominantly of nannofossil-foraminiferal chalk and limestone in this interval.

From the depth range of the Cretaceous section and intervals characterized as limestone a total of 42 water content data were found in the DSDP data base [*DSDP CD-ROM*, 1989]. This was used to estimate sediment compaction of 0.65 ± 0.01.

The hot spot paleolatitude at 70 Ma is $\lambda = -16.2°$ and northward movement $0.27°$ m.y.$^{-1}$. These estimates result in the parameter $a = 0.73 \pm 0.30$, and the uncertainty in a comes mainly from the initial inclination due to low paleolatitude.

4.5.8 DSDP Hole 317A

Hole 317A was cored during leg 33 in 1973 [*Schlanger et al.*, 1976]. Paleomagnetic samples from 577 to 673 m subbottom depth were studied by Robert Cockerham and Richard Jarrard. Additional samples were analyzed by Robert Cockerham and James Hall. The lithology in this interval is mainly nannofossil- nannofossil micritic chalk and limestone. Of the published paleomagnetic data [*Cockerham and Jarrard*, 1976, Table 2, p. 638-639], we deleted two reversed samples (577.34 and

637.25 m), and eight samples from non-calcareous intervals (584.94-584.96 m, 602.65-602.67 m, 653.44 m, and 669-673 m). This leaves 23 stable inclinations of a single polarity from limestone, with mean inclination of –46.8° ± 5.6°, using Kono statistics [*Kono*, 1980*b*]. This is comparable to the original median estimate of I = –48.3° (N = 33) [*Cockerham and Jarrard*, 1976, Table 5, p. 647], mean estimate for carbonate sediments I = –46.7° (N = 59) [*Cockerham and Hall*, 1976, Table 3, p. 4219], and I = –45.7° (λ = –27.1°) [*Cockerham*, 1979].

From the depth range of the paleomagnetic data and intervals characterized as chalk or limestone a total of 21 water content data were found in the DSDP data base [*DSDP CD-ROM*, 1989]. Additional 19 porosity and density data were found [*Schlanger et al.*, 1976, Table 4, p. 174]. The averages are shown in Table 4.3. These were used to estimate sediment compaction of 0.62 ± 0.02.

Biostratigraphy of Hole 317A shows Maastrichtian (65-73 Ma) at 555-569 m, Campanian or younger (73-83 Ma) at 576-584 m, Santonian to Albian (83-113 Ma) at 592-614 m, and possibly Aptian to Barremian (113-125 Ma) at 620-673 m [*Schlanger et al.*, 1976; *Harland et al.*, 1982]. The basement was reached at 910 m and was dated by the K-Ar method at 110-120 Ma [*Lanphere and Dalrymple*, 1976]. This indicates that the paleomagnetic data represents some part of 73-125 Ma and the average age is probably between 100 and 120 Ma. However, accurate time scale is not critical since this site experienced negligible northward movement in this time period. We therefore take average age to be 110 Ma and paleolatitude λ = –35.8° and northward motion is 0.04° m.y.$^{-1}$.

These estimates result in the parameter $a = 0.42 \pm 0.33$, and the uncertainty in a comes equally from the observed inclination and initial inclination.

4.5.9 DSDP Hole 462

Hole 462 was cored during leg 61 in 1978 [*Larson et al.*, 1981]. Paleomagnetic samples from 513 to 552 m subbottom depth were studied by Maureen Steiner. The dominant lithology in this interval is claystone and zeolitic claystone. Of the published data [*Steiner*, 1981, Table 1, p. 714], inclinations from an excursion between 518.06-518.28 m depth were omitted in this study and also two limestone samples (518.81 and 520.04 m). This leaves 19 stable inclinations from claystone, with mean inclination (inverting the reversed directions) of $-12.8° \pm 3.9°$, using Kono statistics [*Kono*, 1980*b*]. This estimate is between the original arithmetic means; lower-Campanian $I = -11.1°$ ($N = 15$, $\lambda = -5.6°$), and Santonian-Cenomanian $I = -14.9°$ ($N = 6$, $\lambda = -7.6°$) [*Steiner*, 1981, Table 2, p. 716]. The normal polarity inclinations are slightly steeper ($-13.9° \pm 4.7°$) than the reversed inclinations ($+10.8° \pm 7.2°$). This difference is insignificant and may be partly due to rapid northward movement and age difference of the data sets.

From the depth range of the paleomagnetic data and intervals characterized as claystone a total of 11 water content and 10 density and porosity data were found in the DSDP data base [*DSDP CD-ROM*, 1989]. The averages are shown in Table 4.3. These were used to estimate sediment compaction of 0.62 ± 0.04.

Biostratigraphy of Hole 462 shows lower-Campanian (79-83 Ma) between 513-521 m, Santonian to Coniacian (86-88 Ma) at 531-536 m, and Cenomanian to late-Albian (91-103 Ma) at 549-551 m [*Larson et al.*, 1981; *Harland et al.*, 1982]. The paleomagnetic data includes a clear reversed zone between 516.5-524.3 m whose age corresponds to chron 33r (78.53-82.93 Ma). This fits very well to the biostratigraphy and indicates that the paleomagnetic data are within the time period 77-103 Ma with average age of 84 Ma. The hot spot paleolatitude at 84 Ma is $\lambda = -26.3°$ and northward movement 0.45° m.y.$^{-1}$.

These estimates result in the parameter $a = 1.24 \pm 0.16$, and the uncertainty in a comes equally from the observed inclination and initial inclination.

4.5.10 DSDP Hole 462A

Hole 462A was cored during leg 61 in 1978 [*Larson et al.*, 1981]. Paleomagnetic samples from 515 to 565 m subbottom depth were studied by Maureen Steiner. The dominant lithology in this interval is claystone and zeolitic claystone. Of the published data [*Steiner*, 1981, Table 1, p. 714], inclinations from excursions between 519.17-519.23 m, 529.43 m and at 536.11 m depth were omitted in this study, one tilted strata sample (564.32 m) and also three limestone samples (515.62, 516.84, and 518.86 m). This leaves 24 stable inclinations from claystone, with mean inclination (inverting the reversed directions) of $-16.0° \pm 3.9°$, using Kono statistics [*Kono*, 1980*b*]. This estimate is comparable to the original arithmetic means; lower-Campanian $I = -15.3°$ ($N = 19$, $\lambda = -7.8°$), and Santonian-Cenomanian $I = -17.2°$ ($N = 9$, $\lambda = -8.8°$)

[*Steiner*, 1981, Table 2, p. 716]. The normal inclinations (–18.4° ± 4.5°) are slightly steeper than the reversed (+11.1° ± 5.8°), which may be partly due to rapid northward movement and age difference of the sediments.

From the depth range of the paleomagnetic data and intervals characterized as claystone a total of 13 density-porosity data were found in the DSDP data base [*DSDP CD-ROM*, 1989]. The averages are shown in Table 4.3. These were used to estimate sediment compaction of 0.61 ± 0.03.

Biostratigraphy of Hole 462A shows lower-Campanian (74-83 Ma) at 487-523 m, and Cenomanian to late-Albian (91-103 Ma) at 544-555 m [*Larson et al.*, 1981; *Harland et al.*, 1982]. As in hole 462 the paleomagnetic data includes a clear reversed zone from 517.9-525.6 m whose age corresponds to chron 33r (78.53-82.93 Ma). This fits very well to the biostratigraphy and indicates that the paleomagnetic data is within 74-100 Ma with average age of 87 Ma. The expected paleolatitude is $\lambda = -27.7°$ and northward movement of 0.45° m.y.$^{-1}$.

These estimates result in the parameter $a = 1.19 \pm 0.16$, and the uncertainty in a comes equally from the observed inclination and initial inclination.

4.5.11 DSDP Hole 463

Hole 463 was cored during leg 62 in 1978 [*Thiede et al.*, 1981]. Paleomagnetic samples from 481 to 692 m subbottom depth were studied by William Sayre. The dominant lithology in this interval is nannofossil limestone, and the interval 613-642 m is composed of silicified

limestone. Of the published data [*Sayre*, 1981, Table 1, p. 985], we have extracted his "reliability category 1" samples (a total of 51 stable inclinations). From these data we omitted an excursion at 636.31 m and three samples at 623.75 m, 625.28 m, and 625.69 m depth, characterized as ash layers [*DSDP CD-ROM*, 1989]. This leaves 47 selected samples from a single polarity from limestone, with mean inclination of –28.3° ± 3.2°, using Kono statistics [*Kono*, 1980*b*]. This estimate is comparable to an original arithmetic mean $I = -27.1°$ ($N = 67$) [*Sayre*, 1981, Table 4, p. 992]. Our estimate for 114 Ma is very similar to the estimate of *Tarduno* [1990] who split the data for 108 and 118 Ma ($I = -30.9° \pm 2.4°$ and $I = -24.8° \pm 3.4°$).

From the depth range of the paleomagnetic data and intervals characterized as limestone a total of 41 density-porosity data were found in the DSDP data base [*DSDP CD-ROM*, 1989]. The averages are shown in Table 4.3. These were used to estimate sediment compaction of 0.62 ± 0.01.

As an age estimate we use linear interpolation between boundaries of Cenomanian/Albian (97.5 Ma at 433 m), Albian/Aptian (113 Ma at 528 m), and Aptian/Barremian (119 Ma at 718 m) [*Thiede et al.*, 1981, Table 4, p. 61; *Harland et al.*, 1982]. This selection imposes a sharp sedimentation rate change at the Albian/Aptian boundary. However, dating errors are not important for this data set since the northward movement of the plate is extremely slow in this time period. This choice indicates that the paleomagnetic data is from approximately 105-118 Ma with average age of 114 Ma. The paleolatitude for this age is $\lambda = -17.8°$ and northward movement is very low 0.03° m.y.$^{-1}$.

These estimates result in the parameter $a = 0.26 \pm 0.46$, and the uncertainty in a comes mainly from the initial inclination due to the low paleolatitude.

4.5.12 DSDP Hole 465A

Hole 465A was cored during leg 62 in 1978 [*Thiede et al.*, 1981]. Sediment paleomagnetic samples from 277-412 m sub-bottom depth were studied by William Sayre. The lithology from 276 m to 412 m is characterized as limestone and nannofossil ooze. Of the published data [*Sayre*, 1981, Table 2, p. 987], we consider his eight "reliability category 1" samples from the limestone interval and obtained a mean inclination of 1.6° ± 3.6°, using Kono statistics [*Kono*, 1980*b*]. We assume that there is no polarity mixing since these sediments were deposited during the middle of the Cretaceous long normal polarity interval (see below). This estimate is shallower than an original arithmetic mean $I = \pm 7.5°$ ($N = 15$) [*Sayre*, 1981, Table 4, p. 992], and $I = 5.3° \pm 3.9°$ ($\theta_{63} = 10.9°$, $N = 18$) [*Tarduno*, 1990], probably because of our choice of only considering the most reliable samples and assuming a normal polarity for the data.

From the depth range of the paleomagnetic data and intervals characterized as limestone a total of 12 density-porosity data points were found in the DSDP data base [*DSDP CD-ROM*, 1989]. The averages are shown in Table 4.3. These were used to estimate sediment compaction of 0.62 ± 0.04.

The sediment from 276 m to 411 m is of early-Cenomanian to late-Albian age [*Thiede et al.*, 1981, Table 4, p. 221]. This indicates that the

paleomagnetic data is from approximately 94-103 Ma with average age of 98 Ma. The hot spot paleolatitude for 98 Ma is $\lambda = -3.5°$ and northward movement is 0.41° m.y.$^{-1}$. The equatorial crossing is predicted in the hot spot model at 90 Ma.

These estimates can not constrain the parameter a due to the equatorial paleolatitude of the site.

4.5.13 DSDP Hole 577

Hole 577 was cored during leg 86 in 1982 [*Heath et al.*, 1985*a*] using the hydraulic piston corer. The entire hole consists of nannofossil ooze. Paleomagnetic samples from 0 to 118 m subbottom depth were studied by Ulrich Bleil. The Tertiary/Cretaceous boundary was recovered at 109.10 m depth. The paleomagnetic data from the Cretaceous section were published in a graph [*Bleil*, 1985, Figure 5, p. 446], but not in numerical tables. Ulrich Bleil has kindly provided his measurements of 47 paleomagnetic samples from the Cretaceous section, of which we omit two excursions at 114.20 m and 117.00 m depth. This leaves 45 selected samples from nannofossil ooze, with mean inclination of 23.3° ± 1.8°, using Kono statistics [*Kono*, 1980*b*]. This estimate is comparable to the original estimate $I \approx$ 23-25° ($\lambda \approx$ 12-13°N) [*Bleil*, 1985, Figure 12, p. 456]. The normal (+21.6° ± 1.5°) and reversed (–24.6° ± 3.0°) inclinations are comparable.

From the depth range of the paleomagnetic data no density-porosity data points were found in the DSDP data base [*DSDP CD-ROM*, 1989]. In order to estimate the compaction we use five section averages of

GRAPE density-porosity data. The averages are shown in Table 4.3. These were used to estimate sediment compaction of 0.36 ± 0.03.

The Tertiary/Cretaceous boundary (65 Ma) is at 109.10 m. Polarities in this part of the hole fit well to the magnetic polarity time scale. The boundary between anomalies 29r/30n (65.39 Ma) is at 112.60 m [*Bleil*, 1985, Table 3, p. 450; *Harland et al.*, 1982]. As an age-depth transform for DSDP hole 577 we use linear interpolation and extrapolation between these two boundaries. This age data indicates that the paleomagnetic data is from 65-66 Ma with average age of 65.4 Ma. The hot spot paleolatitude at 65 Ma is $\lambda = +9.0°$ and northward movement $0.7°$ m.y.$^{-1}$.

These estimates can not constrain the parameter a mainly due to the low paleolatitude and therefore high uncertainty in the initial inclination.

4.5.14 DSDP Hole 577A

Hole 577A was cored during leg 86 in 1982 [*Heath et al.*, 1985*a*] using the hydraulic piston corer. The entire hole consists of nannofossil ooze. Paleomagnetic samples from 0 to 123 m subbottom depth were studied by Ulrich Bleil. The Tertiary/Cretaceous boundary was recovered at 109.62 m depth. The paleomagnetic data from the Cretaceous section was published in a graph [*Bleil*, 1985, Figure 6, p. 447], but not in numerical tables. Ulrich Bleil has kindly provided his measurements of 54 paleomagnetic samples from the Cretaceous section, of which we omit one excursion at 116.70 m depth. The 53 selected samples from nannofossil ooze, have a mean inclination of 28.3° ± 2.6°, using Kono statistics [*Kono*, 1980*b*]. This estimate is comparable to the

original estimate $I \approx 28\text{-}30°$ ($\lambda \approx 15\text{-}16°$N) [*Bleil*, 1985, Figure 12, p. 456]. The normal ($+31.4° \pm 2.4°$) are slightly steeper than the reversed ($-22.5° \pm 4.3°$).

From the depth range of the paleomagnetic data no density-porosity data points were found in the DSDP data base [*DSDP CD-ROM*, 1989]. In order to estimate the compaction we use nine section averages of GRAPE density-porosity data, and density-porosity data for three samples [*Schultheiss*, 1985, Table 1, p. 706]. The averages are shown in Table 4.3. These were used to estimate sediment compaction of 0.26 ± 0.06.

The Tertiary/Cretaceous boundary (65 Ma) is at 109.62 m. Polarities in this part of the hole fit well to the magnetic polarity time scale. The boundary between anomalies 29r/30n (65.39 Ma) is at 113.09 m and anomalies 30n/30r (66.88 Ma) is located at 121.18 m [*Bleil*, 1985, Table 3, p. 450; *Harland et al.*, 1982]. As age estimates for this hole we use linear interpolation and extrapolation between these three boundaries. This choice indicates that the paleomagnetic data is from 65-67 Ma with average age of 66.0 Ma. Hot spot paleolatitude at 66 Ma is $\lambda = +8.3°$ and northward movement $0.7°$ m.y.$^{-1}$.

These estimates can not constrain the parameter a mainly due to the low paleolatitude and therefore high uncertainty in the initial inclination.

4.5.15 DSDP Hole 585

Hole 585 was cored during leg 89 in 1982 [*Moberly et al.*, 1986]. Paleomagnetic samples from 367 to 757 m subbottom depth were studied by James Ogg. Most of the data comes from intervals of claystone. The

inclinations are scattered about zero during the late Cretaceous, and magnetostratigraphy was not possible. In order to minimize possible polarity mixing we constrain this study to the long normal polarity (>83 Ma, 483 m). Of the published data [*Ogg*, 1986, p. 644-645], we only consider his "A-rated reliability" samples. We omit samples from non-claystone intervals: (549-559 m, 572-573 m, 629-630 m, 658-671 m, 677-678 m, 681-757 m). This leaves 49 stable A-class inclinations from claystone, with single polarity mean inclination of $-17.2° \pm 3.9°$, using Kono statistics [*Kono*, 1980*b*]. This estimate is between the original estimates; Santonian to late-Albian, $I = -14.7° \pm 3.5°$ ($N = 43$), and Albian to Aptian, $I = -26.4° \pm 3.3°$ ($N = 39$) [*Ogg*, 1986, Table 1, p. 633].

From the depth range of the paleomagnetic data and intervals characterized as claystone a total of 9 water content, density and porosity data points were found in the DSDP data base [*DSDP CD-ROM*, 1989]. The averages are shown in Table 4.3. These were used to estimate sediment compaction of 0.64 ± 0.03.

Biostratigraphy of Hole 585 shows the Tertiary/Cretaceous boundary (65 Ma) at 381 m depth, the Maastrichtian/Campanian boundary (73 Ma) at 420 m, Santonian (83-87.5 Ma) at 494-500 m, the Turonian/ Cenomanian boundary (91 Ma) at 534.2 m, Albian (97.5-113 Ma) at 599-721 m, and Aptian (113-119 Ma) at 722-759 m [*Moberly et al.*, 1986; *Harland et al.*, 1982]. This indicates that the paleomagnetic data is from approximately 83-110 Ma with average age of about 93 Ma. The hot spot paleolatitude at 93 Ma is $\lambda = -25.3°$ and northward motion $0.46°$ m.y.$^{-1}$.

These estimates result in the parameter $a = 1.05 \pm 0.18$, and the uncertainty in a comes equally from the observed inclination and the initial inclination.

4.5.16 DSDP Hole 585A

Hole 585A was cored during leg 89 in 1982 [*Moberly et al.*, 1986]. Paleomagnetic samples from 0 to 887 m subbottom depth were studied by James Ogg. Most of the data comes from intervals of claystone. The inclinations are scattered about zero during the late Cretaceous, and magnetostratigraphy is not possible. In order to minimize possible polarity mixing we constrain this study to the long normal polarity (>83 Ma, 495 m). Of the published data [*Ogg*, 1986, p. 644-645], we only consider his "A-rated" samples. We omit samples from non-claystone intervals: (800-802 m, 819-824 m, 843-845 m). This leaves 39 stable A-class inclinations from claystone, with single polarity mean inclination of $-21.5° \pm 3.8°$, using Kono statistics [*Kono*, 1980*b*]. This estimate is between the original estimates; Santonian to late-Albian, $I = -15.7° \pm 5.1°$ ($N = 16$), and Albian to Aptian, $I = -27.1° \pm 3.8°$ ($N = 32$) [*Ogg*, 1986, Table 1, p. 633].

From the depth range of the paleomagnetic data and intervals characterized as claystone a total of 23 water content data points were found in the DSDP data base [*DSDP CD-ROM*, 1989]. Additional porosity and density data were found [*Moberly et al.*, 1986, Table 16, p. 86-87]. The averages are shown in Table 4.3. These were used to estimate the sediment compaction, $\Delta V = 0.64 \pm 0.02$.

Biostratigraphy of Hole 585A shows the Tertiary/Cretaceous boundary (65 Ma) at 383.8 m depth, Santonian (83-87.5 Ma) between 502-506 m, the Turonian/Cenomanian boundary (91 Ma) at 544 m, and late-Aptian (113-119 Ma) at 772-834 m [*Moberly et al.*, 1986; *Harland et al.*, 1982]. The age at the bottom is uncertain, but the slow northward movement of the plate before 100 Ma discounts the importance of the age uncertainty. This indicates that the paleomagnetic data is from the interval 83-119 Ma with average age of about 102 Ma. The hot spot paleolatitude for 102 Ma is $\lambda = -28.6°$ and northward motion $0.03°$ m.y.$^{-1}$.

These estimates result in the parameter $a = 1.00 \pm 0.16$, and the uncertainty in a comes equally from the observed inclination and the initial inclination.

4.5.17 Additional Cretaceous Sections from ODP Cores

Cretaceous sediments from the Pacific plate have also been recovered in late 1989 and early 1990 by the Ocean Drilling Program (ODP which is the continuation of the DSDP) legs 129 and 130. On leg 130 Cretaceous sediment was apparently recovered in two holes 803D (2.43°N, 160.54°E, 3412 m water depth) and 807C (3.61°N, 156.62°E, 2806 m water depth) [*Kroenke et al.*, 1991]. Quantitative paleomagnetic results from the Cretaceous sediment of ODP leg 130 have not been published but the inclinations appear to be very shallow.

Preliminary paleomagnetic results were recently published for ODP leg 129 [*Lancelot et al.*, 1990]. Cretaceous sections were recovered in holes 800A (21.92°N, 152.32°E, 5686 m water depth), 801A and 801B

(18.64°N, 156.36°E, 5674 m water depth) and 802A (12.10°N, 153.21°E, 5969 m water depth). At site 801 Jurassic sediments from the Pacific plate were recovered for the first time. Paleomagnetism of these sites is currently being studied by Maureen Steiner and Brian Wallick. Some discussion of the data is warranted, although the paleomagnetic data are preliminary in nature, showing signs of uncleaned recent overprint and remanent measurements are available only from whole-core magnetometer.

At ODP hole 800A the Cretaceous long normal is recovered in cores 8R through 50R. The average inclination is approximately $I \approx -18°$ [*Lancelot et al.*, 1990, Table 3, p. 55], and the average age is close to the Albian/Aptian boundary where the hot spot paleolatitude is about $\lambda \approx -21°$. Density porosity data indicates compaction of about $\Delta V \approx 0.65$ (from [*Lancelot et al.*, 1990, Table 5, p. 61] selecting limestone and claystone intervals separately). These preliminary data result in the parameter $a \approx 0.9$.

At ODP hole 801B the Cretaceous long normal is recovered in cores 1R-13R (203-319 m). The average paleolatitude is approximately 10°S [*Lancelot et al.*, 1990, Figure 26, p. 122], or $I \approx -19°$. Density and porosity data in these cores indicates a compaction of about $\Delta V \approx 0.58$ [*Lancelot et al.*, 1990, Table 6, p. 127] (assuming initial values of claystone). The average age of the data is approximately middle-Albian when a hot spot paleolatitude is $\lambda \approx -23°$. These numbers result in the parameter $a \approx 1.0$.

At ODP hole 802A there is some disagreement between biostratigraphy and magnetostratigraphy in the position of the

Cretaceous long normal, but it appears that at least the interval between cores 47R-56R is within the long normal polarity. The average inclination in this interval is about $I \approx -16°$ (estimated from [*Lancelot et al.*, 1990, Table 4, p. 204]). The average age is probably about Santonian/Coniacian (~87 Ma) where the hot spot paleolatitude is $\lambda \approx -24°$. Claystone density and porosity data [*Lancelot et al.*, 1990, Table 6, p. 210] in the paleomagnetic data interval indicates a compaction of about $\Delta V \approx 0.61$. This would result in the parameter $a \approx 1.1$.

Due to the similarity of the values of the parameter a from these clay rich ODP sediments ($a \approx 0.9$ to 1.1) to the values obtained from the clay rich DSDP cores of this study it appears that paleolatitude discrepancies in these recent ODP inclination data may be explained by the same processes responsible for the inclination shallowing in the DSDP data. The ODP paleomagnetic data are not discussed further in this chapter due to their preliminary nature.

4.6 DISCUSSION

The greatest shallowing in the Cretaceous DSDP inclinations appears to be at sites 462 and 585, 31° and 26° respectively (20° and 17° latitude anomaly). It is very difficult to attribute this to inaccuracies in the paleolatitude estimates. Therefore, we look at processes that might affect the paleomagnetic inclination estimates. It is important to note that the sites in Table 4.2 with two holes (462, 577, and 585) have very similar inclinations with differences on the order of 3°-5°. Therefore, inclination shallowing due to the coring itself are unlikely unless such problems were systematic and persistent.

A possible source of systematic deviations is a later stage remagnetization, which could result in inclination shallowing for the northward moving southern hemisphere sites. However, total remagnetization would destroy the magnetostratigraphy. Of the seven holes in Table 4.2 that include both polarities (the other eight are from the Cretaceous long normal), all show very good correspondence between the biostratigraphic age and the magnetic polarity time scale [*Harland et al.*, 1982]. Therefore, total remagnetization did not occur. There is the possibility of a systematic late stage partial remanence growth or that the paleomagnetic data has remnants of unidentified overprint, possibly a Brunhes or present field overprint, or drilling-induced remanence [e.g., *Backman et al.*, 1988, p. 475-476] similar to drilling-induced remanence documented in basalt cores [*Audunsson and Levi*, 1989]. The effect of a later stage normal overprint would be to shallow the inclinations of normal polarity from southern hemisphere

sites, but it would steepen the reversed inclinations. This can be tested. Significant differences between normal and reversed inclinations may identify persistent secondary overprints. Seven of the holes in Table 4.2 show both polarities, and we compare the normal and reversed inclinations in Figure 4.6. There is no evidence for significant undemagnetized secondary overprints in the stable inclinations.

Undetected random tilting of core pieces inside the core barrel would result in a net inclination shallowing, similar to the process discussed by *Griffiths et al.* [1960]. Random tilting as a source of net inclination shallowing was suggested by *Calderone and Butler* [1988; 1991]. However, this mechanism can only account for few degrees of inclination shallowing, assuming reasonable tilt angles.

Therefore, we consider the possibility that sediment compaction through the rearrangement of the sediment fabric is responsible for the inclination shallowing and try to compare the DSDP data set to compaction-induced shallowing models [e.g., *Arason and Levi*, 1990*a*]. We do this by estimating the parameter a.

The parameter a was estimated by equation (4.2). This estimate is very uncertain for low (equatorial) paleolatitudes and it turns out that only the data from DSDP sites 167, 288, 289, 315, 316, 317, 462, 463, and 585 give practical constraints on this parameter. All of these estimates show positive values of a, indicating inclination shallowing (inclination steepening would result in negative values of a). In Table 4.7 and Figure 4.7 we show our estimates. We have attempted to estimate the clay content for the depth range of the paleomagnetic data from smearslide data in the DSDP data base [*DSDP CD-ROM*, 1989].

Many of the original estimates were based on qualitative descriptions and should only be interpreted qualitatively. It appears that the clayey sediments have higher a values than the calcareous sediments.

Our results are very comparable to estimated a values from laboratory experiments with synthetic sediment of *Lu et al.* [1990], who observed that the inclination shallowing increased with increasing clay concentration. The compaction experiments of *Anson and Kodama* [1987] with synthetic clays resulted in the parameter a of about 0.6 $\pm$ 0.2. *Arason and Levi* [1990*b*] estimated the parameter a for Plio-Pleistocene clays in the top 120 m of DSDP hole 578 to be between 1 and 2, comparable to the estimate from these much older Cretaceous clayey sediments.

Recently, it was suggested that the occurrence of recording or preservation inclination error might be identified by measurements of anisotropy of anhysteretic remanent magnetization (ARM) [*Collombat et al.*, 1990; *Jackson et al.*, 1991]. The equations of *Jackson et al.* [1991] relating ARM anisotropy to inclination shallowing can be transformed to

$$\tan (I - \Delta I) = (1 - b \, \Delta A) \tan I \qquad (4.8)$$

where we define

$$\Delta A = \left(\frac{ARM_x - ARM_z}{ARM_x} \right)_{sample} \qquad (4.9)$$

$$b = \frac{\left(\frac{ARM_{//}}{ARM_{\perp}}\right)_{particle} + 2}{\left(\frac{ARM_{//}}{ARM_{\perp}}\right)_{particle} + 1} \tag{4.10}$$

ΔA is related to the ARM anisotropy of the sample, and the parameter b accounts for anisotropy of the magnetic grains and can be between 1 and 1.5; needles with infinite anisotropy lead to $b = 1.0$ and isotropic grains have $b = 1.5$. The range of probable values of b in natural sediments are not known. Comparison of equations (4.1) and (4.8) leads to

$$a\,\Delta V = b\,\Delta A \tag{4.11}$$

This relationship could be tested by ARM anisotropy measurements of samples from compacted sediments.

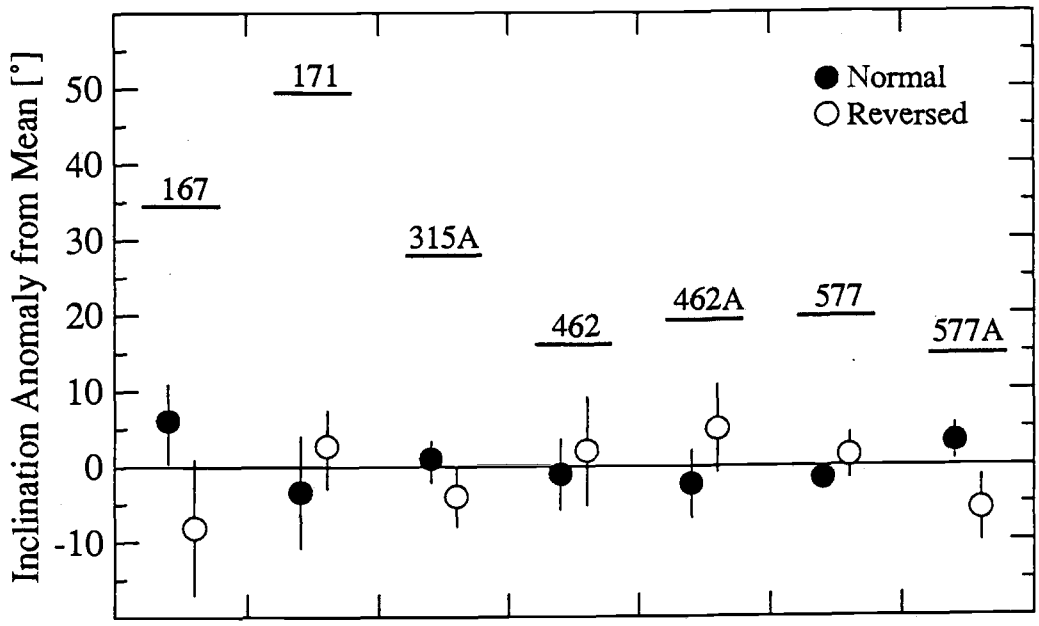

Figure 4.6. Comparison of normal and reversed inclinations in DSDP holes. The zero line represents the mean inclination for each hole. The values are listed in Table 4.2. The bars above (with DSDP hole numbers) show the present field inclination (IGRF 1985) relative to the mean inclinations. The reversed inclinations have been inverted for comparison to the normal means. The error bars represent 95% confidence intervals. If these data were contaminated by the present field (or any later stage normal overprint), the normal inclinations (filled) would be attracted up to the present inclination and the reversed inclinations (open) repulsed down. There appears to be no significant difference between the polarities and no systematic overprint can be detected.

TABLE 4.7. Constraints on the Parameter *a* from Cretaceous DSDP Sediments.

Hole	Depth, m	Age, Ma	Clay Content, %	Observed Inclination, deg	Initial Inclination, deg	Compaction	Estimate of Parameter *a*
				Clayey sediments:			
DSDP 315A	830	71	> 50 ?	–17.0 ± 2.8	–25.0 ± 8.6	0.74 ± 0.02	0.47 ± 0.42
DSDP 462	526	84	?	–12.8 ± 3.9	–44.7 ± 6.3	0.62 ± 0.04	1.24 ± 0.16
DSDP 462A	532	87	70-85	–16.0 ± 3.9	–46.4 ± 6.1	0.61 ± 0.03	1.19 ± 0.16
DSDP 585	550	93	70-90	–17.2 ± 3.9	–43.4 ± 6.5	0.64 ± 0.03	1.05 ± 0.18
DSDP 585A	666	102	70-90	–21.5 ± 3.8	–47.5 ± 5.9	0.64 ± 0.02	1.00 ± 0.16
				Calcareous sediments:			
DSDP 167	832	83	5-25	–23.2 ± 5.1	–38.1 ± 7.2	0.55 ± 0.06	0.82 ± 0.37
DSDP 288A	(880)	92	< 10	–41.6 ± 2.6	–62.2 ± 4.1	0.58 ± 0.03	0.92 ± 0.17
DSDP 289	(1235)	115	< 10	–37.6 ± 5.8	–61.5 ± 4.2	0.64 ± 0.19	0.91 ± 0.35
DSDP 315A	827	70	< 50 ?	–16.6 ± 3.4	–24.4 ± 8.7	0.65 ± 0.01	0.53 ± 0.51
DSDP 316	(640)	70	< 10	–17.1 ± 1.7	–30.2 ± 8.1	0.65 ± 0.01	0.73 ± 0.30
DSDP 317A	621	110	< 10	–46.8 ± 5.6	–55.3 ± 5.0	0.62 ± 0.02	0.42 ± 0.33
DSDP 463	562	114	< 10	–28.3 ± 3.2	–32.7 ± 7.8	0.62 ± 0.01	0.26 ± 0.46

* The clay content estimates are very uncertain, see text.

Estimates of the parameter *a* were calculated using equation (4.2). Poorly constrained values of *a* are not shown, but discussed in the text. The observed inclinations are from Table 4.2, the initial inclinations from Table 4.6, and the compaction estimates from Table 4.3.

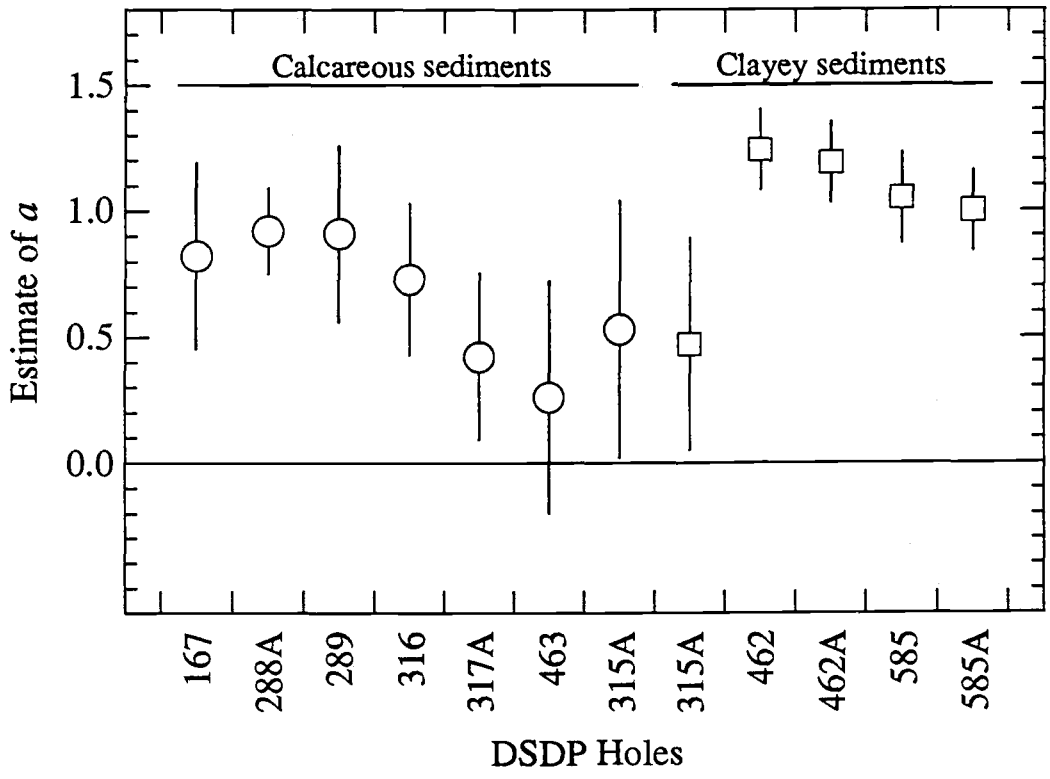

Figure 4.7. The values of the parameter *a* in this study for the holes that give constraints on its value. The values are listed in Table 4.7. Note that the clayey sediments appear to have a slightly higher values and much lower uncertainties than the calcareous sediments. The data from hole 315A shows no difference between intervals characterized as "clayey limestone" and "limey claystone".

4.7 CONCLUSIONS

Cretaceous DSDP sediments from the Pacific plate have considerably shallower inclinations than expected from the geocentric axial dipole hypothesis and plate tectonic reconstructions. Our model for compaction-induced inclination shallowing can account for the observed anomaly. The magnitude of inclination shallowing is affected by lithology; inclination shallowing is greater for clay rich sediments than calcareous sediments. The predictability of the compaction-induced inclination shallowing offers hope for possibly restoring the inclinations, resulting in more accurate paleolatitude estimates.

4.8 REFERENCES

Andrews, J. A., True polar wander: An analysis of Cenozoic and Mesozoic paleomagnetic poles, *J. Geophys. Res., 90*, 7737-7750, 1985.

Andrews, J. E., et al., *Initial Reports of the Deep Sea Drilling Project, 30*, 753 pp., U.S. Government Printing Office, Washington, D.C., 1975.

Anson, G. L., and K. P. Kodama, Compaction-induced inclination shallowing of the post-depositional remanent magnetization in a synthetic sediment, *Geophys. J. R. Astron. Soc., 88*, 673-692, 1987.

Arason, P., and S. Levi, Inclination shallowing recorded in some deep sea sediments (abstract), *Eos Trans. AGU, 67*, 916, 1986.

Arason, P., and S. Levi, Models of inclination shallowing during sediment compaction, *J. Geophys. Res., 95*, 4481-4499, 1990*a*.

Arason, P., and S. Levi, Compaction and inclinations shallowing in deep-sea sediments from the Pacific ocean, *J. Geophys. Res., 95*, 4501-4510, 1990*b*.

Audunsson, H., and S. Levi, Drilling-induced remanent magnetization in basalt drill cores, *Geophys. J. Int., 98*, 613-622, 1989.

Backman, J., et al., *Proceedings of the Ocean Drilling Program, Initial Reports, 115*, 1085 pp., Ocean Drilling Program, College Station, Texas, 1988.

Baldwin, B., Ways of deciphering compacted sediments, *J. Sediment. Petrol., 41*, 293-301, 1971.

Baldwin, B., and C. O. Butler, Compaction curves, *Am. Assoc. Pet. Geol. Bull.*, *69*, 622-629, 1985.

Besse, J., and V. Courtillot, Revised and synthetic apparent polar wander paths of the African, Eurasian, North American and Indian plates, and true polar wander since 200 Ma, *J. Geophys. Res.*, *96*, 4029-4050, 1991.

Bleil, U., The magnetostratigraphy of northwest Pacific sediments, deep sea drilling project leg 86, *Initial Rep. Deep Sea Drill. Proj.*, *86*, 441-458, 1985.

Blow, R. A., and N. Hamilton, Effect of compaction on the acquisition of a detrital remanent magnetization in fine-grained sediments, *Geophys. J. R. Astron. Soc.*, *52*, 13-23, 1978.

Calderone, G. J., and R. F. Butler, The effects of randomly directed noise on paleomagnetic directions (abstract), *Eos Trans. AGU*, *69*, 1158-1159, 1988.

Calderone, G. J., and R. F. Butler, The effects of noise due to random undetected tilts and paleosecular variation on regional paleomagnetic directions, *J. Geophys. Res.*, *96*, 3973-3977, 1991.

Celaya, M. A., and B. M. Clement, Inclination shallowing in deep sea sediments from the north Atlantic, *Geophys. Res. Lett.*, *15*, 52-55, 1988.

Cockerham, R. S., A paleomagnetic and magnetic property study of DSDP Pacific basalts and sediments of Cretaceous age (abstract), *Eos Trans. AGU*, *60*, 239, 1979.

Cockerham, R. S., and J. M. Hall, Magnetic properties and paleomagnetism of some DSDP leg 33 basalts and sediments and their tectonic implications, *J. Geophys. Res.*, *81*, 4207-4222, 1976.

Cockerham, R. S., and R. D. Jarrard, Paleomagnetism of some leg 33 sediments and basalts, *Initial Rep. Deep Sea Drill. Proj.*, *33*, 631-647, 1976.

Collombat, H., P. Rochette, and M. J. Jackson, Possible correction of the inclination error in deep sea sediments using the anisotropy of anhysteretic remanence (ARM) (abstract), *Eos Trans. AGU*, *71*, 1288, 1990.

Courtillot, V., and J. Besse, Magnetic field reversals, polar wander, and core-mantle coupling, *Science*, *237*, 1140-1147, 1987.

Deamer, G. A., and K. P. Kodama, Compaction-induced inclination shallowing in synthetic and natural clay-rich sediments, *J. Geophys. Res.*, *95*, 4511-4529, 1990.

DSDP CD-ROM, *Marine Geological and Geophysical data from the Deep Sea Drilling Project*, CD-ROM data set, National Geophysical Data Center, Colorado, 1989.

Duncan, R. A., and D. A. Clague, Pacific plate motion recorded by linear volcanic chains, in *The Ocean Basins and Margins*, vol. 7A, edited by A. E. M. Nairn, F. G. Stehli, and S. Uyeda, pp. 89-121, Plenum, New York, 1985.

Duncan, R. A., and M. A. Richards, Hotspots, mantle plumes, flood basalts, and true polar wander, *Rev. Geophys.*, *29*, 31-50, 1991.

Gordon, R. G., Late Cretaceous apparent polar wander of the Pacific plate: Evidence for a rapid shift of the Pacific hotspots with respect to the spin axis, *Geophys. Res. Lett.*, *10*, 709-712, 1983.

Gordon, R. G., Test for bias in paleomagnetically determined paleolatitudes from Pacific plate deep sea drilling project sediments, *J. Geophys. Res.*, *95*, 8397-8404, 1990.

Gordon, R. G., and R. A. Livermore, Apparent polar wander of the mean-lithosphere reference frame, *Geophys. J. Roy. Astron. Soc.*, *91*, 1049-1057, 1987.

Griffiths, D. H., R. F. King, A. I. Rees, and A. E. Wright, Remanent magnetism of some recent varved sediments, *Proc. R. Soc. London, Ser. A*, *256*, 359-383, 1960.

Hamilton, E. L., Variations of density and porosity with depth in deep-sea sediments, *J. Sediment. Petrol.*, *46*, 280-300, 1976.

Hammond, S. R., L. W. Kroenke, and F. Theyer, Northward motion of the Ontong-Java plateau between -110 and -30 m.y.: A paleomagnetic investigation of DSDP site 289, *Initial Rep. Deep Sea Drill. Proj.*, *30*, 415-418, 1975.

Harland, W. B., A. V. Cox, P. G. Llewellyn, C. A. G. Pickton, A. G. Smith, and R. Walters, *A Geologic Time Scale*, 131 pp., Cambridge University Press, New York, 1982.

Heath, G. R., et al., *Initial Reports of the Deep Sea Drilling Project*, *86*, 804 pp., U.S. Government Printing Office, Washington, D.C., 1985*a*.

Jackson, M. J., S. K. Banerjee, J. A. Marvin, R. Lu, and W. Gruber, Detrital remanence, inclination errors, and anhysteretic remanence

anisotropy: Quantitative model and experimental results, *Geophys. J. Int.*, *104*, 95-103, 1991.

Jarrard, R. D., Paleomagnetism of leg 17 sediment cores, *Initial Rep. Deep Sea Drill. Proj.*, *17*, 365-376, 1973.

Johnson, T. C., E. L. Hamilton, and W. H. Berger, Physical properties of calcareous ooze: Control by dissolution at depth, *Mar. Geol.*, *24*, 259-277, 1977.

Kent, D. V., and D. J. Spariosu, Magnetostratigraphy of Caribbean site 502 hydraulic piston cores, *Initial Rep. Deep Sea Drill. Proj.*, *68*, 419-433, 1982.

Kono, M., Paleomagnetism of DSDP leg 55 basalts and implications for the tectonics of the Pacific plate, *Initial Rep. Deep Sea Drill. Proj.*, *55*, 737-752, 1980*a*.

Kono, M., Statistics of paleomagnetic inclination data, *J. Geophys. Res.*, *85*, 3878-3882, 1980*b*.

Kroenke, L. W., et al., *Proceedings of the Ocean Drilling Program, Initial Reports*, *130*, 1240 pp., Ocean Drilling Program, College Station, Texas, 1991.

Lancelot, Y., et al., *Proceedings of the Ocean Drilling Program, Initial Reports*, *129*, 488 pp., Ocean Drilling Program, College Station, Texas, 1990.

Lanphere, M. A., and G. B. Dalrymple, K-Ar ages of basalts from DSDP leg 33: sites 315 (Line Islands) and 317 (Manihiki Plateau), *Initial Rep. Deep Sea Drill. Proj.*, *33*, 649-653, 1976.

Larson, R. L., et al., *Initial Reports of the Deep Sea Drilling Project*, *61*, 885 pp., U.S. Government Printing Office, Washington, D.C., 1981.

Le Pichon, X., Sea-floor spreading and continental drift, *J. Geophys. Res.*, *73*, 3661-3697, 1968.

Livermore, R. A., F. J. Vine, and A. G. Smith, Plate motions and the geomagnetic field - II. Jurassic to Tertiary, *Geophys. J. Roy. Astron. Soc.*, *79*, 939-961, 1984.

Lu, R., S.K. Banerjee, and J. Marvin, The effects of clay mineralogy and solution conductivity on DRM acquisition in sediments (abstract), *Eos Trans. AGU*, *69*, 1159, 1988.

Lu, R., S.K. Banerjee, and J. Marvin, Effects of clay mineralogy and the electrical conductivity of water on the acquisition of depositional remanent magnetization in sediments, *J. Geophys. Res.*, *95*, 4531-4538, 1990.

Moberly, R., et al., *Initial Reports of the Deep Sea Drilling Project*, *89*, 678 pp., U.S. Government Printing Office, Washington, D.C., 1986.

Morgan, G. E., Paleomagnetic results from DSDP site 398, *Initial Rep. Deep Sea Drill. Proj.*, *47*, 599-611, 1979.

Ogg, J. G., Paleolatitudes and magnetostratigraphy of Cretaceous and lower Tertiary sedimentary rocks, deep sea drilling project site 585, Mariana basin, western central Pacific, *Initial Rep. Deep Sea Drill. Proj.*, *89*, 629-645, 1986.

Peirce, J. W., Assessing the reliability of DSDP paleolatitudes, *J. Geophys. Res.*, *81*, 4173-4187, 1976.

Pitman, W. C. III, R. L. Larson, and E. M. Herron, The age of the ocean basins, *Geol. Soc. Amer. Map and Chart Series MC-6*, 1974.

Sager, W. W., Paleomagnetism of Abbott Seamount and implications for the latitudinal drift of the Hawaiian hot spot, *J. Geophys. Res.*, *89*, 6271-6284, 1984.

Sager, W. W., and U. Bleil, Latitudinal shift of the Pacific hotspots during the late Cretaceous and early Tertiary, *Nature*, *326*, 488-490, 1987.

Sager, W. W., and M. S. Pringle, Mid-Cretaceous to early Tertiary apparent polar wander path of the Pacific plate, *J. Geophys. Res.*, *93*, 11,753-11,771, 1988.

Sayre, W. O., Preliminary report on the paleomagnetism of Aptian and Albian limestones and trachytes from the mid-Pacific mountains and Hess rise, deep sea drilling project leg 62, *Initial Rep. Deep Sea Drill. Proj.*, *62*, 983-994, 1981.

Schlanger, S. O., et al., *Initial Reports of the Deep Sea Drilling Project*, *33*, 973 pp., U.S. Government Printing Office, Washington, D.C., 1976.

Schlanger, S. O., M. O. Garcia, B. H. Keating, J. J. Naughton, W. W. Sager, J. A. Haggerty, J. A. Philpotts, and R. A. Duncan, Geology and geochronology of the Line Islands, *J. Geophys. Res.*, *89*, 11261-11272, 1984.

Schneider, D. A., and D. V. Kent, Influence of non-dipole field on determination of Plio-Pleistocene true polar wander, *Geophys. Res. Lett.*, *13*, 471-474, 1986.

Schultheiss, P. J., Physical and geotechnical properties of sediments from the northwest Pacific: Deep sea drilling project leg 86, *Initial Rep. Deep Sea Drill. Proj.*, *86*, 701-722, 1985.

Sclater, J. G., and R. D. Jarrard, Preliminary paleomagnetic results, leg 7, *Initial Rep. Deep Sea Drill. Proj.*, *7*, 1227-1234, 1971.

Skempton, A. W., The consolidation of clays by gravitational compaction, *Q. J. Geol. Soc. London*, *125*, 373-411, 1970.

Steiner, M. B., Paleomagnetism of the Cretaceous section, site 462, *Initial Rep. Deep Sea Drill. Proj.*, *61*, 711-716, 1981.

Tarduno, J. A., Absolute inclination values from deep sea sediments: A reexamination of the Cretaceous Pacific record, *Geophys. Res. Lett.*, *17*, 101-104, 1990.

Tarduno, J. A., W. V. Sliter, T. J. Bralower, M. McWilliams, I. Premoli-Silva, and J. G. Ogg, M-sequence reversals recorded in DSDP sediment cores from the western Mid-Pacific Mountains and Magellan Rise, *Bull. Geol. Soc. Am.*, *101*, 1306-1316, 1989.

Tauxe, L., P. Tucker, N. P. Petersen, and J. L. LaBrecque, Magnetostratigraphy of leg 73 sediments, *Initial Rep. Deep Sea Drill. Proj.*, *73*, 609-621, 1984.

Thiede, J., et al., *Initial Reports of the Deep Sea Drilling Project*, *62*, 1120 pp., U.S. Government Printing Office, Washington, D.C., 1981.

Watts, A. B., J. K. Weissel, R. A. Duncan, and R. L. Larson, Origin of the Louisville ridge and its relationship to the Eltanin fracture zone system, *J. Geophys. Res.*, *93*, 3051-3077, 1988.

Winterer, E. L., et al., *Initial Reports of the Deep Sea Drilling Project*, *7*, 1757 pp., U.S. Government Printing Office, Washington, D.C., 1971.

Winterer, E. L., et al., *Initial Reports of the Deep Sea Drilling Project, 17*, 930 pp., U.S. Government Printing Office, Washington, D.C., 1973.

CHAPTER 5

Comparison of Statistical Methods in the Analysis of Paleomagnetic Inclination Data

Several methods have been used in analyzing inclinations-only paleomagnetic data, when declinations are not available. To facilitate comparisons between these methods we have conducted a systematic study of the statistical parameters calculated from these methods. The parameters from the several methods are estimated using data sets generated by random sampling of true distributions with known statistical parameters. We show that for true inclinations below 60° all methods give reasonable estimates. The average inclination calculated by the method of *McFadden and Reid* [1982], as presented in the original article is very similar to the arithmetic mean of the inclinations and should not be used in its published form; however, we suggest a simple modification to their method. The method of *Kono* [1980*b*] appears to provide a reasonable estimate for higher inclinations than the modified McFadden and Reid method. We show that for steep, near vertical inclinations the average inclination and the precision parameter can not be separated. The lack of declination data implies the loss of the ability

to uniquely estimate the average inclination for very steep and scattered inclinations.

5.1 INTRODUCTION

In paleomagnetism it is usually assumed that either directions or virtual geomagnetic poles follow the Fisher distribution, which is analogous to the normal distribution on the sphere. For a given data set of individual directions (inclinations and declinations) we can calculate the maximum likelihood estimate of the mean direction as well as estimates of dispersion, confidence intervals and make statistical tests, using Fisher statistics [*Fisher*, 1953; *Watson*, 1956*a*, *b*; *Watson and Williams*, 1956; *Mardia*, 1972; *McFadden*, 1980*a*, *b*]. On the other hand, borecores are usually azimuthally unoriented, and so the absolute declinations are not available, and even relative declinations within selected depth intervals are often unreliable due to possible core twisting.

Briden and Ward [1966] pointed out that the arithmetic average of inclination-only data was biased toward a shallower inclination than when declinations were also available for calculating a Fisher average. They gave an example of this effect for a true inclination of 90°. Given any scatter in the directions, individual inclinations will all be less than or equal to 90° and the arithmetic average of the inclinations will be less than 90°. This is an extreme example, because this problem is seldom encountered. In addition, Fisher statistics for completely oriented directions distributed about the vertical will always give a slightly shallow average inclination estimate, as the average can not exceed 90°, and random scatter is likely to move the estimated direction away from the true mean, especially when dealing with only few samples. However, even for true mean inclinations not close to ±90°, where there is scatter

in individual directions, the arithmetic mean will be biased toward shallower inclinations. The geometry of the sphere dictates that steeper inclinations represent smaller surface area than shallower inclinations, see Figure 5.1. Therefore, any circularly symmetric distribution about a true mean on the sphere will be represented by more shallow than steep inclinations (compared to the true mean) except for true inclination of zero. *Briden and Ward* [1966] produced tables and graphs, designed to estimate the precision parameter k, which is an inverse measure of variance, and the average inclination I, but tabular and graphic interpolation is neither very accurate nor convenient. This correction is often on the order of 1°-2°, and has been ignored in many studies. In Figure 5.2 we show the inclination shallowing associated with the arithmetic average of inclinations versus the true inclination for various values of the precision parameter.

Harrison [1974] made a correction for this effect by comparing the standard deviation of the inclinations to those of randomly generated Fisher distributed directions with known mean and dispersion. By matching the arithmetic mean inclination and standard deviation of the random data set and the real data Harrison could estimate the true inclination and precision parameter. In a review of Deep Sea Drilling Project (DSDP) paleomagnetic data *Peirce* [1976] outlined the so called Cox's method for correcting the bias in the arithmetic mean of inclination-only data. The method was later used by *Gordon and Cox* [1980]. This method assumes that the dispersion of the data is related to secular variation of the geomagnetic field, and knowledge of the field's dispersion is used to constrain the true precision parameter, from which

a correction term is applied to the arithmetic average inclination. Detailed description of Cox's method was published by *Cox and Gordon* [1984]. Cox's method is only applicable to paleomagnetic results from lava flows, representing spot recordings of the geomagnetic field, where each inclination represents a single flow. Care must be taken to assess whether the data adequately represents the spectrum of geomagnetic secular variation. Since Cox's method assumes some a priori knowledge of κ, it is better to use other available methods where we can obtain an estimate of κ based on the data alone. Therefore, we do not include the Cox's method in the comparisons of this study.

Kono [1980*a*, *b*] extended the work of *Briden and Ward* [1966] and made it possible to estimate statistical parameters for any data set. *McFadden and Reid* [1982] criticized the Kono method and suggested a different method to solve the problem. Since then some workers have used the Kono method [e.g., *Bleil*, 1985; *Ogg*, 1986; *Levi and Karlin*, 1989; *Arason and Levi*, 1990*b*; *Lancelot et al.*, 1990], while others are using the McFadden and Reid method [e.g., *Celaya and Clement*, 1988; *Schneider and Kent*, 1990; *Tarduno*, 1990]. It is very important to document possible differences between the estimates resulting from these two methods. In this study we make such a comparison.

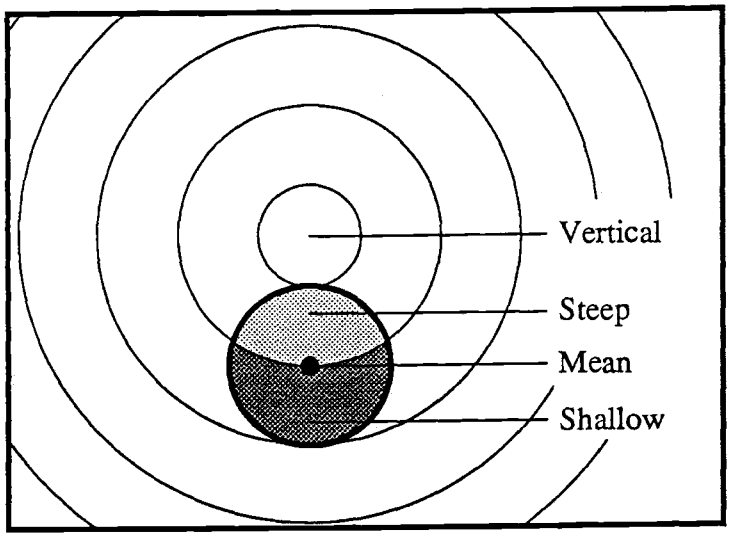

Figure 5.1. The geometry of the sphere dictates that any circularly symmetric distribution about a true mean will be represented by more shallow inclinations than steep as compared to the mean. This figure shows that the area of shallow inclinations (dark shade) is greater than the area represented by the steep inclinations (light shade). Arithmetic average of inclinations will therefore result in a too shallow estimate of the mean.

Figure 5.2. The inclination shallowing resulting from the arithmetic mean of inclination data versus the true inclination. Values of the precision parameter κ are 10, 20, 40, and 100. We show expanded scale on the lower panel. These curves were calculated numerically from equation (5.9). For high κ or low inclination this is effect is not very serious. If κ were known one could apply a simple correction to arithmetic average of inclination-only data. However, κ is usually not known and one needs to estimate κ and I simultaneously using the methods of *Briden and Ward* [1966], *Kono* [1980*a*, *b*], or *McFadden and Reid* [1982].

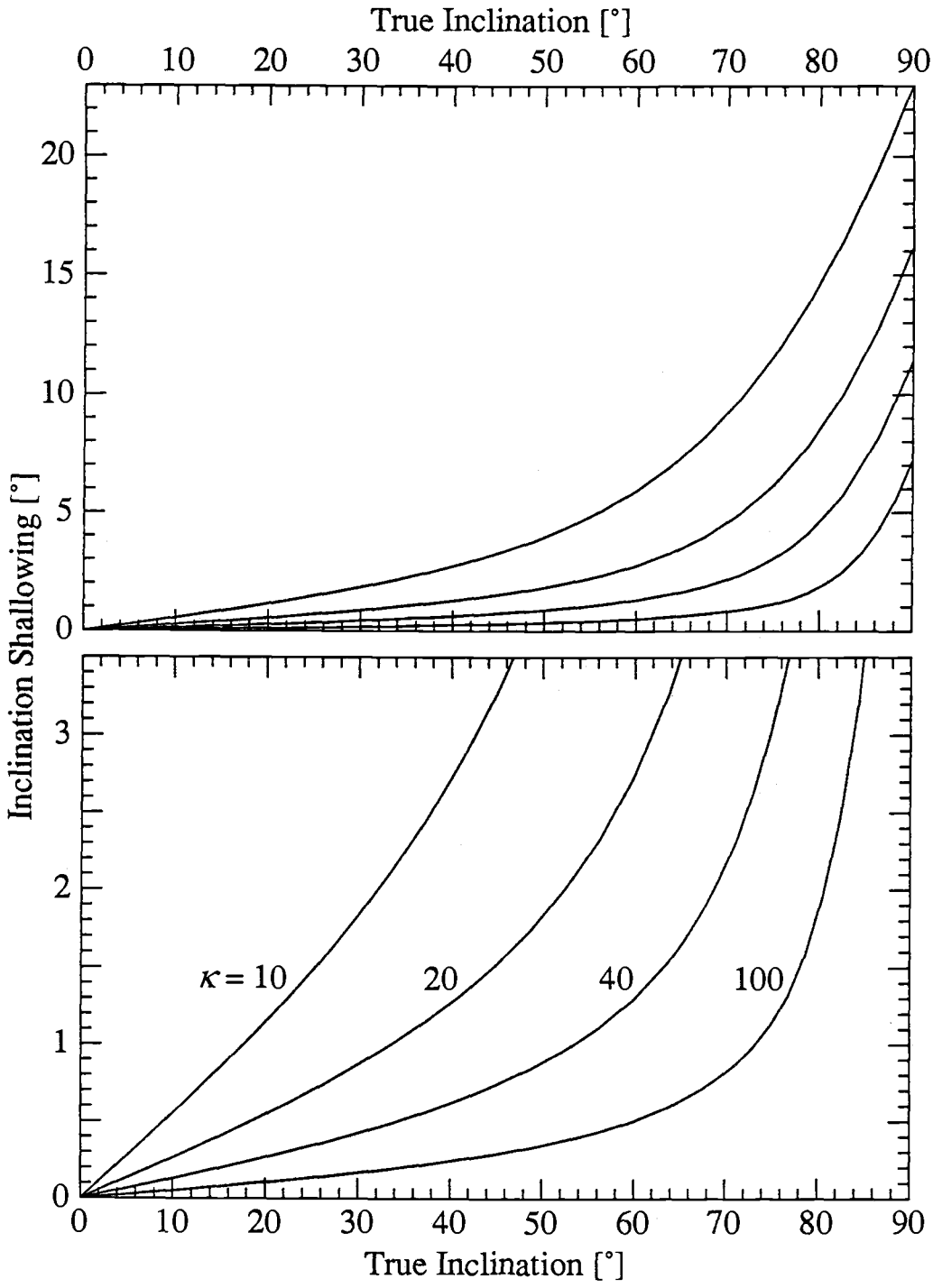
True Inclination [°]
0
10
20
30
40
50
60
70
80
90
Inclination Shallowing [°]
20
15
10
5
0
3
2
1
0
κ = 10
20
40
100
0
10
20
30
40
50
60
70
80
90
True Inclination [°]

Figure 5.2.

5.2 THE METHOD OF BRIDEN AND WARD

Briden and Ward [1966] outlined a method to estimate the average inclination I and the precision parameter κ from inclination-only data. A rough outline of their method is as follows: The Fisher probability distribution is

$$P(\theta', \phi')\, d\theta'\, d\phi' = \frac{\kappa}{4\pi \sinh \kappa}\, e^{\kappa \cos \theta'} \sin \theta'\, d\theta'\, d\phi' \qquad (5.1)$$

where κ is the Fisher precision parameter, θ' is the polar angle between an observation and the mean direction, and ϕ' is the azimuth of the observation about the mean. This expression can be transformed so that the angle between the vertical and the mean direction is θ_0 (the complement of the mean inclination $I_0 = 90° - \theta_0$) and an observation (θ, ϕ) is given relative to the vertical rather than the mean direction

$$P(\theta, \phi)\, d\theta\, d\phi =$$

$$= \frac{\kappa}{4\pi \sinh \kappa}\, e^{\kappa (\cos \theta_0 \cos \theta + \sin \theta_0 \sin \theta \cos \phi)} \sin \theta\, d\theta\, d\phi \qquad (5.2)$$

Since ϕ (declination data) is not available we find the marginal distribution of θ

$$P(\theta) = \int_0^{2\pi} P(\theta, \phi)\, d\phi \qquad (5.3)$$

$$P(\theta) = \frac{\kappa}{2 \sinh \kappa}\, e^{\kappa \cos \theta_0 \cos \theta}\, I_0(\kappa \sin \theta_0 \sin \theta) \sin \theta \qquad (5.4)$$

where $I_0(x)$ is the hyperbolic Bessel function of order zero.

The Briden and Ward method is based on equating functions of the data to the expectation value of the same functions, using knowledge of the probability distribution. They chose to use the functions sin θ and cos θ for this purpose

$$E(\sin\theta) = \frac{1}{N}\sum_{i=1}^{N}\sin\theta_i \tag{5.5}$$

$$E(\cos\theta) = \frac{1}{N}\sum_{i=1}^{N}\cos\theta_i \tag{5.6}$$

From knowledge of the probability distribution one can in principle calculate the expectation values $E(\sin\theta)$ and $E(\cos\theta)$.

$$E(\sin\theta) = \int_0^{\pi} P(\theta)\sin\theta\, d\theta \tag{5.7}$$

$$E(\cos\theta) = \int_0^{\pi} P(\theta)\cos\theta\, d\theta \tag{5.8}$$

However, *Briden and Ward* [1966] were unsuccessful in finding simple expressions for these expectation values. Instead they calculated the functions numerically and gave tables and graphs to estimate κ and θ_0 for a given data set.

The bias in the arithmetic average can be calculated using

$$\Delta I = \theta_0 - \int_0^{\pi} \theta\, P(\theta)\, d\theta \tag{5.9}$$

where θ_0 is the true average and $P(\theta)$ is from equation (5.4). The bias was calculated numerically with the function in equation (5.4) for selected values of κ. The results are shown in Figure 5.2.

5.3 THE METHOD OF KONO

Kono [1980*a*, *b*] was able to derive a simple expression of the expectation value $E(\cos^n\theta)$ for any power n. Since we want to identify two parameters, I_0 and κ, Kono suggested to equate the expectation values of the first two terms ($n = 1$, and 2) to the data. This is in principle a correct method of moments estimation, and is asymptotically unbiased as $N \rightarrow \infty$

$$E(\cos\,\theta) = \cos\,\theta_0\, L(\kappa)$$

$$= \frac{1}{N}\sum_{i=1}^{N}\cos\,\theta_i \tag{5.10}$$

$$E(\cos^2\theta) = \cos^2\theta_0 + \frac{1-3\cos^2\theta_0}{\kappa}\, L(\kappa)$$

$$= \frac{1}{N}\sum_{i=1}^{N}\cos^2\theta_i \tag{5.11}$$

where $L(\kappa)$ is the Langevin function.

$$L(\kappa) = \coth\,\kappa - \frac{1}{\kappa} \tag{5.12}$$

The Langevin function is a smooth concave function that goes from (0,0) and approaches 1 asymptotically as $\kappa \rightarrow \infty$. The function coth κ is nearly identical to $1/\kappa$ for $\kappa \approx 0$, and approaches 1 exponentially for $\kappa > 1$.

We note here that the expectation value $E(\cos\theta)$ for the Fisher distribution was essentially derived by *Langevin* [1905]. Langevin found the direction distribution of N magnetic moments in a paramagnetic gas. This distribution is the Fisher distribution about the pole (θ_0=0°). In order to estimate the net moment Langevin found the expectation value of cos θ', later called the Langevin function.

In this manner, *Kono* [1980*a*, *b*] was able to modify the method of *Briden and Ward* [1966] so that the true mean inclination I_0 and the precision parameter k could be estimated by a computer through the two equations

$$\sin I_0 \,(\coth k - 1/k) = \frac{1}{N}\sum_{i=1}^{N} \sin I_i \qquad (5.13)$$

$$\sin^2 I_0 + (1 - 3\sin^2 I_0)\,(\coth k - 1/k)/k = \frac{1}{N}\sum_{i=1}^{N} \sin^2 I_i \qquad (5.14)$$

[*Kono*, 1980*a*, equations A11 and A12, p. 752; *Kono*, 1980*b*, equation 10, p. 3880] where I_i, (I_1, I_2, ..., I_N) are the observed inclinations.

5.3.1 The K-Method

Following is a description of how we use the Kono method. We call this the K-method. For convenience we define the statistics S_1 and S_2

$$S_1 = \frac{1}{N}\sum_{i=1}^{N} \sin I_i \qquad (5.15)$$

$$S_2 = \frac{1}{N}\sum_{i=1}^{N} \sin^2 I_i \qquad (5.16)$$

The term sin I_0 can be isolated from equations (5.13) and (5.14). We are careful here not make new solutions by zero division and note that the nominators are never zero for $k > 0$

$$\sin I_0 = S_1/L(k) \tag{5.17}$$

$$\sin^2 I_0 = \frac{S_2 - L(k)/k}{1 - 3\,L(k)/k} \tag{5.18}$$

we combine equations (5.17) and (5.18) to eliminate I_0

$$\frac{S_1^2}{L(k)^2} = \frac{S_2 - L(k)/k}{1 - 3\,L(k)/k} \tag{5.19}$$

and this can be simplified to

$$A(k) = L(k)^3/k - S_2\,L(k)^2 - 3\,S_1^2\,L(k)/k + S_1^2 = 0 \tag{5.20}$$

We use this equation to find a k such that $A(k) = 0$. Then we use equations (5.17) and (5.18) to calculate I_0. The function $A(k)$ is symmetric about zero ($A(k) = A(-k)$) and $A(0)$ is always zero. It turns out that there are often several solutions (instances of one (k=0) to seven solutions have been found, depending on the data constants S_1 and S_2) to equation (5.20).

We have found it convenient to constrain the search of solutions by identifying a minimum value of k by the fact that

$$|\sin I_0| \leq 1 \tag{5.21}$$

Since the Langevin function is positive for all $k > 0$, equation (5.17) becomes

$$1 \cdot L(k) \geq | S_1 | \qquad \text{or} \qquad L(k_{min}) = | S_1 | \tag{5.22}$$

This constraint ($k_{min} \leq k$) turns out to be very successful for all cases in decreasing the number of solutions to equation (5.20) to either one or zero. The function $A(k)$ is always negative for very high k. If there is one solution then $A(k_{min})$ is positive. If on the other hand there exists no solution to equations (5.13) and (5.14) then $A(k_{min})$ is negative. After successfully identifying boundaries k_{neg} and k_{pos} such that $A(k_{neg}) \leq 0 \leq A(k_{pos})$, the solution is iteratively squeezed between the approaching boundaries.

There is some question as to what is the best thing to do when a situation with no solution of $A(k) = 0$ is encountered. One possibility is to rewrite equations (5.13) and (5.14) to include error terms E_1 and E_2, and find a solution that minimizes the sum of the squared errors: $\text{Min}(E_1^2 + E_2^2)$. However, a no solution encounter may have to do with a non-uniqueness of the underlying problem for low κ and steep I_0. Therefore, we have chosen to report instances of no solution to $A(k) = 0$ as a "no solution", see discussion later.

When (and if) k is determined the other parameters can be calculated. The average inclination I_0 is the average from equations (5.17) and (5.18).

An expression for the dispersion can be derived from the Fisher distribution for a known precision parameter κ. We want to find the angle θ_t so that the probability of a direction deviating less than θ_t from the mean is t, or $P(\theta < \theta_t) = t$. This can be calculated from the probability distribution

$$P_\theta \, d\theta = \frac{\kappa}{2 \sinh \kappa} \, e^{\kappa \cos \theta} \sin \theta \, d\theta \tag{5.23}$$

and the probability of having a direction less than θ_t from the mean is

$$t = \int_0^{\theta_t} P_\theta \, d\theta \tag{5.24}$$

$$= \frac{\kappa}{2 \sinh \kappa} \int_0^{\theta_t} e^{\kappa \cos \theta} \sin \theta \; d\theta \tag{5.25}$$

with the solution

$$t = \frac{e^{\kappa} - e^{\kappa \cos \theta_t}}{e^{\kappa} - e^{-\kappa}} \tag{5.26}$$

rearranging and solving for cos θ_t we find that

$$\theta_t = \arccos \left(1 + \frac{\ln \left(1 - t \left(1 - e^{-2\kappa} \right) \right)}{\kappa} \right) \tag{5.27}$$

now choosing $t = 63\%$ ($t = 0.63$) in equation (5.27)

$$\theta_{63} = \arccos \left(1 + \frac{\ln \left(1 - 0.63 \left(1 - e^{-2\kappa} \right) \right)}{\kappa} \right) \tag{5.28}$$

At last we calculate the 95% confidence limits of the average inclination. Here equation (5.29) (from *Kono* [1980*b*, equation 12]) is slightly changed from *Fisher* [1953], and is only valid for $k > 3$.

$$\alpha_{95} = \arccos\left(1 - \frac{N - 1}{N\,(k-1) + 1}\left(20^{1/(N-1)} - 1\right)\right) \qquad (5.29)$$

For all ordinary data sets in paleomagnetism the estimate of the average inclination I_0, the precision parameter k, angular standard deviation θ_{63}, and 95% confidence limits of the average α_{95} are calculated in a fraction of a second by the program KONO. The program is listed in Appendix C.

5.4 THE METHOD OF MCFADDEN AND REID

McFadden and Reid [1982] criticized the Kono method and pointed to examples of steep inclinations and low kappa where the Kono method gives poor results. Furthermore, they criticized the Kono method on grounds of formalism, because neither *Kono* [1980*a*, *b*] nor *Briden and Ward* [1966] define the meaning of the "best" solution that they seek. *McFadden and Reid* [1982] derived equations for calculating the maximum likelihood estimates of the inclination I, precision parameter k and 95% confidence interval for inclination-only data. In their derivation they chose to use θ the complement of the inclinations ($\theta = 90° - I$).

5.4.1 Maximum Likelihood Estimates

From the marginal distribution in equation (5.4) *McFadden and Reid* [1982] derive the log likelihood function $h(\theta, \kappa)$, which is a function of the mean θ, the precision parameter κ ($0° \leq \theta \leq 180°$, $0 \leq \kappa < \infty$) and a given data set θ_i ($\theta_1, \theta_2, ..., \theta_N$). The objective is to locate $\theta = \theta_0$ and $\kappa = k$ that maximizes $h(\theta, \kappa)$. The log likelihood function is

$$h(\theta, \kappa) = N \ln(\kappa) - N \ln(\sinh \kappa) + \kappa \sum_{i=1}^{N} \cos \theta \cos \theta_i + \sum_{i=1}^{N} \ln(G_i) + \sum_{i=1}^{N} \ln(\sin \theta_i) - N \ln(2) \qquad (5.30)$$

[*McFadden and Reid*, 1982, Equation 7, p. 310] where the function G_i is a solution to

$$G_i = \frac{1}{2\pi} \int_0^{2\pi} e^{\kappa \sin\theta \sin\theta_i \cos\phi} \, d\phi \tag{5.31}$$

$$= \sum_{r=0}^{\infty} \frac{(\kappa \sin\theta \sin\theta_i)^{2r}}{2^{2r} (r!)^2} \tag{5.32}$$

[*McFadden and Reid*, 1982, Equation 6, p. 308]. To evaluate this infinite sum for high κ turns out to be a significant task since it can become higher than 10^{1000} for legitimate paleomagnetic data. However, the function G was identified as a Bessel function [*Briden and Ward*, 1966], more specifically the hyperbolic Bessel function of order zero $I_0(x)$ [*Kono*, 1980*b*; *Cox and Gordon*, 1984]

$$G_i = I_0(\kappa \sin\theta \sin\theta_i) \tag{5.33}$$

One of the advantages with this representation is that the Bessel function is easily differentiable

$$I_0'(x) = I_1(x) \quad , \quad I_0''(x) = I_2(x) + I_1(x)/x \tag{5.34}$$

where $I_1(x)$, and $I_2(x)$ are the hyperbolic Bessel functions of first and second order [e.g., *Beyer*, 1984, p. 352]. Although the Bessel functions take on very high values for high x there exist very good approximations for both low and high x [e.g., *Beyer*, 1984, p. 352 (low x); *Gradshteyn and Ryzhik*, 1980, equation 8.451.5, p. 962 (high x)]. For κ close to zero the terms $\ln(\kappa)$ and $\ln(\sinh \kappa)$ in equation (5.30) reach $-\infty$ but their most violent terms can be cancelled analytically from equation (5.30).

Similarly for high κ the terms sinh κ and G_i blow up to extremely high values, but their most violent term (e^x) can be cancelled analytically from equation (5.30). Therefore, with carefully selected approximations to individual terms (dependent on θ and κ), one can calculate the value of the very smooth and well behaved function $h(\theta, \kappa)$ in equation (5.30) and its derivatives for all θ, κ and $(\theta_1, \theta_2, ..., \theta_N)$. This way one might solve the exact form of the maximum likelihood problem. The maximum value of $h(\theta, \kappa)$ could be a local maxima

$$\frac{dh(\theta, \kappa)}{d\theta} = 0 \quad \text{and} \quad \frac{dh(\theta, \kappa)}{d\kappa} = 0 \tag{5.35}$$

Monte Carlo experiments showed that for low κ and steep inclinations $h(\theta, \kappa)$ may take on a maximum value on one of the boundaries of the parameter space ($\kappa = 0$, $\kappa \rightarrow \infty$, $\theta = 0°$, or $\theta = 180°$) without possessing any local maxima in the interior.

5.4.2 Approximate Solution

Due to difficulties in calculating $h(\theta, \kappa)$ in equation (5.30) *McFadden and Reid* [1982] made approximations to simplify the problem. They assume that insubstantial portion of the distribution folds back at the vertical, but this assumption breaks down for steep inclinations and low kappa. For a particular θ they calculate the functions S and C

$$S(\theta) = \sum_{i=1}^{N} \sin(\theta - \theta_i) \tag{5.36}$$

$$C(\theta) = \sum_{i=1}^{N} \cos(\theta - \theta_i) \tag{5.37}$$

[*McFadden and Reid*, 1982, equation 34, p. 314]. Their approximate solution is obtained by finding θ_0 that satisfies $A(\theta_0) = 0$

$$A(\theta) = N \cos\theta + (\sin^2\theta - \cos^2\theta) \sum_{i=1}^{N} \cos\theta_i - 2 \sin\theta \cos\theta \sum_{i=1}^{N} \sin\theta_i \qquad (5.38)$$

[*McFadden and Reid*, 1982, equation 19, p. 316] provided that $U(\theta_0) < 0$

$$U(\theta) = \frac{N}{2}\left(\frac{1}{\sin^2\theta} - \frac{C(\theta)}{N - C(\theta)}\right) \qquad (5.39)$$

[*McFadden and Reid*, 1982, equation 19a, p. 317] and an estimate for $(1/\kappa)$ is obtained from

$$k = \frac{N - 1}{2\,(N - C(\theta_0))} \qquad (5.40)$$

[*McFadden and Reid*, 1982, equation 20, p. 317].

It is worth noting that it is possible to calculate the asymptotic bias ($N \rightarrow \infty$) in equation (5.38). When $N \rightarrow \infty$ we replace the sums with the expectation values $E(\cos\theta)$ (equation (5.10)) and $E(\sin\theta)$ (equation (5.7) which needs to be numerically integrated). In Figure 5.3 we show the asymptotic bias versus the true inclination for selected values of κ. For example when $I = 70°$, $\kappa = 10$, and $N \rightarrow \infty$, equation (5.38) has a solution 4.60° shallower than the true value.

In order to estimate θ_0 in equation (5.38) we first find the range $(\theta_{min}, \theta_{max})$ where the function $U(\theta)$ in equation (5.39) is negative, and later restrict our search for a solution to that interval. Assuming some variability in the data, i.e. that the inclination data values are not all identical, then $-N < C(\theta) < N$ for all θ and the function U is U-shaped; it blows up to $+\infty$ for both $\theta = 0°$ and 180° and has a single minima and no local maxima. For very dispersed data it is possible that U is positive for all θ (in which case it is a very smooth and broad trough), and then there is no solution to the problem. This is identified if the value of U at its minima is positive. Even though this method may result in no solution, there always exists a solution that results in a maximum value of $h(\theta, \kappa)$ in equation (5.30); however, some of the approximations might not be valid in such cases.

After successful location of the range $(\theta_{min}, \theta_{max})$ where $U(\theta) < 0$, we find θ_0 that satisfies $A(\theta_0) = 0$ in equation (5.38). For dispersed data there is a distinct possibility of no solution, i.e. $A(\theta) > 0$ for all θ in the interval $(\theta_{min}, \theta_{max})$, or $A(\theta) < 0$ for all θ in the interval $(\theta_{min}, \theta_{max})$. It turns out that in this interval there is either one solution or none. To verify a no solution we compare the sign of $A(\theta_{min})$ and $A(\theta_{max})$. If they are of same sign then the method can not identify a solution.

5.4.3 The Original-MR Method

First, we apply the method of *McFadden and Reid* [1982] as it is presented in their article. We call this the original-MR method. Later we try to correct their approximate method, as we think it should be done. Their article is followed by a numerical example [*McFadden and*

Reid, 1982, Appendix, p. 318], but unfortunately two of their 10 inclinations I_i are not compatible with the given 10 inclination compliments θ_i. *Schneider and Kent* [1990, p. 75] refer to personal communication with P. L. McFadden in 1986 on an ambiguity in the *McFadden and Reid* [1982] article. However, it is not obvious to us how *Schneider and Kent* [1990] modified the method and we have not found any published correction to the *McFadden and Reid* [1982] paper. Furthermore, it appears that some paleomagnetists are using the original-MR method. For example, *Tarduno* [1990, Table 1, p. 102] uses the data of *Steiner* [1981, Table 1, p. 714] to estimate average inclinations and other statistical parameters using *McFadden and Reid* [1982]. Reevaluation of Steiner's data shows that Tarduno is using the original-MR method.

The original-MR method is as follows: After successful identification of θ_0 that solves $A(\theta_0) = 0$ in equation (5.38), we calculate $S_0 = S(\theta_0)$ and $C_0 = C(\theta_0)$ from equations (5.36) and (5.37) and k from equation (5.40). The estimate for the average inclination is then

$$I = 90^\circ - \theta_0 + \frac{180\, S_0}{\pi\, C_0} \tag{5.41}$$

and 95% confidence interval for the inclination is

$$\alpha_{95} = \arccos\left[\, 1 - \frac{1}{2}\left(\frac{S_0}{C_0}\right)^2 - \frac{f\,(N - C_0)}{C_0\,(N - 1)}\,\right] \tag{5.42}$$

where f is the critical value of the F distribution with 1 and $(N - 1)$ degrees of freedom.

5.4.4 The Modified-MR Method

We have noticed that the term $(180\ S_0/\pi\ C_0)$ in equation (5.41) moves the inclination estimate from the approximate maximum likelihood estimate to a value very close to the arithmetic mean. We think that this is an error in the original-MR method. Therefore, we modified the method of *McFadden and Reid* [1982]. We call this the modified-MR method and it is as follows: After successful identification of θ_0 that solves $A(\theta_0) = 0$ in equation (5.38), we calculate $S_0 = S(\theta_0)$ and $C_0 = C(\theta_0)$ from equation (5.36) and (5.37) and k from equation (5.40), the same way as before. On the other hand our estimate for the average inclination is

$$I = 90^\circ - \theta_0 \tag{5.43}$$

and we see no convenience in the approximation of the 95% confidence limits shown in equation (5.42) [*McFadden and Reid*, 1982, equation 42, p. 315] but use the asymmetric form

$$\alpha_{95} = \frac{180\ S_0}{\pi\ C_0} \pm \frac{180}{\pi}\sqrt{\left(\frac{S_0}{C_0}\right)^2 + \frac{2\,f\,(N - C_0)}{C_0\,(N-1)}} \tag{5.44}$$

(minor modifications from [*McFadden and Reid*, 1982, equation 37c, p. 315]) where f is the critical value of the F distribution with 1 and $(N-1)$ degrees of freedom.

Figure 5.3. The asymptotic bias for the modified-MR method. This shows the theoretical bias (too shallow inclination estimate) of the method as the sample size N goes to infinity. Values of the precision parameter κ are 10, 20, 40, and 100. We show expanded scale on the lower panel. These curves were calculated numerically from equation (5.38) where the finite sums of cos θ_i and sin θ_i were replaced by the expectation values $E(\cos\ \theta)$, from equation (5.10), and $E(\sin\ \theta)$, evaluated numerically from equation (5.7). The modified-MR method introduces significant bias for true inclinations over 60°.

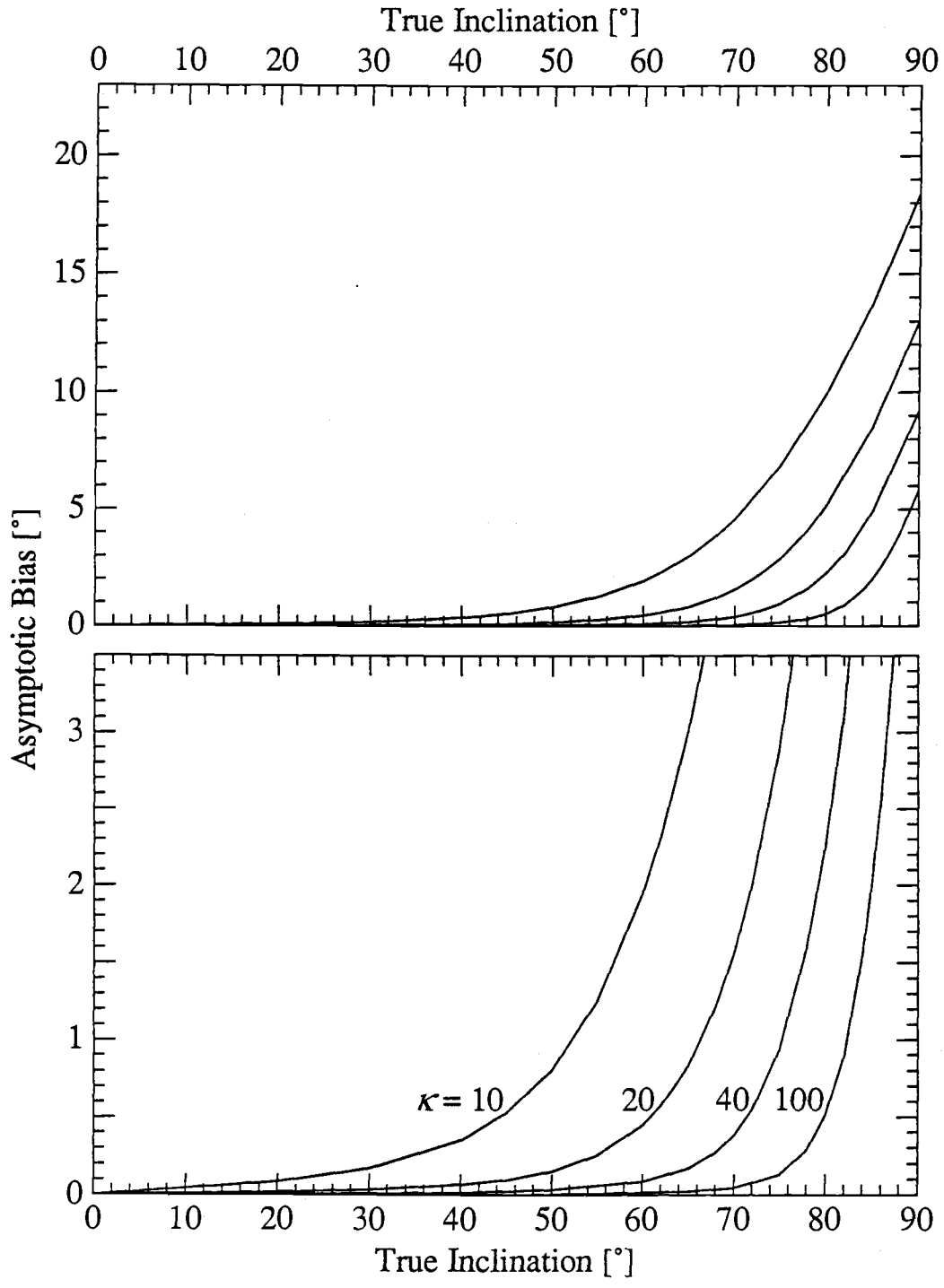
True Inclination [°]
0
10
20
30
40
50
60
70
80
90
20
15
10
5
0
Asymptotic Bias [°]
3
2
1
0
κ = 10
20
40
100
0
10
20
30
40
50
60
70
80
90
True Inclination [°]

Figure 5.3.

5.5 COMPARISON OF THE METHODS

We compared parameters from different methods numerically using random-generated Fisher-distributed data on a computer. We generated both inclinations and declinations so a full Fisher average could be compared to the inclination-only estimates of the K-method and the MR-methods. Two versions of the MR-methods were used, the original-MR method and the modified-MR method, which includes our modifications. We also calculated the arithmetic mean of the inclinations. The essential programs used in this study are listed in Appendix C. With these programs it should be possible to repeat our data generation and the calculations.

In Table 5.1 we show a summary of the simulations. For a given distribution with true inclination I (I = 0°, 10°, 20°, 30°, 40°, 50°, 60°, 70°, 80°, and 90°) and true precision parameter κ (κ = 10, 20, 40, and 100) we created many data sets each with finite number of samples N (N = 5, 10, 20, and 100). Figure 5.4 shows the distributions of the inclinations according to equation (5.4). We created 109 different combinations of (I, κ, N). For each combination of (I, κ, N) we created 1000 directional data sets, a total of 3.3 million directions for this study. As an example of the results we show histograms for the combination (I = 40°, κ = 40, N = 10), the 1000 inclination estimates in Figure 5.5, and the 1000 precision parameter estimates in Figure 5.6. Another example with steep inclinations is given in Figures 5.7 and 5.8 for the combination (I = 70°, κ = 10, N = 20). The initial seed for the random number generator for each combination is given in Table 5.1. We also

show in Table 5.1 the number of solutions found by the K-method and the MR-methods. For some data sets there exist no solutions by these methods, especially for steep inclinations and low precision parameter. This problem is more common in the MR-methods than in the K-method (ratio of 3 to 2).

For each of the 109,000 data sets we calculated the following sixteen parameters: (1) The arithmetic mean of the N inclinations. (2) The Fisher average of N directions (inclination and declination). (3) The Fisher estimate of the precision parameter. (4) The Fisher estimate of 95% confidence interval for the average. (5) We calculated the angular distance between the Fisher average direction and the true mean and checked if the angular distance exceeded the 95% confidence limits. (6) The K-method estimate of the average inclination using only the N inclinations. (7) The K-method estimate of the precision parameter. (8) The K-method estimate of 95% confidence interval for the average. (9) We calculated the difference between the K-method estimate of the average inclination and the true mean and checked if it exceeded the 95% confidence limits. (10) The original-MR method estimate for the average of N inclinations. (11) The modified-MR method estimate of the average of N inclinations. (12) The MR-method estimate of the precision parameter. (13) The original-MR method estimate of 95% confidence interval for the average. (14) For this estimate we calculated the difference between the average inclination and the true mean and checked if it exceeded the 95% confidence limits. (15) The modified-MR method estimate of 95% confidence interval for the average. (16) For this second estimate we calculated the difference between the

average inclination and the true mean and checked if it exceeded the 95% confidence limits.

In Table 5.2 we show the mean inclination anomaly of the 1000 inclination estimates for each (I, κ, N) combination. Here we define the inclination anomaly as

$$\Delta I = \frac{1}{m} \sum_{i=1}^{m} (I_i - I) \tag{5.45}$$

where I is the true inclination and m is the number of solutions, usually 1000 (listed in Table 5.1).

In Table 5.3 we show the harmonic average relative anomaly in the estimated precision parameter. Here we define the precision parameter anomaly as

$$\Delta\kappa\,(\%) = (100\%)\frac{\kappa_H - \kappa}{\kappa} \tag{5.46}$$

where κ is the true precision parameter and κ_H is the harmonic average of the 1000 precision parameter estimates

$$\frac{1}{\kappa_H} = \frac{1}{m} \sum_{i=1}^{m} \frac{1}{\kappa_i} \tag{5.47}$$

As before, m is the number of solutions, usually 1000 (listed in Table 5.1). We use the harmonic average since $1/\kappa$ is proportional to the variance of the Fisher distribution and the observed values of $1/\kappa$ appear to be symmetrically distributed.

In Table 5.4 we show the results of our comparison of the 95% confidence limits of the methods. For each of the 109 (I, κ, N) combinations we counted how many of the 1000 estimates ($I \pm \alpha_{95}$) included the true mean inclination. Ideally these numbers should be close to 95%.

The inclination estimates in Table 5.2 are summarized in Figure 5.9, where we split the results into three groups based on true inclination values of 0° to 60°, values of 70° and 80°, and values of 90°. For true inclinations of 0° to 60° all the methods give reasonable inclination estimates, but the arithmetic average and the original-MR method are clearly the worst, see Figure 5.9*a*. There does not appear to be significant difference between the full Fisher average, the K-method average and the modified-MR method average. For true inclinations of 70° and 80° there are significant discrepancies in the estimates. In Figure 5.9*b* we note that the original-MR method is no better than the arithmetic average. This is also true for the lower inclinations. For these steep inclinations we note that the K-method and the modified-MR method are collapsing, and show significant anomalies. Still the K-method is able to retrieve the inclinations for some combinations (high κ), where the modified-MR method is not as efficient. For true inclinations of 90° the inclination-only methods break down and can not be trusted, see Figure 5.9*c*.

The estimates of the precision parameter in Table 5.3 are summarized in Figure 5.10, where we split the results as before into three groups based on the true inclination values of 0° to 60°, values of 70° and 80°, and values of 90°. The precision parameter is more sensitive to the lack

of declination data than the inclination estimates. In Figure 5.10*a* we show the anomalies of the precision parameter for true inclinations of 0° to 60°. The K-method estimate can easily become 25% too high and reaches up to 60% too high. The MR-method estimate is better and similar to the Fisher estimate, although up to 50% anomalies are observed. For true inclinations of 70° and 80° there are significant discrepancies in the precision parameter estimates, as seen in Figure 5.10*b*. For these steep inclinations the inclination-only methods can result in 100% too high values and are not reliable. For true inclinations of 90° the inclination-only methods break down and can not be trusted, see Figure 5.10*c*.

The successes of the 95% confidence limits, listed in Table 5.4 are summarized in Figure 5.11, where we split the results as before into three groups based on the true inclination values of 0° to 60°, values of 70° and 80°, and values of 90°. In Figure 5.11*a* we show the success of the 95% confidence interval for true inclinations of 0° to 60°. The K-method and the Fisher estimates seem to be in good order. The MR-methods usually overestimates the α_{95} so that 97-98% of the estimates include the true mean. On top of this there are also a few instances of underestimation of α_{95} for low κ and high N. By overestimating the precision parameter when the true inclinations are 70° and 80° the inclination-only methods, particularly the MR-methods also underestimate the 95% confidence limits, see Figure 5.11*b*. For true inclinations of 90° the inclination-only methods break down and can not be trusted, see Figure 5.11*c*.

We note in Figure 5.4 that the probability distributions for 80° and 90° at $\kappa = 10$ are very similar. For highly scattered data (low κ), due to a fold-back near the vertical, it may be difficult to ascertain the original (true) inclination. In Figure 5.12 we plot the probability distributions for true inclinations of 75°, 80°, and 85° and we vary the precision parameter of 8.6, 10, and 12, respectively. It is obviously impossible to distinguish I_0 and κ from data sets drawn from these three distributions, and any attempt to do so will depend critically on the assumptions of the calculation method that may not be true. Therefore, at very steep inclinations and low precision parameters the absence of declinations imply that some crucial information is irretrievably lost. However, with a priori knowledge of either the inclination or the precision parameter, the other parameter can be retrieved.

TABLE 5.1. Summary of the Simulations.

Simulation Parameters				Number of Parameter Solutions Out of 1000 Simulations	
I	κ	N	Seed	Kono	McFadden and Reid
0	10	5	51	1000	1000
0	10	100	17	1000	1000
0	20	5	45	1000	1000
0	20	100	27	1000	1000
0	40	5	36	1000	1000
0	40	100	107	1000	1000
0	100	5	28	1000	1000
0	100	100	109	1000	1000
10	10	5	52	1000	1000
10	10	100	18	1000	1000
10	20	5	46	1000	1000
10	40	5	37	1000	1000
10	100	5	29	1000	1000
20	10	5	53	999	1000
20	10	100	19	1000	1000
20	20	5	47	1000	1000
20	40	5	38	1000	1000
20	100	5	30	1000	1000
30	10	5	54	995	992
30	10	10	67	1000	1000
30	10	100	20	1000	1000
30	20	5	48	1000	1000
30	20	10	74	1000	1000
30	20	100	4	1000	1000
30	40	5	39	1000	1000
30	40	10	80	1000	1000
30	40	100	108	1000	1000
30	100	5	3	1000	1000
30	100	10	87	1000	1000
30	100	100	1	1000	1000
40	10	5	55	993	982
40	10	10	68	997	996
40	10	100	21	1000	1000
40	20	5	49	1000	1000
40	20	10	75	1000	1000
40	40	5	40	1000	1000
40	40	10	81	1000	1000

TABLE 5.1 continued.

Simulation Parameters				Number of Parameter Solutions Out of 1000 Simulations	
I	κ	N	Seed	Kono	McFadden and Reid
40	100	5	31	1000	1000
40	100	10	88	1000	1000
50	10	5	56	963	925
50	10	10	69	985	960
50	10	100	22	1000	1000
50	20	5	50	992	987
50	20	10	76	1000	1000
50	40	5	41	1000	1000
50	40	10	82	1000	1000
50	100	5	32	1000	1000
50	100	10	89	1000	1000
60	10	5	57	926	819
60	10	10	70	918	835
60	10	20	94	982	928
60	10	100	23	1000	967
60	20	5	7	968	933
60	20	10	77	985	951
60	20	20	98	994	978
60	40	5	42	1000	996
60	40	10	83	1000	998
60	40	20	101	1000	1000
60	100	5	33	1000	1000
60	100	10	90	1000	1000
60	100	20	2	1000	1000
70	10	5	58	851	729
70	10	10	71	843	688
70	10	20	95	834	690
70	10	100	24	869	645
70	20	5	10	911	784
70	20	10	78	889	777
70	20	20	99	892	765
70	20	100	60	1000	954
70	40	5	43	968	900
70	40	10	84	964	922
70	40	20	9	991	969
70	40	100	62	1000	1000
70	100	5	34	999	997
70	100	10	91	1000	1000

TABLE 5.1 continued.

Simulation Parameters				Number of Parameter Solutions Out of 1000 Simulations	
I	κ	N	Seed	Kono	McFadden and Reid
70	100	20	104	1000	1000
70	100	100	65	1000	1000
80	10	5	59	803	654
80	10	10	72	739	570
80	10	20	96	694	476
80	10	100	25	584	360
80	20	5	11	835	683
80	20	10	79	747	557
80	20	20	100	700	523
80	20	100	8	583	310
80	40	5	44	860	722
80	40	10	85	816	653
80	40	20	102	765	575
80	40	100	63	804	449
80	100	5	6	934	832
80	100	10	92	924	845
80	100	20	105	980	934
80	100	100	5	1000	1000
90	10	5	16	816	640
90	10	10	73	750	579
90	10	20	97	684	506
90	10	100	26	521	219
90	20	5	12	799	636
90	20	10	13	757	579
90	20	20	14	658	480
90	20	100	61	544	238
90	40	5	15	822	658
90	40	10	86	722	553
90	40	20	103	648	448
90	40	100	64	538	254
90	100	5	35	812	642
90	100	10	93	708	501
90	100	20	106	659	463
90	100	100	66	548	338

Figure 5.4. The probability distributions used for this study. These curves were calculated from equation (5.4). True inclination values I of 0°, 10°, 20°, 30°, 40°, 50°, 60°, 70°, 80°, and 90° were chosen and the precision parameter κ of 10, 20, 40, and 100.

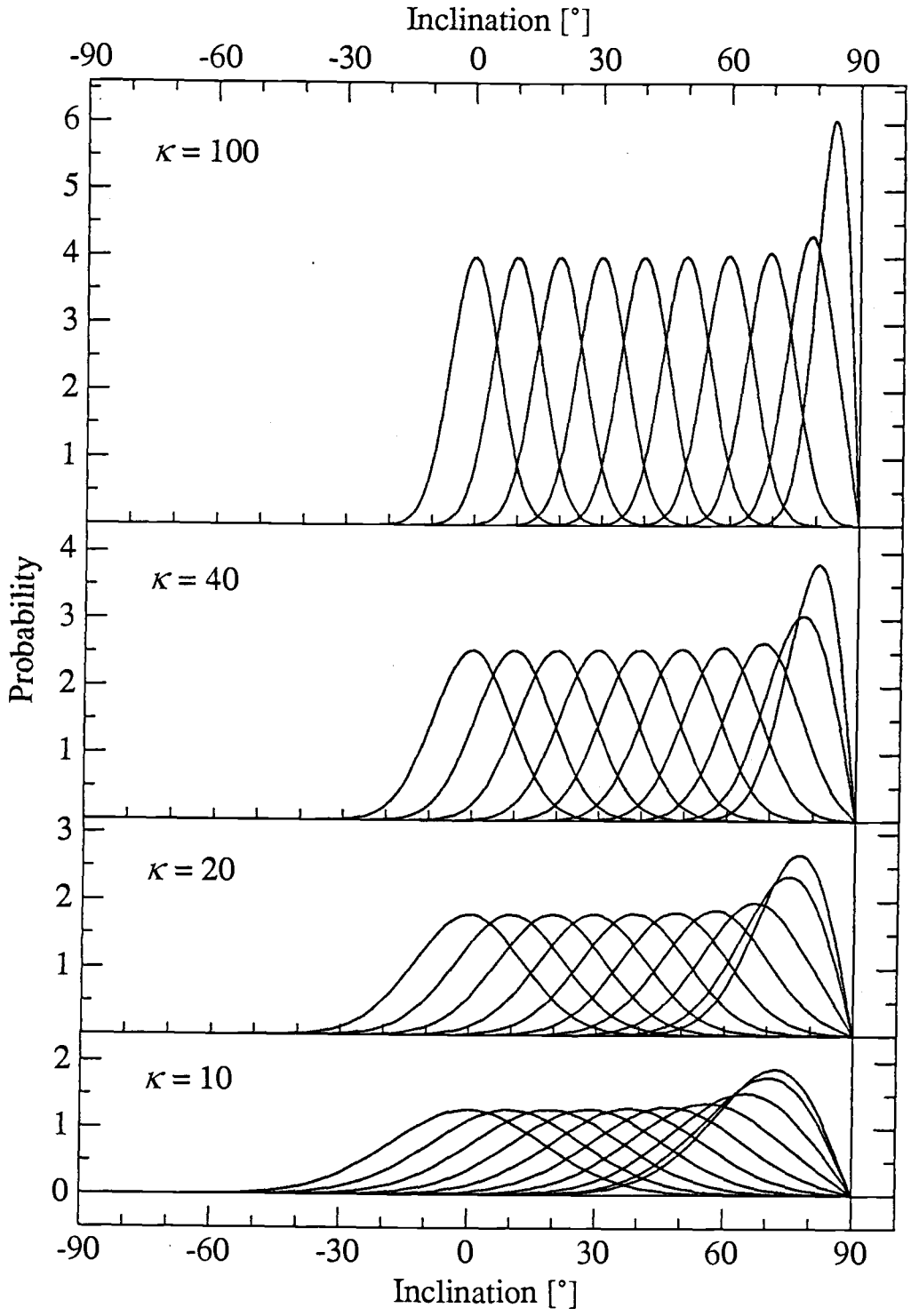
Inclination [°]
-90
-60
-30
0
30
60
90
κ = 100
κ = 40
κ = 20
κ = 10
Probability
Inclination [°]

Figure 5.4.

Figure 5.5. Histograms of inclination estimates of the several statistical methods for 1000 data sets generated from a Fisher distribution with true inclination I = 40°, true precision parameter κ = 40 and N = 10 samples in each set. Both inclinations and declinations were generated. The arithmetic mean of the inclinations (1000 estimates) is 39.44°, slightly shallower than 40°. The Fisher average using both the random-generated inclinations and the declinations is 40.01° showing no apparent bias. The K-method (Kono) and the modified-MR (McFadden and Reid) method for inclination-only data have arithmetic average values for the 1000 estimates of 40.00° and 39.98°, respectively, similar to the full Fisher average. However, the original-MR method has an apparent bias in the average inclination I = 39.44°, identical to the arithmetic mean.

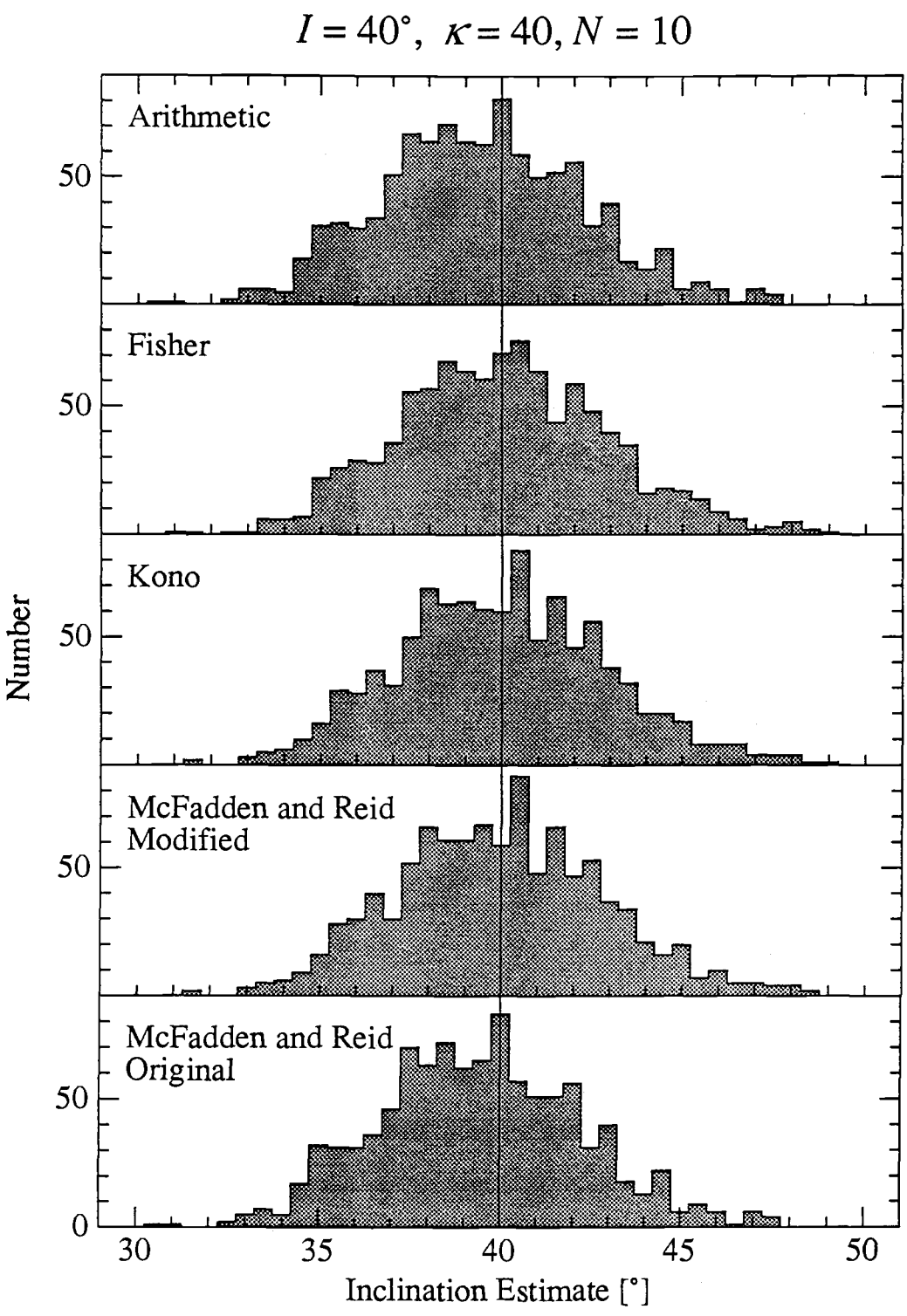
$I = 40°,\ \kappa = 40, N = 10$
Arithmetic
Fisher
Kono
McFadden and Reid
Modified
McFadden and Reid
Original
Number
50
50
50
50
50
0
30
35
40
45
50
Inclination Estimate [°]

Figure 5.5.

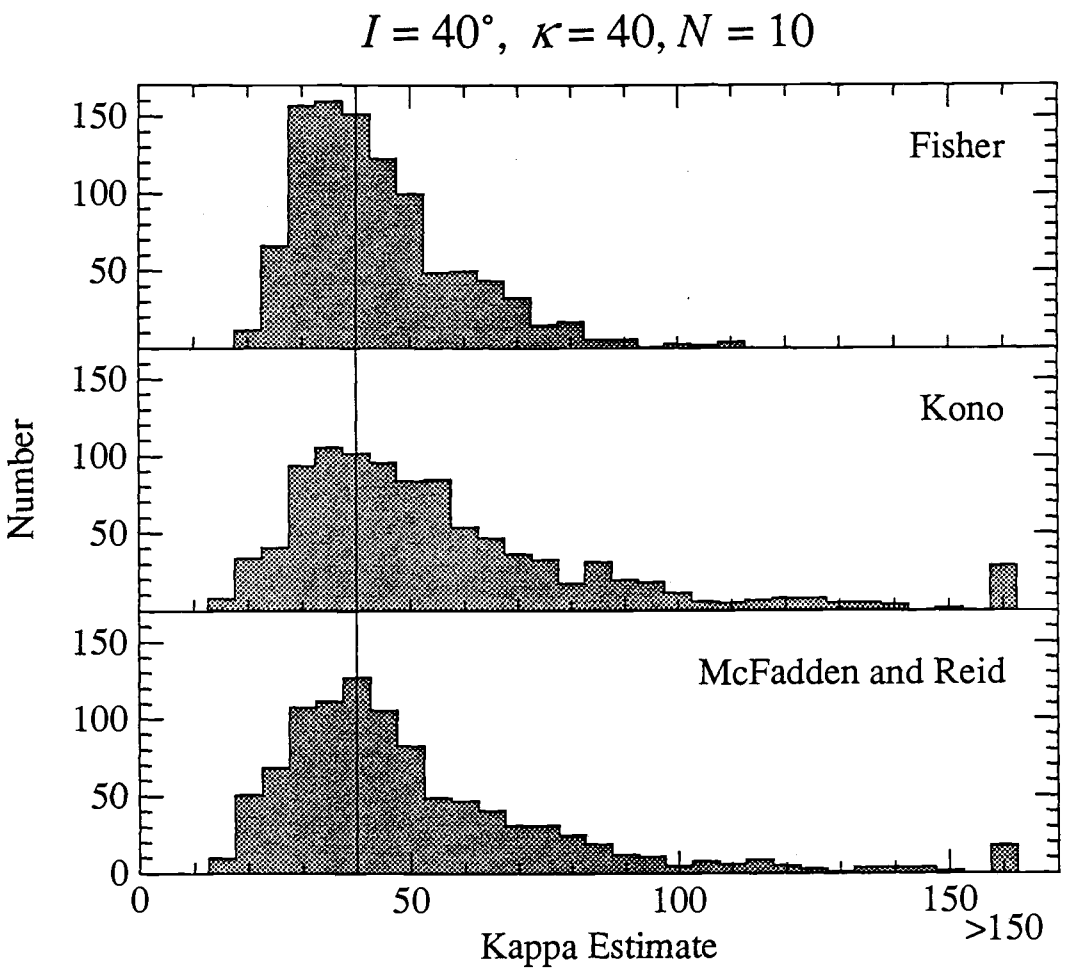

Figure 5.6. Histograms of precision parameter estimates of the statistical methods for 1000 data sets generated from a Fisher distribution with true inclination I = 40°, true precision parameter κ = 40, and N = 10 samples in each set. The data sets are the same as in Figure 5.5. The estimates of κ are more scattered when declination data are not available, and harmonic averages of the estimates for the methods of Fisher, Kono, and McFadden and Reid are 39.96, 44.9, and 40.9, respectively.

Figure 5.7. Histograms of inclination estimates of the statistical methods for 1000 data sets generated from a Fisher distribution with true inclination $I = 70°$, true precision parameter $\kappa = 10$, and $N = 20$ samples in each set. Both inclinations and declinations were generated. The arithmetic mean of the inclinations (1000 estimates) is 60.8°, significantly lower than 70°. The Fisher average using both the random-generated inclinations and the declinations is 69.6° showing no apparent bias. Of the 1000 data sets, 166 had no solution by the K-method (Kono); the remaining 834 solutions had mean inclination of 67.1°. For the MR-methods (McFadden and Reid) 310 of 1000 data sets had no solution, and the 690 solutions are biased to shallower values. The modified-MR method is slightly better than the original-MR method; mean of the 690 values are 63.5° and 60.2°, respectively. Note that the K-method estimates are spread out, while the MR-method shows less variance than the Fisher estimates. The asymptotic bias ($N \rightarrow \infty$) of the MR-method for this combination of I and κ is 4.6° too shallow, while there is no asymptotic bias in the K-method.

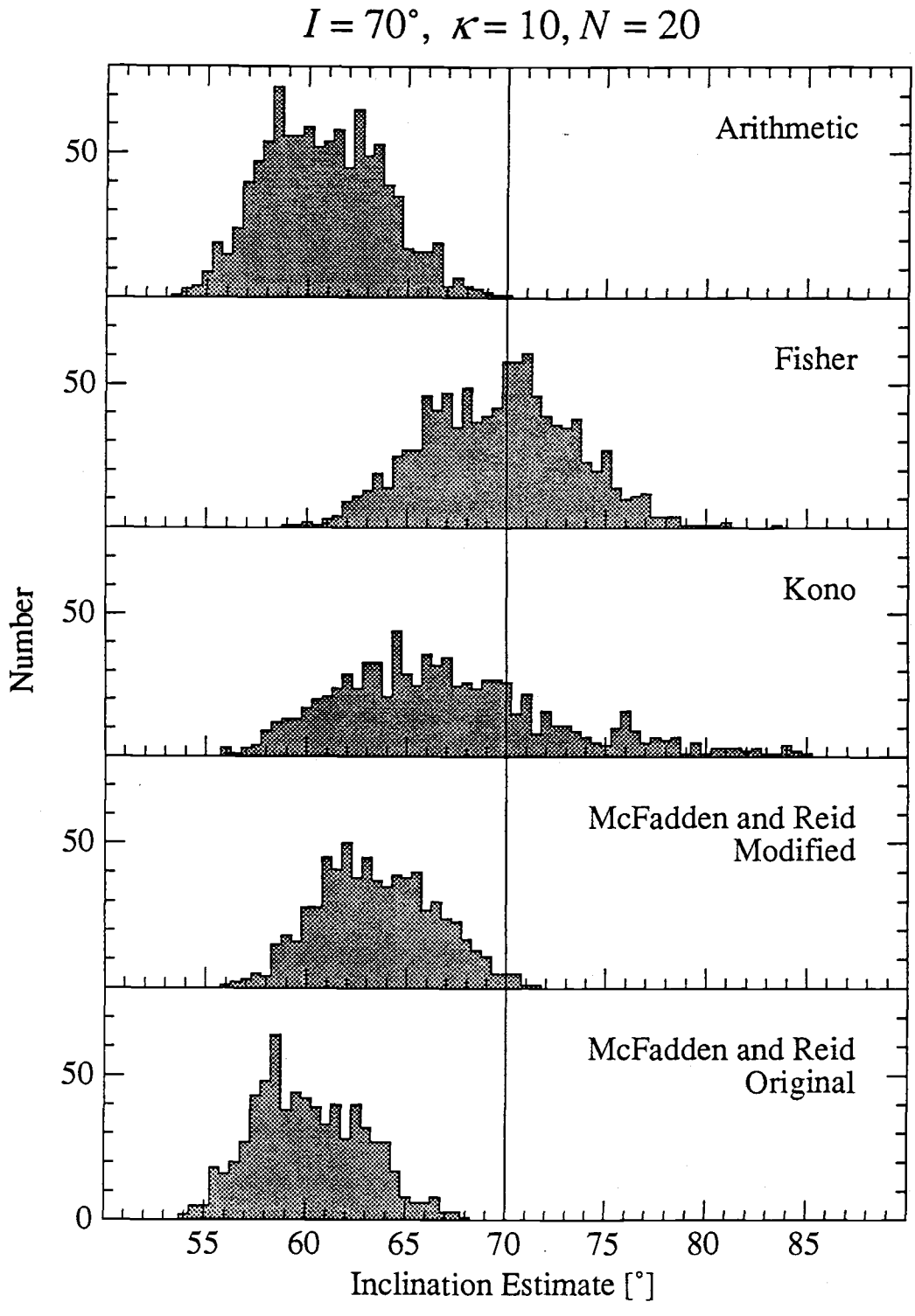
$I = 70°,\ \kappa = 10, N = 20$
Arithmetic
Fisher
Kono
McFadden and Reid Modified
McFadden and Reid Original
Number
50
50
50
50
0
55
60
65
70
75
80
85
Inclination Estimate [°]

Figure 5.7.

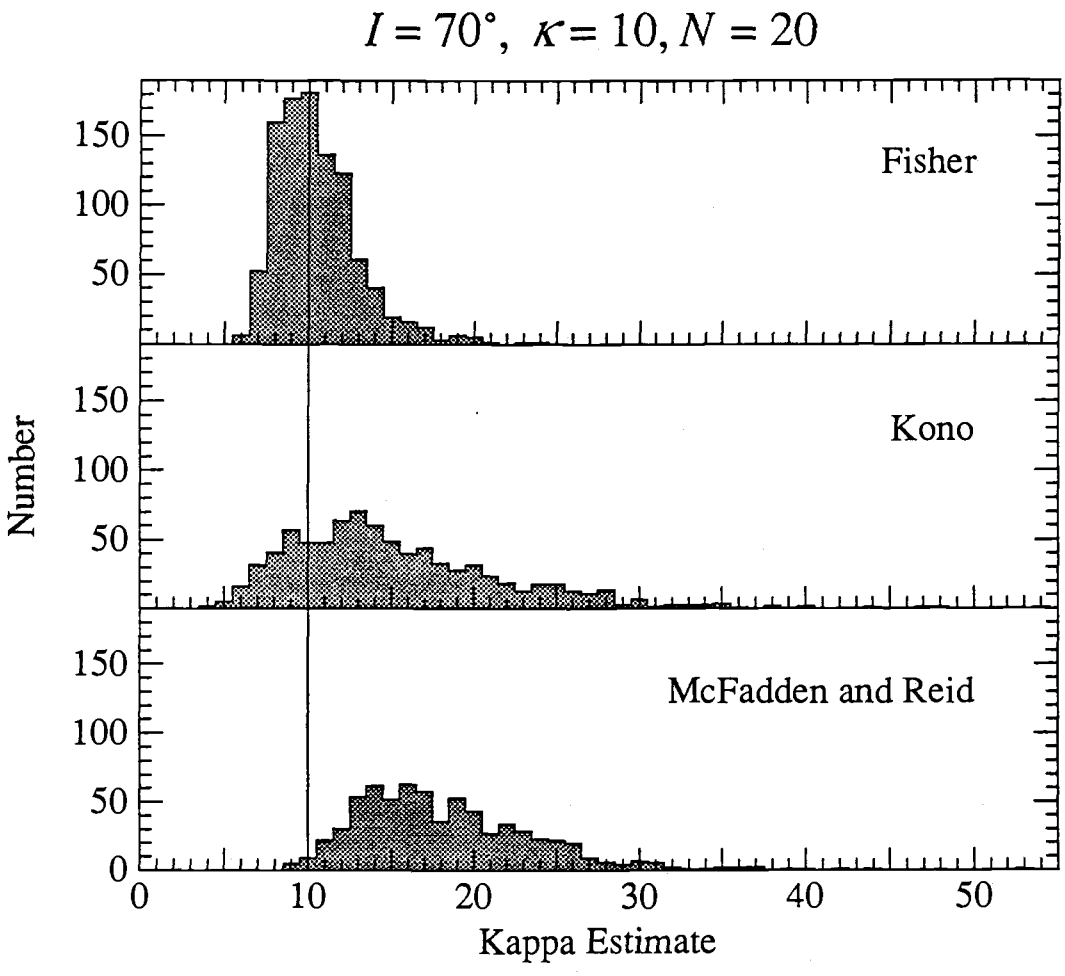

Figure 5.8. Histograms of precision parameter estimates of the statistical methods for 1000 data sets generated from a Fisher distribution with true inclination I = 70°, true precision parameter κ = 10, and N = 20 samples in each set. The data sets are the same as in Figure 5.7. The estimates of κ are more scattered when declination data are not available, and harmonic averages of the estimates for the methods of Fisher, Kono, and McFadden and Reid are 9.98, 13.0, and 17.0, respectively.

TABLE 5.2. Average Inclination Anomalies.

Simulation Parameters			Estimates of Inclination Anomaly				
						McFadden and Reid	
I	κ	N	Arithmetic deg	Fisher deg	Kono deg	Presented deg	Modified deg
0	10	5	0.24	0.26	0.27	0.24	0.26
0	10	100	0.54	0.58	0.59	0.55	0.59
0	20	5	0.39	0.40	0.40	0.39	0.40
0	20	100	0.37	0.38	0.38	0.37	0.38
0	40	5	0.47	0.48	0.48	0.47	0.48
0	40	100	0.27	0.27	0.27	0.27	0.27
0	100	5	0.26	0.26	0.26	0.26	0.26
0	100	100	0.03	0.03	0.03	0.03	0.03
10	10	5	–0.50	–0.04	0.04	–0.50	–0.06
10	10	100	–0.03	0.57	0.62	–0.02	0.57
10	20	5	0.16	0.38	0.41	0.16	0.39
10	40	5	–0.18	–0.07	–0.07	–0.18	–0.07
10	100	5	0.08	0.12	0.12	0.08	0.12
20	10	5	–1.12	–0.22	0.03	–1.11	–0.18
20	10	100	–0.64	0.57	0.68	–0.61	0.56
20	20	5	–0.25	0.21	0.26	–0.25	0.22
20	40	5	–0.04	0.18	0.20	–0.04	0.19
20	100	5	–0.04	0.05	0.06	–0.04	0.06
30	10	5	–1.25	0.27	0.76	–1.34	0.13
30	10	10	–1.36	0.40	0.91	–1.32	0.41
30	10	100	–1.35	0.56	0.76	–1.31	0.50
30	20	5	–0.87	–0.16	–0.14	–0.87	–0.19
30	20	10	–0.19	0.56	0.62	–0.19	0.57
30	20	100	–0.51	0.38	0.45	–0.50	0.40
30	40	5	0.04	0.36	0.39	0.04	0.38
30	40	10	–0.19	0.20	0.24	–0.18	0.23
30	40	100	–0.17	0.26	0.29	–0.17	0.28
30	100	5	0.04	0.17	0.18	0.04	0.18
30	100	10	–0.07	0.08	0.09	–0.07	0.09
30	100	100	–0.14	0.02	0.02	–0.14	0.02
40	10	5	–2.69	–0.50	–0.16	–2.86	–0.94
40	10	10	–3.12	–0.82	–0.29	–3.13	–0.96
40	10	100	–2.29	0.53	0.83	–2.24	0.30
40	20	5	–0.91	0.12	0.31	–0.91	0.15
40	20	10	–0.96	0.22	0.39	–0.95	0.25
40	40	5	–0.40	0.11	0.17	–0.39	0.13
40	40	10	–0.56	0.01	0.00	–0.56	–0.02

TABLE 5.2 continued.

Simulation Parameters			Estimates of Inclination Anomaly				
						McFadden and Reid	
I	κ	N	Arithmetic deg	Fisher deg	Kono deg	Presented deg	Modified deg
40	100	5	–0.27	–0.07	–0.08	–0.27	–0.08
40	100	10	–0.39	–0.18	–0.17	–0.39	–0.17
50	10	5	–3.89	–0.70	–1.03	–4.49	–2.29
50	10	10	–3.02	0.54	0.77	–3.27	–0.50
50	10	100	–2.91	0.96	1.11	–2.86	0.27
50	20	5	–1.59	–0.10	0.15	–1.70	–0.24
50	20	10	–1.45	0.26	0.57	–1.44	0.25
50	40	5	–0.76	–0.03	–0.02	–0.76	–0.05
50	40	10	–0.63	0.18	0.26	–0.63	0.20
50	100	5	–0.27	0.01	0.03	–0.27	0.02
50	100	10	–0.17	0.15	0.18	–0.17	0.17
60	10	5	–4.97	–0.08	–1.83	–6.07	–3.74
60	10	10	–5.98	–0.56	–1.28	–6.70	–3.64
60	10	20	–5.90	–0.16	–0.17	–6.02	–2.54
60	10	100	–4.93	0.94	1.24	–4.89	–1.06
60	20	5	–2.44	–0.14	–0.15	–2.70	–0.92
60	20	10	–2.49	0.08	0.49	–2.69	–0.53
60	20	20	–2.45	0.27	0.75	–2.48	–0.13
60	40	5	–1.05	0.02	0.22	–1.08	0.02
60	40	10	–1.10	0.10	0.23	–1.11	0.08
60	40	20	–1.08	0.18	0.35	–1.08	0.19
60	100	5	–0.18	0.21	0.23	–0.18	0.23
60	100	10	–0.36	0.11	0.16	–0.36	0.13
60	100	20	–0.36	0.13	0.17	–0.36	0.15
70	10	5	–9.16	–1.48	–6.06	–10.23	–7.88
70	10	10	–9.26	–1.37	–4.43	–9.90	–7.03
70	10	20	–9.24	–0.38	–2.94	–9.81	–6.47
70	10	100	–9.34	–0.20	0.03	–9.72	–5.69
70	20	5	–3.87	–0.15	–1.73	–4.70	–2.97
70	20	10	–4.41	–0.08	–0.92	–4.91	–2.62
70	20	20	–4.39	0.17	–0.01	–4.79	–2.21
70	20	100	–4.67	–0.39	0.14	–4.70	–1.75
70	40	5	–1.55	0.16	–0.11	–1.94	–0.70
70	40	10	–2.08	–0.07	–0.12	–2.29	–0.75
70	40	20	–2.18	–0.14	0.07	–2.24	–0.51
70	40	100	–1.97	0.25	0.52	–1.96	–0.05
70	100	5	–0.72	–0.05	–0.04	–0.73	–0.07
70	100	10	–0.68	0.07	0.17	–0.68	0.09

TABLE 5.2 continued.

Simulation Parameters			Estimates of Inclination Anomaly				
						McFadden and Reid	
I	κ	N	Arithmetic deg	Fisher deg	Kono deg	Presented deg	Modified deg
70	100	20	–0.49	0.26	0.28	–0.49	0.25
70	100	100	–0.48	0.30	0.33	–0.48	0.29
80	10	5	–14.78	–4.04	–11.84	–15.84	–13.76
80	10	10	–14.62	–2.30	–10.17	–15.29	–12.69
80	10	20	–14.81	–0.54	–8.50	–15.59	–12.44
80	10	100	–13.96	0.82	–4.16	–14.14	–10.65
80	20	5	–7.91	–1.21	–5.86	–8.50	–6.99
80	20	10	–8.51	–0.69	–5.25	–9.28	–7.29
80	20	20	–8.51	–0.08	–4.29	–9.01	–6.69
80	20	100	–8.53	0.29	–1.63	–8.80	–6.02
80	40	5	–4.69	–0.97	–3.22	–5.16	–4.03
80	40	10	–4.60	–0.39	–2.35	–5.01	–3.59
80	40	20	–4.56	0.02	–1.60	–4.90	–3.17
80	40	100	–4.55	0.23	0.21	–4.69	–2.58
80	100	5	–1.84	–0.36	–0.87	–2.06	–1.29
80	100	10	–1.87	–0.32	–0.54	–2.11	–1.09
80	100	20	–1.82	–0.05	–0.13	–1.86	–0.70
80	100	100	–1.82	0.01	–0.05	–1.82	–0.56
90	10	5	–23.52	–11.05	–20.60	–24.27	–22.38
90	10	10	–22.61	–7.65	–18.15	–22.90	–20.45
90	10	20	–22.60	–5.56	–16.44	–22.67	–19.77
90	10	100	–23.44	–2.32	–14.31	–24.18	–20.48
90	20	5	–16.41	–7.55	–14.56	–17.06	–15.66
90	20	10	–15.88	–5.20	–12.86	–16.07	–14.36
90	20	20	–16.47	–3.74	–12.76	–16.89	–14.85
90	20	100	–16.46	–1.67	–10.30	–16.92	–14.33
90	40	5	–11.53	–5.28	–10.39	–11.95	–11.04
90	40	10	–11.59	–3.86	–9.82	–12.00	–10.76
90	40	20	–11.58	–2.62	–8.97	–11.96	–10.52
90	40	100	–11.60	–1.14	–7.53	–11.84	–10.02
90	100	5	–7.27	–3.24	–6.56	–7.56	–6.96
90	100	10	–7.15	–2.25	–5.93	–7.40	–6.64
90	100	20	–7.12	–1.68	–5.51	–7.25	–6.40
90	100	100	–7.11	–0.76	–4.68	–7.21	–6.17

TABLE 5.3. Harmonic Averages of the Precision Parameter.

Simulation Parameters			Estimates of Relative Anomaly of κ		
I	κ	N	Fisher %	Kono %	McFadden and Reid %
0	10	5	–0.9	17.8	3.0
0	10	100	–4.3	–6.9	–4.4
0	20	5	–2.9	14.4	–4.5
0	20	100	–4.2	–6.4	–5.8
0	40	5	4.5	26.1	2.5
0	40	100	–4.3	–6.5	–6.7
0	100	5	2.2	26.9	2.1
0	100	100	0.0	1.7	1.0
10	10	5	–0.4	18.8	3.6
10	10	100	–4.3	–7.0	–4.2
10	20	5	–1.8	17.3	–2.5
10	40	5	–0.9	22.9	0.0
10	100	5	–3.1	17.5	–5.3
20	10	5	–0.7	14.6	0.0
20	10	100	–4.3	–7.4	–3.7
20	20	5	–3.2	15.4	–3.8
20	40	5	–1.7	17.9	–3.7
20	100	5	–4.6	16.1	–6.3
30	10	5	–1.8	13.0	1.3
30	10	10	–4.4	–3.1	–3.6
30	10	100	–4.3	–7.7	–2.6
30	20	5	–0.1	24.0	2.7
30	20	10	3.9	12.7	3.9
30	20	100	–4.2	–7.0	–5.4
30	40	5	3.8	26.0	2.0
30	40	10	–3.9	2.1	–6.4
30	40	100	–4.1	–6.6	–6.3
30	100	5	–3.1	17.0	–5.6
30	100	10	–2.9	5.7	–4.1
30	100	100	–0.1	2.0	1.3
40	10	5	–0.9	21.2	7.9
40	10	10	2.2	7.1	6.1
40	10	100	–4.1	–7.7	0.2
40	20	5	–1.5	15.9	–1.8
40	20	10	–3.9	1.1	–4.4
40	40	5	–2.9	15.6	–5.0
40	40	10	–0.1	12.2	2.3

TABLE 5.3 continued.

Simulation Parameters			Estimates of Relative Anomaly of κ		
			Fisher	Kono	McFadden and Reid
I	κ	N	%	%	%
40	100	5	0.6	28.1	3.4
40	100	10	1.9	10.2	–0.1
50	10	5	–0.1	35.8	23.7
50	10	10	3.4	14.9	18.3
50	10	100	3.4	2.9	14.3
50	20	5	–2.6	16.2	0.2
50	20	10	–3.5	0.6	–2.7
50	40	5	–2.8	22.5	–0.5
50	40	10	–3.0	3.6	–3.8
50	100	5	–2.1	18.7	–4.2
50	100	10	–3.5	2.4	–6.6
60	10	5	2.6	59.4	54.4
60	10	10	–1.8	19.8	33.3
60	10	20	–0.5	8.9	29.2
60	10	100	3.5	2.9	28.3
60	20	5	–2.9	27.0	15.0
60	20	10	–4.0	1.2	6.6
60	20	20	–4.0	–5.3	4.2
60	40	5	–3.4	14.1	–4.1
60	40	10	–3.4	3.4	–2.0
60	40	20	–4.1	–4.4	–4.2
60	100	5	3.6	27.0	1.9
60	100	10	–4.1	1.5	–6.6
60	100	20	–4.1	–2.7	–5.9
70	10	5	–2.3	89.9	87.2
70	10	10	2.6	50.9	80.7
70	10	20	–0.2	30.3	70.3
70	10	100	–1.2	1.3	51.5
70	20	5	3.4	66.4	61.0
70	20	10	–3.6	22.4	39.4
70	20	20	–4.0	6.7	32.4
70	20	100	1.8	–2.6	23.3
70	40	5	4.2	42.0	28.6
70	40	10	–2.9	10.4	14.1
70	40	20	–1.5	0.2	8.2
70	40	100	–4.2	–8.6	3.3
70	100	5	–2.9	21.4	–1.3
70	100	10	–3.9	1.3	–4.9

TABLE 5.3 continued.

Simulation Parameters			Estimates of Relative Anomaly of κ		
I	κ	N	Fisher %	Kono %	McFadden and Reid %
70	100	20	3.5	7.8	4.9
70	100	100	3.5	2.7	4.2
80	10	5	–2.8	139.5	150.4
80	10	10	1.0	94.4	140.8
80	10	20	–3.7	56.9	113.3
80	10	100	3.5	27.4	120.0
80	20	5	3.2	139.6	147.7
80	20	10	–3.5	70.3	109.3
80	20	20	–3.8	48.2	97.6
80	20	100	–4.3	12.8	80.6
80	40	5	–0.8	105.9	104.6
80	40	10	–0.4	58.6	90.3
80	40	20	–4.2	28.6	70.0
80	40	100	–4.3	–0.6	52.0
80	100	5	0.5	57.9	52.3
80	100	10	2.5	24.8	32.0
80	100	20	–0.3	10.0	25.6
80	100	100	0.0	3.8	22.0
90	10	5	–3.4	159.2	192.0
90	10	10	4.2	116.4	181.9
90	10	20	4.0	81.5	162.5
90	10	100	–4.3	35.9	110.4
90	20	5	–2.8	173.1	192.1
90	20	10	4.0	125.1	191.8
90	20	20	–4.2	88.6	154.2
90	20	100	–4.2	39.6	116.4
90	40	5	–1.0	213.3	219.9
90	40	10	–3.2	128.3	171.1
90	40	20	–3.9	87.3	155.8
90	40	100	–4.3	44.9	121.7
90	100	5	–2.9	204.9	205.4
90	100	10	0.2	128.1	191.3
90	100	20	2.1	110.2	184.4
90	100	100	1.8	60.8	153.9

TABLE 5.4. The 95% Confidence Limits of Inclinations.

Simulation Parameters			Estimates ($I \pm \alpha_{95}$) that Include True Mean			
					McFadden and Reid	
I	κ	N	Fisher %	Kono %	Presented %	Modified %
0	10	5	95.5	93.7	97.5	97.4
0	10	100	99.1	100.0	100.0	100.0
0	20	5	93.4	94.4	97.8	97.8
0	20	100	97.8	100.0	99.6	99.6
0	40	5	95.0	94.4	97.3	97.3
0	40	100	97.3	99.1	99.1	99.1
0	100	5	95.1	93.9	97.0	97.0
0	100	100	92.5	98.9	98.5	98.5
10	10	5	96.1	94.8	97.2	97.2
10	10	100	97.9	98.9	99.9	99.9
10	20	5	94.4	94.5	97.9	97.9
10	40	5	93.6	94.3	97.2	97.2
10	100	5	94.8	94.7	98.2	98.2
20	10	5	94.1	93.6	97.5	97.5
20	10	100	98.1	99.1	99.0	99.0
20	20	5	94.2	94.0	97.7	97.7
20	40	5	92.8	92.5	96.8	96.8
20	100	5	95.1	94.7	98.1	98.1
30	10	5	93.2	94.1	98.1	98.1
30	10	10	95.1	96.1	97.7	97.7
30	10	100	99.1	100.0	98.1	98.1
30	20	5	95.3	93.6	96.7	96.7
30	20	10	94.2	95.4	96.6	96.6
30	20	100	98.0	99.1	98.5	98.5
30	40	5	94.9	95.5	97.7	97.7
30	40	10	94.3	96.7	97.8	97.8
30	40	100	97.9	99.9	99.8	99.8
30	100	5	94.2	94.7	98.6	98.6
30	100	10	94.4	96.5	97.6	97.6
30	100	100	92.4	98.6	99.0	99.0
40	10	5	96.1	94.8	97.8	97.8
40	10	10	94.7	95.7	95.6	95.5
40	10	100	98.6	98.8	92.8	92.8
40	20	5	94.2	93.2	97.1	97.1
40	20	10	93.9	96.8	97.8	97.8
40	40	5	94.4	93.9	97.8	97.8
40	40	10	95.1	96.7	97.8	97.8

TABLE 5.4 continued.

Simulation Parameters			Estimates ($I \pm \alpha_{95}$) that Include True Mean			
					McFadden and Reid	
I	κ	N	Fisher %	Kono %	Presented %	Modified %
40	100	5	95.7	95.1	97.6	97.6
40	100	10	94.9	96.5	97.1	97.1
50	10	5	94.5	92.3	96.2	96.2
50	10	10	94.7	94.9	95.1	95.1
50	10	100	89.7	92.8	85.0	85.0
50	20	5	94.6	93.5	97.5	97.5
50	20	10	94.7	95.9	97.5	97.5
50	40	5	95.1	94.4	97.7	97.7
50	40	10	94.5	96.2	97.4	97.4
50	100	5	96.4	94.7	97.7	97.7
50	100	10	96.1	96.8	97.7	97.7
60	10	5	95.0	92.2	95.2	95.2
60	10	10	94.8	91.7	90.9	90.9
60	10	20	95.5	92.7	82.7	82.5
60	10	100	89.0	87.2	58.2	58.2
60	20	5	93.8	93.6	96.6	96.6
60	20	10	95.1	94.9	95.4	95.4
60	20	20	94.3	95.5	94.8	94.8
60	40	5	93.5	94.3	97.5	97.5
60	40	10	95.5	95.6	96.6	96.6
60	40	20	94.5	97.3	96.5	96.5
60	100	5	95.1	95.4	97.9	97.9
60	100	10	96.3	96.9	97.3	97.3
60	100	20	95.2	97.5	97.7	97.7
70	10	5	93.8	85.7	90.7	90.4
70	10	10	95.0	84.9	71.4	70.9
70	10	20	96.0	78.9	30.3	30.3
70	10	100	91.4	65.1	0.0	0.0
70	20	5	95.2	92.4	95.5	95.5
70	20	10	94.3	91.8	89.3	89.3
70	20	20	94.0	90.0	79.4	79.4
70	20	100	92.4	89.4	26.1	26.0
70	40	5	94.8	93.7	96.7	96.7
70	40	10	96.1	94.1	94.9	94.9
70	40	20	96.4	95.1	90.2	90.2
70	40	100	98.1	95.9	85.0	85.0
70	100	5	93.9	95.2	97.8	97.8
70	100	10	93.8	96.0	97.1	97.1

TABLE 5.4 continued.

Simulation Parameters			Estimates ($I \pm \alpha_{95}$) that Include True Mean			
					McFadden and Reid	
I	κ	N	Fisher %	Kono %	Presented %	Modified %
70	100	20	94.4	95.4	94.6	94.6
70	100	100	88.9	92.8	97.4	97.4
80	10	5	94.4	58.9	67.1	66.7
80	10	10	95.0	48.0	3.3	3.3
80	10	20	94.4	44.8	0.0	0.0
80	10	100	89.2	41.1	0.0	0.0
80	20	5	95.3	76.1	81.3	81.3
80	20	10	96.5	68.1	29.6	29.6
80	20	20	94.2	61.4	1.7	1.7
80	20	100	97.1	57.3	0.0	0.0
80	40	5	93.7	84.0	87.5	87.5
80	40	10	95.1	82.1	67.4	67.4
80	40	20	94.4	83.1	31.7	31.7
80	40	100	99.0	74.3	0.0	0.0
80	100	5	94.1	89.3	94.5	94.5
80	100	10	94.7	93.1	90.9	90.9
80	100	20	96.3	92.9	85.1	85.1
80	100	100	92.5	89.3	37.2	37.2
90	10	5	93.8	21.5	0.2	0.0
90	10	10	93.9	11.2	0.0	0.0
90	10	20	94.6	8.0	0.0	0.0
90	10	100	97.9	3.7	0.0	0.0
90	20	5	93.8	18.3	0.0	0.0
90	20	10	94.3	9.8	0.0	0.0
90	20	20	94.6	4.6	0.0	0.0
90	20	100	98.0	0.0	0.0	0.0
90	40	5	94.2	14.6	0.0	0.0
90	40	10	94.0	6.9	0.0	0.0
90	40	20	94.5	4.6	0.0	0.0
90	40	100	99.1	0.0	0.0	0.0
90	100	5	94.7	14.8	0.0	0.0
90	100	10	94.8	7.8	0.0	0.0
90	100	20	94.4	3.0	0.0	0.0
90	100	100	91.8	0.4	0.0	0.0

Figure 5.9. Histograms of the average inclination anomalies of the methods. These data are listed in Table 5.2. For each combination of (I, κ, N) a 1000 data sets were generated and the mean of these 1000 inclination estimates were compared to the true value. (*a*) Histograms for the 61 combinations where the true inclination was 0° to 60°. Both the arithmetic mean and the original-MR method show significant anomalies. However, both the K-method and the modified-MR method give reasonable estimates, although both the MR-method estimates have more outliers for I = 60° and κ = 10. (*b*) Histograms for the 32 combinations where the true inclination was 70° and 80°. For these steep inclinations both the K-method and the modified-MR method are collapsing. However, the K-method still has a cluster of estimates close to the true value. (*c*) Histograms for the 16 combinations where the true inclination was 90°. For this inclination both the Kono method and the McFadden and Reid method have collapsed.

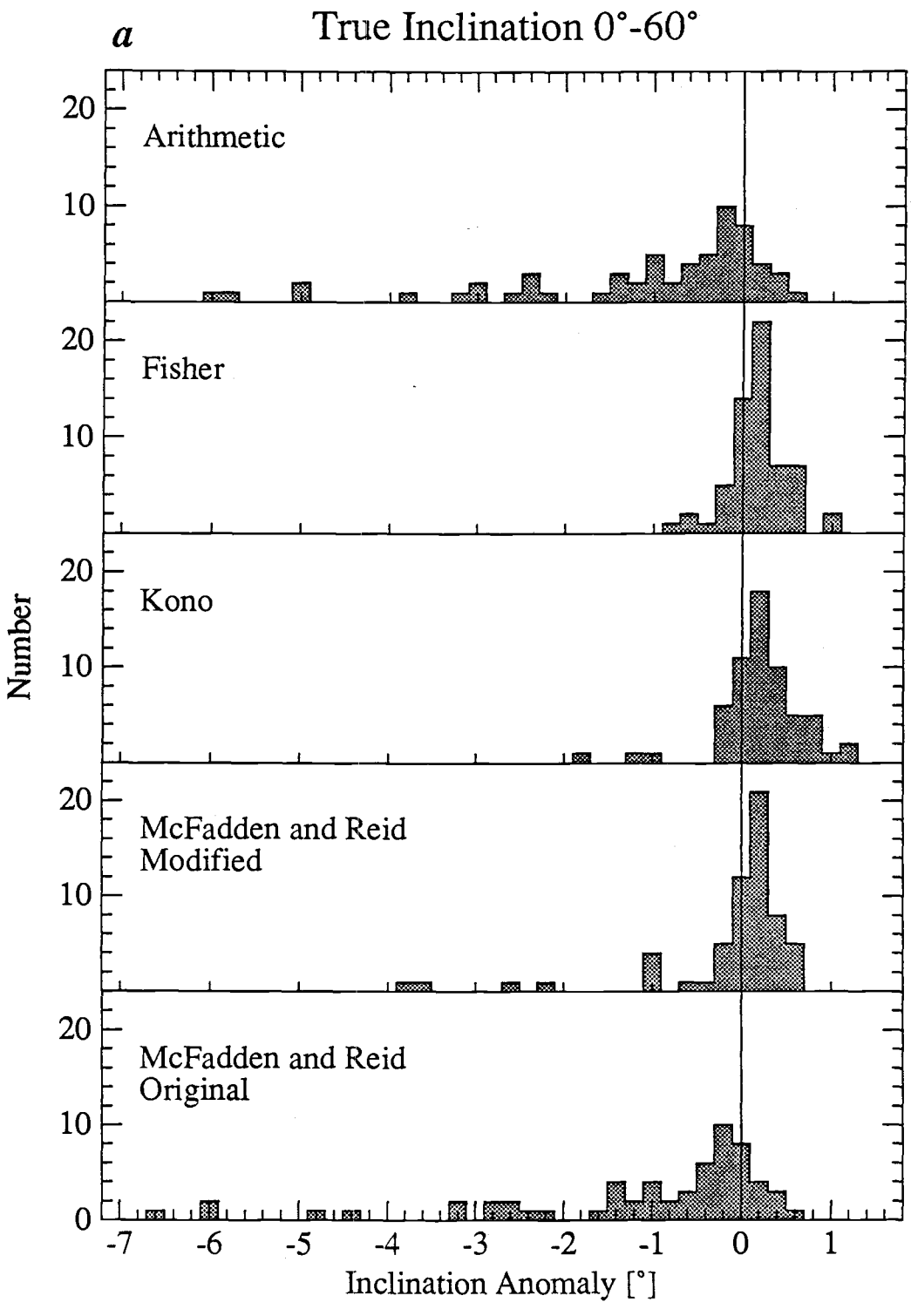
a
True Inclination 0°-60°
Arithmetic
Fisher
Kono
McFadden and Reid
Modified
McFadden and Reid
Original
Number
20
10
0
-7
-6
-5
-4
-3
-2
-1
0
1
Inclination Anomaly [°]

Figure 5.9.

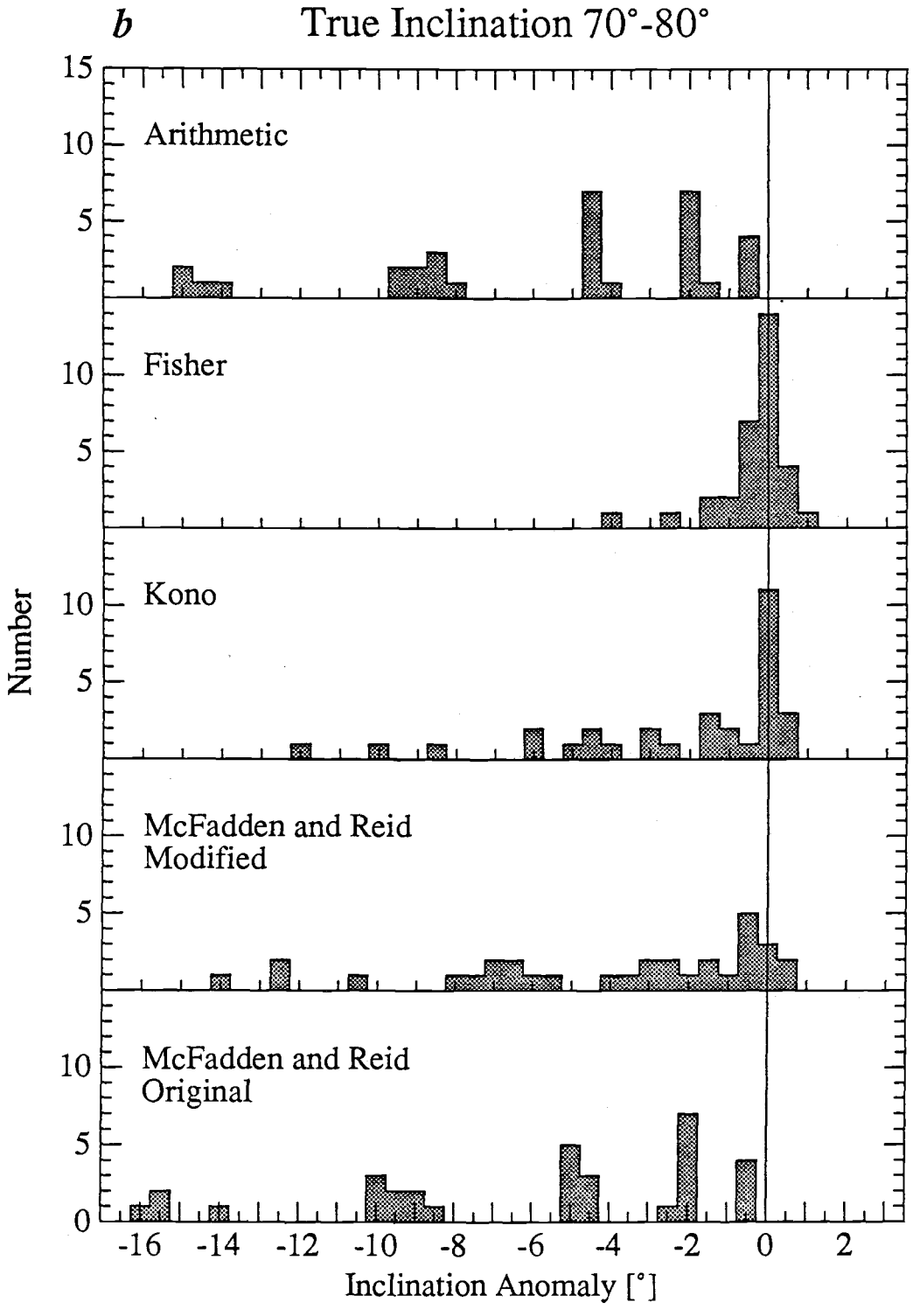

Figure 5.9 continued.

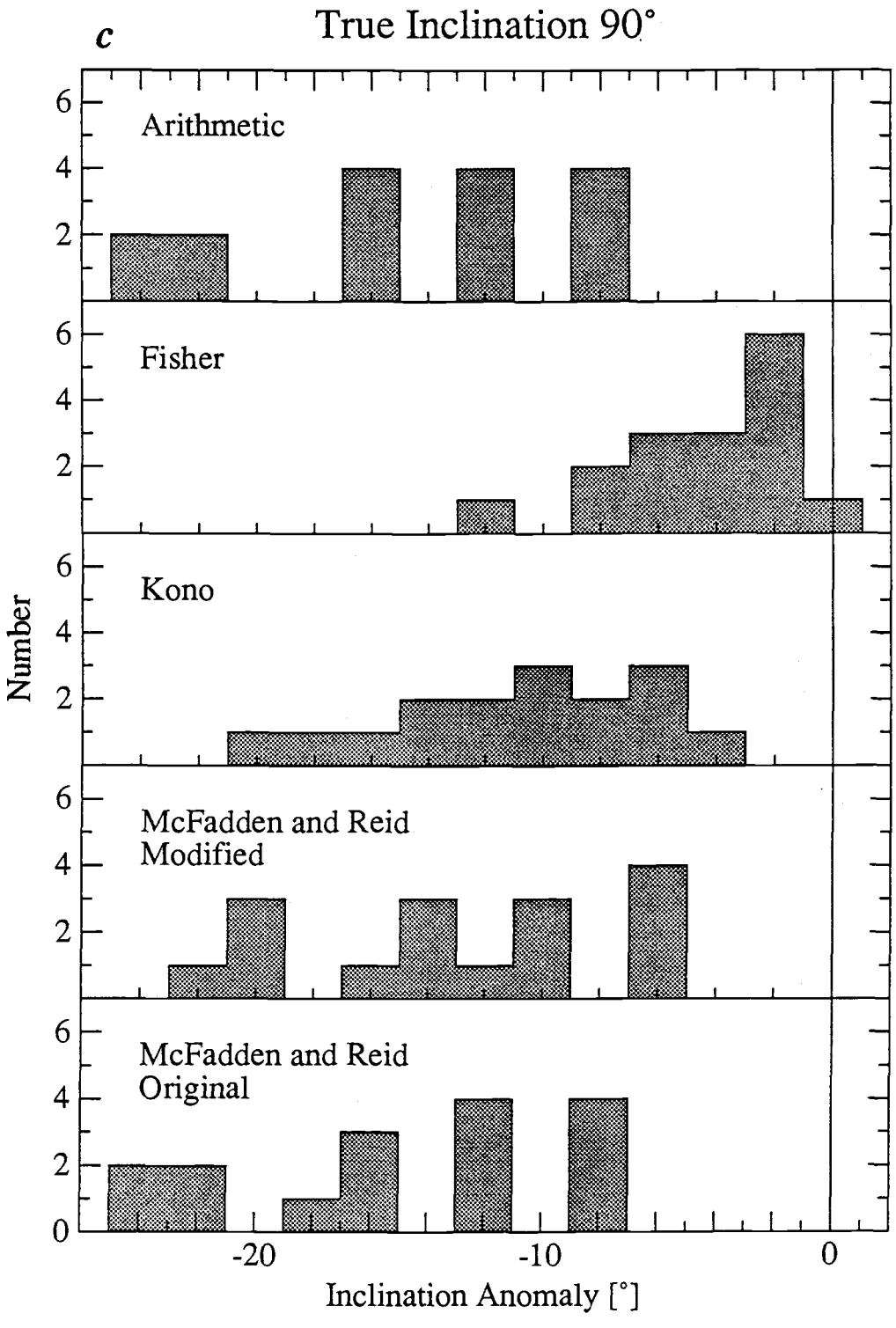

Figure 5.9 continued.

Figure 5.10. Histograms of the harmonic averages of the precision parameter of the methods. The data are listed in Table 5.3. For each combination of (I, κ, N) a 1000 data sets were generated and the harmonic average of these 1000 precision parameter estimates were compared to the true value. (a) Histograms for the 61 combinations where the true inclination was 0° to 60°. With the lack of the declination the Kono method and the McFadden and Reid method cannot give as accurate estimate of the precision parameter as the Fisher method. (b) Histograms for the 32 combinations where the true inclination was 70° and 80°. For these steep inclinations both the Kono method and the McFadden and Reid method are collapsing and the precision parameter estimate can on average be biased to double its true value. (c) Histograms for the 16 combinations where the true inclination was 90°. For this inclination both the Kono method and the McFadden and Reid method have collapsed.

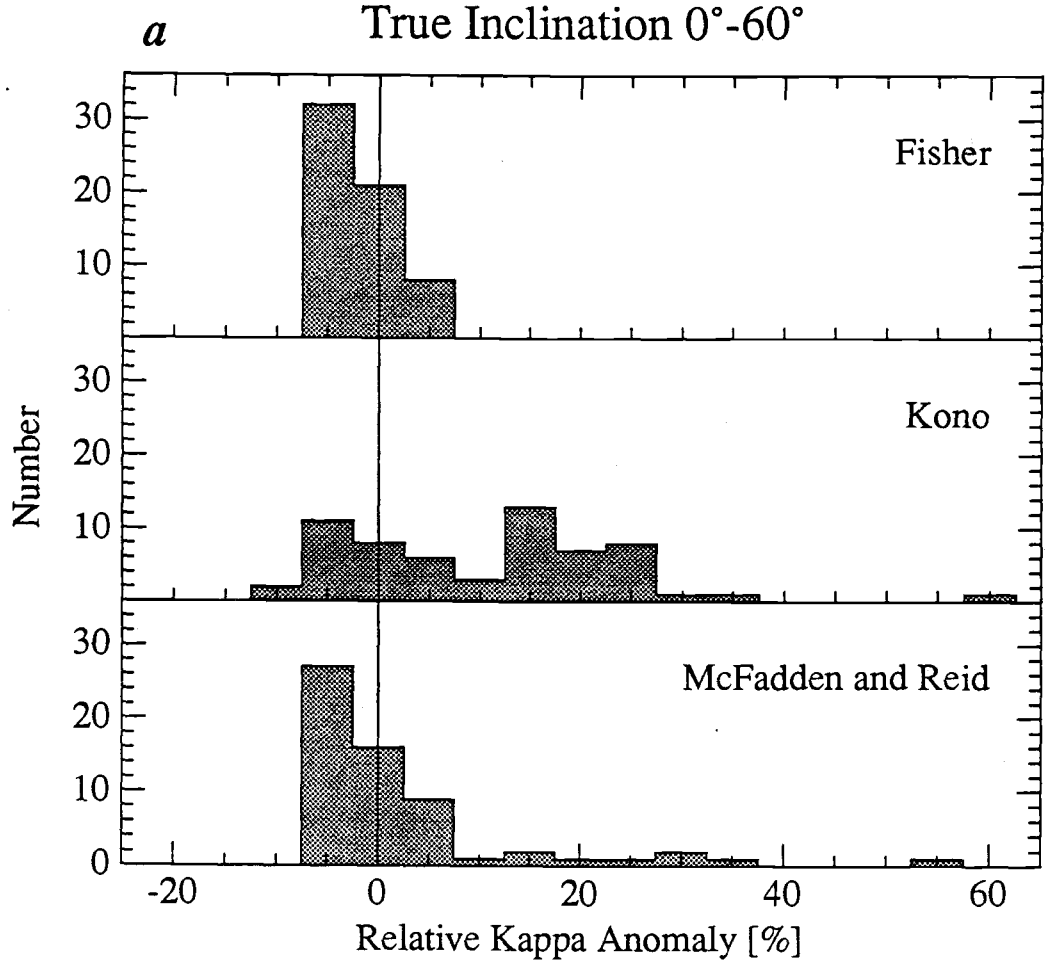
a
True Inclination 0°-60°
Fisher
Kono
McFadden and Reid
Number
30
20
10
0
-20
0
20
40
60
Relative Kappa Anomaly [%]

Figure 5.10.

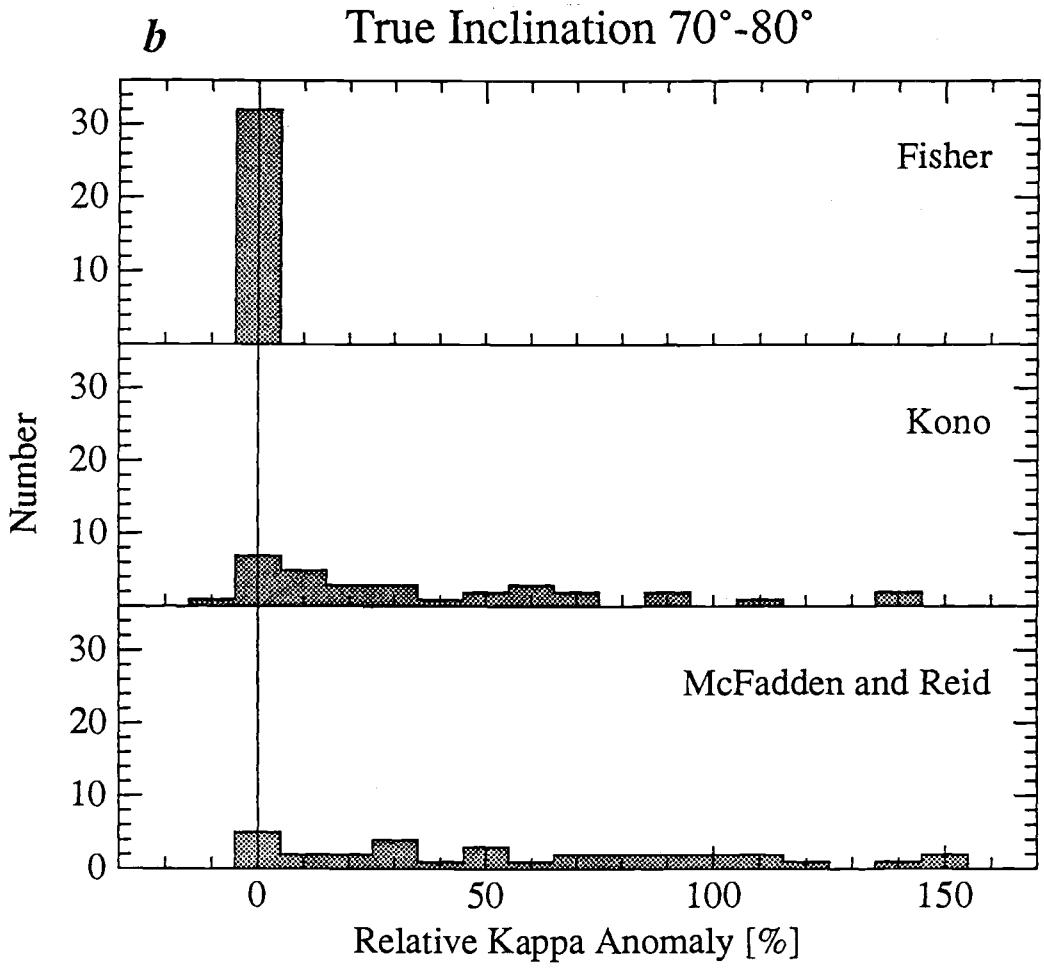

Figure 5.10 continued.

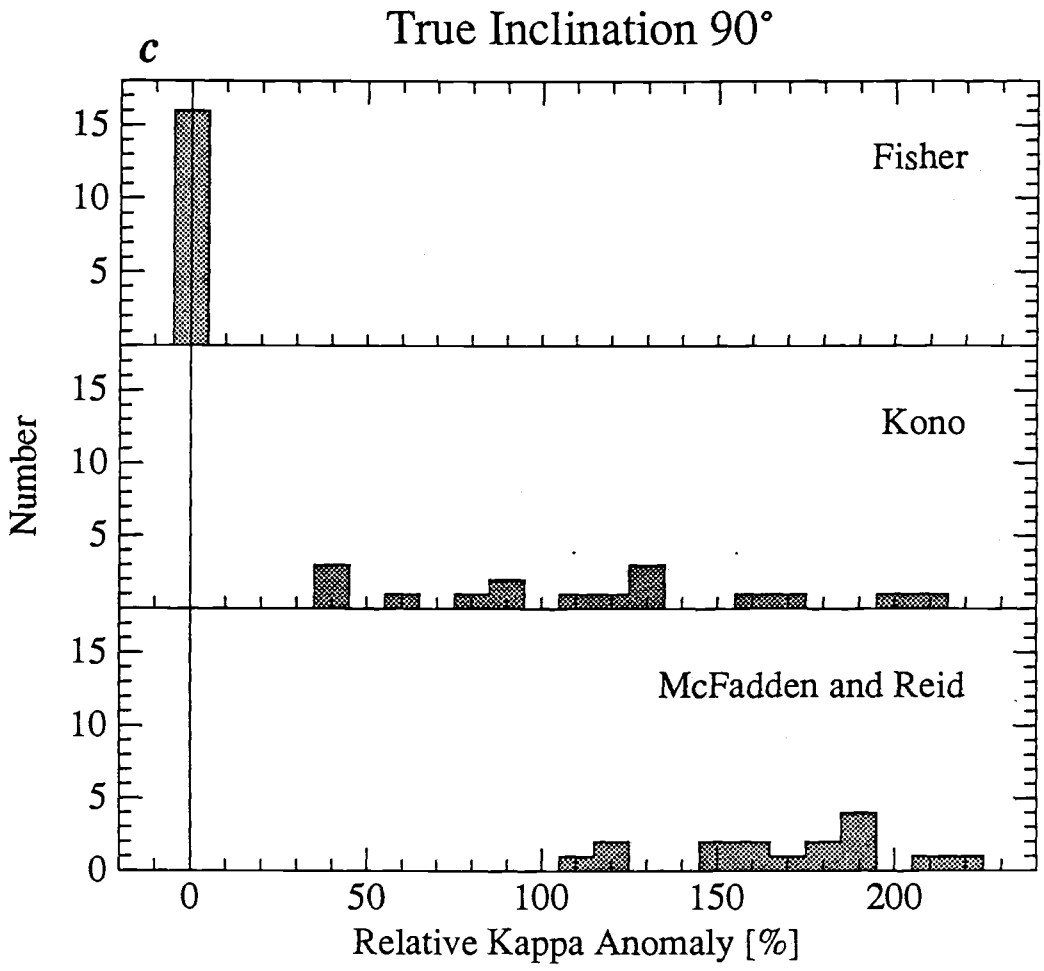

Figure 5.10 continued.

Figure 5.11. Histogram of the success of the 95% confidence interval of the methods. The data are listed in Table 5.4. For each combination of (I, κ, N) a 1000 data sets were generated and we counted how many (%) of the estimates ($I \pm \alpha_{95}$) included the true mean. Ideally 95% of the estimates should include the true mean, lower count indicates an underestimate of the α_{95}. (*a*) Histograms for the 61 combinations where the true inclination was 0° to 60°. The Fisher and Kono estimates of α_{95} appear to be in good order. However, the estimates of the McFadden and Reid methods usually overestimate α_{95}, and in a few cases severely underestimates it. (*b*) Histograms for the 32 combinations where the true inclination was 70° and 80°. For these steep inclinations both the Kono method and the McFadden and Reid method are collapsing and the 95% confidence limits they give can not be trusted. (*c*) Histograms for the 16 combinations where the true inclination was 90°. For this inclination both the Kono method and the McFadden and Reid method have collapsed.

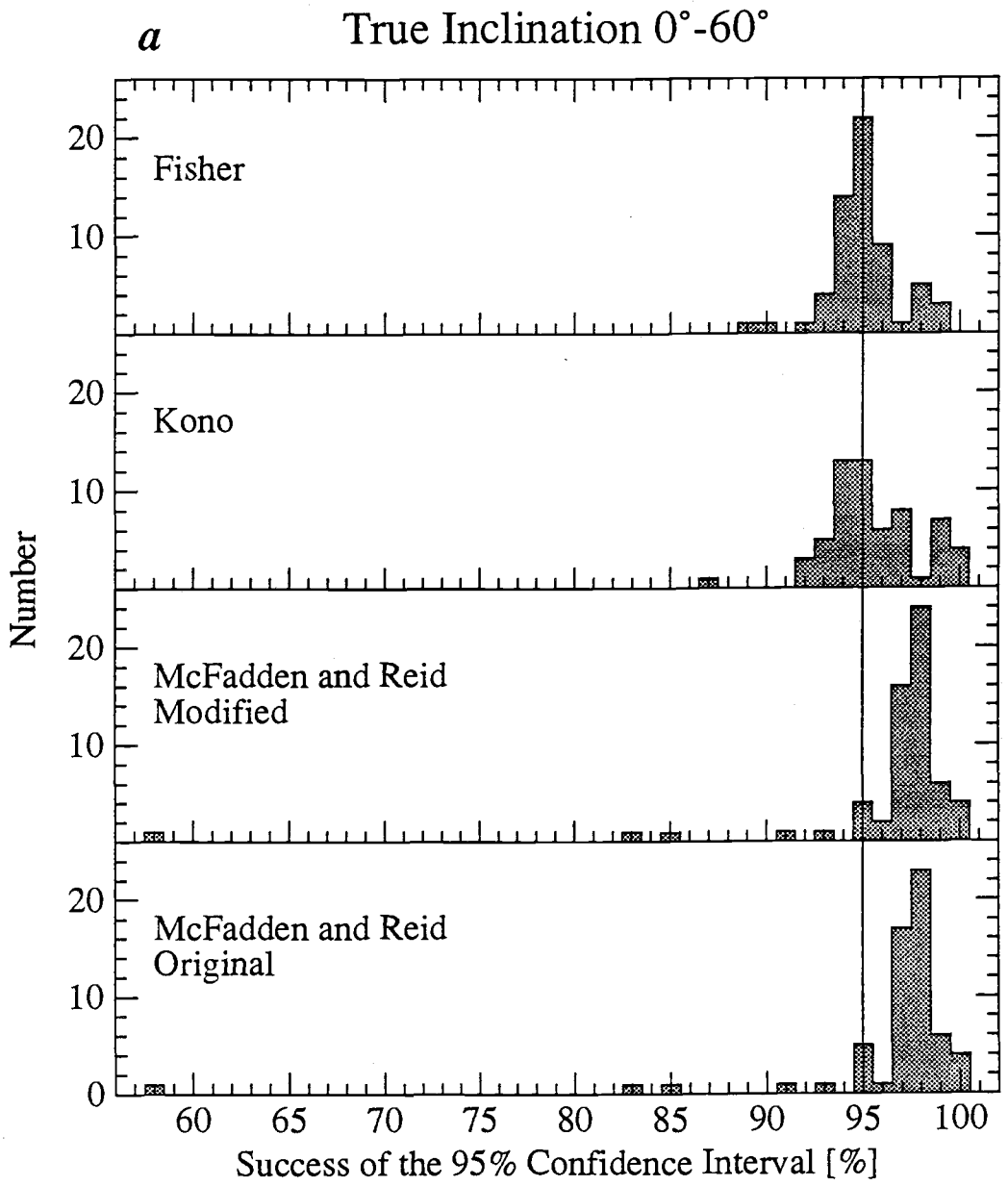
a
True Inclination 0°-60°
Fisher
Kono
McFadden and Reid
Modified
McFadden and Reid
Original
Number
20
10
0
60
65
70
75
80
85
90
95
100
Success of the 95% Confidence Interval [%]

Figure 5.11.

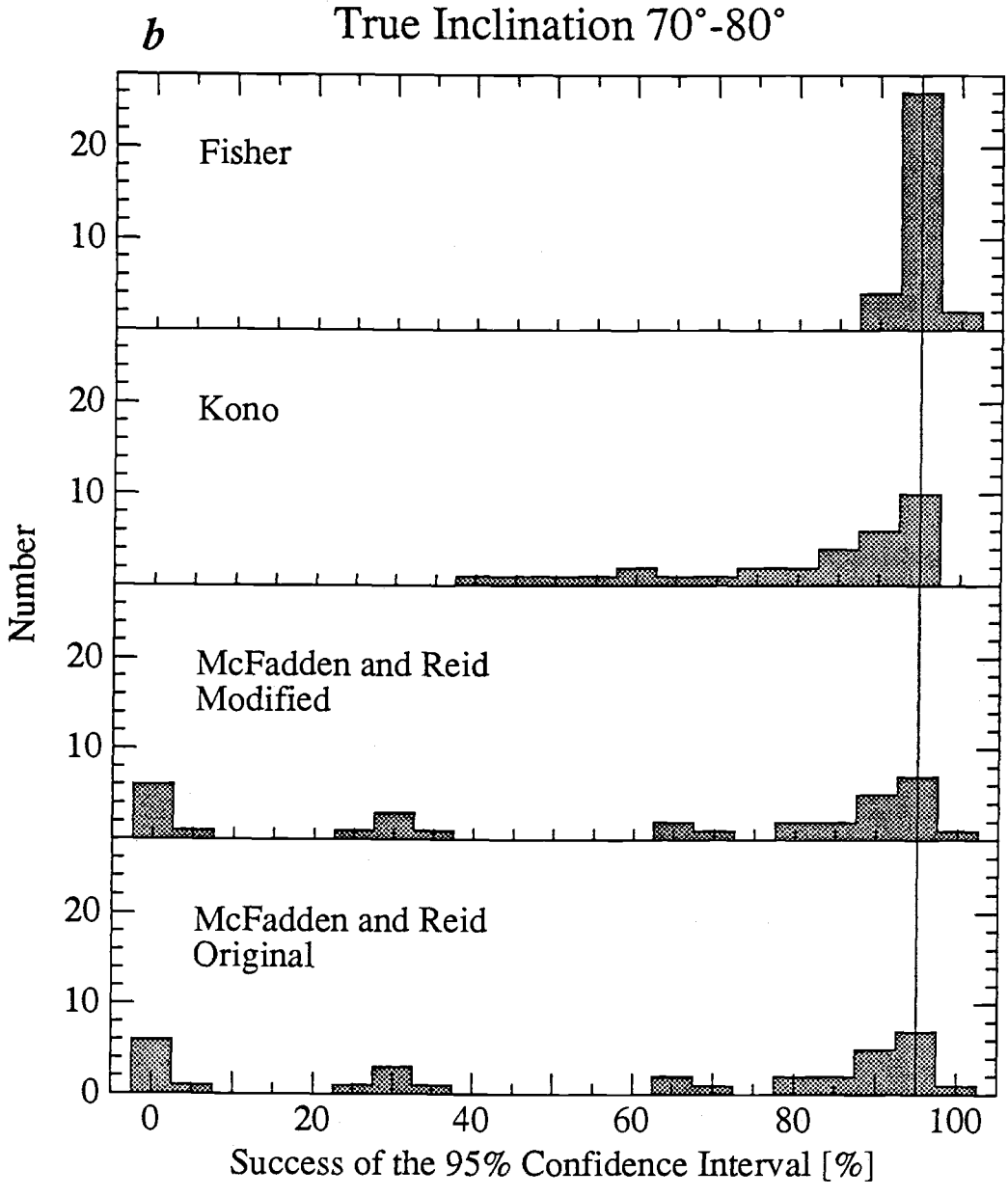

Figure 5.11 continued.

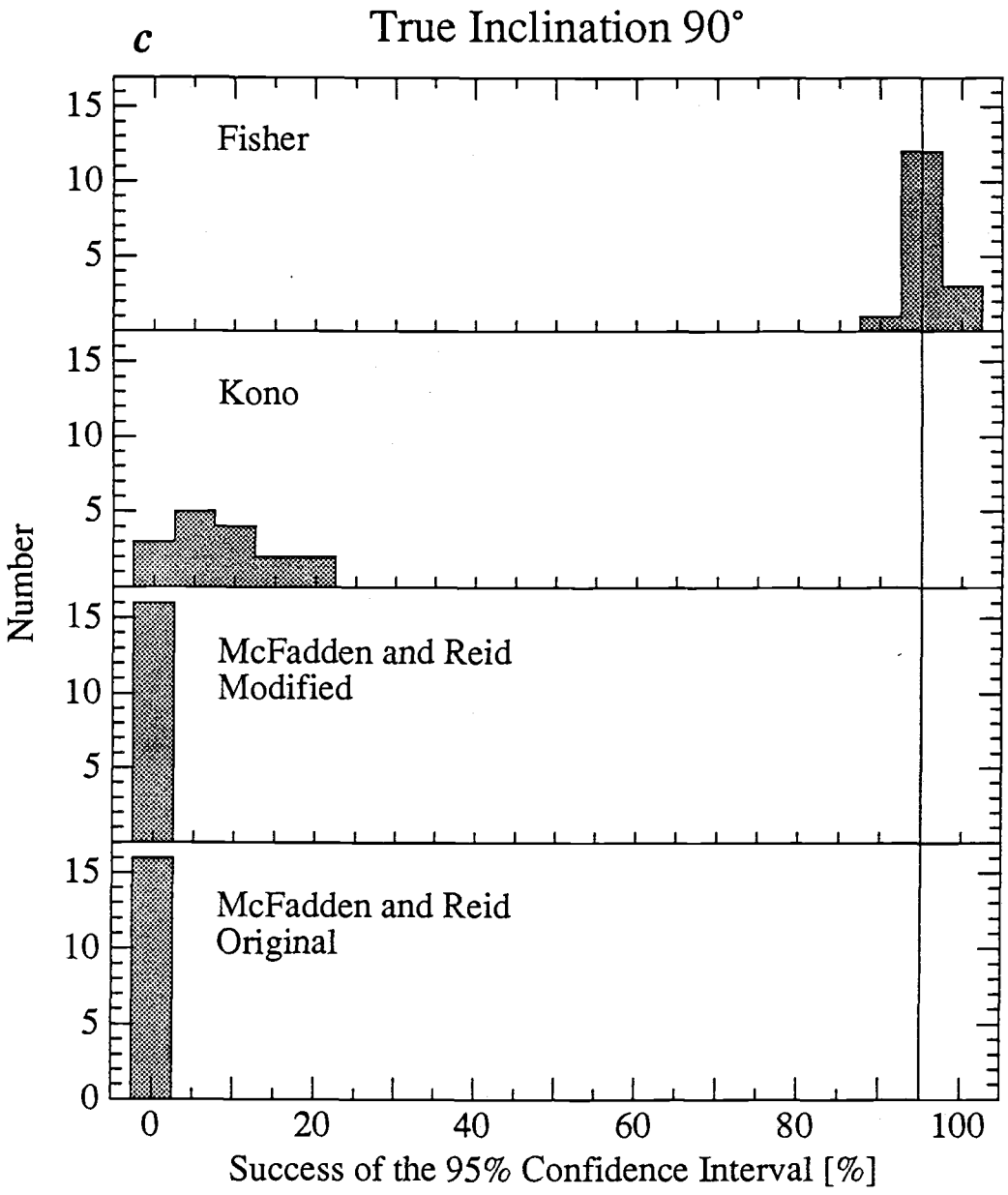

Figure 5.11 continued.

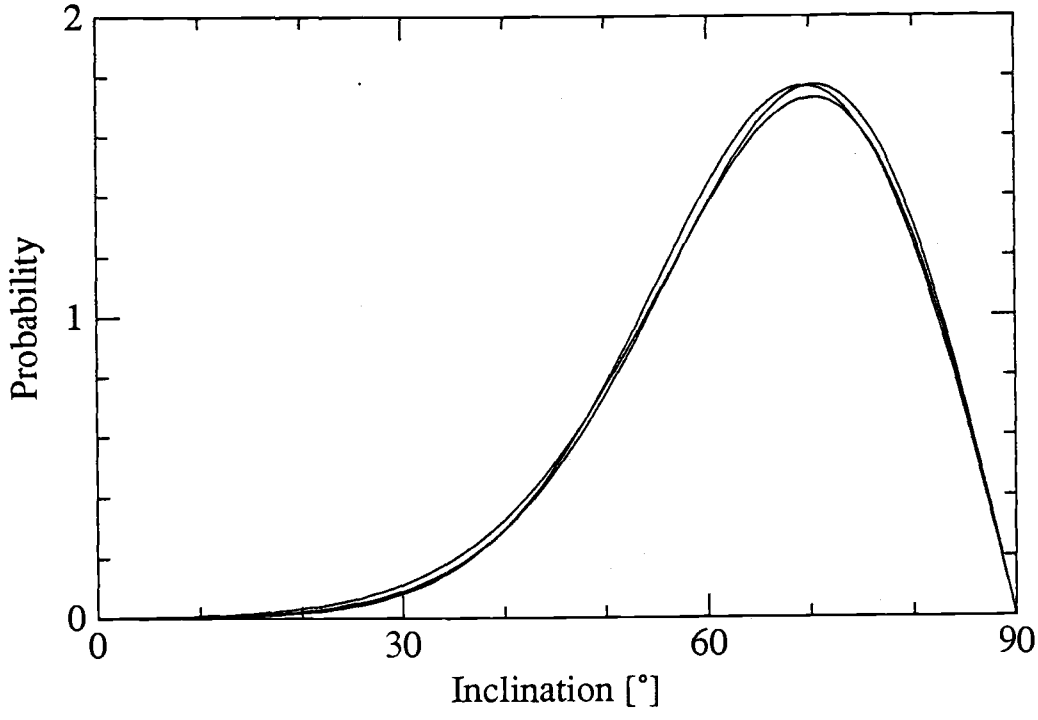

Figure 5.12. The distribution from equation (5.4) of observed inclinations for three combinations of the true values (I_0, κ). The values are ($I_0 = 75°$, $\kappa = 8.6$), ($I_0 = 80°$, $\kappa = 10$), and ($I_0 = 85°$, $\kappa = 12$) (it is not important in this context to identify the curves). For these steep true inclinations and low kappa it becomes impossible to extract information on both I_0 and κ from a finite set of observed inclinations, and any attempt to do so will depend critically on the assumptions of the calculation method.

5.6 A NUMERICAL EXAMPLE

As a numerical example we present the paleomagnetic data used in numerical examples by *Fisher* [1953] and *Briden and Ward* [1966], listed in Table 5.5. The paleomagnetic samples were taken by J. Hospers from the 1947-1948 lava flow of Hekla in Iceland (64.0°N, 19.7°W). In Table 5.6 we analyze the Table 5.5 data using the several methods. First we show the arithmetic average of the inclinations, declinations and a 95% confidence limits on the average inclination assuming normal distribution. Then we present the Fisher statistics estimate [*Fisher*, 1953]. We show the graphical estimate made by *Briden and Ward* [1966, p. 137]. These are followed by an estimate from the method of *Kono* [1980*b*]. Finally, three estimates based on the method of *McFadden and Reid* [1982] are shown. First the solution of θ_0 ($I = 90° - \theta_0$) and κ that maximize the exact form of the likelihood function in equation (5.30). Then the solution of the original-MR method. Last is the solution of the modified-MR method, which includes our modifications to their original method. Note that the bivariate estimate of α_{95} of the Fisher statistics should not be compared to the other univariate estimates. Note also that the original-MR method results in the same average inclination as the arithmetic average. The exact form of the maximum likelihood estimate of *McFadden and Reid* [1982] resembles most the results of the *Kono* [1980*b*] method.

TABLE 5.5. Nine Specimens From an Icelandic Lava Flow*

Specimen Number	Declination, deg	Inclination, deg
631	343.2	66.1
632	62.0	68.7
633	36.9	70.1
634	27.0	82.1
635	359.0	79.5
636	5.7	73.0
642A	50.4	69.3
643A	357.6	58.8
644	44.0	51.4

* From *Fisher* [1953, Table 1, p. 304].

TABLE 5.6. Different Methods Used to Estimate Statistical Parameters

Method	Average Inclination, deg	Average Declination, deg	Precision Parameter	95% Confidence Limits, deg
Arithmetic Average	68.78	22.87	—	7.48
Fisher [1953]:	70.89	24.27	35.08	8.81
Briden and Ward [1966]:	72	—	33	—
Kono [1980]:	71.99	—	31.64	9.29
McFadden and Reid [1982]:				
Maximum Likelihood*	71.85	—	32.45	—
Original	68.79	—	34.62	9.25
Modified	70.95	—	34.62	-2.16 ± 9.24

*Solution to the exact form of equation (5.30).

5.7 CONCLUSIONS

This study shows that care is needed when the *McFadden and Reid* [1982] method is used, and it should never be used as it is presented in their article. For true inclinations up to 60° comparable results are obtained from the *Kono* [1980*b*] method and the modified McFadden and Reid method. Above 60° the Kono method becomes a better choice. However, approaching the vertical all methods break down and, for low κ the loss of declination data implies that estimates of inclination and precision parameter can not be made.

5.8 REFERENCES

Arason, P., and S. Levi, Compaction and inclination shallowing in deep-sea sediments from the Pacific ocean, *J. Geophys. Res., 95*, 4501-4510, 1990*b*.

Beyer, W. H. (Ed.), *CRC Standard Mathematical Tables*, 27th ed., 615 pp., CRC Press, Boca Raton, Fla., 1984.

Bleil, U., The magnetostratigraphy of northwest Pacific sediments, Deep Sea Drilling Project leg 86, *Initial Rep. Deep Sea Drill. Proj., 86*, 441-458, 1985.

Briden, J. C., and M. A. Ward, Analysis of magnetic inclinations in borecores, *Pure Appl. Geophys., 63*, 133-152, 1966.

Celaya, M. A., and B. M. Clement, Inclination shallowing in deep sea sediments from the north Atlantic, *Geophys. Res. Lett., 15*, 52-55, 1988.

Cox, A., and R. G. Gordon, Paleolatitudes determined from paleomagnetic data from vertical cores, *Rev. Geophys., 22*, 47-72, 1984.

Fisher, R., Dispersion on a sphere, *Proc. R. Soc. London, Ser. A, 217*, 295-305, 1953.

Gordon, R. G., and A. Cox, Calculating paleomagnetic poles for oceanic plates *Geophys. J. R. Astron. Soc., 63*, 619-640, 1980.

Gradshteyn, I. S., and I. M. Ryzhik, *Table of Integrals, Series, and Products*, 1160 pp., 4th ed., Academic, San Diego, Calif., 1980.

Harrison, C. G. A., The paleomagnetic record from deep-sea sediment cores, *Earth Sci. Rev., 10*, 1-36, 1974.

Kono, M., Paleomagnetism of DSDP leg 55 basalts and implications for the tectonics of the Pacific plate, *Initial Rep. Deep Sea Drill. Proj.*, *55*, 737-752, 1980*a*.

Kono, M., Statistics of paleomagnetic inclination data, *J. Geophys. Res.*, *85*, 3878-3882, 1980*b*.

Lancelot, Y., et al., *Proceedings of the Ocean Drilling Program, Initial Reports*, *129*, 488 pp., Ocean Drilling Program, College Station, Texas, 1990.

Langevin, P., Magnétisme et théorie des électrons (in French), *Ann. Chim. Phys.*, *5*, 70-127, 1905.

Levi, S., and R. Karlin, A sixty thousand year paleomagnetic record from Gulf of California sediments: Secular variation, late Quaternary excursions and geomagnetic implications, *Earth Planet. Sci. Lett.*, *92*, 219-233, 1989.

Mardia, K. V., *Statistics of Directional Data*, 357 pp., Academic, San Diego, Calif., 1972.

McFadden, P. L., Determination of the angle in a Fisher distribution which will be exceeded with a given probability, *Geophys. J. R. Astron. Soc.*, *60*, 391-396, 1980*a*.

McFadden, P. L., The best estimate of Fisher's precision parameter κ, *Geophys. J. R. Astron. Soc.*, *60*, 397-407, 1980*b*.

McFadden, P. L., and A. B. Reid, Analysis of paleomagnetic inclination data, *Geophys. J. R. Astron. Soc.*, *69*, 307-319, 1982.

Ogg, J. G., Paleolatitudes and magnetostratigraphy of Cretaceous and lower Tertiary sedimentary rocks, deep sea drilling project site 585,

Mariana basin, western central Pacific, *Initial Rep. Deep Sea Drill. Proj.*, *89*, 629-645, 1986.

Peirce, J. W., Assessing the reliability of DSDP paleolatitudes, *J. Geophys. Res.*, *81*, 4173-4187, 1976.

Schneider, D. A., and D. V. Kent, The time-averaged paleomagnetic field, *Rev. Geophys.*, *28*, 71-96, 1990.

Steiner, M. B., Paleomagnetism of the Cretaceous section, site 462, *Initial Rep. Deep Sea Drill. Proj.*, *61*, 711-716, 1981.

Tarduno, J. A., Absolute inclination values from deep sea sediments: A reexamination of the Cretaceous Pacific record, *Geophys. Res. Lett.*, *17*, 101-104, 1990.

Watson, G. S., Analysis of dispersion on a sphere, *Mon. Notic. R. Astron. Soc. Geophys. Suppl.*, *7*, 153-159, 1956*a*.

Watson, G. S., A test for randomness of directions, *Mon. Notic. R. Astron. Soc. Geophys. Suppl.*, *7*, 160-161, 1956*b*.

Watson, G. S., and E. J. Williams, On the construction of significance tests on the circle and the sphere, *Biometrica*, *43*, 344-352, 1956.

CHAPTER 6

Intrinsic Bias in Averaging Paleomagnetic Data

Simulations of paleomagnetic data show that the transformation of isotropically distributed geomagnetic poles to local site directions introduces slight apparent inclination shallowing if the averaging is done in directional space. This effect depends on the site latitude and pole dispersions. For typical dispersions of poles (θ_{63} = 10° to 20°) the average inclination will appear too shallow by 1° to 2° for site latitudes of 10° to 50° North or South. On the other hand by averaging all the data in polar space, when some of the scatter might be due to isotropic scatter in directions will introduce a steepening effect. For most individual paleomagnetic studies this slight intrinsic inclination bias will not be significant, because typical uncertainties of the order of 5° to 10° are considerably larger than the proposed effect. However, for integrated high resolution studies of certain aspects of the geomagnetic field this methodological problem can bias the results, and we caution against averaging data only in directional space, a method that has been used by some workers.

6.1 INTRODUCTION

When interpreting paleomagnetic data it is more meaningful to reduce the scatter of the data by assembling several measurements to a mean by applying Fisher statistics [*Fisher*, 1953]. Such calculations of the average make the fundamental assumption that the data obey the Fisher distribution, which is an isotropic distribution. One can either assume that the directions are Fisher distributed or that the virtual geomagnetic poles are Fisher distributed. The problem in paleomagnetism is that scatter in directions is often due to both local isotropic noise and isotropic scatter of the geomagnetic poles. The transformation of a dipole field to local directions is non-linear and an isotropic distribution in one space is skewed in the other.

To illustrate the problem consider a site at magnetic latitude $\lambda_0 = 20°$. The corresponding dipole inclination I_0 can be calculated from the dipole equation

$$\tan I_0 = 2 \tan \lambda_0 \qquad (6.1)$$

which turns out to give $I_0 = 36.1°$. The transformation of the dipole equation is shown in Figure 6.1. Consider now isotropic noise in the directions. Two inclinations $(I_0 + 10°)$ and $(I_0 - 10°)$, transform to magnetic latitudes $(\lambda_0 + 7.4°)$ and $(\lambda_0 - 6.3°)$. The average of these magnetic latitudes will give us higher latitude than λ_0, and we have created a near-sided virtual geomagnetic pole by 0.6° of latitude. Now consider isotropic scatter in poles. The two magnetic latitudes $(\lambda_0 + 7°)$

and ($\lambda_0 - 7°$) correspond to the inclinations ($I_0 + 9.5°$) and ($I_0 - 11.3°$). The average of the inclinations is lower than I_0 and we have introduced 0.9° of inclination shallowing. The problem is that it may be difficult to determine which space is geophysically appropriate, because usually the scatter is a mixture of noise from both polar and directional space of unknown proportions.

The problem of the inconsistency between these two averaging spaces has received little attention in the literature. Some textbooks on paleomagnetism mention parts of the problem: *Irving* [1964, p. 52-71] describes in some detail the possible sources of the within-site dispersion; orientation and measurement of specimens (usually 2°-5°), rock magnetic problems (sediment compaction, rock anisotropy), secondary overprinting, within-site tilting, fundamental recording noise problems, and field changes during recording of a site. Sources of between-site dispersion include; statistical effects, between-site tilting, and variations of the field. Irving discusses the problems of the progression of going from directions of individual specimens to the site mean. In going from site directions to a single rock unit direction he gives two possibilities: assume either the directions or the poles to be Fisher distributed. He notes that the resulting pole positions are approximately the same and that the difference is of uncertain physical significance. *Tarling* [1971, p. 90-91] discusses whether directions or poles are Fisher distributed and concludes that neither does so exactly, but the differences are small. *McElhinny* [1973, p. 81-83] discusses the problem of transfering the statistical parameters of the scatter through the dipole equation, but does not mention any problem in choosing where to average the data.

In his revised and significantly expanded book on paleomagnetism *Tarling* [1983, p. 127] discusses very briefly the problem of choosing either the directions or the poles to be Fisher distributed. A circular pole distribution will transform to a 2:1 elliptical distribution on the equator. He argues that since the directions are acquired in a geomagnetic field and since the field approximates to an axial geocentric dipole, it is physically more plausible to assume that the virtual poles are Fisher distributed. Tarling states that most workers use directional space for averaging and transform their results to polar space. He does not mention that this practice may cause bias. *Collinson* [1983, p. 394-398] mentions the two alternatives, i.e. of assuming the directions or the poles to be Fisher distributed and states that if the poles are Fisherian then we expect the directions to have an oval distribution, which he states is not generally observed. Collinson considers oval distributed directions to be associated with viscous remanent magnetization streaking towards the present local field direction. He does not mention that the particular choice may affect estimates of the mean. *Merrill and McElhinny* [1983, p. 84-87] address the problem of whether to assume the directions or the poles to be Fisher distributed. Their main conclusion is that the within-site scatter is most likely due to a combination of the sample orientation error, local magnetic anomalies, and laboratory procedures in removing secondary components, and should be isotropic in directional space. On the other hand the between-site scatter is usually assumed to be due to secular variation of the geomagnetic field, and therefore isotropic in polar space. They believe that in practice the data will be a combination

of a Fisher distributed poles and Fisher distributed directions, therefore an oval distribution viewed from both directional and polar perspective.

Few articles have mentioned this subject. *Shuey et al.* [1970] in describing a different problem, noted that there is an inclination error associated with the choice of data space, but they did not address the problem further. *McElhinny and Merrill* [1975] show in considerable detail how the dispersion gets skewed through the dipole equation and becomes oval, but do not mention that the dipole equation may affect the mean. *Creer* [1983] showed that several types of simple synthetic field variations will result in an inclination error arising from the use of unit directional vectors. True inclinations can be obtained by weighting the data by the intensity. However, paleointensities are very difficult to obtain as compared to paleomagnetic directions. Creer does not present detailed evaluation of the magnitude of the apparent inclination shallowing due to this misuse of directions, but notes that this may play a significant role in estimating persistent non-dipole terms of the field.

The validity of the dipole assumption and possible long-term non-dipole components of the geomagnetic field are not important in this context. The fact that the dipole model is approximately true [e.g., *Opdyke and Henry*, 1969] is sufficient for the current analysis. In this study we estimate the magnitude of the bias that may be introduced by a particular selection of averaging method.

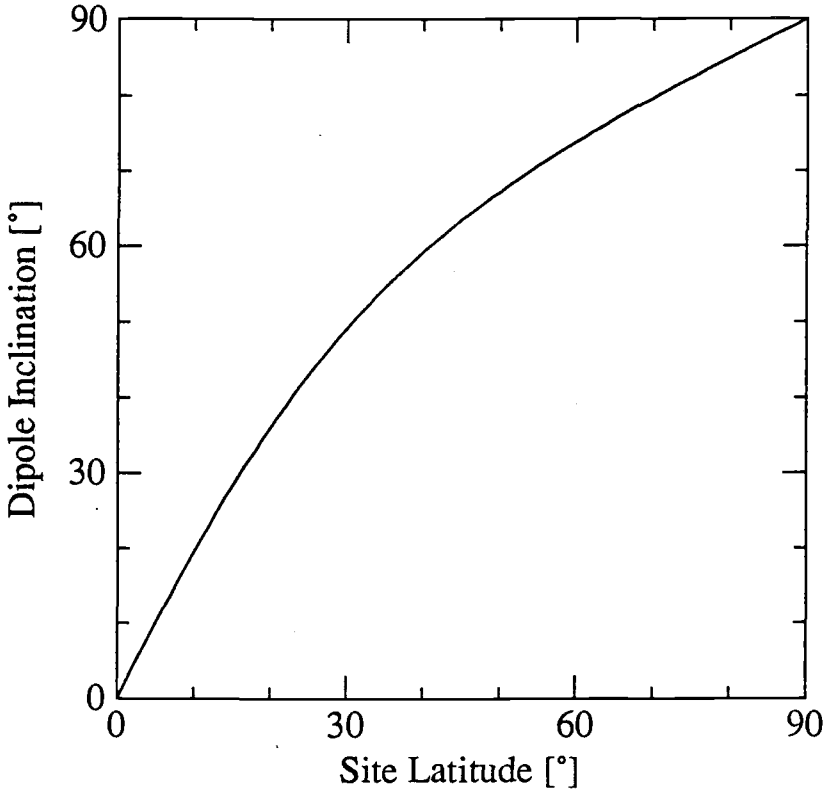

Figure 6.1. The transformation of the dipole equation: $\tan I = 2 \tan \lambda$.

6.2 ISOTROPIC POLES VERSUS ISOTROPIC DIRECTIONS

In averaging paleomagnetic data it is important to know the origin of the scatter in the data. To a first approximation we assume that local disturbances and experimental noise cause isotropic scatter of the directions, and geomagnetic disturbances isotropic scatter of the poles. Disturbances which produce anisotropic scatter are not considered in this study.

Ideally one wants to average the local scatter in directional space and the polar scatter in polar space, but it is usually difficult to distinguish between the sources for the scatter. Assuming that most of the within-site scatter is due to local disturbances and the between-site scatter is mainly due to secular variation of the field, many but not all workers average the within-site scatter in directional space and the between-site scatter in polar space. For lava flows and other examples of instantaneous recordings of the geomagnetic field this scenario may be approximately true, and this method is recommended as the best approach to minimize the averaging problems described in this study.

This scheme is questionable for sediment cores and large intrusions, where there are difficulties in defining "sites", and the remanence in samples already represents some time average of isotropic local and experimental scatter and of the secular variation, and there is question about the origin of the between sample scatter.

6.3 SIMULATIONS OF THIS STUDY

To transform the Fisher distribution analytically from polar space, through the dipole equation and spherical trigonometry to a distribution of local directions is fairly complicated. For this simple study we chose to assess this numerically by transforming isotropic poles to directions. The distribution of these directions turns out to be oval. Then we average the directions using Fisher statistics and transform the average direction to a pole that can be compared to the original average pole. These calculations were performed for various site latitudes and selected pole dispersions.

We generated two simple types of isotropic pole distributions: One made of a dipole precessing around the Earth's rotation axis, i.e. the poles are at a fixed latitude but various longitudes. The other type consists of a very large number of random generated Fisher distributed poles with known dispersion.

The dipole precession was generated by fixed-latitude poles (the latitudes of the poles were 70°, 75°, and 80°N). For each latitude we generated 180 poles in a longitude steps of 2°. Then the 180 pole positions were transformed to a direction at a site via the dipole equation and spherical trigonometry. The circle of poles around the rotation axis transforms into an oval in directional space, and the geocentric axial dipole direction is noticeably removed from the center of the oval. An example of this effect is shown in Figure 6.2. The result of the Fisher average of the skewed directions shows that we have introduced an apparent inclination shallowing, that depends on the site and pole

latitudes. However, the inclination shallowing is smaller than appears from the displacement of the oval, because of unequal data density on each side of the dipole direction.

The method of generating a large number of random Fisher distributed poles has the main disadvantage that a very large number is required to average out statistical fluctuations. Typically, on the order of thousands to millions of poles are needed. These calculations are needed for a number of site latitudes to get a continuous function of latitude and for different pole dispersions. The calculations were performed for the angular standard deviations of the poles θ_{63} = 10°, 15°, and 20°. Thirty thousand Fisher distributed poles were generated for each set of pole dispersions and for each site latitude, which were varied from 0° to 90° in steps of 2°. The statistical fluctuations were decreased by taking into account that the mean of the poles in polar space is not exactly at 90°N. In Figure 6.3 we show an example of Fisher-distributed poles that are skewed when transformed into directional space. In Figure 6.4 we show the apparent inclination shallowing for circularly distributed poles as a function of site latitude for the two versions of pole distributions and various pole dispersions.

Figure 6.2. Example of the data generated for the dipole precession. (*a*) Expanded view of the center of a stereographic polar projection. The centered cross represents the Earth's rotation axis and the circles represent 70°, and 80°N of latitude. A total of 180 magnetic poles were generated at 2° increments of longitude. (*b*) Transformed paleomagnetic directions in Hoffman's stereographic projection [*Hoffman*, 1984] (he calls it (D', I') space), showing the 180 directions seen at site latitude of 20°N corresponding to the 180 poles in *a*. The solid circles represent 10° and 20° deviation from the direction of the geocentric axial dipole (GAD), represented by the centered cross. The average of the 180 directions gives shallower inclination (higher on the graph) than the GAD value.

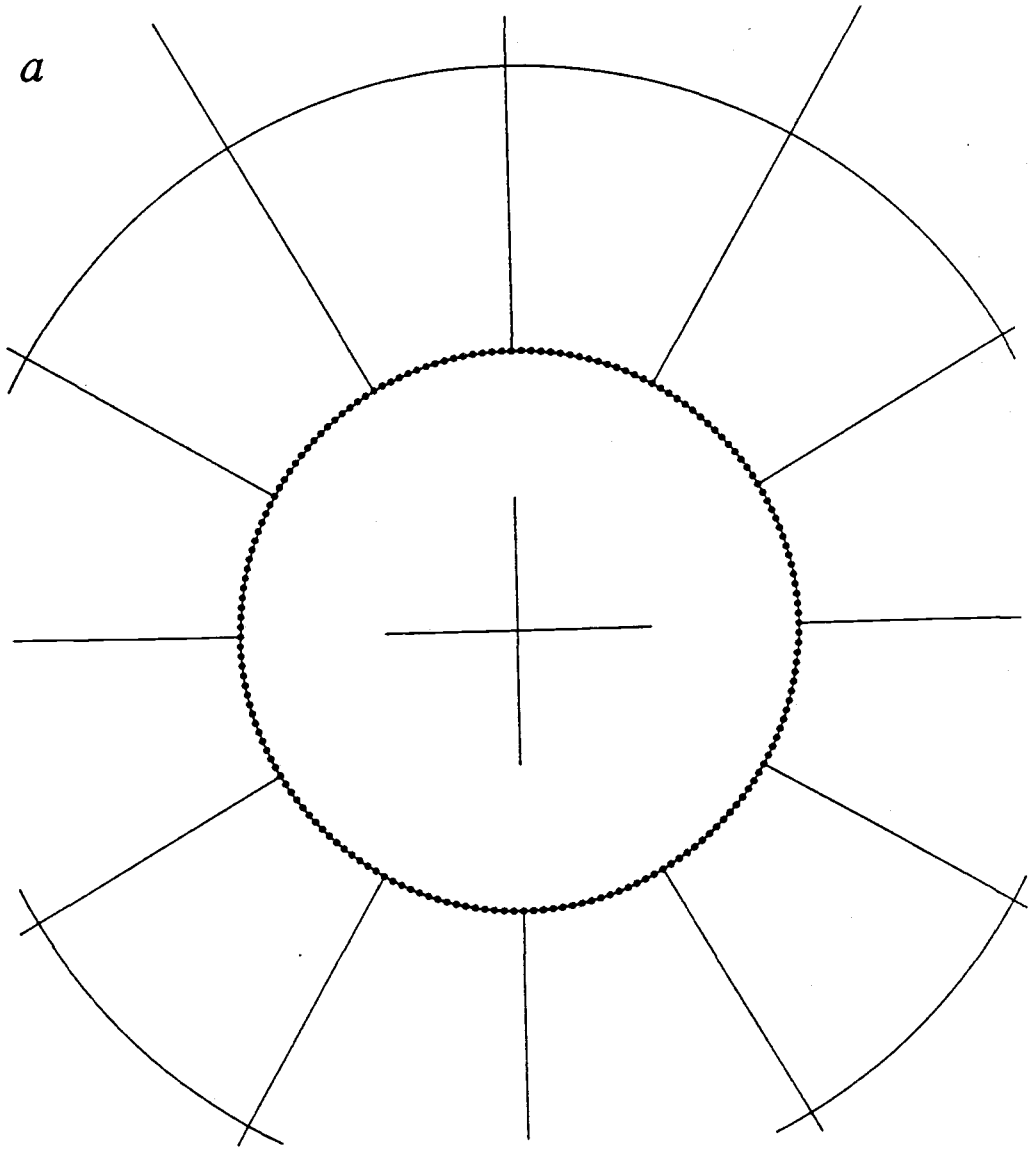

Figure 6.2.

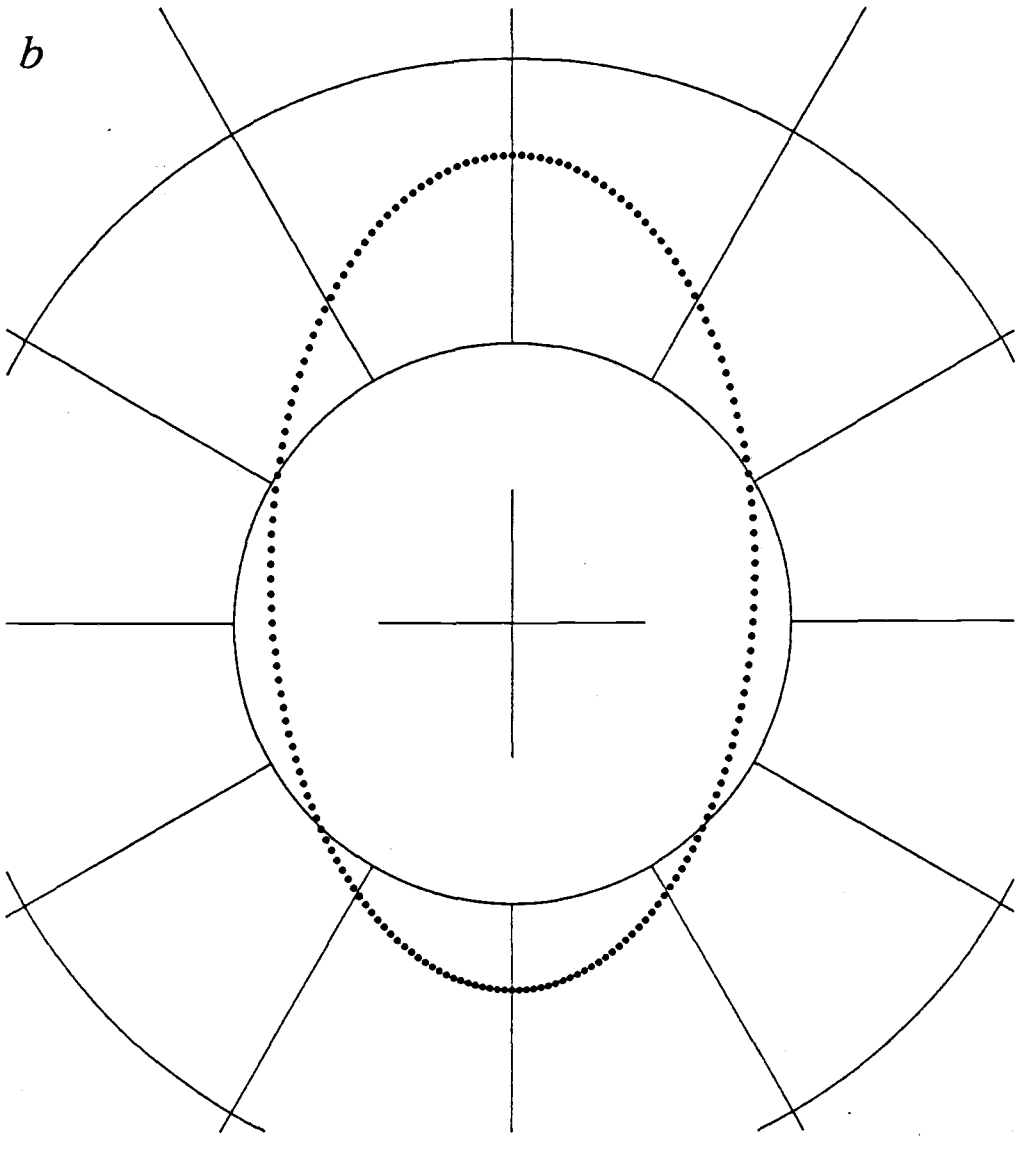

Figure 6.2 continued.

Figure 6.3. Stereographic projections of Fisher distributed polar data. (*a*) Here nine circles represent θ_{10}, θ_{20}, ... , θ_{90}, (θ_{90} encircles 90% of the distribution) of a Fisher distribution with $\theta_{63} = 20°$ on a pole centered stereographic projection. The star represents a site at 20°N. (*b*) the nine circles have been transformed to the directional space seen at 20°N in a Hoffman's projection. The interval between crosses is 10° of latitude in *a* and 10° of direction in *b*.

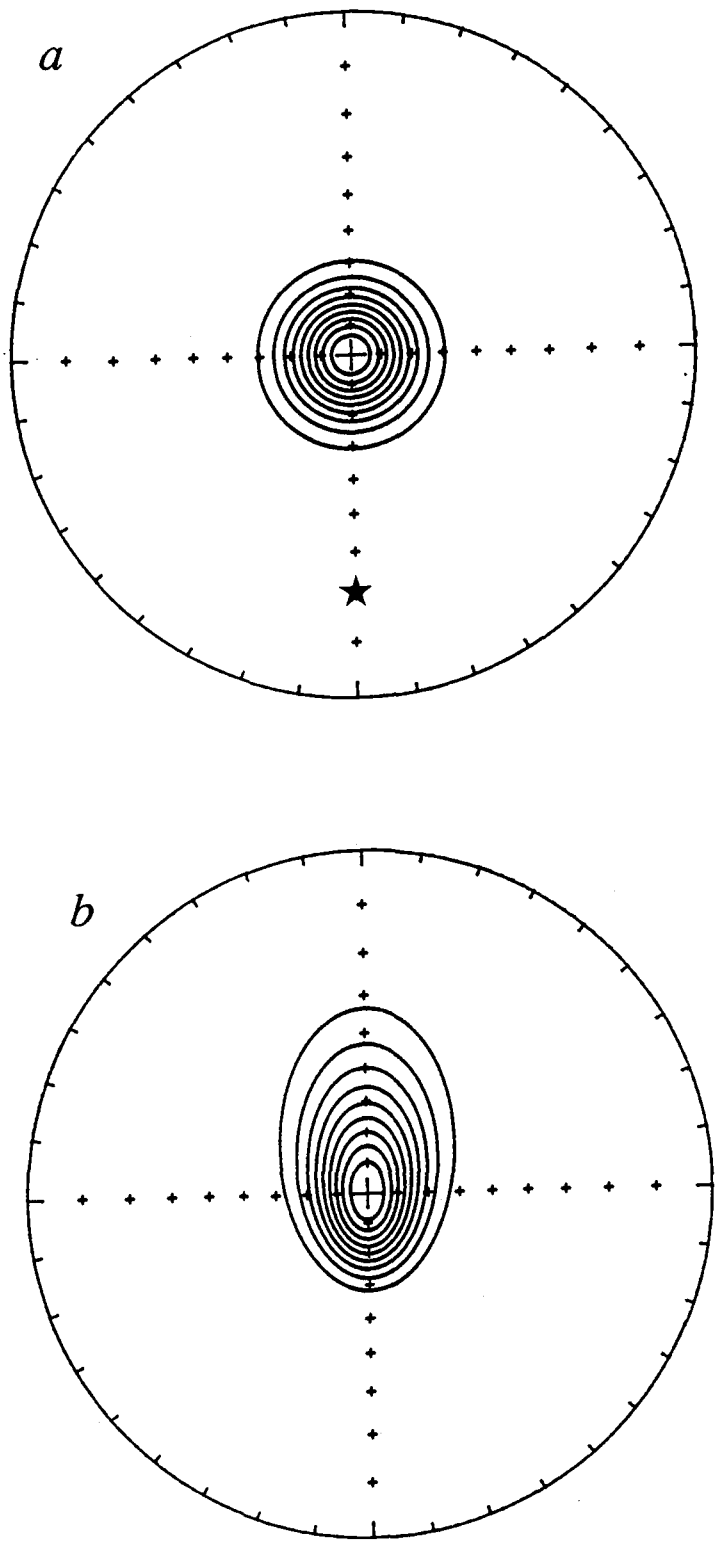

Figure 6.3.

Figure 6.4. The simulated apparent inclination shallowing obtained by averaging isotropic polar data in directional space as a function of site latitude. (*a*) Results of dipole precession about the rotation axis, with deviations of $\Delta\theta = 10°$, 15°, and 20° away from the rotation axis. (*b*) Results of random generated Fisher distributed poles for $\theta_{63} = 10°$, 15°, and 20°. This simple study shows that averaging in directional space of isotropically distributed poles will introduce an inclination shallowing (far-sided poles) effect of a few degrees.

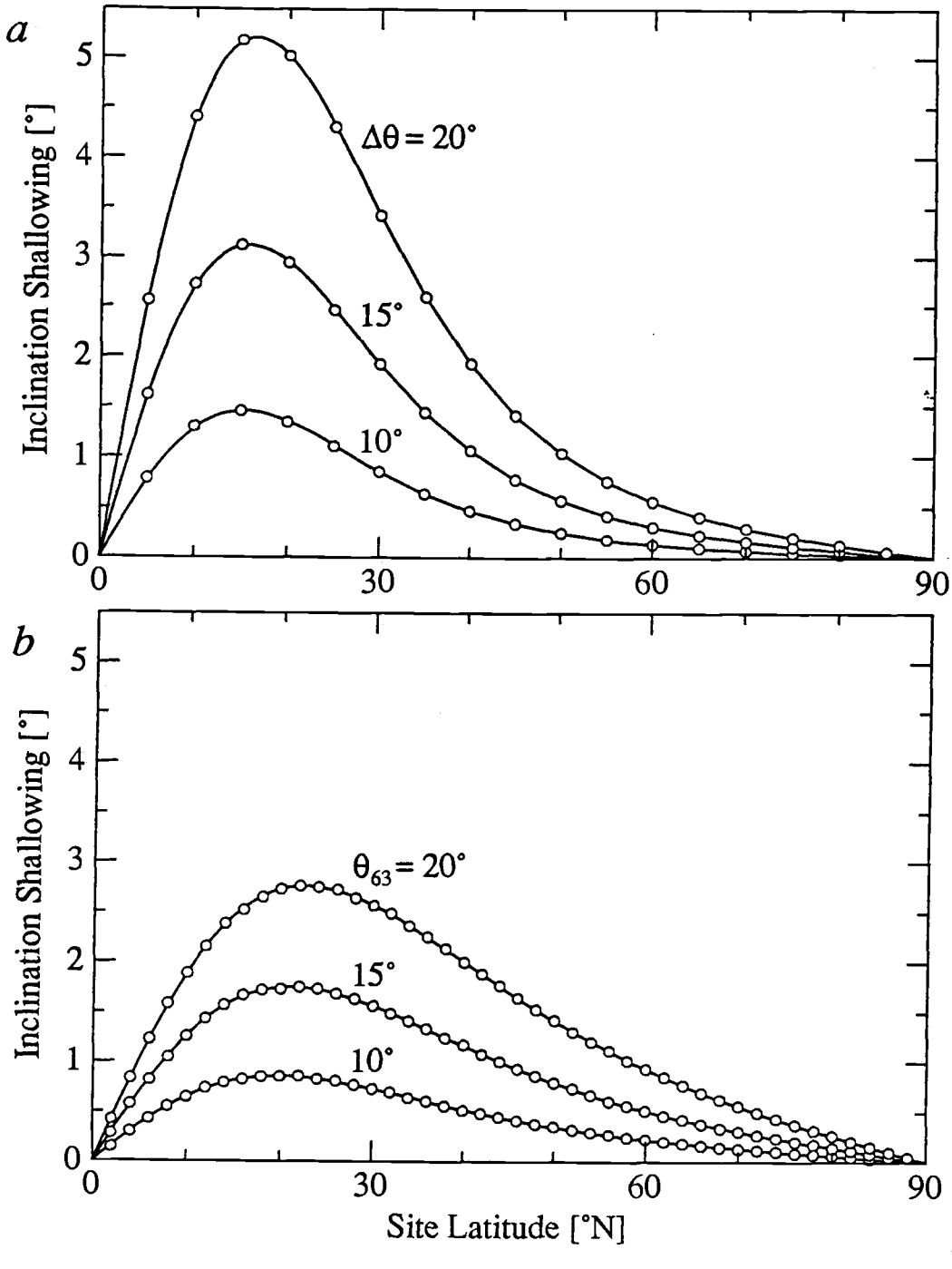
a
Inclination Shallowing [°]
Δθ = 20°
15°
10°
0
1
2
3
4
5
0
30
60
90
b
Inclination Shallowing [°]
θ63 = 20°
15°
10°
0
1
2
3
4
5
0
30
60
90
Site Latitude [°N]

Figure 6.4.

6.4 DISCUSSION

Estimates of the angular dispersion of virtual geomagnetic poles due to secular variation gives latitude dependent observations, but θ_{63} (angular standard deviation) is in the range of 10° to 20° [*Merrill and McElhinny*, 1983, p. 204]. We see that for such dispersions, we can introduce an apparent inclination shallowing or far-sided poles by doing all the averages in directional space. The apparent inclination anomaly is on the order of 1° to 2° for site latitudes of 20° to 60°, see Figure 6.4*b*. Some paleomagnetists averaged their data in directional space only, even for rock units of several sites, see for instance a review by *Harrison and Lindh* [1982, p. 1906]. Therefore, some bias probably exists in large data sets that are used to estimate apparent polar wander paths. Alternatively, polar space should not be too hastily embraced, for then averaging of local scatter might introduce false inclination steepening in the data.

Analyzing the ovality of the distribution may assist in choosing the space for data averaging [e.g. *Merrill and McElhinny*, 1983]. This is not necessarily true because non-dipole terms in the field will affect the ovality of the directions, even though those terms may on average cancel out. It has been postulated that virtual geomagnetic poles do not obey the Fisher distribution exactly. *Harrison* [1980] showed that the true distribution of the virtual geomagnetic poles derived from some Icelandic lavas is better described by a mixture of 10% totally random distribution and 90% Fisher distribution. This results in additional anomalous poles which will exaggerate the apparent inclination

shallowing of this study. Thus, paleomagnetic data bases are possibly contaminated by an intrinsic bias due to improper averaging of paleomagnetic directions.

6.5 REFERENCES

Collinson, D. W., *Methods in Rock Magnetism and Palaeomagnetism; Techniques and Instrumentation*, 503 pp., Chapman and Hall, London, 1983.

Creer, K. M., Computer synthesis of geomagnetic palaeosecular variations, *Nature, 304*, 695-699, 1983.

Fisher, R., Dispersion on a sphere, *Proc. Roy. Soc., Ser. A, 217*, 295-305, 1953.

Harrison, C. G. A., Secular variation and excursions of the earth's magnetic field, *J. Geophys. Res., 85*, 3511-3522, 1980.

Harrison, C. G. A., and T. Lindh, A polar wandering curve for North America during the Mesozoic and Cenozoic, *J. Geophys. Res., 87*, 1903-1920, 1982.

Hoffman, K. A., A method for the display and analysis of transitional paleomagnetic data, *J. Geophys. Res., 89*, 6285-6292, 1984.

Irving, E., *Paleomagnetism; and Its Application to Geological and Geophysical Problems*, 399 pp., John Wiley, New York, 1964.

McElhinny, M. W., *Palaeomagnetism and Plate Tectonics*, 358 pp., Cambridge University Press, Cambridge, 1973.

McElhinny, M. W., and R. T. Merrill, Geomagnetic secular variation over the past 5 m.y., *Rev. Geophys., 13*, 687-708, 1975.

Merrill, R. T., and M. W. McElhinny, *The Earth's Magnetic Field; Its History, Origin and Planetary Perspective*, 401 pp., Academic, New York, 1983.

Opdyke, N. D., and K. W. Henry, A test of the dipole hypothesis, *Earth Planet. Sci. Lett.*, *6*, 139-151, 1969.

Shuey, R. T., E. R. Cole, and M. J. Mikulich, Geographic correction of archeomagnetic data, *J. Geomag. Geoelectr.*, *22*, 485-489, 1970.

Tarling, D. H., *Principles and Applications of Palaeomagnetism*, 164 pp., Chapman and Hall, London, 1971.

Tarling, D. H., *Palaeomagnetism; Principles and Applications in Geology, Geophysics and Archaeology*, 379 pp., Chapman and Hall, London, 1983.

CHAPTER 7

Conclusions

The main conclusions of this thesis include:

(1) Progressive sediment compaction is responsible for downhole shallowing of the paleomagnetic inclinations of Plio- Pleistocene sediments at DSDP hole 578.

(2) We show that a variety of mechanical models can lead to inclination shallowing, and to a first approximation they can be expressed as

$$\tan (I - \Delta I) = (1 - a \, \Delta V) \tan I \qquad (7.1)$$

where I is the ambient field inclination, ΔI the inclination shallowing, ΔV the compaction, and a is a constant, chosen to fit inclination shallowing data from laboratory experiments and natural sediments.

(3) Cretaceous DSDP sediments from the Pacific plate have considerably shallower inclinations than expected, and our model

for compaction-induced inclination shallowing successfully accounts for the observed discrepancy. The magnitude of inclination shallowing is affected by lithology; inclination shallowing is more pronounced in clay-rich sediments than in calcareous sediments.

(4) The predictability of the compaction-induced inclination shallowing offers hope for possibly restoring the inclinations, resulting in more accurate paleolatitude estimates.

(5) We show that in analyzing azimuthally unoriented inclination-only data care is needed when the *McFadden and Reid* [1982] method is used, and it should never be used as it is presented in their article. For true inclinations up to 60° comparable results are obtained from the *Kono* [1980*b*] method and our modification of the McFadden and Reid method. As inclinations approach the vertical, all methods break down, and for low κ, the absence of declination data implies that simultaneous estimates of inclination and precision parameter cannot be made.

(6) We show that commonly encountered dispersions of paleomagnetic directions can introduce apparent inclination shallowing by performing all the averages in directional space when some of the scatter is isotropic in polar space.

BIBLIOGRAPHY

Andrews, J. A., True polar wander: An analysis of Cenozoic and Mesozoic paleomagnetic poles, *J. Geophys. Res., 90*, 7737-7750, 1985.

Andrews, J. E., et al., *Initial Reports of the Deep Sea Drilling Project, 30*, 753 pp., U.S. Government Printing Office, Washington, D.C., 1975.

Anson, G. L., and K. P. Kodama, Compaction-induced shallowing of the post-depositional remanent magnetization in a synthetic sediment, *Geophys. J. R. Astron. Soc., 88*, 673-692, 1987.

Arason, P., and S. Levi, Inclination shallowing recorded in some deep sea sediments (abstract), *Eos Trans. AGU, 67*, 916, 1986.

Arason, P., and S. Levi, Models of inclination shallowing during sediment compaction, *J. Geophys. Res., 95*, 4481-4499, 1990*a*.

Arason, P., and S. Levi, Compaction and inclination shallowing in deep-sea sediments from the Pacific ocean, *J. Geophys. Res., 95*, 4501-4510, 1990*b*.

Audunsson, H., and S. Levi, Drilling-induced remanent magnetization in basalt drill cores, *Geophys. J. Int., 98*, 613-622, 1989.

Backman, J., et al., *Proceedings of the Ocean Drilling Program, Initial Reports, 115*, 1085 pp., Ocean Drilling Program, College Station, Texas, 1988.

Baldwin, B., Ways of deciphering compacted sediments, *J. Sediment. Petrol., 41*, 293-301, 1971.

Baldwin, B., and C. O. Butler, Compaction curves, *Am. Assoc. Pet. Geol. Bull., 69*, 622-629, 1985.

Barker, F. S., et al., International geomagnetic reference field revision 1985, *Eos Trans. AGU, 67*, 523-524, 1986.

Barton, C. E., M. W. McElhinny, and D. J. Edwards, Laboratory studies of depositional DRM, *Geophys. J. R. Astron. Soc., 61*, 355-377, 1980.

Bennett, R. H., W. R. Bryant, and G. H. Keller, Clay fabric of selected submarine sediments: Fundamental properties and models, *J. Sediment. Petrol., 51*, 217-232, 1981.

Besse, J., and V. Courtillot, Revised and synthetic apparent polar wander paths of the African, Eurasian, North American and Indian plates, and true polar wander since 200 Ma, *J. Geophys. Res., 96*, 4029-4050, 1991.

Beyer, W. H. (Ed.), *CRC Standard Mathematical Tables*, 27th ed., 615 pp., CRC Press, Boca Raton, Fla., 1984.

Bleil, U., The magnetostratigraphy of northwest Pacific sediments, Deep Sea Drilling Project leg 86, *Initial Rep. Deep Sea Drill. Proj., 86*, 441-458, 1985.

Blow, R. A., and N. Hamilton, Effect of compaction on the acquisition of a detrital remanent magnetization in fine-grained sediments, *Geophys. J. R. Astron. Soc.*, *52*, 13-23, 1978.

Briden, J. C., and M. A. Ward, Analysis of magnetic inclination in borecores, *Pure Appl. Geophys.*, *63*, 133-152, 1966.

Calderone, G. J., and R. F. Butler, The effects of randomly directed noise on paleomagnetic directions (abstract), *Eos Trans. AGU*, *69*, 1158-1159, 1988.

Calderone, G. J., and R. F. Butler, The effects of noise due to random undetected tilts and paleosecular variation on regional paleomagnetic directions, *J. Geophys. Res.*, *96*, 3973-3977, 1991.

Castro, J., and L. Brown, Shallow paleomagnetic directions from historic lava flows, Hawaii, *Geophys. Res. Lett.*, *14*, 1203-1206, 1987.

Celaya, M. A., and B. M. Clement, Inclination shallowing in deep sea sediments from the North Atlantic, *Geophys. Res. Lett.*, *15*, 52-55, 1988.

Chikazumi, S., *Physics of Magnetism*, 554 pp., John Wiley, New York, 1964.

Cockerham, R. S., A paleomagnetic and magnetic property study of DSDP Pacific basalts and sediments of Cretaceous age (abstract), *Eos Trans. AGU*, *60*, 239, 1979.

Cockerham, R. S., and J. M. Hall, Magnetic properties and paleomagnetism of some DSDP leg 33 basalts and sediments and their tectonic implications, *J. Geophys. Res.*, *81*, 4207-4222, 1976.

Cockerham, R. S., and R. D. Jarrard, Paleomagnetism of some leg 33 sediments and basalts, *Initial Rep. Deep Sea Drill. Proj.*, *33*, 631-647, 1976.

Cogné, J.-P., and H. Perroud, Unstraining paleomagnetic vectors: The current state of debate, *Eos Trans. AGU*, *68*, 705-712, 1987.

Collinson, D. W., Depositional remanent magnetization in sediments, *J. Geophys. Res.*, *70*, 4663-4668, 1965.

Collinson, D. W., *Methods in Rock Magnetism and Palaeomagnetism; Techniques and Instrumentation*, 503 pp., Chapman and Hall, London, 1983.

Collombat, H., P. Rochette, and M. J. Jackson, Possible correction of the inclination error in deep sea sediments using the anisotropy of anhysteretic remanence (ARM) (abstract), *Eos Trans. AGU*, *71*, 1288, 1990.

Coupland, D. H., and R. Van der Voo, Long-term nondipole components in the geomagnetic field during the last 130 m.y., *J. Geophys. Res.*, *85*, 3529-3548, 1980.

Courtillot, V., and J. Besse, Magnetic field reversals, polar wander, and core-mantle coupling, *Science*, *237*, 1140-1147, 1987.

Cox, A., and R. G. Gordon, Paleolatitudes determined from paleomagnetic data from vertical cores, *Rev. Geophys.*, *22*, 47-72, 1984.

Creer, K. M., Computer synthesis of geomagnetic palaeosecular variations, *Nature*, *304*, 695-699, 1983.

Deamer, G. A., and K. P. Kodama, Compaction-induced inclination shallowing in synthetic and natural clay-rich sediments, *J. Geophys. Res.*, *95*, 4511-4529, 1990.

DSDP CD-ROM, *Marine Geological and Geophysical Data From the Deep Sea Drilling Project*, CD-ROM data set, National Geophysical Data Center, Colorado, 1989.

Duncan, R. A., and D. A. Clague, Pacific plate motion recorded by linear volcanic chains, in *The Ocean Basins and Margins*, vol. 7A, edited by A. E. M. Nairn, F. G. Stehli, and S. Uyeda, pp. 89-121, Plenum, New York, 1985.

Duncan, R. A., and M. A. Richards, Hotspots, mantle plumes, flood basalts, and true polar wander, *Rev. Geophys.*, *29*, 31-50, 1991.

Faas, R. W., and D. S. Crocket, Clay fabric development in a deep-sea core: Site 515, Deep Sea Drilling Project leg 72, *Initial Rep. Deep Sea Drill. Proj.*, *72*, 519-535, 1983.

Fisher, R., Dispersion on a sphere, *Proc. R. Soc. London, Ser. A, 217*, 295-305, 1953.

Forsythe, G. E., M. A. Malcolm, and C. B. Moler, *Computer Methods for Mathematical Computations*, 259 pp., Prentice Hall, Englewood Hills, N. J., 1977.

Gordon, R. G., Late Cretaceous apparent polar wander of the Pacific plate: Evidence for a rapid shift of the Pacific hotspots with respect to the spin axis, *Geophys. Res. Lett.*, *10*, 709-712, 1983.

Gordon, R. G., Test for bias in paleomagnetically determined paleolatitudes from Pacific plate deep sea drilling project sediments, *J. Geophys. Res.*, *95*, 8397-8404, 1990.

Gordon, R. G., and A. Cox, Calculating paleomagnetic poles for oceanic plates *Geophys. J. R. Astron. Soc., 63*, 619-640, 1980.

Gordon, R. G., and R. A. Livermore, Apparent polar wander of the mean-lithosphere reference frame, *Geophys. J. Roy. Astron. Soc., 91*, 1049-1057, 1987.

Gradshteyn, I. S., and I. M. Ryzhik, *Table of Integrals, Series, and Products*, 1160 pp., 4th ed., Academic, San Diego, Calif., 1980.

Griffiths, D. H., R. F. King, A. I. Rees, A. E. Wright, Remanent magnetism of some recent varved sediments, *Proc. R. Soc. London, Ser. A, 256*, 359-383, 1960.

Hamilton, E. L., Thickness and consolidation of deep-sea sediments, *Geol. Soc. Am. Bull., 70*, 1399-1424, 1959.

Hamilton, E. L., Variations of density and porosity with depth in deep-sea sediments, *J. Sediment Petrol., 46*, 280-300, 1976.

Hammond, S. R., L. W. Kroenke, and F. Theyer, Northward motion of the Ontong-Java plateau between -110 and -30 m.y.: A paleomagnetic investigation of DSDP site 289, *Initial Rep. Deep Sea Drill. Proj., 30*, 415-418, 1975.

Harland, W. B., A. V. Cox, P. G. Llewellyn, C. A. G. Pickton, A. G. Smith, and R. Walters, *A Geologic Time Scale*, 131 pp., Cambridge University Press, New York, 1982.

Harrison, C. G. A., Paleomagnetism of deep sea sediments, *J. Geophys. Res., 71*, 3035-3043, 1966.

Harrison, C. G. A., The paleomagnetic record from deep-sea sediment cores, *Earth Sci. Rev., 10*, 1-36, 1974.

Harrison, C. G. A., Secular variation and excursions of the earth's magnetic field, *J. Geophys. Res.*, *85*, 3511-3522, 1980.

Harrison, C. G. A., and T. Lindh, A polar wandering curve for North America during the Mesozoic and Cenozoic, *J. Geophys. Res.*, *87*, 1903-1920, 1982.

Heath, G. R., et al., *Initial Reports of the Deep Sea Drilling Project*, *86*, 804 pp., U.S. Government Printing Office, Washington, D.C., 1985*a*.

Heath, G. R., D. H. Rea, and S. Levi, Paleomagnetism and accumulation rates of sediments at sites 576 and 578, Deep Sea Drilling Project leg 86, western north Pacific, *Initial Rep. Deep Sea Drill. Proj.*, *86*, 459-502, 1985*b*.

Heath, G. R., R. B. Kovar, C. Lopez, and G. L. Campi, Elemental composition of Cenozoic pelagic clays from deep sea drilling project sites 576 and 578, western north Pacific, *Initial Rep. Deep Sea Drill. Proj.*, *86*, 605-646, 1985*c*.

Hoffman, K. A., A method for the display and analysis of transitional paleomagnetic data, *J. Geophys. Res.*, *89*, 6285-6292, 1984.

Irving, E., *Paleomagnetism; and Its Application to Geological and Geophysical Problems*, 399 pp., John Wiley, New York, 1964.

Irving, E., and A. Major, Post-depositional detrital remanent magnetization in a synthetic sediment, *Sedimentology*, *3*, 135-143, 1964.

Jackson, M. J., S. K. Banerjee, J. A. Marvin, R. Lu, and W. Gruber, Detrital remanence, inclination errors, and anhysteretic remanence anisotropy: Quantitative model and experimental results, *Geophys. J. Int.*, *104*, 95-103, 1991.

Jarrard, R. D., Paleomagnetism of leg 17 sediment cores, *Initial Rep. Deep Sea Drill. Proj.*, *17*, 365-376, 1973.

Johnson, T. C., E. L. Hamilton, and W. H. Berger, Physical properties of calcareous ooze: Control by dissolution at depth, *Mar. Geol.*, *24*, 259-277, 1977.

Karlin, R., and S. Levi, Preliminary paleomagnetic results of laminated sediments from deep sea drilling project hydraulic piston core site 480, Guaymas basin, Gulf of California, *Initial Rep. Deep Sea Drill. Proj.*, *64*, 1255-1258, 1982.

Karlin, R., and S. Levi, Geochemical and sedimentological control of the magnetic properties of hemipelagic sediments, *J. Geophys. Res.*, *90*, 10,373-10,392, 1985.

Kent, D. V., Post-depositional remanent magnetization in deep-sea sediment, *Nature*, *246*, 32-34, 1973.

Kent, D. V., and D. J. Spariosu, Magnetostratigraphy of Caribbean site 502 hydraulic piston cores, *Initial Rep. Deep Sea Drill. Proj.*, *68*, 419-433, 1982.

Khramov, A. N., Orientational magnetization of finely dispersed sediments, *Izv. Acad. Sci. USSR Phys. Solid Earth*, *1*, 63-66, 1968.

King, R. F., Remanent magnetism of artificially deposited sediments, *Mon. Not. R. Astron. Soc., Geophys. Suppl.*, *7*, 115-134, 1955.

King, R. F., and A. J. Rees, Detrital magnetism in sediments: An examination of some theoretical models, *J. Geophys. Res.*, *71*, 561-571, 1966.

Kono, M., Paleomagnetism of DSDP leg 55 basalts and implications for the tectonics of the Pacific plate, *Initial Rep. Deep Sea Drill. Proj.*, *55*, 737-752, 1980*a*.

Kono, M., Statistics of paleomagnetic inclination data, *J. Geophys. Res.*, *85*, 3878-3882, 1980*b*.

Kroenke, L. W., et al., *Proceedings of the Ocean Drilling Program, Initial Reports*, *130*, 1240 pp., Ocean Drilling Program, College Station, Texas, 1991.

Ku, T. L., J. R. Southon, J. S. Vogel, Z. C. Liang, M. Kusakabe, and D. E. Nelson, ^{10}Be distributions in deep sea drilling project site 576 and site 578 sediments studied by accelerator mass spectrometry, *Initial Rep. Deep Sea Drill. Proj.*, *86*, 539-546, 1985.

Lancelot, Y., et al., *Proceedings of the Ocean Drilling Program, Initial Reports*, *129*, 488 pp., Ocean Drilling Program, College Station, Texas, 1990.

Langevin, P., Magnétisme et théorie des électrons (in French), *Ann. Chim. Phys.*, *5*, 70-127, 1905.

Lanphere, M. A., and G. B. Dalrymple, K-Ar ages of basalts from DSDP leg 33: sites 315 (Line Islands) and 317 (Manihiki Plateau), *Initial Rep. Deep Sea Drill. Proj.*, *33*, 649-653, 1976.

Larson, R. L., et al., *Initial Reports of the Deep Sea Drilling Project, 61*, 885 pp., U.S. Government Printing Office, Washington, D.C., 1981.

Le Pichon, X., Sea-floor spreading and continental drift, *J. Geophys. Res.*, *73*, 3661-3697, 1968.

Lenôtre, N., H. Chamley, and M. Hoffert, Clay stratigraphy at Deep Sea Drilling Project sites 576 and 578, leg 86 (western north Pacific), *Initial Rep. Deep Sea Drill. Proj.*, *86*, 571-579, 1985.

Levi, S., and R. T. Merrill, Properties of single-domain, pseudo-single-domain, and multidomain magnetite, *J. Geophys. Res.*, *83*, 309-323, 1978.

Levi, S., and R. Karlin, A sixty thousand year paleomagnetic record from Gulf of California sediments: Secular variation, late Quaternary excursions and geomagnetic implications, *Earth Planet. Sci. Lett.*, *92*, 219-233, 1989.

Levi, S., and S. Banerjee, On the origin of inclination shallowing in redeposited sediments, *J. Geophys. Res.*, *95*, 4383-4389, 1990.

Livermore, R. A., F. J. Vine, and A. G. Smith, Plate motions and the geomagnetic field - I. Quaternary and late Tertiary, *Geophys. J. Roy. Astron. Soc.*, *73*, 153-171, 1983.

Livermore, R. A., F. J. Vine, and A. G. Smith, Plate motions and the geomagnetic field - II. Jurassic to Tertiary, *Geophys. J. Roy. Astron. Soc.*, *79*, 939-961, 1984.

Lu, R., S.K. Banerjee, and J. Marvin, The effects of clay mineralogy and solution conductivity on DRM acquisition in sediments (abstract), *Eos Trans. AGU*, *69*, 1159, 1988.

Lu, R., S.K. Banerjee, and J. Marvin, Effects of clay mineralogy and the electrical conductivity of water on the acquisition of depositional remanent magnetization in sediments, *J. Geophys. Res.*, *95*, 4531-4538, 1990.

Mardia, K. V., *Statistics of Directional Data*, 357 pp., Academic, San Diego, Calif., 1972.

McElhinny, M. W., *Palaeomagnetism and Plate Tectonics*, 358 pp., Cambridge University Press, Cambridge, 1973.

McElhinny, M. W., and R. T. Merrill, Geomagnetic secular variation over the past 5 m.y., *Rev. Geophys.*, *13*, 687-708, 1975.

McFadden, P. L., Determination of the angle in a Fisher distribution which will be exceeded with a given probability, *Geophys. J. R. Astron. Soc.*, *60*, 391-396, 1980*a*.

McFadden, P. L., The best estimate of Fisher's precision parameter κ, *Geophys. J. R. Astron. Soc.*, *60*, 397-407, 1980*b*.

McFadden, P. L., and A. B. Reid, Analysis of paleomagnetic inclination data, *Geophys. J. R. Astron. Soc.*, *69*, 307-319, 1982.

Merrill, R. T., and M. W. McElhinny, Anomalies in the time-averaged paleomagnetic field and their implications for the lower mantle, *Rev. Geophys.*, *15*, 309-323, 1977.

Merrill, R. T., and M. W. McElhinny, *The Earth's Magnetic Field; Its History, Origin and Planetary Perspective*, 401 pp., Academic, New York, 1983.

Moberly, R., et al., *Initial Reports of the Deep Sea Drilling Project*, *89*, 678 pp., U.S. Government Printing Office, Washington, D.C., 1986.

Morgan, G. E., Paleomagnetic results from DSDP site 398, *Initial Rep. Deep Sea Drill. Proj.*, *47*, 599-611, 1979.

Nagata, T., Notes on detrital remanent magnetization of sediments, *J. Geomagn. Geoelectr.*, *14*, 99-106, 1962.

Ness, G., S. Levi, and R. Couch, Marine magnetic anomaly timescales for the Cenozoic and Late Cretaceous: A précis, critique, and synthesis, *Rev. Geophys., 18*, 753-770, 1980.

Nobes, D. C., H. Villinger, E. E. Davis, and L. K. Law, Estimation of marine sediment bulk physical properties at depth from seafloor geophysical measurements, *J. Geophys. Res., 91*, 14,033-14,043, 1986.

Ogg, J. G., Paleolatitudes and magnetostratigraphy of Cretaceous and lower Tertiary sedimentary rocks, deep sea drilling project site 585, Mariana basin, western central Pacific, *Initial Rep. Deep Sea Drill. Proj., 89*, 629-645, 1986.

Opdyke, N. D., Paleomagnetism of deep-sea cores, *Rev. Geophys., 10*, 213-249, 1972.

Opdyke, N. D., and K. W. Henry, A test of the dipole hypothesis, *Earth Planet. Sci. Lett., 6*, 139-151, 1969.

Ozima, M., Effects of plastic deformation on the remanent magnetization of a Cu-Co alloy, *Earth Planet. Sci. Lett., 47*, 121-123, 1980.

Payne, M. A., and K. L. Verosub, The acquisition of post-depositional detrital remanent magnetization in a variety of natural sediments, *Geophys. J. R. Astron. Soc., 68*, 625-642, 1982.

Peirce, J. W., Assessing the reliability of DSDP paleolatitudes, *J. Geophys. Res., 81*, 4173-4187, 1976.

Petronotis, K. E., and R. G. Gordon, Age dependence of skewness of magnetic anomalies above seafloor formed at the Pacific-Kula spreading center, *Geophys. Res. Lett., 16*, 315-318, 1989.

Pitman, W. C. III, R. L. Larson, and E. M. Herron, The age of the ocean basins, *Geol. Soc. Amer. Map and Chart Series MC-6*, 1974.

Sager, W. W., Paleomagnetism of Abbott Seamount and implications for the latitudinal drift of the Hawaiian hot spot, *J. Geophys. Res.*, *89*, 6271-6284, 1984.

Sager, W. W., and U. Bleil, Latitudinal shift of the Pacific hotspots during the late Cretaceous and early Tertiary, *Nature*, *326*, 488-490, 1987.

Sager, W. W., and M. S. Pringle, Mid-Cretaceous to early Tertiary apparent polar wander path of the Pacific plate, *J. Geophys. Res.*, *93*, 11,753-11,771, 1988.

Sayre, W. O., Preliminary report on the paleomagnetism of Aptian and Albian limestones and trachytes from the mid-Pacific mountains and Hess rise, deep sea drilling project leg 62, *Initial Rep. Deep Sea Drill. Proj.*, *62*, 983-994, 1981.

Schlanger, S. O., et al., *Initial Reports of the Deep Sea Drilling Project*, *33*, 973 pp., U.S. Government Printing Office, Washington, D.C., 1976.

Schlanger, S. O., M. O. Garcia, B. H. Keating, J. J. Naughton, W. W. Sager, J. A. Haggerty, J. A. Philpotts, and R. A. Duncan, Geology and geochronology of the Line Islands, *J. Geophys. Res.*, *89*, 11261-11272, 1984.

Schneider, D. A., An estimate of the long-term non-dipole field from marine magnetic anomalies, *Geophys. Res. Lett.*, *15*, 1105-1108, 1988.

Schneider, D. A., and D. V. Kent, Influence of non-dipole field on determination of Plio-Pleistocene true polar wander, *Geophys. Res. Lett.*, *13*, 471-474, 1986.

Schneider, D. A., and D. V. Kent, Inclination anomalies from Indian ocean sediments and the possibility of a standing nondipole field, *J. Geophys. Res.*, *93*, 11,621-11,630, 1988*a*.

Schneider, D. A., and D. V. Kent, The paleomagnetic field from equatorial deep-sea sediments: Axial symmetry and polarity asymmetry, *Science*, *242*, 252-256, 1988*b*.

Schneider, D. A., and D. V. Kent, The time-averaged paleomagnetic field, *Rev. Geophys.*, *28*, 71-96, 1990.

Schultheiss, P. J., Physical and geotechnical properties of sediments from the northwest Pacific: Deep Sea Drilling Project leg 86, *Initial Rep. Deep Sea Drill. Proj.*, *86*, 701-722, 1985.

Sclater, J. G., and R. D. Jarrard, Preliminary paleomagnetic results, leg 7, *Initial Rep. Deep Sea Drill. Proj.*, *7*, 1227-1234, 1971.

Shuey, R. T., E. R. Cole, and M. J. Mikulich, Geographic correction of archeomagnetic data, *J. Geomag. Geoelectr.*, *22*, 485-489, 1970.

Skempton, A. W., The consolidation of clays by gravitational compaction, *Q. J. Geol. Soc. London*, *125*, 373-411, 1970.

Stacey, F. D., On the role of Brownian motion in the control of detrital remanent magnetization of sediments, *Pure Appl. Geophys.*, *98*, 139-145, 1972.

Steele, W. K., Directional errors in remanent magnetization of non-cubic soft sediment specimens measured with spinner magnetometers, *Geophys. J.*, *96*, 333-341, 1989.

Steiner, M. B., Paleomagnetism of the Cretaceous section, site 462, *Initial Rep. Deep Sea Drill. Proj.*, *61*, 711-716, 1981.

Stober, J. C., and R. Thompson, Magnetic remanence acquisition in Finnish lake sediments, *Geophys. J. R. Astron. Soc.*, *57*, 727-739, 1979.

Tanguy, J.-C., Abnormal shallow palaeomagnetic inclinations from the 1950 and 1972 lava flows, Hawaii, *Geophys. J. Int.*, *103*, 281-283, 1990.

Tarduno, J. A., Absolute inclination values from deep sea sediments: A reexamination of the Cretaceous Pacific record, *Geophys. Res. Lett.*, *17*, 101-104, 1990.

Tarduno, J. A., W. V. Sliter, T. J. Bralower, M. McWilliams, I. Premoli-Silva, and J. G. Ogg, M-sequence reversals recorded in DSDP sediment cores from the western Mid-Pacific Mountains and Magellan Rise, *Bull. Geol. Soc. Am.*, *101*, 1306-1316, 1989.

Tarling, D. H., *Principles and Applications of Palaeomagnetism*, 164 pp., Chapman and Hall, London, 1971.

Tarling, D. H., *Palaeomagnetism; Principles and Applications in Geology, Geophysics and Archaeology*, 379 pp., Chapman and Hall, London, 1983.

Tauxe, L., P. Tucker, N. P. Petersen, and J. L. LaBrecque, Magnetostratigraphy of leg 73 sediments, *Initial Rep. Deep Sea Drill. Proj.*,*73*, 609-621, 1984.

Thiede, J., et al., *Initial Reports of the Deep Sea Drilling Project*, *62*, 1120 pp., U.S. Government Printing Office, Washington, D.C., 1981.

Tomlinson, M. J., *Foundation Design and Construction*, 793 pp., 4th ed., Pitman Advanced Publishing Program, Boston, Mass., 1980.

Tschebotarioff, G. P., *Soil Mechanics, Foundations and Earth Structures*, 655 pp., McGraw-Hill, New York, 1951.

Tucker, P., Selective post-depositional realignment in a synthetic sediment, *Phys. Earth Planet. Inter.*, *20*, 11-14, 1979.

Tucker, P., Stirred remanent magnetization: A laboratory analogue of post-depositional realignment, *J. Geophys.*, *48*, 153-157, 1980.

Verosub, K. L., Depositional and postdepositional processes in the magnetization of sediments, *Rev. Geophys.*, *15*, 129-143, 1977.

Von Mises, R., Über die "ganzzahligkeit" der atomgewichte und verwandte fragen (in German), *Phys. Z.*, *19*, 490-500, 1918.

Watson, G. S., Analysis of dispersion on a sphere, *Mon. Notic. R. Astron. Soc. Geophys. Suppl.*, *7*, 153-159, 1956*a*.

Watson, G. S., A test for randomness of directions, *Mon. Notic. R. Astron. Soc. Geophys. Suppl.*, *7*, 160-161, 1956*b*.

Watson, G. S., and E. J. Williams, On the construction of significance tests on the circle and the sphere, *Biometrica*, *43*, 344-352, 1956.

Watts, A. B., J. K. Weissel, R. A. Duncan, and R. L. Larson, Origin of the Louisville ridge and its relationship to the Eltanin fracture zone system, *J. Geophys. Res.*, *93*, 3051-3077, 1988.

Wilson, R. L., Permanent aspects of the Earth's non-dipole magnetic field over upper Tertiary times, *Geophys. J. R. Astron. Soc.*, *19*, 417-437, 1970.

Wilson, R. L., Dipole offset – The time-average palaeomagnetic field over the past 25 million years, *Geophys. J. R. Astron. Soc.*, *22*, 491-504, 1971.

Winterer, E. L., et al., *Initial Reports of the Deep Sea Drilling Project*, *7*, 1757 pp., U.S. Government Printing Office, Washington, D.C., 1971.

Winterer, E. L., et al., *Initial Reports of the Deep Sea Drilling Project*, *17*, 930 pp., U.S. Government Printing Office, Washington, D.C., 1973.

Wolejszo, J., R. Schlich, and J. Segoufin, Paleomagnetic studies of basalt samples, Deep Sea Drilling Project, leg 25, *Initial Rep. Deep Sea Drill. Proj.*, *25*, 555-572, 1974.

APPENDICES

APPENDIX A

Data From DSDP Hole 578

In this appendix we list the paleomagnetic data from DSDP hole 578 (33.93°N, 151.63°E, 6010 m water depth). These data were used in chapter 2: "Compaction and Inclination Shallowing in Deep-Sea Sediments From the Pacific Ocean". The samples were obtained in 1982 during DSDP leg 86 onboard the *D/V Glomar Challenger*. These data include probably the most complete Neogene magnetostratigraphy from a single hole of the DSDP program.

TABLE A.1. Paleomagnetic Data From DSDP Hole 578.

Sample ID	Sample Number	Depth in Hole, m	Stable Direction: Declination, deg	Stable Direction: Inclination, deg	Intensity, 10^{-3} A m^{-1}: NRM	Intensity, 10^{-3} A m^{-1}: AFD-Level 10mT	Intensity, 10^{-3} A m^{-1}: AFD-Level 20mT	Data Source
86-578-1-1,16	901	0.16	173.2	46.8	98.23	88.13	-	(2)
86-578-1-1,38	902	0.38	165.6	49.6	85.61	78.97	-	(2)
86-578-1-1,53	903	0.53	150.4	52.8	88.11	75.92	-	(2)
86-578-1-1,66	904	0.66	147.0	48.4	43.87	40.01	-	(2)
86-578-1-1,86	905	0.86	115.5	43.9	14.19	10.39	-	(2)
86-578-1-1,106	906	1.06	95.8	52.3	45.63	39.43	-	(2)
86-578-1-1,126	907	1.26	98.7	47.9	52.34	-	-	(2)
86-578-1-1,146	908	1.46	90.5	54.7	63.19	53.53	-	(2)
86-578-1-2,6	909	1.56	97.0	55.0	52.95	49.80	-	(2)
86-578-1-2,26	910	1.76	65.6	47.8	38.29	34.31	25.54	(1)
86-578-1-2,50	911	2.00	79.2	50.3	52.79	38.96	-	(2)
86-578-1-2,66	912	2.16	93.8	46.4	67.88	58.73	44.81	(1)
86-578-1-2,86	913	2.36	96.3	55.3	29.65	28.09	-	(2)
86-578-1-2,106	914	2.56	109.2	44.8	19.30	16.56	12.34	(1)
86-578-1-2,126	915	2.76	112.2	63.7	44.81	39.93	-	(2)
86-578-1-2,146	916	2.96	81.6	54.4	49.55	39.69	-	(2)
86-578-1-3,6	917	3.06	117.2	47.5	-	51.08	-	(2)
86-578-1-3,27	918	3.27	135.9	46.9	78.17	68.58	-	(2)
86-578-1-3,46	919	3.46	125.9	51.4	-	74.48	-	(2)
86-578-1-3,66	920	3.66	130.3	29.9	58.94	44.99	-	(2)
86-578-1-3,86	921	3.86	149.2	41.0	56.45	43.76	-	(2)
86-578-1-3,106	922	4.06	129.7	57.9	59.82	50.84	38.65	(1)
86-578-1-3,126	923	4.26	152.6	44.3	66.18	55.42	-	(2)
86-578-1-3,146	924	4.46	135.7	41.4	66.12	58.65	44.96	(1)
86-578-2-1,6	925	4.86	200.5	39.9	63.86	52.96	-	(2)
86-578-2-1,29	926	5.09	216.9	51.4	47.65	42.18	33.37	(1)
86-578-2-1,43	927	5.23	219.3	55.9	57.51	46.56	-	(2)
86-578-2-1,66	928	5.46	210.8	47.5	39.65	34.20	26.91	(1)
86-578-2-1,86	929	5.66	218.4	30.3	31.48	25.48	-	(2)
86-578-2-1,106	930	5.86	226.1	47.6	51.13	45.82	36.65	(1)
86-578-2-1,126	931	6.06	251.2	61.7	57.60	52.76	-	(2)
86-578-2-1,146	932	6.26	232.3	47.5	59.48	52.91	41.32	(2)
86-578-2-2,5	933	6.35	231.8	–28.4	34.30	26.36	20.73	(2)
86-578-2-2,26	934	6.56	237.3	42.4	52.90	43.63	32.96	(2)
86-578-2-2,46	935	6.76	221.8	54.3	44.85	37.30	-	(2)
86-578-2-2,69	936	6.96	222.3	41.7	16.15	12.49	8.91	(1)
86-578-2-2,86	937	7.16	242.1	54.2	56.89	49.19	-	(2)
86-578-2-2,106	938	7.36	239.9	48.5	66.78	59.05	45.85	(1)
86-578-2-2,126	939	7.56	235.3	64.1	51.76	45.32	-	(2)
86-578-2-2,146	940	7.76	246.8	43.6	43.85	35.24	27.37	(1)
86-578-2-3,41	942	8.21	233.7	47.5	115.80	83.05	-	(2)
86-578-2-3,66	943	8.46	189.4	18.5	61.38	50.86	-	(2)

86-578-2-3,86	944	8.66	175.5	55.0	54.93	49.96	-	(2)
86-578-2-3,106	945	8.86	178.4	51.2	66.49	51.05	-	(2)
86-578-2-3,128	946	9.06	183.3	51.3	47.45	39.13	28.58	(1)
86-578-2-3,144	947	9.24	172.3	53.9	45.97	36.24	-	(2)
86-578-2-4,6	948	9.36	171.6	46.7	44.77	37.66	29.26	(1)
86-578-2-4,26	949	9.56	167.1	59.4	86.49	70.93	-	(2)
86-578-2-4,46	950	9.76	176.5	55.6	66.28	56.80	43.27	(1)
86-578-2-4,64	951	9.94	169.1	60.9	80.73	65.83	-	(2)
86-578-2-4,86	952	10.16	189.2	51.3	58.23	47.19	35.25	(1)
86-578-2-4,106	953	10.36	173.7	48.7	53.19	43.63	-	(2)
86-578-2-4,126	954	10.56	192.6	55.2	9.83	7.90	5.43	(1)
86-578-2-4,146	955	10.76	177.6	48.8	5.83	4.64	-	(2)
86-578-2-5,5	956	10.86	171.1	49.7	20.82	17.15	13.36	(1)
86-578-2-5,26	957	11.06	177.0	59.4	61.67	52.25	-	(2)
86-578-2-5,46	958	11.26	181.3	46.4	55.36	48.11	36.16	(1)
86-578-2-5,66	959	11.46	187.3	60.0	79.92	68.15	-	(2)
86-578-2-5,86	960	11.66	185.2	56.7	102.50	89.63	70.68	(1)
86-578-2-5,106	961	11.86	180.0	58.6	83.08	66.93	-	(2)
86-578-2-5,127	962	12.07	180.9	53.0	121.77	101.26	77.69	(1)
86-578-2-6,6	963	12.36	185.8	54.7	95.13	74.51	-	(2)
86-578-2-6,27	964	12.57	186.5	51.1	84.91	72.81	56.38	(1)
86-578-3-1,4	965	14.34	350.5	44.7	119.54	99.47	-	(2)
86-578-3-1,26	966	14.56	356.8	53.1	16.96	15.53	11.45	(1)
86-578-3-1,46	967	14.76	2.5	63.9	8.91	7.43	-	(2)
86-578-3-1,68	968	14.96	358.5	49.8	19.41	17.23	12.56	(1)
86-578-3-1,86	969	15.16	355.0	54.2	20.57	17.16	-	(2)
86-578-3-1,106	970	15.36	4.5	53.3	48.09	40.28	29.07	(2)
86-578-3-1,126	971	15.56	5.2	−57.8	38.41	33.98	22.68	(2)
86-578-3-1,146	972	15.76	357.1	47.3	49.86	41.15	32.06	(2)
86-578-3-2,6	973	15.86	8.8	55.2	45.34	37.37	-	(2)
86-578-3-2,26	974	16.06	3.4	55.1	27.62	24.01	18.24	(1)
86-578-3-2,46	975	16.26	357.9	51.0	27.06	23.94	-	(2)
86-578-3-2,66	976	16.46	11.4	51.6	43.60	40.15	31.09	(1)
86-578-3-2,86	977	16.66	8.0	59.5	61.84	51.96	-	(2)
86-578-3-2,106	978	16.86	10.8	53.4	56.99	52.29	39.91	(1)
86-578-3-2,126	979	17.06	18.4	58.4	57.84	48.08	-	(2)
86-578-3-2,146	980	17.26	23.3	54.1	58.37	49.57	32.92	(2)
86-578-3-3,6	981	17.36	51.5	−13.4	52.58	42.56	31.45	(2)
86-578-3-3,26	982	17.56	15.3	52.8	86.43	72.52	55.57	(2)
86-578-3-3,46	983	17.76	28.1	54.9	52.66	41.74	-	(2)
86-578-3-3,66	984	17.96	23.4	55.6	35.42	31.72	23.20	(1)
86-578-3-3,83	985	18.13	21.9	55.5	60.09	53.35	-	(2)
86-578-3-3,101	986	18.31	24.8	46.7	47.82	43.00	32.89	(1)
86-578-3-3,126	987	18.56	38.2	53.9	75.11	64.74	-	(2)
86-578-3-3,146	988	18.76	5.9	55.5	81.86	77.09	60.86	(1)
86-578-3-4,6	989	18.86	34.1	52.1	67.67	58.42	-	(2)
86-578-3-4,26	990	19.06	51.6	52.5	36.32	32.29	24.04	(1)
86-578-3-4,46	991	19.26	43.7	54.3	51.53	43.72	-	(2)
86-578-3-4,66	992	19.46	45.2	56.0	45.60	41.07	30.72	(1)
86-578-3-4,86	993	19.66	43.4	53.7	56.18	53.77	-	(2)
86-578-3-4,106	994	19.86	39.7	48.1	39.59	33.69	24.88	(1)
86-578-3-4,126	995	20.06	49.3	56.6	79.95	70.84	-	(2)

86-578-3-4,146	996	20.26	34.7	53.8	57.92	52.00	39.23	(1)
86-578-3-5,6	997	20.36	49.7	48.4	92.82	80.56	-	(2)
86-578-3-5,26	998	20.56	50.0	50.7	93.81	84.18	64.85	(1)
86-578-3-5,46	999	20.76	48.1	53.6	72.61	65.03	-	(2)
86-578-3-5,66	1000	20.96	49.9	50.0	37.76	33.70	25.56	(1)
86-578-3-5,86	1001	21.16	57.9	58.0	76.31	61.87	-	(2)
86-578-3-5,106	1002	21.36	53.1	51.9	126.27	105.06	74.75	(1)
86-578-3-5,126	1003	21.56	67.2	52.1	105.76	93.29	-	(2)
86-578-3-5,146	1004	21.76	63.7	54.2	58.33	52.52	39.79	(1)
86-578-3-6,6	1005	21.86	79.3	47.5	47.16	38.93	-	(2)
86-578-3-6,26	1006	22.06	65.7	59.7	58.72	51.75	38.01	(1)
86-578-3-6,50	1007	22.30	78.8	66.0	8.47	6.61	-	(2)
86-578-3-6,66	1008	22.46	58.7	53.3	1.80	1.57	1.31	(1)
86-578-3-6,86	1009	22.66	62.8	55.7	2.05	1.71	-	(2)
86-578-3-6,105	1010	22.85	77.3	54.2	12.38	10.88	7.70	(1)
86-578-3-7,6	1011	23.36	67.2	49.3	41.98	32.44	-	(2)
86-578-3-7,25	1012	23.55	67.0	59.7	42.87	38.13	28.76	(1)
86-578-3-7,46	1013	23.76	65.9	52.8	39.54	33.26	-	(2)
86-578-4-1,6	1014	23.86	27.6	52.0	5.24	3.96	1.73	(1)
86-578-4-1,26	1015	24.06	332.8	74.7	9.33	7.91	-	(2)
86-578-4-1,46	1016	24.26	283.2	55.4	21.66	18.48	13.68	(1)
86-578-4-1,66	1017	24.46	328.7	46.6	47.99	41.28	-	(2)
86-578-4-1,84	1018	24.64	328.6	52.9	38.35	35.60	26.64	(1)
86-578-4-1,113	1019	24.93	340.2	47.2	43.62	38.54	-	(2)
86-578-4-1,131	1020	25.11	343.8	50.1	46.59	42.27	33.60	(1)
86-578-4-1,145	1021	25.25	329.1	52.7	40.06	34.69	-	(2)
86-578-4-2,6	1022	25.36	321.2	53.9	39.65	36.62	28.07	(1)
86-578-4-2,25	1023	25.55	328.1	46.0	46.58	39.51	-	(2)
86-578-4-2,46	1024	25.76	312.7	48.0	47.72	43.83	33.16	(1)
86-578-4-2,66	1025	25.96	321.1	51.0	62.95	54.87	-	(2)
86-578-4-2,86	1026	26.16	341.7	55.7	42.07	36.83	28.05	(1)
86-578-4-2,108	1027	26.38	329.4	57.5	64.93	54.50	-	(2)
86-578-4-2,126	1028	26.56	321.0	50.1	78.44	69.61	52.76	(1)
86-578-4-2,146	1029	26.76	332.3	55.6	58.44	53.07	-	(2)
86-578-4-3,6	1040	26.86	320.9	52.9	68.10	62.38	48.65	(1)
86-578-4-3,26	1039	27.06	312.4	50.2	43.58	36.34	-	(2)
86-578-4-3,66	1041	27.46	313.5	28.6	78.41	64.66	-	(2)
86-578-4-3,86	1042	27.66	266.3	49.1	42.81	35.93	-	(2)
86-578-4-3,105	1043	27.85	116.0	–12.0	6.47	8.88	8.12	(2)
86-578-4-3,126	1044	28.06	95.4	–60.5	36.14	34.52	-	(2)
86-578-4-3,146	1045	28.26	79.2	–51.7	58.22	60.56	-	(2)
86-578-4-4,6	1030	28.36	88.4	–52.7	36.14	38.83	33.72	(1)
86-578-4-4,25	1031	28.55	98.8	–58.4	41.12	43.55	-	(2)
86-578-4-4,46	1032	28.76	82.5	–41.1	31.69	31.50	26.29	(1)
86-578-4-4,65	1033	28.95	64.6	–29.0	0.52	0.64	0.48	(2)
86-578-4-4,85	1034	29.15	105.9	–58.4	0.37	0.49	0.37	(1)
86-578-4-4,110	1035	29.40	65.0	–50.0	0.95	0.91	0.72	(2)
86-578-4-4,129	1036	29.59	75.5	–34.1	0.78	0.68	0.64	(1)
86-578-4-3,146	1038	29.76	292.3	49.6	38.93	33.76	25.00	(1)
86-578-4-4,146	1037	29.76	68.1	–51.9	6.03	5.64	-	(2)
86-578-4-5,6	1046	29.86	55.7	–49.4	15.31	14.87	10.66	(1)
86-578-4-5,32	1047	30.12	49.5	–49.8	21.02	21.56	-	(2)

86-578-4-5,50	1048	30.30	62.0	–62.8	26.45	25.15	20.03	(1)
86-578-4-5,66	1049	30.46	48.5	–46.2	9.62	9.71	-	(2)
86-578-4-5,86	1050	30.66	49.5	–53.4	32.62	32.92	26.15	(1)
86-578-4-5,106	1051	30.86	40.9	–58.8	15.35	19.03	-	(2)
86-578-4-5,126	1052	31.06	28.3	–56.3	55.36	56.78	47.72	(1)
86-578-4-5,146	1053	31.26	22.0	–54.3	46.46	50.07	-	(2)
86-578-4-5,6	1054	31.36	28.7	–61.1	38.72	40.54	33.79	(1)
86-578-4-6,26	1055	31.56	10.3	–55.0	37.28	41.42	-	(2)
86-578-4-6,46	1056	31.76	9.6	–51.3	39.80	43.80	-	(2)
86-578-4-6,66	1057	31.96	2.2	57.2	27.30	33.23	23.76	(2)
86-578-4-6,85	1058	32.15	181.2	40.3	38.90	31.41	22.96	(1)
86-578-4-6,114	1059	32.44	161.3	55.7	55.55	43.81	-	(2)
86-578-5-1,26	1060	33.56	320.9	30.8	40.59	35.66	27.89	(1)
86-578-5-1,47	1061	33.77	330.1	47.9	50.12	44.58	-	(2)
86-578-5-1,106	1062	34.36	2.0	66.9	19.31	15.09	8.52	(2)
86-578-5-1,126	1063	34.56	153.9	–57.0	37.98	38.78	-	(2)
86-578-5-2,145	1064	34.75	145.4	–58.1	66.14	65.86	56.79	(1)
86-578-5-2,6	1065	34.86	161.8	–47.1	62.64	59.65	-	(2)
86-578-5-2,26	1066	35.06	165.1	–40.3	53.99	55.59	51.48	(1)
86-578-5-2,51	1067	35.31	155.7	–42.2	43.11	45.15	-	(2)
86-578-5-2,68	1068	35.48	152.2	–50.3	41.15	43.38	36.11	(1)
86-578-5-2,85	1069	35.65	142.6	–39.2	10.35	12.77	-	(2)
86-578-5-2,106	1070	35.86	168.7	–42.2	12.49	12.86	12.02	(1)
86-578-5-2,126	1072	36.06	166.2	–49.0	84.67	83.36	71.42	(1)
86-578-5-2,126	1071	36.06	167.0	–48.8	53.29	53.86	-	(2)
86-578-5-3,6	1073	36.36	164.9	–49.1	68.79	69.06	-	(2)
86-578-5-3,26	1074	36.56	162.0	–49.6	103.14	102.51	86.13	(1)
86-578-5-3,45	1075	36.75	168.3	–51.3	43.53	44.75	-	(2)
86-578-5-3,65	1076	36.95	163.7	–49.6	56.48	57.11	50.89	(1)
86-578-5-3,86	1077	37.16	167.3	–51.6	35.10	39.07	-	(2)
86-578-5-3,105	1078	37.35	178.0	–44.3	16.19	19.90	-	(2)
86-578-5-3,128	1079	37.58	355.9	43.9	21.83	16.61	8.81	(2)
86-578-5-3,146	1080	37.76	45.5	–45.0	40.44	4.54	4.99	(2)
86-578-5-4,6	1081	37.86	167.0	–38.4	11.02	12.70	-	(2)
86-578-5-4,26	1082	38.06	172.7	–43.9	54.39	58.00	49.86	(1)
86-578-5-4,46	1083	38.26	175.5	–46.2	33.21	31.77	-	(2)
86-578-5-4,66	1084	38.46	171.3	–36.2	33.20	32.71	28.21	(1)
86-578-5-4,86	1085	38.66	174.1	–48.0	36.01	36.66	-	(2)
86-578-5-4,106	1086	38.86	180.6	–56.8	53.94	52.99	44.43	(1)
86-578-5-4,126	1087	39.06	181.4	–52.4	18.73	19.99	-	(2)
86-578-5-4,146	1088	39.26	129.6	–55.1	0.45	0.37	0.31	(1)
86-578-5-5,6	1089	39.36	150.6	–51.7	0.70	0.55	-	(2)
86-578-5-5,26	1090	39.56	180.5	–39.9	5.49	4.65	3.52	(1)
86-578-5-5,46	1091	39.76	184.4	–54.3	9.56	8.07	-	(2)
86-578-5-5,66	1092	39.96	174.3	–43.1	15.36	12.31	9.29	(1)
86-578-5-5,86	1093	40.16	197.2	–52.3	26.32	23.18	-	(2)
86-578-5-5,107	1094	40.37	192.7	–55.3	41.50	37.85	29.64	(1)
86-578-5-5,128	1095	40.58	175.4	–50.6	17.53	15.44	-	(2)
86-578-5-5,146	1096	40.76	186.6	–53.5	13.49	10.70	8.49	(1)
86-578-5-6,6	1097	40.86	188.0	–51.7	24.85	21.29	-	(2)
86-578-5-6,26	1098	41.06	184.0	–57.9	35.70	32.08	24.56	(1)
86-578-5-6,46	1099	41.26	176.6	–52.3	61.02	59.38	-	(2)

86-578-5-6,66	1100	41.46	190.8	–57.2	62.59	58.28	46.71	(1)
86-578-5-6,86	1101	41.66	191.3	–54.3	79.63	72.40	-	(2)
86-578-5-6,106	1102	41.86	186.8	–53.8	62.94	59.07	46.29	(1)
86-578-5-6,126	1103	42.06	193.6	–55.0	76.99	72.54	-	(2)
86-578-5-7,6	1104	42.36	189.5	–52.1	50.52	48.95	39.75	(1)
86-578-5-7,22	1105	42.52	189.7	–56.0	40.73	37.43	-	(2)
86-578-5-7,40	1106	42.70	170.4	–57.2	28.83	29.93	26.80	(1)
86-578-6-1,51	1108	43.31	33.5	–59.2	54.83	55.77	47.10	(1)
86-578-6-1,67	1109	43.47	31.1	–51.0	33.09	34.85	-	(2)
86-578-6-1,86	1110	43.66	41.2	–39.2	50.52	51.81	44.95	(1)
86-578-6-1,106	1111	43.86	42.8	–56.6	40.49	35.98	-	(2)
86-578-6-1,126	1112	44.06	36.0	–51.3	2.08	2.16	1.83	(1)
86-578-6-1,146	1113	44.26	62.7	–55.8	12.37	10.56	-	(2)
86-578-6-2,6	1114	44.36	42.4	–50.0	37.01	35.83	28.62	(1)
86-578-6-2,26	1115	44.56	35.1	–47.5	33.26	32.26	-	(2)
86-578-6-2,46	1116	44.76	52.6	–49.9	39.38	39.82	32.65	(1)
86-578-6-2,66	1117	44.96	53.1	–50.6	34.50	36.43	-	(2)
86-578-6-2,86	1118	45.16	61.4	–50.6	29.12	29.61	24.84	(1)
86-578-6-2,106	1119	45.36	56.0	–41.3	58.31	56.71	-	(2)
86-578-6-2,126	1120	45.56	77.0	–38.2	62.02	61.28	50.97	(1)
86-578-6-2,146	1121	45.76	70.7	–45.9	70.53	73.30	-	(2)
86-578-6-3,6	1122	45.86	62.5	–52.9	71.93	73.02	61.64	(1)
86-578-6-3,26	1123	46.06	66.0	–55.0	50.79	47.99	-	(2)
86-578-6-3,41	1124	46.21	67.9	–52.3	68.84	67.34	55.68	(1)
86-578-6-3,63	1125	46.43	80.5	–53.7	73.11	72.22	-	(2)
86-578-6-3,80	1126	46.60	65.5	–53.6	49.32	48.16	39.24	(1)
86-578-6-3,102	1127	46.82	87.7	–53.2	33.94	33.14	-	(2)
86-578-6-3,126	1128	47.06	75.1	–46.4	1.34	1.31	1.23	(1)
86-578-6-3,146	1129	47.26	62.6	–57.1	0.68	0.69	0.60	(2)
86-578-6-4,6	1130	47.36	92.5	–53.9	2.08	1.92	1.74	(1)
86-578-6-4,24	1131	47.54	81.1	–47.5	2.40	2.22	-	(2)
86-578-6-4,46	1132	47.76	97.9	–52.3	2.34	2.10	1.78	(1)
86-578-6-4,66	1133	47.96	86.3	–52.3	18.41	16.99	-	(2)
86-578-6-4,86	1134	48.16	77.9	–58.9	51.20	49.51	39.75	(1)
86-578-6-4,106	1135	48.36	82.8	–51.2	27.61	26.68	-	(2)
86-578-6-4,125	1136	48.55	88.2	–61.9	20.10	21.37	17.63	(1)
86-578-6-4,146	1137	48.76	98.8	–55.1	28.93	33.67	-	(2)
86-578-6-5,6	1138	48.85	83.8	–53.3	55.72	54.67	46.65	(1)
86-578-6-5,46	1140	49.26	76.8	–54.7	53.51	53.72	44.00	(1)
86-578-6-5,66	1141	49.46	67.5	–59.2	39.64	43.35	-	(2)
86-578-6-5,86	1142	49.66	67.7	–54.1	44.25	46.87	39.95	(1)
86-578-6-5,106	1143	49.86	66.9	–52.0	21.43	24.57	-	(2)
86-578-6-5,125	1144	50.06	76.9	–55.1	57.53	59.56	49.08	(1)
86-578-6-5,146	1145	50.26	79.0	–48.8	26.29	23.53	-	(2)
86-578-6-6,11	1146	50.41	68.7	–42.3	16.58	15.84	11.71	(1)
86-578-6-6,34	1147	50.64	71.5	–36.8	1.37	1.24	-	(2)
86-578-6-6,66	1148	50.96	76.0	–52.1	30.08	30.79	24.26	(1)
86-578-6-6,86	1149	51.16	75.1	–49.9	23.21	21.11	-	(2)
86-578-6-6,107	1150	51.37	58.7	–54.6	45.49	44.66	36.70	(1)
86-578-6-7,3	1151	51.83	72.9	–55.8	42.78	40.16	-	(2)
86-578-6-7,23	1152	52.03	62.1	–45.7	27.16	25.45	19.75	(1)
86-578-6-7,43	1153	52.23	69.8	–56.5	26.53	24.31	-	(2)

86-578-7-1,19	1154	52.39	287.7	10.1	13.96	12.83	9.67	(1)
86-578-7-1,46	1155	52.66	300.9	–38.4	35.78	31.65	-	(2)
86-578-7-1,66	1156	52.86	299.4	–58.1	70.68	67.42	54.19	(1)
86-578-7-1,86	1157	53.06	298.0	–59.8	72.81	63.41	-	(2)
86-578-7-1,106	1158	53.26	281.1	–45.9	38.12	37.65	30.50	(1)
86-578-7-1,126	1159	53.46	298.2	–61.2	11.45	11.57	-	(2)
86-578-7-1,146	1160	53.66	121.8	49.6	36.63	31.82	27.66	(2)
86-578-7-2,6	1161	53.76	123.4	57.6	32.85	29.74	22.13	(2)
86-578-7-2,28	1162	53.98	262.5	–44.2	15.95	14.18	-	(2)
86-578-7-2,46	1163	54.16	114.1	46.6	39.48	36.96	-	(2)
86-578-7-2,66	1164	54.36	101.2	46.7	25.20	23.55	19.20	(1)
86-578-7-2,86	1165	54.56	133.3	46.8	68.29	58.82	-	(2)
86-578-7-2,106	1166	54.76	156.2	55.2	41.66	37.11	30.23	(1)
86-578-7-2,131	1167	55.01	121.7	48.5	53.17	44.89	-	(2)
86-578-7-2,146	1168	55.16	122.5	54.5	42.32	38.66	31.18	(1)
86-578-7-3,6	1169	55.26	115.8	45.5	42.55	35.19	-	(2)
86-578-7-3,26	1170	55.46	127.5	48.4	53.49	50.20	42.22	(1)
86-578-7-3,46	1171	55.66	129.1	46.0	42.65	36.46	-	(2)
86-578-7-3,66	1172	55.86	120.7	53.8	116.65	106.32	86.07	(1)
86-578-7-3,86	1173	56.06	122.1	58.4	67.92	69.68	-	(2)
86-578-7-3,106	1174	56.26	124.2	59.7	79.63	73.73	60.81	(1)
86-578-7-3,126	1175	56.46	124.5	58.0	63.72	53.30	-	(2)
86-578-7-3,146	1176	56.66	137.4	56.0	91.49	83.26	67.44	(1)
86-578-7-4,6	1177	56.76	142.9	56.6	82.32	76.65	-	(2)
86-578-7-4,26	1178	56.96	136.9	56.6	89.60	81.43	65.39	(1)
86-578-7-4,47	1179	57.17	140.0	52.3	51.54	40.50	-	(2)
86-578-7-4,66	1180	57.36	150.3	47.7	68.31	61.29	47.35	(1)
86-578-7-4,86	1181	57.56	147.6	58.2	80.95	76.38	-	(2)
86-578-7-4,106	1182	57.76	140.7	53.5	72.46	64.13	51.42	(1)
86-578-7-4,126	1183	57.96	160.3	49.5	26.98	21.58	-	(2)
86-578-7-4,146	1184	58.16	325.4	–56.0	23.40	27.15	-	(2)
86-578-7-5,6	1185	58.26	328.0	–54.7	34.87	38.19	-	(2)
86-578-7-5,26	1186	58.46	320.5	–51.7	64.38	70.34	62.70	(1)
86-578-7-5,46	1187	58.66	316.4	–78.0	11.87	19.23	18.21	(2)
86-578-7-5,66	1188	58.86	323.2	–56.2	50.57	54.86	45.76	(1)
86-578-7-5,86	1189	59.06	320.9	–48.5	62.15	67.44	-	(2)
86-578-7-5,106	1190	59.26	309.4	–50.2	49.18	52.59	45.14	(1)
86-578-7-5,126	1191	59.46	312.1	–55.8	62.57	64.26	-	(2)
86-578-7-5,146	1192	59.66	308.9	–55.6	65.05	69.32	61.69	(1)
86-578-7-6,6	1193	59.76	306.3	–46.0	45.63	46.33	-	(2)
86-578-7-6,25	1194	59.95	310.9	–46.5	54.64	56.34	47.01	(1)
86-578-7-6,45	1195	60.15	315.2	–47.9	51.23	51.66	-	(2)
86-578-7-6,66	1196	60.36	324.3	–47.1	47.58	50.40	43.69	(1)
86-578-7-6,86	1197	60.56	322.9	–47.2	46.69	52.63	-	(2)
86-578-7-6,106	1198	60.76	308.0	–49.6	47.09	47.53	39.91	(1)
86-578-7-6,126	1199	60.96	308.0	–49.6	41.98	42.82	-	(2)
86-578-7-6,146	1200	61.16	309.7	–47.9	61.58	61.22	47.96	(1)
86-578-7-7,11	1201	61.31	304.0	–57.9	53.80	53.43	-	(2)
86-578-7-7,46	1202	61.66	295.1	–58.8	46.57	46.97	-	(2)
86-578-8-1,26	1203	62.06	164.9	54.3	15.04	13.33	10.86	(2)
86-578-8-1,46	1204	62.26	314.5	–62.2	1.12	1.06	0.97	(2)
86-578-8-1,66	1205	62.46	271.5	41.7	12.02	10.35	-	(2)

86-578-8-1,87	1206	62.67	74.8	–58.7	0.75	0.66	-	(2)
86-578-8-1,92	1207	62.72	92.4	–50.0	1.92	1.87	-	(2)
86-578-8-1,111	1208	62.91	253.1	44.3	0.99	0.98	0.80	(1)
86-578-8-1,126	1209	63.06	80.6	–53.2	1.48	1.40	-	(2)
86-578-8-1,146	1210	63.26	89.8	–52.0	1.89	1.62	1.24	(1)
86-578-8-2,6	1211	63.36	72.9	–45.2	2.49	2.41	-	(2)
86-578-8-2,26	1212	63.56	77.7	–52.4	26.32	23.53	18.59	(1)
86-578-8-2,46	1213	63.76	60.9	–50.6	43.87	39.52	-	(2)
86-578-8-2,66	1214	63.96	76.4	–49.7	40.21	37.92	30.10	(1)
86-578-8-2,86	1215	64.16	64.4	–49.0	64.11	58.85	-	(2)
86-578-8-2,106	1216	64.36	65.7	–52.6	70.40	68.34	56.19	(1)
86-578-8-2,126	1217	64.56	54.0	–55.1	60.24	54.16	-	(2)
86-578-8-2,146	1218	64.76	106.7	–23.1	17.17	14.62	11.41	(1)
86-578-8-3,6	1219	64.86	68.0	–55.9	66.18	64.01	-	(2)
86-578-8-3,26	1220	65.06	60.0	–47.1	64.48	61.29	47.91	(1)
86-578-8-3,46	1221	65.26	64.4	–55.6	71.44	65.61	-	(2)
86-578-8-3,66	1222	65.46	76.0	–42.6	17.59	18.02	15.24	(1)
86-578-8-3,86	1223	65.66	65.1	–50.3	55.53	58.90	-	(2)
86-578-8-3,106	1224	65.86	59.9	–57.3	60.20	58.20	47.82	(1)
86-578-8-3,126	1225	66.06	64.7	–45.7	44.65	45.30	-	(2)
86-578-8-3,146	1226	66.26	68.2	–51.9	60.91	60.07	50.45	(1)
86-578-8-4,6	1227	66.36	48.4	–42.5	42.88	46.36	-	(2)
86-578-8-4,26	1228	66.56	53.1	–49.3	53.62	53.70	47.98	(1)
86-578-8-4,48	1229	66.78	51.8	–51.1	63.47	60.89	-	(2)
86-578-8-4,53	1230	66.83	40.3	–45.5	28.17	27.13	22.83	(1)
86-578-8-4,86	1231	67.16	59.4	–34.0	44.46	42.95	-	(2)
86-578-8-4,106	1232	67.36	59.3	–49.9	23.67	24.07	20.53	(1)
86-578-8-4,126	1233	67.56	63.5	–43.7	45.65	45.79	-	(2)
86-578-8-4,146	1234	67.76	79.7	–64.5	52.48	52.32	44.33	(1)
86-578-8-5,6	1235	67.86	61.2	–40.6	48.55	47.37	-	(2)
86-578-8-5,26	1236	68.06	66.5	–53.2	59.06	59.60	50.06	(1)
86-578-8-5,46	1237	68.26	69.9	–42.7	40.80	40.01	-	(2)
86-578-8-5,86	1239	68.66	73.3	–44.5	15.11	18.06	-	(2)
86-578-8-5,64	1238	68.84	74.8	–51.2	45.46	47.94	39.56	(1)
86-578-8-5,106	1240	68.86	80.7	–51.8	23.53	26.20	23.23	(1)
86-578-8-5,123	1241	69.03	77.7	–50.1	57.91	63.02	-	(2)
86-578-8-5,136	1242	69.16	74.9	–41.2	49.28	51.09	43.39	(1)
86-578-8-6,6	1243	69.36	82.3	–49.1	39.33	42.70	-	(2)
86-578-8-6,26	1244	69.56	80.1	–44.4	50.97	52.10	46.93	(1)
86-578-8-6,46	1245	69.76	73.2	–56.0	104.65	102.27	-	(2)
86-578-8-6,66	1246	69.96	69.5	–54.0	49.89	51.15	41.04	(1)
86-578-8-6,91	1247	70.21	83.4	–59.8	75.49	79.68	-	(2)
86-578-8-6,108	1248	70.38	73.1	–48.1	69.75	69.18	56.48	(1)
86-578-8-6,126	1249	70.56	75.0	–47.1	66.29	62.96	-	(2)
86-578-8-6,146	1250	70.76	69.2	–50.0	78.79	77.03	64.05	(1)
86-578-8-7,5	1251	70.85	75.4	–48.7	80.53	79.36	-	(2)
86-578-8-7,21	1252	71.01	64.7	–47.9	86.38	86.71	74.16	(1)
86-578-8-7,36	1253	71.16	87.8	–54.7	86.28	90.06	-	(2)
86-578-9-1,16	1254	71.46	63.6	–53.6	1.12	1.47	1.37	(1)
86-578-9-1,31	1255	71.61	77.0	–42.5	16.02	17.23	-	(2)
86-578-9-1,46	1256	71.76	73.6	–49.6	56.99	57.14	49.78	(1)
86-578-9-1,66	1257	71.96	60.8	–56.0	40.17	45.08	-	(2)

86-578-9-1,86	1258	72.16	67.1	31.8	56.89	62.37	44.74	(2)
86-578-9-1,106	1259	72.36	71.0	–42.4	61.36	62.31	-	(2)
86-578-9-1,126	1260	72.56	57.6	–45.2	15.12	19.30	-	(2)
86-578-9-2,146	1261	72.76	249.2	49.6	44.25	37.95	25.55	(2)
86-578-9-2,6	1262	72.86	58.2	44.2	50.53	46.77	36.25	(1)
86-578-9-2,26	1263	73.06	61.1	48.3	75.38	71.55	-	(2)
86-578-9-2,46	1264	73.26	53.8	55.4	41.98	36.25	27.85	(1)
86-578-9-2,67	1265	73.47	49.0	55.2	62.44	53.27	-	(2)
86-578-9-2,86	1266	73.86	62.3	48.5	78.03	69.84	55.38	(1)
86-578-9-2,106	1267	73.86	77.7	60.8	38.21	35.32	-	(2)
86-578-9-2,126	1268	74.06	60.3	36.6	47.62	43.56	35.17	(1)
86-578-9-2,146	1269	74.26	61.0	48.8	100.99	80.29	-	(2)
86-578-9-3,6	1270	74.36	109.5	46.4	88.84	83.33	68.98	(1)
86-578-9-3,26	1271	74.56	112.1	42.4	86.63	81.72	-	(2)
86-578-9-3,46	1272	74.76	109.9	41.8	66.51	60.91	51.41	(1)
86-578-9-3,66	1273	74.96	98.7	48.8	49.96	40.38	-	(2)
86-578-9-3,86	1274	75.16	112.0	50.6	75.82	71.21	60.56	(1)
86-578-9-3,106	1275	75.36	103.7	37.0	67.87	62.01	-	(2)
86-578-9-3,126	1276	75.56	111.2	38.9	73.44	66.43	56.08	(1)
86-578-9-3,146	1277	75.76	116.7	44.7	15.79	12.11	9.40	(2)
86-578-9-4,6	1278	75.96	305.8	55.3	42.51	39.40	32.51	(1)
86-578-9-4,26	1279	76.06	297.3	49.9	108.59	105.73	-	(2)
86-578-9-4,46	1280	76.36	304.0	51.2	82.19	77.92	68.03	(1)
86-578-9-4,66	1281	76.46	311.7	40.7	76.33	67.69	54.98	(2)
86-578-9-4,86	1282	76.66	306.4	45.9	107.74	96.45	73.71	(1)
86-578-9-4,106	1283	76.86	312.8	48.2	69.43	57.88	-	(2)
86-578-9-4,126	1284	77.06	323.1	51.0	91.62	84.24	68.11	(1)
86-578-9-4,146	1285	77.26	313.5	49.9	56.20	48.88	-	(2)
86-578-9-5,6	1286	77.46	314.7	50.5	135.35	116.03	88.54	(1)
86-578-9-5,25	1287	77.55	326.5	52.6	116.12	103.96	-	(2)
86-578-9-5,46	1288	77.76	314.2	47.5	88.67	80.05	62.90	(1)
86-578-9-5,66	1289	77.96	321.6	56.9	70.50	53.30	-	(2)
86-578-9-5,83	1290	78.13	320.8	49.1	81.46	74.46	60.64	(1)
86-578-9-5,100	1291	78.30	333.6	50.9	85.89	71.22	-	(2)
86-578-9-5,116	1292	78.46	311.6	50.9	95.90	87.54	67.92	(1)
86-578-9-6,6	1293	78.86	316.2	46.6	67.91	60.92	-	(2)
86-578-9-6,26	1294	79.06	317.3	48.4	44.04	39.34	30.64	(1)
86-578-9-6,46	1295	79.26	315.2	54.2	55.98	53.25	-	(2)
86-578-9-6,66	1296	79.46	315.7	46.4	105.38	95.13	74.09	(1)
86-578-9-6,86	1297	79.66	325.4	54.1	55.60	47.29	-	(2)
86-578-9-6,106	1298	79.86	328.3	51.0	55.30	50.69	39.79	(1)
86-578-9-6,126	1299	80.06	340.0	48.1	83.41	74.01	-	(2)
86-578-9-6,146	1300	80.26	325.6	52.8	112.86	103.67	82.02	(1)
86-578-9-7,6	1301	80.36	336.1	50.4	81.54	73.87	-	(2)
86-578-9-7,26	1302	80.56	305.4	59.3	15.81	10.61	-	(2)
86-578-9-7,48	1303	80.78	140.9	–42.2	11.82	11.74	9.74	(2)
86-578-10-1,28	1304	81.08	30.9	55.3	49.43	43.07	-	(2)
86-578-10-1,46	1305	81.26	33.6	37.7	39.78	36.66	-	(2)
86-578-10-1,78	1306	81.58	234.6	–45.9	68.01	70.09	-	(2)
86-578-10-1,96	1307	81.76	221.2	–36.7	27.74	31.39	-	(2)
86-578-10-1,114	1308	81.94	227.5	–35.1	51.97	51.41	41.91	(1)
86-578-10-1,130	1309	82.10	222.7	–45.0	57.19	60.44	-	(2)

86-578-10-1,146	1310	82.26	217.0	–49.1	51.44	51.10	-	(2)
86-578-10-2,6	1311	82.36	195.5	–43.1	35.38	35.61	-	(2)
86-578-10-2,24	1312	82.54	10.6	47.7	43.38	37.61	-	(2)
86-578-10-2,46	1313	82.76	10.6	44.6	84.54	64.20	-	(2)
86-578-10-2,66	1314	82.96	17.2	41.0	74.24	68.45	52.86	(1)
86-578-10-2,86	1315	83.16	8.0	52.3	74.06	67.96	-	(2)
86-578-10-2,106	1316	83.36	14.4	50.0	97.81	91.17	72.29	(1)
86-578-10-2,126	1317	83.56	18.8	49.6	49.81	40.10	-	(2)
86-578-10-2,146	1318	83.76	182.9	–52.8	17.45	26.62	-	(2)
86-578-10-3,6	1319	83.86	179.9	–45.1	40.50	40.79	-	(2)
86-578-10-3,26	1320	84.06	171.4	–55.9	58.85	57.76	47.74	(1)
86-578-10-3,46	1321	84.26	176.4	–38.0	32.14	31.43	-	(2)
86-578-10-3,66	1322	84.46	182.4	–51.2	63.67	59.88	47.64	(1)
86-578-10-3,86	1323	84.66	178.1	–42.1	76.31	69.28	-	(2)
86-578-10-3,106	1324	84.86	170.4	–46.8	15.47	17.33	-	(2)
86-578-10-3,126	1325	85.06	353.6	53.7	66.84	60.42	-	(2)
86-578-10-3,146	1326	85.26	0.8	50.1	55.29	50.18	38.68	(1)
86-578-10-4,6	1327	85.36	298.9	45.4	44.72	33.56	-	(2)
86-578-10-4,26	1328	85.56	316.9	49.3	68.81	61.98	48.29	(1)
86-578-10-4,46	1329	85.76	310.9	47.6	63.09	54.94	-	(2)
86-578-10-4,66	1330	85.96	305.0	48.2	56.52	50.61	38.13	(1)
86-578-10-4,86	1331	86.16	318.4	49.7	67.50	56.54	-	(2)
86-578-10-4,106	1332	86.46	316.2	49.8	70.21	63.26	49.88	(1)
86-578-10-4,126	1333	86.56	306.9	45.5	60.16	47.13	-	(2)
86-578-10-4,146	1334	86.76	315.9	44.8	60.28	52.87	41.38	(1)
86-578-10-5,6	1335	86.86	296.7	43.6	68.61	58.20	-	(2)
86-578-10-5,26	1336	87.06	301.0	44.8	58.73	51.98	40.97	(1)
86-578-10-5,46	1337	87.26	294.0	45.5	59.62	51.66	-	(2)
86-578-10-5,66	1338	87.46	293.9	45.0	20.63	14.87	-	(2)
86-578-10-5,86	1339	87.66	123.0	–43.6	37.24	37.65	-	(2)
86-578-10-5,106	1340	87.86	107.6	–45.8	52.25	49.65	-	(2)
86-578-10-5,126	1341	88.06	107.6	–45.5	39.14	41.85	-	(2)
86-578-10-5,146	1342	88.26	94.0	–49.3	52.05	50.45	40.25	(1)
86-578-10-6,6	1343	88.36	76.1	–47.4	50.16	47.99	-	(2)
86-578-10-6,26	1344	88.56	69.9	–34.3	25.78	28.67	23.63	(1)
86-578-10-6,46	1345	88.76	63.5	–40.7	39.57	45.88	-	(2)
86-578-10-6,66	1346	88.96	59.7	–50.0	55.05	56.35	46.03	(1)
86-578-10-6,86	1347	89.16	61.8	–36.9	41.67	46.65	-	(2)
86-578-11-1,6	1348	90.36	199.5	–50.2	45.73	41.94	33.26	(1)
86-578-11-1,26	1349	90.56	199.2	–53.8	60.15	58.68	-	(2)
86-578-11-1,46	1350	90.76	183.4	–49.0	94.61	89.01	70.72	(1)
86-578-11-1,66	1351	90.96	196.3	–54.5	53.62	56.84	-	(2)
86-578-11-1,86	1352	91.16	201.6	–38.7	42.62	41.58	32.06	(1)
86-578-11-1,106	1353	91.36	195.6	–51.7	50.78	51.96	-	(2)
86-578-11-1,126	1354	91.56	198.8	–47.6	55.60	52.33	41.68	(1)
86-578-11-1,143	1355	91.76	191.5	–48.7	25.99	27.94	-	(2)
86-578-11-2,6	1356	91.86	207.8	–46.6	55.43	53.68	42.08	(1)
86-578-11-2,26	1357	92.06	196.3	–50.7	25.44	25.01	-	(2)
86-578-11-2,46	1358	92.26	200.1	–50.8	42.41	39.71	31.33	(1)
86-578-11-2,66	1359	92.46	197.8	–33.3	35.02	33.62	-	(2)
86-578-11-2,86	1360	92.56	205.0	–51.7	48.96	46.13	35.59	(1)
86-578-11-2,106	1361	92.86	199.8	–44.5	46.65	49.71	-	(2)

86-578-11-2,126	1362	93.06	202.5	–42.3	49.92	46.76	36.99	(1)
86-578-11-2,146	1363	93.26	202.6	–58.3	45.04	48.17	-	(2)
86-578-11-3,6	1364	93.36	225.0	–53.0	31.67	33.90	-	(2)
86-578-11-3,26	1365	93.56	25.6	54.6	49.16	39.87	-	(2)
86-578-11-3,46	1366	93.76	55.8	54.8	23.63	20.45	16.16	(1)
86-578-11-3,66	1367	93.96	21.7	46.5	42.20	35.02	-	(2)
86-578-11-3,86	1368	94.16	23.2	53.1	28.37	25.15	19.54	(1)
86-578-11-3,106	1369	94.36	16.8	46.7	63.59	58.31	-	(2)
86-578-11-3,126	1370	94.56	14.4	53.5	37.33	31.20	-	(2)
86-578-11-3,146	1371	94.76	199.9	–28.7	6.26	7.83	-	(2)
86-578-11-4,6	1372	94.96	201.0	–48.7	11.84	11.85	9.00	(1)
86-578-11-4,26	1373	95.06	204.8	–47.3	40.83	43.64	-	(2)
86-578-11-4,46	1374	95.26	202.5	–49.1	30.98	28.89	23.68	(1)
86-578-11-4,66	1375	95.46	210.2	–42.0	25.94	26.78	-	(2)
86-578-11-4,86	1376	95.66	205.5	–47.6	27.28	25.94	19.99	(1)
86-578-11-4,106	1377	95.86	207.8	–51.9	23.29	24.67	-	(2)
86-578-11-4,126	1378	95.96	202.9	–52.0	29.55	27.29	21.20	(1)
86-578-11-4,146	1379	96.26	198.9	–51.7	29.65	31.23	-	(2)
86-578-11-5,6	1380	96.36	196.1	–56.8	8.61	10.54	-	(2)
86-578-11-5,26	1381	96.56	42.1	51.1	26.45	21.01	-	(2)
86-578-11-5,46	1382	96.76	34.5	46.0	42.42	37.87	28.78	(1)
86-578-11-5,66	1383	96.96	42.3	47.2	35.62	29.86	-	(2)
86-578-11-5,80	1384	97.10	33.8	51.1	45.27	40.43	29.82	(1)
86-578-11-5,97	1385	97.27	41.3	48.8	41.41	34.15	-	(2)
86-578-11-5,116	1386	97.46	85.0	4.0	8.05	3.72	1.75	(2)
86-578-11-5,134	1387	97.64	207.1	–48.4	42.31	42.79	-	(2)
86-578-11-6,6	1388	97.86	223.4	–59.4	27.45	26.50	21.25	(1)
86-578-11-6,26	1389	98.06	228.3	–52.9	29.45	32.19	-	(2)
86-578-11-6,46	1390	98.26	229.7	–48.1	37.83	35.54	28.66	(1)
86-578-11-6,66	1391	98.46	227.5	–41.9	32.02	32.41	-	(2)
86-578-11-6,86	1392	98.66	230.9	–44.9	53.15	49.16	38.60	(1)
86-578-11-6,106	1393	98.86	225.3	–46.9	46.96	42.46	-	(2)
86-578-11-6,126	1394	99.06	216.5	–44.0	26.80	25.54	-	(2)
86-578-11-6,146	1395	99.26	45.0	56.4	34.65	26.12	-	(2)
86-578-11-7,6	1396	99.36	46.2	50.1	17.23	14.05	10.43	(1)
86-578-11-7,21	1397	99.51	44.1	44.7	46.94	39.83	-	(2)
86-578-12-1,76	1398	99.93	150.6	46.7	42.79	36.32	27.06	(1)
86-578-12-1,96	1399	100.04	159.5	31.7	37.09	31.11	-	(2)
86-578-12-1,116	1400	100.33	154.2	41.9	38.98	32.15	24.08	(1)
86-578-12-1,146	1401	100.54	144.6	35.9	19.00	14.76	-	(2)
86-578-12-2,4	1402	100.62	168.7	27.6	6.67	4.93	3.30	(2)
86-578-12-2,34	1403	100.92	306.3	–27.0	32.46	37.97	28.29	(2)
86-578-12-2,51	1404	101.09	304.4	–49.2	35.13	39.05	33.33	(1)
86-578-12-2,67	1405	101.25	311.0	–22.0	8.69	7.19	7.83	(2)
86-578-12-2,86	1406	101.44	313.3	–51.8	46.20	49.31	39.93	(1)
86-578-12-2,106	1407	101.64	313.8	–48.9	28.26	32.13	-	(2)
86-578-12-2,126	1408	101.84	142.1	54.7	39.17	29.85	-	(2)
86-578-12-2,146	1409	102.04	141.8	47.2	56.24	44.47	-	(2)
86-578-12-3,6	1410	102.14	125.4	48.4	52.05	43.14	32.93	(1)
86-578-12-3,26	1411	102.34	132.6	48.8	48.37	40.22	-	(2)
86-578-12-3,46	1412	102.54	136.4	46.5	49.67	40.62	31.09	(1)
86-578-12-3,66	1413	102.74	136.1	49.7	47.37	35.80	-	(2)

86-578-12-3,86	1414	102.94	129.3	49.0	47.69	39.04	30.29	(1)
86-578-12-3,111	1415	103.19	138.5	51.9	47.42	35.98	-	(2)
86-578-12-4,6	1416	103.64	144.8	44.1	21.73	10.56	-	(2)
86-578-12-4,26	1417	103.84	313.1	–50.9	21.52	27.01	-	(2)
86-578-12-4,46	1418	104.04	320.9	–49.0	27.04	29.91	25.20	(1)
86-578-12-4,66	1419	104.24	326.6	–38.0	20.76	24.13	-	(2)
86-578-12-4,86	1420	104.44	315.6	–51.2	25.15	28.58	22.70	(1)
86-578-12-4,106	1421	104.64	306.6	–57.5	16.31	21.27	-	(2)
86-578-12-4,126	1422	104.84	309.1	–52.2	25.86	26.99	20.73	(1)
86-578-12-4,146	1423	105.04	313.3	–48.9	23.02	25.13	-	(2)
86-578-12-5,6	1424	105.14	302.1	–49.6	28.62	29.74	22.95	(1)
86-578-12-5,26	1425	105.34	309.9	–44.4	19.29	22.99	-	(2)
86-578-12-5,46	1426	105.54	322.9	–50.1	18.18	19.66	15.67	(1)
86-578-12-5,66	1427	105.74	319.9	–51.0	28.65	32.27	-	(2)
86-578-12-5,86	1428	105.94	310.0	–47.0	25.32	27.08	20.99	(1)
86-578-12-5,106	1429	106.14	315.8	–31.3	12.19	16.74	-	(2)
86-578-12-5,126	1430	106.34	294.9	–44.3	24.72	25.99	21.14	(1)
86-578-12-5,146	1431	106.54	307.1	–43.9	19.68	22.28	-	(2)
86-578-12-6,66	1432	107.24	301.9	–49.9	20.08	21.65	16.79	(1)
86-578-12-6,86	1433	107.44	289.0	–51.9	21.39	23.17	-	(2)
86-578-12-6,106	1434	107.64	267.0	–24.5	27.75	27.07	20.68	(1)
86-578-12-6,123	1435	107.81	274.2	–51.0	15.86	17.49	-	(2)
86-578-12-6,140	1436	107.98	267.3	–44.0	23.76	23.48	17.86	(1)
86-578-13-1,26	1437	109.56	352.5	–49.1	8.24	12.39	-	(2)
86-578-13-1,46	1438	109.76	158.9	47.9	33.11	25.97	-	(2)
86-578-13-1,66	1439	109.96	167.9	49.2	35.35	27.80	-	(2)
86-578-13-1,86	1440	110.16	163.7	52.4	45.64	34.70	-	(2)
86-578-13-1,106	1441	110.36	156.0	47.7	25.97	17.77	-	(2)
86-578-13-1,126	1442	110.56	160.8	39.5	31.00	22.18	-	(2)
86-578-13-1,146	1443	110.76	168.9	58.8	14.94	9.17	-	(2)
86-578-13-2,6	1444	110.86	154.1	36.4	20.60	15.34	-	(2)
86-578-13-2,26	1445	111.06	160.0	46.6	30.59	23.51	-	(2)
86-578-13-2,46	1446	111.26	165.1	44.7	39.59	27.61	-	(2)
86-578-13-2,66	1447	111.46	166.5	44.4	32.94	25.47	-	(2)
86-578-13-2,86	1448	111.66	159.3	45.8	34.18	27.15	-	(2)
86-578-13-2,106	1449	111.86	172.0	–60.0	7.37	1.52	0.97	(2)
86-578-13-2,126	1450	112.06	340.3	–50.7	10.65	14.48	-	(2)
86-578-13-2,146	1451	112.26	7.5	–48.5	19.68	21.73	-	(2)
86-578-13-3,6	1452	112.36	340.1	–44.1	12.94	15.16	-	(2)
86-578-13-3,26	1453	112.56	3.4	–33.1	1.42	3.57	3.59	(2)
86-578-13-3,46	1454	112.76	351.2	–43.5	14.49	17.11	-	(2)
86-578-13-3,66	1455	112.96	356.4	–33.1	9.72	16.08	-	(2)
86-578-13-3,86	1456	113.16	358.2	–46.8	11.85	14.65	-	(2)
86-578-13-3,106	1457	113.36	176.8	32.2	17.70	9.77	-	(2)
86-578-13-3,126	1458	113.56	187.4	44.2	29.36	19.79	-	(2)
86-578-13-3,146	1459	113.76	192.0	46.7	36.60	24.97	-	(2)
86-578-13-4,6	1460	113.86	203.9	50.6	35.11	25.31	-	(2)
86-578-13-4,26	1461	114.06	196.2	44.9	28.04	20.18	-	(2)
86-578-13-4,46	1462	114.26	162.2	–40.5	40.35	31.89	-	(2)
86-578-13-4,66	1463	114.46	208.1	39.6	19.56	15.05	-	(2)
86-578-13-4,86	1464	114.66	13.0	15.0	4.20	3.24	-	(2)
86-578-13-4,106	1465	114.86	212.4	47.3	34.81	23.37	-	(2)

86-578-13-4,126	1466	115.06	210.6	44.5	23.80	17.55	-	(2)
86-578-13-4,146	1467	115.26	212.7	48.5	27.96	19.77	-	(2)
86-578-13-5,6	1468	115.36	210.0	46.3	41.90	31.83	-	(2)
86-578-13-5,26	1469	115.56	213.9	49.0	29.37	21.02	-	(2)
86-578-13-5,46	1470	115.76	211.8	41.4	28.36	19.05	-	(2)
86-578-13-5,66	1471	115.96	56.0	64.0	8.75	2.18	1.76	(2)
86-578-13-5,86	1472	116.16	35.4	–42.9	13.54	18.16	-	(2)
86-578-13-5,106	1473	116.36	29.8	–43.7	17.29	24.30	-	(2)
86-578-13-5,126	1474	116.56	31.7	–44.6	17.40	22.17	-	(2)
86-578-13-5,146	1475	116.76	24.3	–38.9	15.43	19.15	-	(2)
86-578-13-6,6	1476	116.86	26.6	–33.8	15.14	18.52	-	(2)
86-578-13-6,26	1477	117.06	27.7	–41.4	17.92	23.64	-	(2)
86-578-13-6,46	1478	117.26	29.6	–44.8	25.48	28.66	-	(2)
86-578-13-6,66	1479	117.46	29.5	–43.9	18.07	23.76	-	(2)
86-578-13-6,86	1480	117.66	29.7	–48.6	13.85	17.80	-	(2)
86-578-13-6,106	1481	117.86	15.8	–44.1	14.04	22.64	-	(2)
86-578-13-6,126	1482	118.06	173.0	–9.7	2.59	5.18	-	(2)
86-578-13-6,146	1483	118.26	28.5	–38.5	19.24	28.46	-	(2)
86-578-13-7,6	1484	118.36	26.7	–47.0	13.12	17.08	-	(2)
86-578-13-7,26	1485	118.56	21.6	–47.8	12.00	19.36	-	(2)
86-578-14-1,31	1486	118.66	188.5	52.7	25.33	17.23	-	(2)
86-578-14-1,56	1487	118.91	245.7	40.6	46.24	34.75	-	(2)
86-578-14-1,86	1488	119.21	36.3	–59.6	8.27	12.64	-	(2)
86-578-14-1,106	1489	119.41	216.7	45.7	40.58	27.65	-	(2)
86-578-14-1,146	1490	119.81	36.9	–54.2	1.46	7.05	5.39	(2)
86-578-14-2,6	1491	119.91	39.0	–49.5	13.04	20.80	-	(2)
86-578-14-2,26	1492	120.11	32.5	–46.0	9.75	14.74	-	(2)
86-578-14-2,46	1493	120.31	34.9	–47.4	12.31	19.18	-	(2)
86-578-14-2,66	1494	120.51	235.2	49.9	21.19	11.94	-	(2)
86-578-14-2,86	1495	120.71	207.0	53.9	14.77	7.28	-	(2)
86-578-14-2,106	1496	120.91	31.0	–46.9	9.36	13.69	-	(2)
86-578-14-2,126	1497	121.11	210.2	50.1	25.54	14.93	-	(2)
86-578-14-2,146	1498	121.31	208.1	47.5	34.86	24.17	-	(2)
86-578-14-3,6	1499	121.41	214.5	43.5	41.12	26.63	-	(2)
86-578-14-3,26	1500	121.61	21.1	–44.7	3.14	8.15	-	(2)
86-578-14-3,46	1501	121.81	214.3	45.3	15.90	7.08	-	(2)
86-578-14-3,66	1502	122.01	216.3	48.0	23.41	14.42	-	(2)
86-578-14-3,86	1503	122.21	220.7	45.7	36.61	23.73	-	(2)
86-578-14-3,106	1504	122.41	209.1	48.0	51.63	40.87	-	(2)
86-578-14-3,126	1505	122.61	217.5	45.1	51.22	33.40	-	(2)
86-578-14-3,146	1506	122.81	216.7	49.3	40.75	26.51	-	(2)
86-578-14-4,6	1507	122.91	220.1	40.1	43.12	31.29	-	(2)
86-578-14-4,26	1508	123.11	213.0	46.9	39.00	30.51	-	(2)
86-578-14-4,46	1509	123.31	205.8	46.5	36.78	21.83	-	(2)
86-578-14-4,66	1510	123.51	211.1	36.7	31.44	22.71	-	(2)
86-578-14-4,86	1511	123.71	210.3	42.3	41.21	28.22	-	(2)
86-578-14-4,106	1512	123.91	31.5	–50.8	7.91	14.85	-	(2)
86-578-14-4,126	1513	124.11	23.1	–47.0	6.01	6.31	-	(2)
86-578-14-4,146	1514	124.31	8.0	–43.0	23.24	2.95	-	(2)
86-578-14-5,6	1515	124.41	238.4	74.4	35.02	10.38	-	(2)
86-578-14-5,26	1516	124.61	200.1	41.8	35.47	20.18	-	(2)
86-578-14-5,46	1517	124.81	23.8	–40.0	23.95	31.57	-	(2)

86-578-14-5,66	1518	125.01	23.9	–41.0	16.98	22.28	-	(2)
86-578-14-5,86	1519	125.21	28.0	–41.0	23.09	31.41	-	(2)
86-578-14-5,106	1520	125.41	21.3	–40.7	29.72	34.48	-	(2)
86-578-14-5,126	1521	125.61	20.7	–42.9	25.32	31.61	-	(2)
86-578-14-5,146	1522	125.81	17.5	–46.3	29.50	35.79	-	(2)
86-578-14-6,6	1523	125.91	17.6	–39.3	27.63	33.40	-	(2)
86-578-14-6,26	1524	126.11	176.7	45.6	17.97	9.23	-	(2)
86-578-14-6,46	1525	126.31	15.2	–34.9	12.06	21.11	-	(2)
86-578-14-6,66	1526	126.51	196.8	53.0	52.47	33.29	-	(2)
86-578-14-6,86	1527	126.71	200.6	44.2	63.67	41.45	-	(2)
86-578-14-6,106	1528	126.91	200.1	42.5	54.89	35.69	-	(2)
86-578-14-6,126	1529	127.11	203.0	44.6	48.76	31.62	-	(2)
86-578-14-6,138	1530	127.23	196.5	48.4	47.90	28.92	-	(2)
86-578-14-7,6	1531	127.41	350.7	–25.7	9.53	4.19	-	(2)
86-578-14-7,26	1532	127.61	30.5	–37.7	10.18	2.03	-	(2)
86-578-14-7,44	1533	127.79	242.1	46.6	16.44	2.30	-	(2)
86-578-15-1,44	1538	128.44	10.3	35.1	30.02	15.02	-	(2)
86-578-15-1,66	1539	128.66	11.5	50.4	27.63	18.18	-	(2)
86-578-15-1,86	1540	128.86	5.3	45.7	37.03	21.56	-	(2)
86-578-15-1,108	1541	129.08	6.0	47.6	45.06	30.42	-	(2)
86-578-15-1,126	1542	129.26	8.3	37.6	30.70	18.80	-	(2)
86-578-15-1,146	1543	129.46	7.3	43.6	25.48	16.46	-	(2)
86-578-15-2,6	1544	129.56	17.6	45.2	37.06	23.95	-	(2)
86-578-15-2,26	1545	129.76	20.7	40.3	35.96	20.36	-	(2)
86-578-15-2,46	1546	129.96	17.1	43.0	56.65	35.19	-	(2)
86-578-15-2,66	1547	130.16	22.0	44.2	31.96	20.53	-	(2)
86-578-15-2,86	1548	130.36	24.6	43.0	33.78	19.33	-	(2)
86-578-15-2,106	1549	130.56	30.1	38.9	34.28	21.87	-	(2)
86-578-15-2,126	1550	130.76	18.4	43.0	42.59	25.85	-	(2)
86-578-15-2,146	1551	130.96	28.3	43.0	46.67	35.79	-	(2)
86-578-15-3,6	1552	131.06	215.5	–39.6	9.44	13.92	-	(2)
86-578-15-3,26	1553	131.26	215.1	–44.8	30.01	34.88	-	(2)
86-578-15-3,46	1554	131.46	39.4	39.4	43.76	32.94	-	(2)
86-578-15-3,66	1555	131.66	224.2	–42.1	12.35	15.92	-	(2)
86-578-15-3,86	1556	131.86	42.0	45.1	21.21	10.63	-	(2)
86-578-15-3,106	1557	132.06	229.1	–38.0	4.95	10.14	-	(2)
86-578-15-3,126	1558	132.26	223.3	–39.2	6.90	12.48	-	(2)
86-578-15-3,146	1559	132.46	219.8	–46.7	23.87	28.87	-	(2)
86-578-15-4,6	1560	132.56	226.4	–46.3	16.05	16.57	-	(2)
86-578-15-4,26	1561	132.76	227.7	–46.2	14.56	18.03	-	(2)
86-578-15-4,46	1562	132.96	54.1	46.6	31.37	20.54	-	(2)
86-578-15-4,66	1563	133.16	188.9	–35.3	7.43	1.53	-	(2)
86-578-15-4,86	1564	133.36	246.3	–41.5	3.97	11.67	-	(2)
86-578-15-4,106	1565	133.56	230.7	–42.0	14.75	20.04	-	(2)
86-578-15-4,126	1566	133.76	243.4	–35.7	8.42	14.91	-	(2)
86-578-15-4,146	1567	133.96	235.7	–38.8	7.60	11.91	-	(2)
86-578-15-5,6	1568	134.06	243.5	–41.2	16.56	22.28	-	(2)
86-578-15-5,26	1569	134.26	243.8	–38.5	17.89	23.33	-	(2)
86-578-15-5,46	1570	134.46	64.2	47.1	29.98	16.30	-	(2)
86-578-15-5,66	1571	134.66	68.3	48.0	36.57	22.74	-	(2)
86-578-15-5,84	1572	134.84	258.3	–36.4	4.66	3.50	-	(2)
86-578-15-5,100	1573	135.00	247.7	–45.7	12.32	17.37	-	(2)

86-578-15-5,116	1574	135.16	70.3	42.2	17.40	6.58	-	(2)
86-578-15-6,6	1575	135.56	71.8	42.6	40.46	29.43	-	(2)
86-578-15-6,26	1576	135.76	109.0	13.0	11.44	3.18	-	(2)
86-578-15-6,46	1577	135.96	240.9	–41.9	7.02	9.21	-	(2)
86-578-15-6,66	1578	136.16	253.7	–47.8	12.24	18.10	-	(2)
86-578-15-6,86	1579	136.36	202.1	–70.5	10.65	13.99	-	(2)
86-578-15-6,106	1580	136.56	248.8	–42.6	11.01	18.88	-	(2)
86-578-15-6,116	1581	136.66	73.5	50.5	22.54	14.06	-	(2)
86-578-15-6,146	1582	136.96	253.8	–30.4	7.92	12.59	-	(2)
86-578-15-7,6	1583	137.06	249.7	–38.5	7.29	11.48	-	(2)
86-578-15-7,26	1584	137.26	64.5	42.6	31.10	18.72	-	(2)
86-578-15-7,45	1585	137.45	136.9	–72.0	8.06	4.33	-	(2)
86-578-16-1,36	1586	138.11	174.7	–58.0	20.41	19.81	-	(2)
86-578-16-1,56	1587	138.31	179.5	–69.2	19.41	21.04	-	(2)
86-578-16-1,136	1591	139.11	126.5	–36.3	4.59	11.84	-	(2)
86-578-16-2,6	1592	139.31	129.8	–41.3	8.43	10.75	-	(2)
86-578-16-2,26	1593	139.51	310.3	41.9	32.45	17.46	-	(2)
86-578-16-2,46	1594	139.71	305.6	35.1	18.81	6.76	-	(2)
86-578-16-2,66	1595	139.91	311.1	47.1	23.91	14.21	-	(2)
86-578-16-2,86	1596	140.11	116.0	–34.0	5.89	13.42	-	(2)
86-578-16-2,106	1597	140.31	115.2	–39.4	1.06	9.29	-	(2)
86-578-16-2,126	1598	140.51	121.5	–38.5	7.17	6.42	-	(2)
86-578-16-2,146	1599	140.71	306.5	38.4	24.29	13.01	-	(2)
86-578-16-3,6	1600	140.81	292.1	48.2	32.54	18.82	-	(2)
86-578-16-3,26	1601	141.01	299.6	52.0	26.97	17.07	-	(2)
86-578-16-3,46	1602	141.21	295.6	44.3	31.04	16.57	-	(2)
86-578-16-3,66	1603	141.41	299.0	42.6	29.20	16.14	-	(2)
86-578-16-3,86	1604	141.61	298.6	47.6	30.69	16.72	-	(2)
86-578-16-3,106	1605	141.81	118.3	–40.3	4.67	7.21	-	(2)
86-578-16-3,126	1606	142.01	294.7	54.3	20.12	7.35	-	(2)
86-578-16-3,146	1607	142.21	303.5	48.6	34.31	19.78	-	(2)
86-578-16-4,6	1608	142.31	288.3	56.8	38.91	19.45	-	(2)
86-578-16-4,26	1609	142.51	295.4	49.3	25.88	14.19	-	(2)
86-578-16-4,46	1610	142.71	301.5	51.5	33.67	12.91	-	(2)
86-578-16-4,66	1611	142.91	304.4	47.2	18.54	8.91	-	(2)
86-578-16-4,86	1612	143.11	304.8	52.7	34.82	23.41	-	(2)
86-578-16-4,106	1613	143.31	306.8	55.1	24.79	13.43	-	(2)
86-578-16-4,126	1614	143.51	112.9	–52.1	7.81	15.19	-	(2)
86-578-16-4,146	1615	143.71	120.7	–47.6	5.04	10.95	-	(2)
86-578-16-5,6	1616	143.81	122.2	–38.9	3.31	7.87	-	(2)
86-578-16-5,26	1617	144.01	108.0	–51.1	7.53	13.89	-	(2)
86-578-16-5,46	1618	144.21	297.0	58.4	41.91	17.92	-	(2)
86-578-16-5,66	1619	144.41	120.3	–50.8	9.07	5.16	-	(2)
86-578-16-5,86	1620	144.61	264.4	53.1	39.41	18.85	-	(2)
86-578-16-5,106	1621	144.81	294.7	53.8	31.71	18.77	-	(2)
86-578-16-5,126	1622	145.01	90.0	–55.8	9.10	1.78	-	(2)
86-578-16-5,146	1623	145.21	100.8	–55.8	3.76	13.19	-	(2)
86-578-16-6,7	1624	145.32	97.0	–53.1	2.97	11.94	-	(2)
86-578-16-6,21	1625	145.46	120.1	–54.9	3.11	8.72	-	(2)
86-578-17-1,32	1626	147.34	11.1	–27.4	5.59	11.71	-	(2)
86-578-17-1,48	1627	147.50	8.0	–34.8	3.51	13.55	-	(2)
86-578-17-1,67	1628	147.69	358.0	–26.6	-	5.88	-	(2)

86-578-17-1,86	1629	147.88	188.7	41.0	28.75	8.84	-	(2)
86-578-17-1,106	1630	148.08	188.2	32.0	35.65	11.42	-	(2)
86-578-17-1,126	1631	148.28	189.5	35.0	31.24	13.10	-	(2)
86-578-17-1,146	1632	148.48	8.2	–23.0	15.19	3.25	-	(2)
86-578-17-2,11	1633	148.63	28.3	–23.3	14.30	4.90	-	(2)
86-578-17-2,43	1634	148.95	207.8	40.8	25.91	7.43	-	(2)
86-578-17-2,55	1635	149.07	209.0	33.1	33.34	12.51	-	(2)
86-578-17-2,71	1636	149.23	209.3	33.7	29.36	7.85	-	(2)
86-578-17-2,86	1637	149.38	211.7	31.4	34.46	13.32	-	(2)
86-578-17-2,106	1638	149.58	216.0	31.6	31.00	8.91	-	(2)
86-578-17-2,116	1639	149.78	212.9	36.1	26.74	7.60	-	(2)
86-578-17-2,146	1640	149.98	23.8	–37.2	13.04	4.40	-	(2)
86-578-17-3,6	1641	150.08	35.1	–4.1	15.32	2.21	-	(2)
86-578-17-3,26	1642	150.28	35.5	–26.1	9.14	4.80	-	(2)
86-578-17-3,46	1643	150.48	222.8	39.2	25.01	7.12	-	(2)
86-578-17-3,66	1644	150.68	223.6	69.1	25.10	1.94	-	(2)
86-578-17-3,82	1645	150.84	230.4	38.7	28.61	4.05	-	(2)
86-578-17-3,99	1646	151.01	222.3	25.8	27.49	2.73	-	(2)
86-578-17-3,118	1647	151.20	220.6	57.1	27.96	2.34	-	(2)
86-578-17-3,134	1648	151.36	236.0	68.1	26.65	2.44	-	(2)
86-578-17-4,26	1650	151.78	79.8	52.7	36.38	2.57	-	(2)
86-578-17-4,46	1651	151.98	65.6	37.7	30.47	4.41	-	(2)
86-578-17-4,66	1652	152.18	64.9	43.9	32.40	4.17	-	(2)
86-578-17-4,82	1653	152.34	60.4	39.7	47.95	9.31	-	(2)
86-578-17-4,100	1654	152.52	51.8	49.5	52.87	8.29	-	(2)
86-578-17-4,118	1655	152.70	227.4	–53.4	28.77	4.43	-	(2)
86-578-17-4,136	1656	152.88	64.9	43.7	32.12	7.61	-	(2)
86-578-17-5,6	1657	153.08	161.3	–40.9	32.30	1.49	-	(2)
86-578-17-5,26	1658	153.28	26.2	43.1	40.83	5.45	-	(2)
86-578-17-5,46	1659	153.48	170.3	–60.6	40.79	1.87	-	(2)
86-578-17-5,66	1660	153.68	25.5	46.8	51.19	39.99	-	(2)
86-578-17-5,86	1661	153.88	77.2	–3.1	37.79	0.93	-	(2)
86-578-17-5,106	1662	154.08	32.2	30.2	38.19	6.60	-	(2)
86-578-17-5,126	1663	154.28	28.6	38.2	40.74	6.99	-	(2)
86-578-18-1,26	1664	156.86	108.2	19.4	34.34	13.57	-	(2)
86-578-18-1,46	1665	157.06	126.7	30.0	38.03	16.26	-	(2)
86-578-18-1,66	1666	157.26	293.7	–37.7	14.03	9.06	-	(2)
86-578-18-1,86	1667	157.46	292.2	–34.8	12.73	11.68	-	(2)
86-578-18-1,106	1668	157.66	69.0	–62.0	24.75	0.74	-	(2)
86-578-18-1,126	1669	157.86	122.7	56.2	30.54	3.83	-	(2)
86-578-18-1,146	1670	158.06	273.0	–32.0	27.34	1.12	-	(2)
86-578-18-2,6	1671	158.16	108.7	55.3	21.95	2.41	-	(2)
86-578-18-2,29	1672	158.39	279.0	–26.2	24.90	1.75	-	(2)
86-578-18-2,46	1673	158.56	112.3	43.5	48.51	15.34	-	(2)
86-578-18-2,66	1674	158.76	285.1	–38.6	16.73	9.54	-	(2)
86-578-18-2,86	1675	158.96	279.5	–28.5	-	25.65	-	(2)
86-578-18-2,106	1676	159.16	283.7	–27.7	14.03	11.46	-	(2)
86-578-18-2,126	1677	159.36	289.5	–47.9	19.91	2.44	-	(2)
86-578-18-2,146	1678	159.56	102.3	34.7	41.85	9.44	-	(2)
86-578-18-3,6	1679	159.66	104.0	29.1	50.50	21.55	-	(2)
86-578-18-3,26	1680	159.86	95.4	29.4	43.34	18.40	-	(2)
86-578-18-3,46	1681	160.06	93.3	42.8	36.08	10.92	-	(2)

86-578-18-3,66	1682	160.26	100.9	36.4	46.90	19.32	-	(2)
86-578-18-3,86	1683	160.46	267.0	14.7	24.79	5.04	-	(2)
86-578-18-3,106	1684	160.66	99.2	26.1	40.28	9.55	-	(2)
86-578-18-3,117	1685	160.77	306.8	–46.3	22.91	2.27	-	(2)
86-578-18-4,6	1686	161.16	293.0	–31.0	33.53	1.28	-	(2)
86-578-18-4,26	1687	161.36	5.0	–61.0	31.10	3.02	-	(2)
86-578-18-4,46	1688	161.56	309.0	1.0	27.32	1.37	-	(2)
86-578-18-4,66	1689	161.76	260.1	–53.6	23.71	7.73	-	(2)
86-578-18-4,86	1690	161.96	106.5	56.6	39.12	5.39	-	(2)
86-578-18-4,106	1691	162.16	272.0	–11.0	25.85	1.77	-	(2)
86-578-18-4,126	1692	162.36	288.0	–15.0	44.35	1.11	-	(2)
86-578-18-CC,5	1693	162.48	27.1	30.0	37.09	3.85	-	(2)
86-578-18-CC,30	1694	162.73	353.9	35.8	48.99	18.75	-	(2)
86-578-19-1,47	1695	166.34	54.0	–37.8	29.05	19.27	-	(2)
86-578-19-1,66	1696	166.53	195.8	–68.0	19.14	4.10	-	(2)
86-578-19-1,86	1697	166.73	225.0	–28.2	23.65	6.39	-	(2)
86-578-19-1,106	1698	166.93	254.0	–18.0	39.59	1.11	-	(2)
86-578-19-1,126	1699	167.13	86.5	30.7	32.63	2.73	-	(2)
86-578-19-1,146	1700	167.33	66.1	38.0	53.60	12.49	-	(2)
86-578-19-2,32	1741	167.69	134.2	–57.6	33.22	3.20	-	(2)
86-578-19-2,48	1742	167.85	219.9	–23.9	31.12	18.61	-	(2)
86-578-19-2,66	1743	168.03	61.3	37.3	71.16	26.20	-	(2)
86-578-19-2,86	1744	168.23	73.3	52.3	55.39	16.18	-	(2)
86-578-19-2,99	1701	168.36	57.6	37.9	66.68	21.30	-	(2)
86-578-19-2,111	1702	168.48	236.0	–24.0	34.78	3.14	-	(2)
86-578-19-2,125	1703	168.62	66.8	49.7	46.58	9.89	-	(2)
86-578-19-2,138	1704	168.75	52.9	39.6	60.65	14.56	-	(2)
86-578-19-3,6	1705	168.93	65.2	59.5	51.55	8.09	-	(2)
86-578-19-3,26	1706	169.13	39.7	48.2	65.02	18.73	-	(2)
86-578-19-3,46	1707	169.33	40.0	41.6	59.65	19.62	-	(2)
86-578-19-3,66	1708	169.53	57.9	45.1	73.69	12.64	-	(2)
86-578-19-3,86	1709	169.73	36.2	51.5	105.82	45.26	-	(2)
86-578-19-3,106	1710	169.93	47.6	46.7	74.06	21.57	-	(2)
86-578-19-CC,5	1711	170.12	131.3	37.9	60.46	26.48	-	(2)
86-578-19-CC,29	1712	170.36	335.1	–51.4	71.16	24.50	-	(2)
86-578-20-1,6	1534	175.86	21.4	–60.0	34.79	24.73	-	(2)
86-578-20-1,22	1535	176.02	85.0	–82.4	29.95	29.95	-	(2)
86-578-20-1,46	1536	176.26	19.1	–2.4	49.52	6.25	-	(2)
86-578-20-1,71	1537	176.51	170.3	–58.7	35.31	7.58	-	(2)

Data source is (1) This study, (2) *Heath et al.* [1985*b*, Table 6, p. 485-494].

APPENDIX B

Solutions to Some Calculus Problems

In this appendix we derive some equations that were used in chapter 3: "Models of Inclination Shallowing During Sediment Compaction". We derive equations (3.36), (3.39), (3.74), and (3.76): Equation (3.36) is derived from equations (3.30), (3.34), and (3.35). Equation (3.39) from equations (3.30), (3.35), and (3.38). Equation (3.74) from equations (3.66), (3.68), (3.71), and (3.72). And finally, equation (3.76) is derived from equations (3.9), (3.68), (3.71), and (3.72). Furthermore, we show in this appendix that for initially dispersed within-sample magnetic moments equation (3.78) is valid independent of the microscopic mechanism causing the inclination shallowing.

B.1 COLLAPSING RIGID MATRIX

We want to find the exact mathematical solution to

$$F(\Delta V) = \int_0^{\pi/2} \cos \Delta\theta \, P_f(\theta) \, d\theta \tag{B.1}$$

where $\Delta\theta$ is related to θ and ΔV by

$$\sin (\theta - \Delta\theta) = (1 - \Delta V) \sin \theta \tag{B.2}$$

and the normalized probability distribution $P_f(\theta)$ is described by

$$P_f(\theta) \, d\theta = \sin \theta \, d\theta \tag{B.3}$$

a distribution which describes a spherically random fabric flakes. Equation (B.2) can be written with $\Delta\theta$ isolated

$$\Delta\theta = \theta - \arcsin [(1 - \Delta V) \sin \theta] \tag{B.4}$$

We define for ease $a \equiv (1 - \Delta V)$, and now we can write

$$\cos \Delta\theta = \cos [\theta - \arcsin (a \sin \theta)] \tag{B.5}$$

and this can be split, using the angle difference relation, to yield

$$\cos \Delta\theta = \cos \theta \cos [\arcsin (a \sin \theta)] +$$

$$+ \sin\theta \sin [\arcsin(a \sin\theta)] \qquad \text{(B.6)}$$

which can be simplified to

$$\cos\Delta\theta = \cos\theta\sqrt{1-a^2\sin^2\theta} + a\sin^2\theta \qquad \text{(B.7)}$$

We can therefore write equation (B.1) on the form

$$F(\Delta V) = \int_0^{\pi/2} [\cos\theta\sqrt{1-a^2\sin^2\theta} + a\sin^2\theta]\sin\theta\, d\theta \qquad \text{(B.8)}$$

this can be split into two integrals, and the first one simplified by the substitution

$$s \equiv \sqrt{1 - a^2\sin^2\theta} \qquad \text{(B.9)}$$

So we can write equation (B.8) as

$$F(\Delta V) = -a^{-2} \int_1^{\sqrt{1-a2}} s^2\, ds + a\int_0^{\pi/2} \sin^3\theta\, d\theta \qquad \text{(B.10)}$$

and the exact solution to equation (B.1) assuming (B.2) is

$$F(\Delta V) = \frac{1 - (1 - a^2)^{3/2}}{3\, a^2} + \frac{2\, a}{3} \qquad \text{(B.11)}$$

or written out in full with ΔV

$$F(\Delta V) = 1 - \frac{(2\,\Delta V - \Delta V^2)^{3/2} - 3\,\Delta V^2 + 2\,\Delta V^3}{3 - 6\,\Delta V + 3\,\Delta V^2} \qquad \text{(B.12)}$$

this result is used in equation (3.36).

B.2 COLLAPSING SOFT MATRIX

We want to find the exact mathematical solution to (B.1) assuming now that $\Delta\theta$ can be connected to θ and ΔV by

$$\tan (\theta - \Delta\theta) = (1 - \Delta V) \tan \theta \qquad \text{(B.13)}$$

As before we define the variable $a \equiv (1 - \Delta V)$. From equation (B.13) we can now write

$$\cos \Delta\theta = \cos [\theta - \arctan (a \tan \theta)] \qquad \text{(B.14)}$$

using now the angle difference relation, as before, we get

$$\begin{aligned} \cos \Delta\theta = {} & \cos \theta \cos [\arctan (a \tan \theta)] + \\ & + \sin \theta \sin [\arctan (a \tan \theta)] \end{aligned} \qquad \text{(B.15)}$$

This can be simplified by standard relationships between sin x, cos x, tan x, and arctan x [*Beyer*, 1984, pp. 139-140]. We are only interested in the first quadrant $0 \leq x \leq \pi/2$, where the trigonometric functions are positive, so we do not have to worry about sign problems. We define $t \equiv \tan \theta$.

Equation (B.15) is now simplified to

$$\cos \Delta\theta = \frac{1}{\sqrt{1+t^2}} \frac{1}{\sqrt{1+a^2t^2}} + \frac{t}{\sqrt{1+t^2}} \frac{a\,t}{\sqrt{1+a^2t^2}} \qquad \text{(B.16)}$$

or

$$\cos \Delta\theta = \frac{(\ 1 + a\ t^2\ )}{\sqrt{(1 + t^2)\ (1 + a^2 t^2)}} \tag{B.17}$$

and we can write $P_f(\theta)$ from equation (B.3) as

$$\sin \theta = \frac{t}{\sqrt{1 + t^2}} \tag{B.18}$$

By getting rid of $\Delta\theta$ we have now simplified equation (B.1) to

$$F(\Delta V) = \int_0^{\pi/2} \frac{(\ 1 + a\ \tan^2\theta\ )\ \tan\ \theta}{(1 + \tan^2\theta)\ \sqrt{1 + a^2\ \tan^2\theta}} d\theta \tag{B.19}$$

in solving equation (B.19) it is convenient to make the substitution

$$s \equiv \sqrt{1 + a^2\ \tan^2\theta} \tag{B.20}$$

which transforms equation (B.19) to

$$F(\Delta V) = \int_1^{\infty} \frac{a\ (s^2 - (1-a))}{(s^2 - (1-a^2))^2}\ ds \tag{B.21}$$

This can be solved by using standard integral tables [e.g., *Beyer*, 1984, pp. 240-241, integrals 61a, 65, and 69, with $b = 1$, and $m = 1$]. We can now evaluate the integrals

$$g_1 = \int_1^{\infty} \frac{ds}{s^2 - (1-a^2)} = \frac{1}{2\ \sqrt{1-a^2}} \ln \left[\frac{1 + \sqrt{1-a^2}}{1 - \sqrt{1-a^2}} \right] \tag{B.22}$$

$$g_2 = \int_1^{\infty} \frac{ds}{(s^2 - (1-a^2))^2} = \frac{1 - a^2\, g_1}{2\, a^2\, (\, 1 - a^2\,)} \qquad \text{(B.23)}$$

$$g_3 = \int_1^{\infty} \frac{s^2\, ds}{(s^2 - (1-a^2))^2} = \frac{1 + a^2\, g_1}{2\, a^2} \qquad \text{(B.24)}$$

and write the solution to equation (B.21)

$$F(\Delta V) = -a\,(\,1 - a\,)\, g_2 + a\, g_3 \qquad \text{(B.25)}$$

Written out in full, the exact mathematical solution to equation (B.1), assuming (B.13) is then

$$F(\Delta V) = \frac{1}{2\,(2 - \Delta V)} +$$

$$+ \frac{(2 - \Delta V)^2 - 1}{4\,(2 - \Delta V)\,\sqrt{\Delta V(2-\Delta V)}} \ln\left[\frac{1 + \sqrt{\Delta V(2-\Delta V)}}{1 - \sqrt{\Delta V(2-\Delta V)}}\right] \qquad \text{(B.26)}$$

This result is used in equation (3.39).

B.3 INITIAL WITHIN-SAMPLE DISPERSION

We want to solve

$$\tan\,(\,I-\Delta I\,)\;=$$

$$=\frac{\displaystyle\int_{-\pi/2}^{\pi/2}\int_{0}^{2\pi}\cos i\;(1+\kappa\cos\theta)\;\sin(i-\Delta i)\;dd\;di}{\displaystyle\int_{-\pi/2}^{\pi/2}\int_{0}^{2\pi}\cos i\;(1+\kappa\cos\theta)\;\cos(i-\Delta i)\;\cos d\;dd\;di}\qquad\text{(B.27)}$$

where θ is related to I, i, and d through

$$\cos\,\theta\;=\;\sin I\,\sin i\;+\;\cos I\,\cos i\,\cos d\qquad\text{(B.28)}$$

For convenience we define Z, and X

$$Z\;\equiv\;\int_{-\pi/2}^{\pi/2}\int_{0}^{2\pi}\cos i\;(1+\kappa\cos\theta)\;\sin(i-\Delta i)\;dd\;di\qquad\text{(B.29)}$$

$$X\;\equiv\;\int_{-\pi/2}^{\pi/2}\int_{0}^{2\pi}\cos i\;(1+\kappa\cos\theta)\;\cos(i-\Delta i)\;\cos d\;dd\;di\qquad\text{(B.30)}$$

and by applying equation (B.28) in (B.29) and (B.30) we get

$$Z\;=\;\int_{-\pi/2}^{\pi/2}\int_{0}^{2\pi}[\cos i\;(1+\kappa\,\sin I\,\sin i)\;\sin(i-\Delta i)]\;dd\;di\;+$$

$$+\;\int_{-\pi/2}^{\pi/2}\int_{0}^{2\pi}[\cos i\;(\kappa\cos I\,\cos i)\;\sin(i-\Delta i)]\;\cos d\;dd\;di\qquad\text{(B.31)}$$

$$X = \int_{-\pi/2}^{\pi/2} \int_{0}^{2\pi} [\cos i\ (1+\kappa \sin I \sin i)\ \cos(i-\Delta i)]\ \cos d\ dd\ di\ +$$

$$+ \int_{-\pi/2}^{\pi/2} \int_{0}^{2\pi} [\cos i\ \ (\kappa \cos I \cos i)\ \cos(i-\Delta i)]\ \cos^2 d\ dd\ di \quad \text{(B.32)}$$

Integration over d from 0 to 2π is now a simple task and Z and X can be simplified to

$$Z = 2\,\pi\,\kappa \sin I \int_{-\pi/2}^{\pi/2} \cos\, i \sin\, i \sin(i - \Delta i)\, di \quad \text{(B.33)}$$

$$X = \pi\,\kappa \cos I \int_{-\pi/2}^{\pi/2} \cos^2 i \cos(i - \Delta i)\, di \quad \text{(B.34)}$$

The integrals in equations (B.33) and (B.34) are over symmetric functions about zero and can be replaced by double the integrals from 0 to $\pi/2$. At this point we notice that equation (B.27) will take the form

$$\tan\,(\,I - \Delta I\,) = (\,1 - F\,) \tan I \quad \text{(B.35)}$$

where

$$F = 1 - \frac{2 \int_{0}^{\pi/2} \cos\, i \sin\, i \sin(i - \Delta i)\, di}{\int_{0}^{\pi/2} \cos^2 i \cos(i - \Delta i)\ \ di} \quad \text{(B.36)}$$

Equation (B.35) carries great significance: We have not yet, in this derivation, introduced a microscopic relation defining the dependence of Δi on i and ε (or ΔV). Still we get the functional relationship of

equation (B.35). We have, in fact, shown that if the within-sample magnetic moments have dispersed orientations, the macroscopic relationship will take the form shown in equation (B.35), independent of the form of the microscopic relationship between ΔI and ΔV. We note that F is a function of ε but independent of κ and I.

Now we connect $(i - \Delta i)$ to i and ε by

$$\tan (i - \Delta i) = (1 - \varepsilon) \tan i \tag{B.37}$$

and use the relations $\sin x = \tan x/(1+\tan^2 x)^{1/2}$ and $\cos x = 1/(1+\tan^2 x)^{1/2}$ to obtain

$$\sin (i - \Delta i) = \frac{(1 - \varepsilon) \tan i}{\sqrt{1 + (1-\varepsilon)^2 \tan^2 i}} \tag{B.38}$$

$$\cos (i - \Delta i) = \frac{1}{\sqrt{1 + (1-\varepsilon)^2 \tan^2 i}} \tag{B.39}$$

We define $\beta \equiv (1 - \varepsilon)$, and Z' and X'

$$Z' \equiv 2 \beta \int_0^{\pi/2} \frac{\sin^2 i \; di}{\sqrt{1 + \beta^2 \tan^2 i}} \tag{B.40}$$

$$X' \equiv \int_0^{\pi/2} \frac{\cos^2 i \; di}{\sqrt{1 + \beta^2 \tan^2 i}} \tag{B.41}$$

and these give the relation $\tan (I - \Delta I) = (Z'/X') \tan I$. Here it turns out to be convenient to use the substitution $s \equiv 1 + \tan^2 i$, which transforms equations (B.40) and (B.41) to

$$Z' = 4\beta \int_1^{\infty} \frac{s-1}{s^2 A^{1/2}} ds \qquad \text{(B.42)}$$

$$X' = 2 \int_1^{\infty} \frac{1}{s^2 A^{1/2}} ds \qquad \text{(B.43)}$$

where $A \equiv (\beta^2 - 1) + (1 - 2\beta^2)s + \beta^2 s^2$. These integrals can be solved using integral tables [e.g., *Beyer*, 1984, integrals 259 and 261, p. 257] resulting in

$$Z' = \frac{2\beta\,(\arcsin(1-2\beta^2) + \pi/2)}{(1-\beta^2)^{3/2}} - \frac{4\beta^2}{(1-\beta^2)} \qquad \text{(B.44)}$$

$$X' = \frac{(1-2\beta^2)\,(\arcsin(1-2\beta^2) + \pi/2)}{(1-\beta^2)^{3/2}} + \frac{2\beta}{(1-\beta^2)} \qquad \text{(B.45)}$$

And finally we define the function b such that $(1 - b\,\varepsilon) = Z'/X'$, incorporate relationships between arcsin and arccos, and replace β by $(1 - \varepsilon)$ to get

$$(1 - b\,\varepsilon) =$$

$$= \frac{2\,(1-\varepsilon)\arccos(1-4\varepsilon+2\varepsilon^2) - 4\,(1-\varepsilon)^2\sqrt{2\varepsilon-\varepsilon^2}}{-(1-4\varepsilon+2\varepsilon^2)\arccos(1-4\varepsilon+2\varepsilon^2) + 2\,(1-\varepsilon)\sqrt{2\varepsilon-\varepsilon^2}} \qquad \text{(B.46)}$$

This result is used in equation (3.74).

To calculate the effect of initial within-sample dispersion on model 1a, we have to start form equation (B.35) and (B.36), and instead of equation (B.37), we connect $(i - \Delta i)$ to i and ε by

$$\sin(i - \Delta i) = (1 - \varepsilon)\sin i \qquad \text{(B.47)}$$

and use the relation $\cos x = (1 - \sin^2 x)^{1/2}$ to obtain

$$\cos (i - \Delta i) = \sqrt{1 - (1-\varepsilon)^2 \sin^2 i} \qquad \text{(B.48)}$$

As before we define $\beta \equiv (1 - \varepsilon)$, and Z' and X'

$$Z' \equiv 2 \beta \int_0^{\pi/2} \cos i \sin^2 i \, di \qquad \text{(B.49)}$$

$$X' \equiv \int_0^{\pi/2} \cos^2 i \sqrt{1 - \beta^2 \sin^2 i} \, di \qquad \text{(B.50)}$$

and these give the relation $\tan (I - \Delta I) = (Z'/X') \tan I$. Equation (B.49) is easily solved to give $Z' = 2 (1 - \varepsilon) / 3$. However, equation (B.50) is an elliptic integral, which can not be written in terms of elementary functions, but can be written in terms of the special functions $\boldsymbol{K}(k)$ and $\boldsymbol{E}(k)$, called the complete elliptic integrals of the first ($\boldsymbol{K}$) and second ($\boldsymbol{E}$) kind [*Gradshteyn and Ryzhik*, 1980, integral 2.583.6, p. 159]. For model 1a we define $(1 - b' \varepsilon) \equiv (Z'/X')$, which can be written as

$$(1 - b' \varepsilon) = \frac{2 (1-\varepsilon)^3}{((1-\varepsilon)^2-1) \, \boldsymbol{K}(1-\varepsilon) + ((1-\varepsilon)^2+1) \, \boldsymbol{E}(1-\varepsilon)} \qquad \text{(B.51)}$$

This result is used in equation (3.76).

APPENDIX C

Computer Programs for the Analysis of Inclination Data

The computer programs of this appendix were used to generate synthetic directional data and to analyze directional data sets. It should be possible to repeat all the calculations of chapter 5: "Comparison of statistical methods in the analysis of paleomagnetic inclination data" using these programs.

Following is a list of the Fortran subroutines URAND, FRAND, FISHER, FADDEN, KONO, and LANVIN.

C.1 THE PROGRAM URAND

The program URAND is used to generate random numbers that are uniformly distributed between 0 and 1. Zero can occur, but not one. This algorithm is based on *Forsythe et al.* [1977, p. 241-246].

```
c######################################################################
c
c       U R A N D   Function that generates uniform random numbers
c       Based on algorithm in :
c       Forsythe, G.E., M.A. Malcolm and C.B. Moler,
c          Computer Methods for Mathematical Computations, 259 pp.,
c          p. 241-246, Prentice Hall, Englewood Hills, N.J., 1977.
c
c       Subroutines :   none
c
c       iseed   Should be initialized to an arbitrary integer prior
c               to the first call to URAND.  The calling routine
c               should not alter the value of iseed between
c               subsequent calls to URAND.            (input,output)
c       URAND   Random values in the interval [0,1[. (output)
c
c       History:
c               August 1985  Initial version written for LSI 11/23
c               March 1989   Adaption to Macintosh
c               March 1991   Comment clarification
c
c       Pórdur Arason
c       Oregon State University
c       College of Oceanography
c       Corvallis, OR 97331
c
c######################################################################

        real function URAND ( iseed )

        integer*4 iseed

        integer*4 ib, nfirst
        real*8 fullin, y, a, c, yn, b
        real*8 datan, dsqrt

        data nfirst/0/
        data fullin/2147483648.D0/    ! Define largest integer (+1).

        if ( nfirst .ne. 0 ) goto 19
```

```
      nfirst = 1              ! Calculate a and c the first time.
      a = 8*idint( fullin*datan(1.D0)/16.D0 ) + 5
      c = 2*idint( fullin*(0.5D0-dsqrt(3.D0)/6.D0)/2.D0 ) + 1

19    yn = iseed
      y = yn*a + c                    ! Next random number.
      ib = y/fullin
      b = ib

      iseed = y - b*fullin + 0.5D0 ! Next random integer [0,2**31[.

      URAND = float(iseed)/fullin  ! Random real number [0,1[.

      return
      end
```

C.2 THE PROGRAM FRAND

The program FRAND is used to create random numbers that are Fisher distributed on a sphere.

```
c######################################################################
c
c       F R A N D   Subroutine that generates Fisher distributed
c       random data points about a mean inclination or pole on a
c       sphere.
c
c       Subroutines :   URAND  ! Gives uniform random values [0,1[.
c
c       iseed   Should be initialized to an arbitrary integer prior
c               to the first call to RANFIS.  The calling routine
c               should not alter the value of iseed between
c               subsequent calls.                    (input, output)
c       xinc    The mean inclination in degrees or latitude of pole
c                                                    (input, unaltered)
c       xdec    The mean declination in degrees or longitude of pole
c                                                    (input, unaltered)
c       xkappa  The precision parameter of the Fisher distribution
c                                                    (input, unaltered)
c       rinc    Random inclination in degrees or latitude
c               range [-90,90]                       (output)
c       rdec    Random declination in degrees or longitude
c               range [-90,270[                      (output)
c
c       History:
c               May 1985        Initial version written for LSI 11/23
c                               based on a program by W.H. Menke
c               March 1989      Adaption to Macintosh
c               January 1991    User defined true mean
c               March 1991      Comment clarifications
c
c       Pórdur Arason
c       Oregon State University
c       College of Oceanography
c       Corvallis, OR 97331
c
c######################################################################

        subroutine FRAND ( iseed, xinc, xdec, xkappa, rinc, rdec )

        integer*4 iseed
        real xinc, xdec, xkappa, rinc, rdec
```

```
      dr = 0.01745329252            ! Degrees to radians (pi/180).

      do (i=1, 10)                  ! Should only need one loop
        u = URAND ( iseed )
        r = 1. - 2.*u
        if ( xkappa > 0. .and. xkappa < 20. )
     +       r = 1. + alog( 1. - u*(1.-exp(-2.*xkappa)))/xkappa
        if ( xkappa .ge. 20. ) r = 1. + alog( 1. - u )/xkappa
        if ( r .ge. -1. .and. r .le. 1. ) goto 19
      end do
      write (9,*) "Error in FRAND"
      pause
      stop

c     Calculate random data about the pole

19    theta = acos( r )/dr          ! Distance from pole [0,180]
      phi = 360.*URAND ( iseed ) ! Uniform random direction [0,360[

c     Transform the random data to the user defined mean direction
c     First calculate random inclination

      x = sin(xinc*dr)*cos(theta*dr)
     +     + cos(xinc*dr)*sin(theta*dr)*cos(phi*dr)
      if ( x > 1. ) x = 1.
      if ( x < -1. ) x = -1.
      rinc = asin( x )/dr

c     Calculate random declination.
c     Special care must be taken due to roundoff errors close
c     to the poles (I = ± 90)

      if ( xinc > -89.99 .and. xinc < 89.99
     +      .and. rinc > -89.99 .and. rinc < 89.99 ) then
        x = (cos(theta*dr) - sin(xinc*dr)*sin(rinc*dr))
     +       /(cos(xinc*dr)*cos(rinc*dr))
        if ( x > 1. ) x = 1.
        if ( x < -1. ) x = -1.
        dec = acos( x )/dr
        if ( phi > 180. ) dec = -dec
      else
        dec = phi
      end if
      rdec = xdec + dec
      if ( rdec < -90. ) rdec = rdec + 360.
      if ( rdec .ge. 270. ) rdec = rdec - 360.

      return
      end
```

C.3 THE PROGRAM FISHER

The program FISHER is used to calculate Fisher statistics of directional data.

```
c######################################################################
c
c       F I S H E R   Subroutine that calculates Fisher statistics
c       of a given directional data.
c
c       Subroutines :   none
c
c       xinc   String of inclinations in degrees (input, unaltered)
c       xdec   String of declinations in degrees (input, unaltered)
c       np     Number of data points             (input, unaltered)
c       avinc  Average inclination in degrees      (output)
c       avdec  Average declination in degrees      (output)
c       xkappa Precicion parameter kappa           (output)
c       r      Length of vector sum                (output)
c       t63    Angular standard deviation theta-63 (output)
c       a95    95% confidence limits alpha-95      (output)
c
c       History:
c               January 1991   Written for Macintosh
c               March 1991     Comment clarifications
c
c       Pórdur Arason
c       Oregon State University
c       College of Oceanography
c       Corvallis, OR 97331
c
c######################################################################

        subroutine FISHER ( xinc, xdec, np
     +                    , avinc, avdec, xkappa, r, t63, a95 )

        real xinc(1000), xdec(1000)
        real avinc, avdec, xkappa, r, t63, a95
        integer np

        dr = 0.01745329252          ! Degrees to radians (pi/180)
        t63max = 105.070062145      ! 63% area of a sphere
        a95max = 154.158067237      ! 95% area of a sphere

        fn = float(np)

c       Check for illegal use
```

```
      if ( np < 1 ) then
        avinc = 0.
        avdec = 0.
        xkappa = 0.
        r = 0.
        t63 = t63max
        a95 = a95max
        return
      end if
      if ( np = 1 ) then
        avinc = xinc(1)
        avdec = xdec(1)
        xkappa = 0.
        r = 1.
        t63 = t63max
        a95 = a95max
        return
      end if
      if ( np > 1000 ) then
        write (9,*) "Too small dimension in FISHER"
        pause
        stop
      end if

c     Check if all directions are identical

      do (i=2, np)
        if ( xinc(i) .ne. xinc(1)
     +       .or. xdec(i) .ne. xdec(1) ) goto 19
      end do
      avinc = xinc(1)
      avdec = xdec(1)
      xkappa = 1.E10
      r = fn
      t63 = 0.
      a95 = 0.
      return

c     Vector sum of directions

19    sn = 0.
      se = 0.
      sv = 0.
      do (i=1, np)
        sn = sn + cos( xdec(i)*dr )*cos( xinc(i)*dr )
        se = se + sin( xdec(i)*dr )*cos( xinc(i)*dr )
        sv = sv + sin( xinc(i)*dr )
      end do

c     Length of the vector sum
```

```
      if ( sn = 0. .and. se = 0. .and. sv = 0. ) then
        avinc = 0.
        avdec = 0.
        xkappa = 0.
        r = 0.
        t63 = t63max
        a95 = a95max
        return
      else
        r = sqrt( sn*sn + se*se + sv*sv )
      end if

c     Average declination

      if ( sn = 0. .and. se .ne. 0. ) avdec = 90.*sign(1.,se)
      if ( sn < 0. ) avdec = 180. + atan( se/sn )/dr
      if ( sn > 0. ) avdec = atan( se/sn )/dr
      if ( avdec < -90. ) avdec = avdec + 360.
      if ( avdec .ge. 270. ) avdec = avdec - 360.

c     Average inclination

      if ( sn = 0. .and. se = 0. ) then
        avinc = 90.*sign(1.,sv)
        avdec = 0.
      else
        avinc = atan( sv/sqrt( sn*sn + se*se ) )/dr
      end if

c     Precision parameter : Kappa

      if ( fn > r ) then
        xkappa = (fn - 1.)/(fn - r)
      else
        xkappa = 1.E10
      end if

c     Angular standard deviation : Theta 63

      if ( xkappa < 20. )
     +     t63 = acos( 1. + alog( 1.
     +     - 0.63*(1. - exp( -2.*xkappa )) )/xkappa )/dr
      if ( xkappa .ge. 20. )
     +     t63 = acos( 1. + alog( 1. - 0.63 )/xkappa )/dr
      if ( t63 > t63max ) t63 = t63max

c     95% confidence limits : Alpha 95

      x = 1. - ((fn - r)/r)*( (1./(1.-0.95))**(1./(fn-1.)) - 1. )
      if ( x < -1. ) x = -1.
      if ( x > 1. ) x = 1.
      a95 = acos( x )/dr
```

```
if ( a95 > a95max ) a95 = a95max

return
end
```

C.4 THE PROGRAM FADDEN

The program FADDEN is used to calculate statistical parameters from paleomagnetic inclination data. Based on the theory of *McFadden and Reid* [1982]. The program calculates the original-MR method The modified-MR method is shown in comment lines at two places.

```
c#####################################################################
c
c       F A D D E N   Subroutine that uses the method of
c       McFadden and Reid to estimate mean and other
c       statistical parameters of inclination-only data.
c       McFadden, P. L., and A. B. Reid, Analysis of palaeomagnetic
c       inclination data, Geophys. J. R. Astron. Soc., 69, 307-319,
c       1982.
c
c       Subroutines :   none
c
c       xinc   String of inclinations in degrees    (input, unaltered)
c       np     Number of data points                (input, unaltered)
c       avinc  Average inclination in degrees       (output)
c       ak     Precicion parameter kappa            (output)
c       t63    Angular standard deviation theta-63  (output)
c       a95    95% confidence limits alpha-95       (output)
c
c       History:
c               January 1991   Written for Macintosh
c               March 1991     Comment clarifications
c
c       Pórdur Arason
c       College of Oceanography
c       Oregon State University
c       Corvallis,  OR 97331
c
c#####################################################################

        subroutine FADDEN ( xinc, np, avinc, ak, t63, a95 )

        real xinc(1000), avinc, ak, t63, a95
        real fdis(34)
        integer np

c       F-distribution F[1,N](p=0.025) (N=1-30,40,60,120,inf)
c       for estimating 95% confidence limits for mean inclination
```

```
      data fdis / 647.8, 38.51, 17.44, 12.22,
     +            10.01, 8.81, 8.07, 7.57, 7.21,
     +             6.94, 6.72, 6.55, 6.41, 6.30,
     +             6.20, 6.12, 6.04, 5.98, 5.92,
     +             5.87, 5.83, 5.79, 5.75, 5.72,
     +             5.69, 5.66, 5.63, 5.61, 5.59,
     +             5.57, 5.42, 5.29, 5.15, 5.02 /

      dr = 0.01745329252        ! Degrees to radians (pi/180)
      t63max = 105.070062145    ! 63% area of a sphere
      a95max = 154.158067237    ! 95% area of a sphere

c     Check for illegal use

      if ( np < 1 ) then
        avinc = -92.
        ak = -1.
        t63 = -1.
        a95 = -1.
        return
      end if
      if ( np = 1 ) then
        avinc = xinc(1)
        ak = 0.
        t63 = t63max
        a95 = a95max
        return
      end if
      if ( np > 1000 ) then
        write (9,*) "Too small dimension in FADDEN"
        pause
        stop
      end if

c     Check if no variability i.e. all inclinations are the same

      do (i=2, np)
        if ( xinc(i) .ne. xinc(1) ) goto 19
      end do
      avinc = xinc(1)
      ak = 1.E10
      t63 = 0.
      a95 = 0.
      return

c     Sums of cos and sin of (90-incl)

19    sumct = 0.
      sumst = 0.
      fn = float(np)
      do (i=1, np)
        t = (90.-xinc(i))*dr
```

```
          sumct = sumct + cos(t)
          sumst = sumst + sin(t)
        end do

c       Find interval (tmin, tmax) where function U is negative.
c       First we locate a single value tneg, where U(tneg) is
c       negative.  For most data sets U is negative over a broad
c       interval so first we look for negative U in a simple
c       fashion at theta 10, 20, 30, ..., 150, 160, 170 degrees.

        tneg = 200.*dr
        t = 10.*dr
        do (i=1, 17)
          c = cos(t)*sumct + sin(t)*sumst
          u = 1./(sin(t))**2 - c/(fn-c)
          if ( u < 0. ) then
            tneg = t
            goto 29
          end if
          t = t + 10.*dr
        end do

c       If we have not found any negative U yet, we locate the minima
c       of the function U.

29      if ( tneg > 190.*dr ) then     ! We have not found negative U
          tpp = 179.99*dr
          c = cos(tpp)*sumct + sin(tpp)*sumst
          s = sin(tpp)*sumct - cos(tpp)*sumst
          up = -2.*cos(tpp)/(sin(tpp)*sin(tpp)*sin(tpp))
     +         + fn*s/((fn-c)*(fn-c))
          if ( up < 0. ) then              ! Should never happen
            write (9,'(
     +        " FADDEN can not find positive derivative of U")')
            pause
            stop
          endif

          tpn = 0.01*dr
          c = cos(tpn)*sumct + sin(tpn)*sumst
          s = sin(tpn)*sumct - cos(tpn)*sumst
          up = -2.*cos(tpn)/(sin(tpn)*sin(tpn)*sin(tpn))
     +         + fn*s/((fn-c)*(fn-c))
          if ( up > 0. ) then                  ! Should never happen
            write (9,'(
     +        " FADDEN can not find negative derivative of U")')
            pause
            stop
          endif

c         Now we have identified locations where the derivative of U
c         is positive (tpp) and negative (tpn).
```

```
          t = (tpp + tpn)/2.
          do (i=1, 20)
            c = cos(t)*sumct + sin(t)*sumst
            s = sin(t)*sumct - cos(t)*sumst
            up = -2.*cos(t)/(sin(t)*sin(t)*sin(t))
     +           + fn*s/((fn-c)*(fn-c))
            if ( up < 0. ) then
              tpn = t
            end if
            if ( up > 0. ) then
              tpp = t
            end if
            if ( up = 0. ) goto 39
            t = (tpp + tpn)/2.
          end do
39        tpmin = t

          c = cos(tpmin)*sumct + sin(tpmin)*sumst
          u = 1./(sin(tpmin))**2 - c/(fn-c)
          if ( u < 0. ) then
            tneg = tpmin
          else
            write (9,'(" FADDEN no solution to U < 0")')
            avinc = -93.
            ak = -3.
            t63 = -3.
            a95 = -3.
            return
          end if

        end if

c       Now we have located a value (tneg) where U is negative
c       and we can locate tmin

        tpos = 0.                  ! This gives always positive U
        tn = tneg
        t = (tneg + tpos)/2.
        do (i=1, 20)
          c = cos(t)*sumct + sin(t)*sumst
          u = 1./(sin(t))**2 - c/(fn-c)
          if ( u < 0. ) then
            tneg = t
          end if
          if ( u > 0. ) then
            tpos = t
          end if
          if ( u = 0. ) then
            tpos = t - 0.001*dr
          end if
          t = (tneg + tpos)/2.
```

```
      end do
      tmin = tpos

c     In the same way we find tmax

      tpos = 180.*dr              ! This gives always positive U
      tneg = tn
      t = (tneg + tpos)/2.
      do (i=1, 20)
        c = cos(t)*sumct + sin(t)*sumst
        u = 1./(sin(t))**2 - c/(fn-c)
        if ( u < 0. ) then
          tneg = t
        end if
        if ( u > 0. ) then
          tpos = t
        end if
        if ( u = 0. ) then
          tpos = t + 0.001*dr
        end if
        t = (tneg + tpos)/2.
      end do
      tmax = tpos

c     Now we have identified the interval (tmin, tmax) where
c     solution is possible.  The problem is now set up such that
c     there is either one solution or no solution.  If there is one
c     solution (t0) then tmin < t0 < tmax and A(t0) = 0.  In this
c     case the sign of A(tmin) is not the same as A(tmax).  If the
c     sign of A(tmin) is the same as that of A(tmax) then there is
c     no solution.  We check first for this possibility.

      tn = tmin
      tx = tmax
      si = sin(tn)
      co = cos(tn)
      an = (fn*co + (si**2 - co**2)*sumct - 2.*si*co*sumst)
      si = sin(tx)
      co = cos(tx)
      ax = (fn*co + (si**2 - co**2)*sumct - 2.*si*co*sumst)
      sig = 1.
      if ( an/ax < 0. ) then
        if ( an > 0. ) sig = -1.
      else
        write (9,'(" FADDEN no solution to A = 0")')
        avinc = -93.
        ak = -1.
        t63 = -1.
        a95 = -1.
        return
      end if
```

```
c       Now we know that there is a solution and squeze (tn) and (tx)
c       slowly toward this solution

        t = (tn + tx)/2.
        do (i=1, 50)
          si = sin(t)
          co = cos(t)
          a = sig*(fn*co + (si**2 - co**2)*sumct - 2.*si*co*sumst)
          if ( a > 0. ) then
            tx = t
          end if
          if ( a < 0. ) then
            tn = t
          end if
          if ( a = 0. ) goto 49
          t = (tn + tx)/2.
        end do

49      t0 = t                          ! This is the estimate of theta

        c = cos(t0)*sumct + sin(t0)*sumst      ! MR eq (34)
        s = sin(t0)*sumct - cos(t0)*sumst

        if ( c .le. 0. ) then                  ! Should never happen
          write (9,'(" FADDEN problem with negative C")')
          pause
          stop
        end if

c       Calculate mean inclination.
c       The method as presented uses MR eq (40)

        avinc = 90. - (t0 - s/c)/dr

c       The modified method uses the maximum likelihood
c       estimate as the mean.
c
c       avinc = 90. - t0/dr

        if ( avinc < -90. ) avinc = -90.
        if ( avinc > 90. ) avinc = 90.

c       Estimate of precision parameter kappa (1/k)

        if ( fn > c ) then
          ak = 0.5*(fn-1.)/(fn-c)                ! MR eq (20)
        else
          ak = 1.E10
        end if

c       Find F-value from F-distribution table
```

```
      if ( np .ge. 2 .and. np .le. 31 ) fd = fdis(np-1)
      if ( np .gt. 31 .and. np .le. 41 )
     +     fd = fdis(30) - 0.015*(np-31)
      if ( np .gt. 41 .and. np .le. 61 )
     +     fd = fdis(31) - 0.0065*(np-41)
      if ( np .gt. 61 .and. np .le. 121 )
     +     fd = fdis(32) - 0.00233*(np-61)
      if ( np .gt. 121 ) fd = fdis(34)

c     95% confidence interval - Alpha 95.
c     The method as presented uses MR eq (42).

      x = 1 - 0.5*(s/c)**2 - fd*(fn-c)/(c*(fn-1.))
      if ( x < -1. ) x = -1.
      if ( x > 1. ) x = 1.
      a95 = acos( x )/dr

c     The modified method uses the asymmetric form of MR eq (37c)
c     so that a95 = a1 ± a2 where
c
c     a1 = (s/c)/dr
c     a2 = sqrt( 4.*s**2 + 8.*fd*c*(fn-c)/(fn-1) ) / (2.*c*dr)

      if ( a95 > a95max ) a95 = a95max

c     Angular standard deviation - Theta 63

      if ( ak < 20. )
     +     t63 = acos( 1.+alog(1.-0.63*(1.-exp(-2.*ak)))/ak )/dr
      if ( ak .ge. 20. )
     +     t63 = acos( 1.+alog(1.-0.63)/ak )/dr
      if ( t63 > t63max ) t63 = t63max

      return
      end
```

C.5 THE PROGRAM KONO

The program KONO is used to calculate statistical parameters from paleomagnetic inclination data. Based on the theory of *Kono* [1980*a*, *b*].

```
c######################################################################
c
c       K O N O   Subroutine that estimates mean inclination,
c       and precision parameter from several inclinations from
c       borecores, where declination is not available.
c       Kono, M.,  Statistics of paleomagnetic inclination data,
c       J. Geophys. Res., 85, 3878-3882, 1980.
c
c       Subroutines : LANVIN    ! Calculates Langevin functions
c
c       xinc    String of inclinations          (input, unaltered)
c       n       Number of inclinations          (input, unaltered)
c       fisher  Whether directions are assumed Fisherian or
c               the Virtual geomagnetic poles are.
c               'd' -> Directions are Fisherian
c               'p' -> Poles are Fisherian      (input, unaltered)
c       avinc   Mean inclination                      (output)
c       ak      Precision parameter - Kappa           (output)
c       t63     Angular standard deviation - Theta 63 (output)
c       a95     95% confidence limits of the mean inclination
c               - Alpha 95                            (output)
c
c       History:
c               August 1985     Initially written for LSI 11/23
c               March 1989      Adapted for Macintosh
c               February 1991   Algorithm modified to identify
c                               when no solution exists
c               March 1991      Comment clarifications
c
c       Þórdur Arason
c       Oregon State University
c       College of Oceanography
c       Corvallis, OR 97331
c
c######################################################################

        subroutine KONO ( xinc, n, fisher, avinc, ak, t63, a95 )

        real xinc(1000), avinc, ak, t63, a95
        integer n
        character fisher*1
```

```
      real*8 dr, dn, s1, s2, s12, as1, s, xi
      real*8 xlan, dlan, xlox
      real*8 a, aneg, apos
      real*8 dkmin, dkpos, dkneg
      real*8 dsi1, dsi2, dsi, dco, dfac
      real*8 dk, dkold

c     Set constants.

      dr = 0.01745329252          ! Degrees to radians (pi/180)
      t63max = 105.070062145      ! 63 % of a sphere.
      a95max = 154.158067237      ! 95 % of a sphere.
      dn = n

c     Check for illegal use

      if ( n < 1 ) then
        avinc = 0.
        ak = 0.
        t63 = t63max
        a95 = a95max
        return
      end if
      if ( n = 1 ) then
        avinc = xinc(1)
        ak = 0.
        t63 = t63max
        a95 = a95max
        return
      end if
      if ( n > 1000 ) then
        write (9,*) " Too small dimension in KONO"
        pause
        stop
      end if

c     Check if all incl are identical

      do (i=2, n)
        if ( xinc(i) .ne. xinc(1) ) goto 19
      end do
      avinc = xinc(1)
      ak = 1.E10
      t63 = 0.
      a95 = 0.
      return

c     Sum sines and sines squared of incl or VGL

19    s1 = 0.D0
      s2 = 0.D0
      do (i=1, n)
```

```
          xi = dble(xinc(i))*dr
          if ( (fisher = "p" .or. fisher = "P") .and.
     +          (abs(xinc(i)) < 89.9999) ) xi = datan(0.5D0*dtan(xi))
          s = dsin( xi )
          s1 = s1 + s
          s2 = s2 + s**2
        end do
        s1 = s1/dn
        s2 = s2/dn
        s12 = s1**2
        as1 = dabs( s1 )

c       We want to solve
c       A(k) = L**3/k -s2*L**2 -3*s1**2*L/k + s1**2 = 0
c       where L is the Langevin function L = coth k - 1/k
c       First we locate (dkpos) and (dkneg) so that
c       dkpos < dkneg  and  A(dkpos) > 0  and A(dkneg) < 0
c       The solution is then in between these boundaries
c       The search is performed in a way such that if these
c       boundaries can not be found then there is no solution
c       to the problem.

c       First a special rare case

        dkpos = -1.D0
        dkneg = -1.D0
        if ( as1 = 0.D0 ) then
          do (i=-6, 10)
            dk = dble(10.**i)
            call LANVIN ( dk, xlan, dlan, xlox )
            a = xlox - s2
            if ( a > 0.D0 ) then
              dkpos = dk
              apos = a
            end if
            if ( a < 0.D0 ) then
              dkneg = dk
              aneg = a
              goto 29
            end if
          end do
        end if

c       Find minimum value of kappa using Newtons iteration on the
c       equation : |s1| / L(k) ≤ 1

        dkmin = 1.D10
        dkold = 0.D0
        if ( as1 < 1.D0 ) dkmin = 1.D0/( 1.D0 - as1 )
        do (i=1, 100)
          call LANVIN ( dkmin, xlan, dlan, xlox )
          dkmin = dkmin - (xlan - as1)/dlan
```

```
          if ( dabs(dkold-dkmin) < 1.D-10 ) goto 29
            if ( dkmin < 0.D0 ) dkmin = 0.D0
            dkold = dkmin
          end do
          dkmin = 1.D-10

c         Find (dkpos) such that dkmin ≤ dkpos and A(dkpos) > 0

29        do (i=-3, 10)
            dk = dkmin - 1.D-3 + dble(10.**i)
            call LANVIN ( dk, xlan, dlan, xlox )
            a = xlox*xlan**2-s2*xlan**2-3.D0*s12*xlox+s12
            if ( a > 0.D0 ) then
              dkpos = dk
              apos = a
            end if
          end do

c         Find (dkneg) such that dkpos ≤ dkneg and A(dkneg) < 0

          do (i=-3, 10)
            dk = dkpos - 1.D-3 + dble(10.**i)
            call LANVIN ( dk, xlan, dlan, xlox )
            a = xlox*xlan**2-s2*xlan**2-3.D0*s12*xlox+s12
            if ( a < 0.D0 ) then
              dkneg = dk
              aneg = a
              goto 39
            end if
          end do

c         Check if we have found boundaries.

39        if ( dkneg < -0.5D0 .or. dkpos < -0.5D0 ) then
            write (9,*) " Warning - No solution of A=0 in KONO"
            avinc = -95.
            ak = -1.
            t63 = -1.
            a95 = -1.
            return
          end if

c         Squeeze the solution between the boundaries

          do (i=1, 30)
            dk = (dkneg + dkpos)/2.D0
            call LANVIN ( dk, xlan, dlan, xlox )
            a = xlox*xlan**2-s2*xlan**2-3.D0*s12*xlox+s12
            if ( a < 0.D0 ) then
              dkneg = dk
              aneg = a
            end if
```

```
            if ( a > 0.D0 ) then
              dkpos = dk
              apos = a
            end if
            if ( a = 0.D0 ) then
              dkpos = dk
              dkneg = dk
              goto 49
            end if
          end do

c         Estimate of kappa

49        dk = (dkneg + dkpos)/2.D0
          ak = dk

c         Estimate of mean inclination calculated from (ak) and data.

          call LANVIN ( dk, xlan, dlan, xlox )
          dsi1 = s1/xlan
          dsi2 = dsqrt( (s2 - xlox)/(1.D0 - 3.D0*xlox) )
          dsi = (dsi1 + dsign(1.D0,dsi1)*dsi2)/2.D0
          dfac = 2.D0
          if ( fisher .eq. 'd' .or. fisher .eq. 'D' ) dfac = 1.D0
          avinc = dsign(90.D0,dsi)
          if ( dabs(dsi) < 1.D0 )
     +       avinc = datan ( dfac*dsi/dsqrt(1.D0-dsi**2) )/dr

c         Estimate of angular standard deviation : Theta-63
c         calculated from (ak).

          if ( dk .ge. 20.D0 ) dco = 1.D0 + dlog(1.D0-0.63D0)/dk
          if ( dk .gt. 0.1D0 .and. dk .lt. 20.D0 )
     +       dco = 1.D0 + dlog(1.D0 - 0.63D0*
     +             (1.D0-dexp(-2.D0*dk)))/dk
          if ( dk .le. 0.1D0 ) dco = -0.26D0 + 0.4662D0*dk
          t63 = 90.D0 - dsign(90.D0,dco)
          if ( dabs(dco) .lt. 1.D0 )
     +       t63 = 90.D0 - datan( dco/dsqrt(1.D0-dco**2) )/dr
          if ( t63 .gt. t63max ) t63 = t63max

c         Estimate of 95 % circular confidence limit
c         of the mean - Alpha-95

          dco = 1.D0 - (dn - 1.D0) * (20.D0**(1.D0/(dn-1.D0)) - 1.D0)
     +        /(dn*(dk-1.D0) + 1.D0)
          a95 = 90.D0 - dsign(90.D0,dco)
          if ( dabs(dco) .lt. 1.D0 )
     +       a95 = 90.D0 - datan( dco/dsqrt(1.D0-dco**2) )/dr
          if ( a95 .gt. a95max ) a95 = a95max
          return
          end
```

C.6 THE PROGRAM LANVIN

The program LANVIN is used to calculate Langevin functions. These functions are used extensively in the program KONO.

```
c######################################################################
c
c       L A N V I N   Subroutine that calculates the value of the
c       Langevin function L(x) = coth x - 1/x, its derivative
c       L'(x) = -1/(sinh x)**2 + 1/x**2, and L(x)/x.
c         These functions are all smooth and well behaved.
c       However, they are all defined by functions that behave
c       rather wildly (but cancel each other) and care is needed
c       in calculating the functions.
c         The functions are calculated differently depending on
c       the value of (x).  For 20 <= |x| there may be overflow
c       in calculating dexp(x), there an approximation is used.
c       For |x| <= 0.1 there may be division by nearly zero and
c       therefore roundoff error, there a polynomial approximation
c       is used.
c
c       Subroutines :   none
c
c       x      Given x-value                          (input, unaltered)
c       xlan   Value of Langevin function
c              L(x) = coth x - 1/x                    (output)
c       dlan   Derivative of Langevin function
c              dL(x)/dx = -1/(sinh x)**2 + 1/x**2     (output)
c       xlox   Langevin function divided by x
c              L(x)/x = (coth x - 1/x)/x              (output)
c
c       History:
c              August 1985     Initial version written for LSI 11/23
c              March 1989      Adapted for Macintosh
c              February 1991   Simplified
c              March 1991      Comment clarifications
c
c       Pórdur Arason
c       Oregon State University
c       College of Oceanography
c       Corvallis, OR 97331
c
c######################################################################

        subroutine LANVIN ( x, xlan, dlan, xlox )

        real*8 x, xlan, dlan, xlox
```

```
      real*8 en, ep
      real ax

      ax = dabs(x)

c     Functions calculated for 20 ≤ |x|

      if ( ax .ge. 20. ) then
        xlan = dsign(1.D0,x) - 1.D0/x
        dlan = 1.D0/x**2
        xlox = xlan/x
        return
      end if

c     Functions calculated for 0.1 < |x| < 20

      if ( ax > 0.1 .and. ax < 20. ) then
        en = dexp(-x)
        ep = dexp(x)
        xlan = (ep+en)/(ep-en) - 1.D0/x
        dlan = -4.D0/(ep-en)**2 + 1.D0/x**2
        xlox = xlan/x
        return
      end if

c     Functions calculated for |x| ≤ 0.1

      if ( ax .le. 0.1 ) then
        xlan = x/3.D0 - x**3/45.D0 + 2.D0*x**5/945.D0
        dlan = 1.D0/3.D0 - 3.D0*x**2/45.D0 + 10.D0*x**4/945.D0
        xlox = 1.D0/3.D0 - x**2/45.D0 + 2.D0*x**4/945.D0
        return
      end if

      return
      end
```